

The evolution of close binaries with white dwarf components

Proefschrift

ter verkrijging van de graad van doctor
aan de Radboud Universiteit Nijmegen
op gezag van de rector magnificus prof. mr. S.C.J.J. Kortmann,
volgens besluit van het college van decanen
in het openbaar te verdedigen op maandag 7 oktober 2013
om 12.30 uur precies

door

Silvia Gerarda Martina Toonen

geboren op 31 mei 1984
te Nijmegen

PROMOTOREN: Prof. dr. G. Nelemans KU Leuven
Prof. dr. P.J. Groot

MANUSCRIPTCOMMISSIE: Prof. dr. N. de Groot
Prof. dr. B.T. Gaensicke University of Warwick
Prof. dr. D. Maoz Tel-Aviv University
Prof. dr. S. Portegies Zwart Leiden University
dr. O.R. Pols

© 2013, Silvia Toonen

The evolution of close binaries with white dwarf components

Thesis, Radboud University Nijmegen

Illustrated; with bibliographic information and Dutch summary

ISBN: 978-94-6191-884-0

*Optimism is the faith that leads to achievement.
Nothing can be done without hope and confidence.*

Helen Keller

CONTENTS

1	Introduction	1
1.1	Stars	1
1.2	Stellar evolution of low- and intermediate-mass stars	1
1.3	Binary evolution	2
1.3.1	Roche lobe geometry	2
1.3.2	Mass transfer	4
1.3.3	Accretion onto white dwarfs	5
1.3.4	Common-envelope evolution	6
1.4	Supernovae Type Ia	7
1.5	Binary population synthesis	8
1.6	This thesis	9
2	The effect of common-envelope evolution on the visible population of post-common-envelope binaries	13
2.1	Introduction	14
2.2	Method	15
2.2.1	SeBa - a fast stellar and binary evolution code	15
2.2.2	The initial stellar population	16
2.2.3	Common-envelope evolution	16
2.2.4	Galactic model	17
2.2.5	Magnitudes	17
2.2.6	Selection effects	18
2.3	Results	18
2.3.1	The SDSS PCEB sample	25
2.3.2	Variable CE efficiency	31
2.4	Discussion and conclusion	32
2.A	Population synthesis code SeBa	35

CONTENTS

2.B	The spectral type - mass relation	36
3	The single degenerate supernova type Ia progenitors: Studying the influence of different mass retention efficiencies	39
3.1	Introduction	40
3.2	Evolution of single degenerate SNIa progenitors	42
3.2.1	Global evolution	42
3.2.2	Common envelope phase	43
3.2.3	Growth of the white dwarf	45
3.3	Method	47
3.3.1	Retention efficiencies	48
3.3.2	Islands	49
3.4	Results: SNIa rates and delay times	51
3.5	Discussion	54
3.6	Conclusions	55
3.A	Retention efficiencies	57
3.A.1	Retention efficiencies based on Nomoto et al. 2007	57
3.A.2	Retention efficiencies based on Ruiter et al. 2009	58
3.A.3	Retention efficiencies based on Yungelson 2010	59
4	The influence of mass-transfer variability on the growth of the mass of white dwarfs in accreting systems	61
4.1	introduction	62
4.2	Mass-transfer variability	63
4.2.1	Theoretical considerations	64
4.2.2	Observations	65
4.3	Model	66
4.3.1	Mass-transfer variability	66
4.3.2	Integrated retention efficiency	69
4.4	Application to binary stellar evolution	71
4.5	Binary population Synthesis	74
4.6	Results and discussion	75
4.7	Conclusions	77
5	Supernova Type Ia progenitors from merging double white dwarfs: Using a new population synthesis model	83
5.1	Introduction	84
5.2	SeBa - a fast stellar and binary evolution code	87
5.2.1	Impact on the population of double white dwarfs	88
5.3	Two models for common-envelope evolution	90

5.3.1	Impact on the population of double white dwarfs and type Ia supernova progenitors	91
5.4	Evolutionary paths to supernova type Ia from the double degenerate channel	93
5.4.1	common-envelope channel	95
5.4.2	Stable mass transfer channel	97
5.4.3	Formation reversal channel	99
5.5	Delay time distribution	99
5.6	Population of merging double white dwarfs	103
5.7	Conclusion and discussion	107
5.A	Most important changes to the population synthesis code SeBa	110
5.A.1	Treatment of wind mass-loss	110
5.A.2	Accretion onto stellar objects	112
5.A.3	Stability of mass transfer	115
6	PopCORN: Hunting down the differences between binary population synthesis codes	121
6.1	Introduction	122
6.2	Binary evolution	124
6.2.1	Roche lobe overflow	124
6.3	Binary population synthesis codes	128
6.3.1	binary_c/nucsyn	128
6.3.2	The Brussels code	129
6.3.3	SeBa	130
6.3.4	StarTrack	130
6.4	Method	131
6.4.1	Assumptions for this project	132
6.4.2	Normalisation	134
6.5	Results	135
6.5.1	Single white dwarf systems	135
6.5.2	Double white dwarfs	170
6.6	Summary of critical assumptions in BPS studies	184
6.7	Conclusion	187
6.A	Backbones of the BPS codes	189
6.A.1	Single star prescriptions	191
6.A.2	Stability of mass transfer	191
6.A.3	Stable mass transfer	193
6.A.4	Wind mass loss	194
6.A.5	Angular momentum loss from winds	195
6.A.6	Evolution of helium stars	195
6.A.7	Generating the initial stellar population	196

CONTENTS

6.B	Typical variable assumptions in BPS codes	196
6.B.1	Accretion efficiency	198
6.B.2	Angular momentum loss during RLOF	198
6.B.3	Common envelope evolution	199
6.B.4	Wind accretion	200
6.B.5	Tides	200
6.B.6	Magnetic braking	200
6.B.7	Initial population	201
Bibliography		203
Summary		213
	Chapter 2: Common-envelope evolution	213
	Chapter 3: Mass retention efficiency of accreting white dwarfs	214
	Chapter 4: Mass transfer variability towards accreting white dwarfs	215
	Chapter 5: Double white dwarf binaries as supernovae Type Ia progenitors	215
	Chapter 6: Binary population synthesis	216
	Conclusion	217
Samenvatting		219
	Introductie	219
	Het leven van een ster...	219
	.. met zijn tweeën	220
	Supernovae van type Ia	223
	Dit proefschrift	223
	Hoofdstuk 2: Instabiele massa-overdracht	225
	Hoofdstuk 3: Hoe efficiënt kan een witte dwerg groeien door accretie?	226
	Hoofdstuk 4: Variabiliteit van de snelheid van massa-overdracht naar witte dwerfen	226
	Hoofdstuk 5: Supernovae van type Ia veroorzaakt door samensmeltende dubbele witte dwerfen	227
	Hoofdstuk 6: Het simuleren van dubbelsterpopulaties	228
Curriculum vitæ		229
List of Publications		231
Acknowledgements		233

CHAPTER 1

INTRODUCTION

1.1 Stars

A star is a sphere of gas and plasma that holds its shape through hydrostatic and thermal equilibrium. Hydrostatic equilibrium in a star is achieved by a balance between the force of gravity and the pressure gradient force. The force of gravity pushes the stellar material towards the center of the star, while the gas pressure pushes the material outwards into space. The combination of the pressure, density, temperature and chemical composition enforces that stars are gaseous throughout. When a star is in thermal equilibrium, the temperature of the gas is constant over time for a given radius. The temperature is maintained by energy production inside the star. Many energy sources are available, e.g. gravitational, chemical and thermonuclear energy, but only thermonuclear energy can account for the stellar luminosities and lifetimes. In a thermonuclear reaction (‘burning’), energy is produced by the fusing of two nuclei into a more massive nucleus. Energy losses at the surfaces of stars is what we as observers on Earth perceive as starlight.

1.2 Stellar evolution of low- and intermediate-mass stars

The equilibrium structure of a star slowly (and sometimes rapidly) changes in time as the energy production in the star changes. The long-term evolution of the star is driven by successive phases of nuclear burning. Initially stars mainly consist of hydrogen, which is fused into helium in the stellar core. This phase is known as the main-sequence phase. It lasts for about 90% of the stellar lifetime, which is approximately $10^{10}(M/M_{\odot})^{-2.8}\text{yr}$, where M is the mass of the star and M_{\odot} the mass of the Sun¹. When hydrogen is exhausted in the core, the star increases in size and becomes a giant. Core burning ceases, however,

¹This is called the nuclear evolution timescale.

hydrogen burning continues in a shell around the inert core. Since the core is no longer supported by enough thermal pressure, the core contracts. This in turn leads to a dramatic expansion of the stellar envelope to giant dimensions. For low- and intermediate-mass stars ($M \lesssim 8M_{\odot}$) the stellar radius increases by a factor of about 10-100 compared to the main-sequence radius. When the density and the temperature in the core become sufficiently high, core helium burning is ignited and carbon and oxygen are formed. For a low mass star of $M \lesssim 2M_{\odot}$, helium ignition occurs under degenerate conditions, while helium is ignited non-degenerately for more massive stars. When the core runs out of fuel once again, fusion continues in a shell around the carbon-oxygen core. At this stage there are two burning shells embedded in the star, a hydrogen burning shell and a helium burning shell. The envelope has expanded even more to roughly 100-500 solar radii (R_{\odot}). For stars of $M \lesssim 6.5M_{\odot}$ this is the end of the line; the density and temperature in the core will not reach values that are sufficiently high to ignite carbon. In more massive stars of $6.5M_{\odot} \lesssim M \lesssim 8M_{\odot}$, carbon will ignite which leads to an oxygen-neon core. For all low- and intermediate-mass stars, stellar evolution ends when the envelope is dispersed into the interstellar medium by stellar winds. The remaining core continues to contract as it cools down, until it is supported by electron degeneracy pressure; a white dwarf is born.

1.3 Binary evolution

Most stars are not isolated and single stars, like our Sun, but they are members of binary systems [or even multiple stellar systems, e.g. Duchêne & Kraus, 2013]. If a star is in a close binary system, its evolution will be modified by binary interactions. For low- and intermediate-mass stars this occurs if the initial orbital period is less than about 10 years. Examples of binary interactions are mass transfer, mergers and tidal interaction.

1.3.1 Roche lobe geometry

A useful geometry for isolated, circularized binary systems, is the co-rotating frame of the binary. The potential in this frame is called the Roche potential (see Fig. 1.1 top panel). Close to a star the potential field is dominated by the gravitational potential field of that star. The surfaces of equal potential (see Fig. 1.1 bottom panel) are centred on that star and approximately circular. At larger distances the surfaces of equal potential are distorted in tear-drop shapes. The figure of eight that passes through L1 are the Roche lobes of each star. L1 is the first Lagrangian point which is a saddle point of the potential field in which the forces cancel out. If a star overflows its Roche lobe, matter can move freely through L1 to the companion.

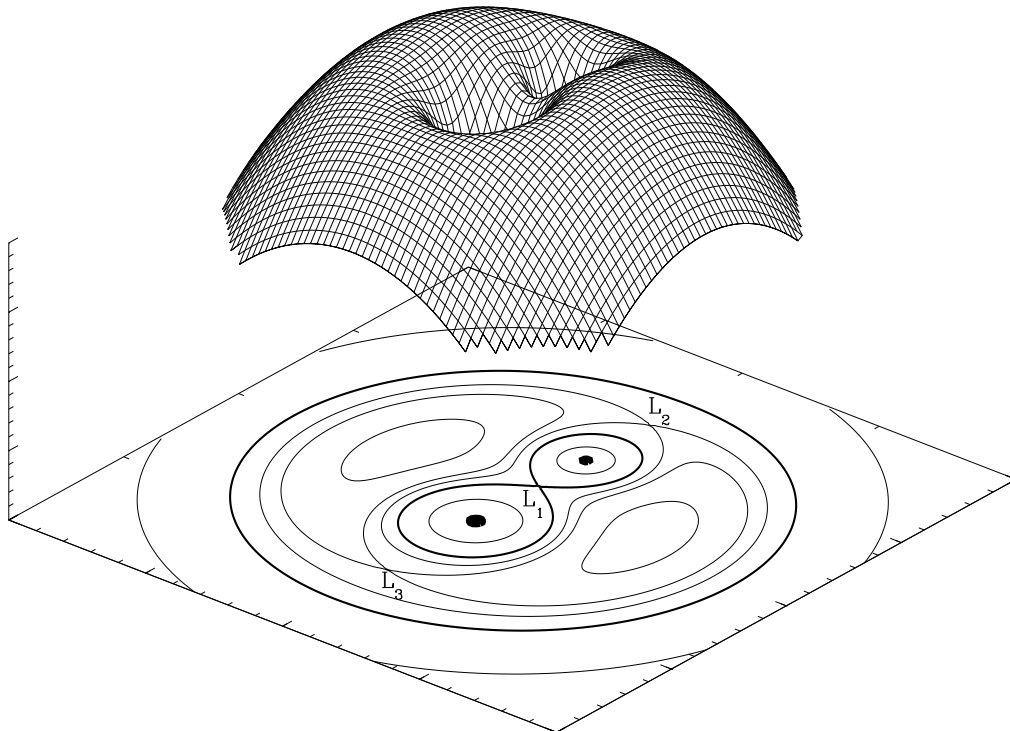


FIGURE 1.1: The Roche potential of a close binary in a binary star with a mass ratio of two in the co-rotating frame. On the top the Roche potential is shown in 3D, where as on the bottom a contour plot is shown of equipotential surfaces. L1, L2 and L3 are the Lagrangian points where forces cancel out. Courtesy of Marc van der Sluys.

The Roche lobe geometry naturally distinguishes between three types of binary stars:

- Detached binaries

These are binaries in which the outer shells of both stars lie within their respective Roche lobes. The stars only influence each other through tidal interactions or through stellar winds.

- Semidetached binaries

In a semidetached binary, one of the star fills its Roche lobe. Mass is transferred from the envelope of the Roche-lobe filling star through L1 towards the detached companion star (see Fig. 1.1). The mass transfer significantly alters the evolution of the two stars. In this thesis we will study how mass transfer affects binaries and their stellar components.

- Contact binaries

Contact binaries are binaries in which both stars fill or overflow their Roche lobes. Both stellar components are gravitationally distorted and surrounded by a common photosphere through which the stars are in physical contact.

1.3.2 Mass transfer

When one of the stars overflows its Roche lobe, it tends to lose most of its envelope. The evolution of the star is significantly shortened or even stopped prematurely. In the latter case, nuclear burning ceases after the mass transfer phase. Consequently, the inert core contracts and cools down to form a white dwarf². On the other hand, the evolution of a star is shortened e.g. for a star that loses its hydrogen-rich envelope but nuclear burning continues in the helium-rich layers of the star.

The companion star can accrete none, a fraction, or all of the mass that is transferred to it. The response of a non-degenerate star to accretion is to re-adjust its structure. This can cause the stellar core to grow in mass adding unprocessed material (a process called ‘rejuvenation’). On the other hand, accretion onto white dwarfs is a complicated process due to possible nuclear burning of the accreted matter (see Sect. 1.3.3).

If the mass transfer phase proceeds in a stable manner [Webbink, 1985; Hjellming & Webbink, 1987; Pols & Marinus, 1994; Soberman et al., 1997], the donor star will stay within its Roche lobe, approximately. The donor has to readjust its structure to recover hydrostatic and thermal equilibrium. The orbit is affected by the re-arrangement (and possible loss) of mass and angular momentum, and it widens in general. When mass transfer becomes unstable, the donor star will overflow its Roche lobe further upon mass loss. Subsequently the mass transfer rate increases even more leading to a runaway situation. A common

²This is strictly only true for the low- and intermediate-mass binaries that this thesis focuses on. More massive stars can evolve into a neutron star or black hole.

envelope develops around both stars (see Sect. 1.3.4). The binary may evolve to a more stable configuration or merge into a single, rapidly rotating star.

Mass transfer can become unstable through a dynamical or tidal instability. The dynamical stability of mass transfer depends on the response to mass loss of the donor star and the Roche lobe of the donor star in the first place. When the Roche lobe of the donor star shrinks faster than the radius of the donor star shrinks, a dynamical instability occurs. Or vice versa, when the Roche lobe increases more slowly than the donor star, mass transfer is dynamically unstable. In the second place the response of the companion star is important. If the accretor star swells up while adjusting to its new equilibrium, it may fill its Roche lobe leading to the formation of a contact binary.

Apart from the dynamical instability, a tidal instability [Darwin, 1879] can take place in compact systems with extreme mass ratios. Tidal forces act to synchronize the rotation of the stars with the orbit, but a stable orbit is not always possible. When there is insufficient orbital angular momentum that can be transferred to the most massive star, the star cannot stay in synchronous rotation. Tidal forces will cause the star to spin up by extracting angular momentum from the orbit, but in turn the binary becomes more compact and spins up. So that now the star needs even more angular momentum to stay in synchronous rotation. The result is a runaway process of orbital decay.

Stable mass transfer can proceed on many timescales depending on the driving mechanism of the mass transfer. The donor star itself can drive Roche lobe overflow on the timescale that it is evolving; due to its nuclear evolution or due to the thermal readjustment of the star to the new mass. The timescale of mass transfer in the former case is the nuclear evolution timescale of the donor (see Sect. 1.2). In the latter case it is the thermal timescale of the donor star. The thermal timescale is approximately $3.1 \cdot 10^7 (M/M_\odot)^2 (R/R_\odot)^{-1} (L/L_\odot)^{-1} \text{yr}$. Mass loss can also be driven by the change in the Roche lobe from the re-arrangement of mass and angular momentum in the binary system. An example is angular momentum loss from the binary due to gravitational wave emission or magnetic braking. Gravitational wave emission affects close binaries [Peters, 1964] which makes them very interesting sources for gravitational wave interferometers such as LIGO, Virgo or eLISA. Magnetic braking extracts angular momentum from a rotating star with a magnetic field by means of a stellar wind. If the system is compact, tidal forces will keep the star in corotation with the orbit such that magnetic braking removes orbital angular momentum from the binary system as well [Verbunt & Zwaan, 1981].

1.3.3 Accretion onto white dwarfs

When a white dwarf accretes material, the matter spreads over the surface of the white dwarf quickly, however, the matter may not be retained by the white dwarf. Depending on the rate of accretion, and the resulting temperature and density structure near the surface of the white dwarf [Nomoto, 1982; Nomoto et al., 2007; Shen & Bildsten, 2007], nuclear

burning can take place in the accumulated surface layer. The burning occurs in a stable way [Whelan & Iben, 1973; Nomoto, 1982] or in an unstable way in a thermo-nuclear runaway [Schatzman, 1950; Starrfield et al., 1974].

At low mass transfer rates, the temperature and pressure in the surface layer are too low for the matter to ignite immediately. The matter piles up on the surface of the white dwarf. When ignition values are reached, nuclear burning quickly spreads through the layer leading to a runaway. These events are observed as nova eruptions. During nova eruptions, some or all of the accreted matter is ejected from the white dwarf, and possibly even surface material of the white dwarf itself can be lost [Priyalnik, 1986; Priyalnik & Kovetz, 1995; Townsley & Bildsten, 2004; Yaron et al., 2005]. At higher accretion rates, the nuclear burning on the surface of the white dwarf occurs in a stable and continuous way. Binaries in which this occurs can be observed as supersoft X-ray sources. At even higher accretion rates, an extended envelope develops around the white dwarf (similar to the envelope of a giant star). Furthermore, the nuclear burning is strong enough to develop a wind from the white dwarf [Kato & Hachisu, 1994; Hachisu et al., 1996; Hachisu et al., 1999b]. A common envelope can be avoided if the wind attenuates the accretion rate sufficiently.

Concluding, even though the growth of white dwarfs is limited to a relatively narrow range of mass accretion rates (for hydrogen accretion $\sim 10^{-7} - 10^{-6} M_{\odot} \text{ yr}^{-1}$), accretion onto white dwarfs gives rise to many interesting processes.

1.3.4 Common-envelope evolution

When mass transfer is dynamically or tidally unstable, the envelope matter from the donor star will quickly engulf the companion star [Paczynski, 1976]. Both the companion star and the core of the donor star experience friction in their orbit around the center of mass and spiral inward through the envelope. One possible outcome is a merger between the companion star and the donor star's core. However, if the common envelope (CE) can be expelled before the merger, the spiral-in phase is halted and a close binary with a compact object is born. Therefore the CE-phase plays an essential role in the formation of many types of compact binary systems. Examples of systems are post-common envelope binaries (PCEBs i.e. detached white dwarf - main-sequence binaries), cataclysmic variables (semidetached white dwarf - main-sequence binaries), detached double white dwarf binaries, semi-detached double white dwarf binaries (AM CVn), X-ray binaries (semidetached binaries with accreting neutron stars or black holes).

Despite of the importance of the CE-phase and the enormous effort of the community, the CE-phase is not well understood. In order for the envelope to be expelled, enough energy and angular momentum must be transferred to it. Much of the discussion on CE-evolution is focused on which energy sources (e.g. orbital energy, recombination energy) can be used to expel the envelope and how efficient these sources can be used. Most of our understanding of CE-evolution comes from theoretical considerations [e.g. Tutukov &

Yungelson, 1979; Webbink, 1984] or binary population studies [e.g. Nelemans et al., 2000; van der Sluys et al., 2006; Zorotovic et al., 2010]. Hydrodynamical simulations of the CE-phase are a numerical challenge due to the large range in time-scales and length-scales, however, due to advances in computer methodologies, it has become possible to simulate parts of the CE-phase.

1.4 Supernovae Type Ia

Type Ia supernovae (SNIa) are one of the most energetic, explosive events known. They cause a burst of radiation that for a brief amount of time outshines entire galaxies. Their light curves show peak luminosities of around $10^{43} \text{erg s}^{-1}$ and a gradual decline over several weeks or months before the SNIa fades from view. The brightness of SNeIa makes allows us to observe them at large distances from Earth. However, most importantly, the uniformity [Phillips, 1993] in the lightcurves of SNeIa makes it possible to use SNIa as standard candles to estimate extragalactic distances. As measuring distances in the Universe is notoriously hard to do, observations of SNIa events have been of great importance in the field of observational cosmology, even indicating that the Universe undergoes accelerated expansion [e.g. Riess et al., 1998; Perlmutter et al., 1999]. SNIa explosions also play an important role in galactic evolution as they enrich the interstellar medium with high mass elements such as iron [e.g. Tsujimoto et al., 1995; Dupke & White, 2000; Sato et al., 2007].

Despite their significance, SNeIa are still poorly understood theoretically. It is generally thought that SNIa are thermonuclear explosions of carbon-oxygen white dwarfs. Once fusion has begun, the temperature of the white dwarf increases. The increase in temperature does not affect the hydrodynamic equilibrium in a degenerate environment, contrary to main-sequence stars which expand when heated and thus cool again. Therefore in a white dwarf the fusion process accelerates dramatically leading to a runaway process. The energy that is released in this process exceeds the binding energy of the white dwarf. Therefore the white dwarf is expected to explode violently such that after a SNIa event no remnant is left.

The details of the ignition are still poorly understood, and several evolutionary channels have been suggested to instigate the fusion process in the WD. The two canonical channels involve white dwarfs accreting material until they reach a maximum mass. A natural mass limit occurs in white dwarfs when the electron degeneracy pressure is not able to support the white dwarf against collapse. This is the case for white dwarfs that are more massive than the Chandrasekhar mass limit, which lies at $1.44M_{\odot}$ for slowly-rotating white dwarfs. However, the Chandrasekhar mass is not reached as carbon fusion commences in the core at slightly lower masses. We note that as carbon-oxygen white dwarfs have masses close to $0.6M_{\odot}$ and up to about $1.1M_{\odot}$, the SNIa progenitors are biased to massive white dwarfs and towards binaries with efficient accretion processes.

One of the canonical SNIa models is the double degenerate (DD) model [Webbink, 1984; Iben & Tutukov, 1984]. In this theory two carbon-oxygen white dwarfs merge due to the emission of gravitational waves that carry away energy and angular momentum from the binary. If the combined mass of the system is above $\sim 1.4M_{\odot}$, it is assumed a SNIa explosion can take place. The other canonical model is the single degenerate (SD) model [Whelan & Iben, 1973] in which a carbon-oxygen white dwarf accretes matter from a non-degenerate companion approaching the maximum mass limit. Understanding the accretion process onto white dwarfs is of vital importance for this channel (see Sect. 1.3.3).

There are serious concerns about the viability of both models. The most important concern about the single-degenerate channel is that the white dwarf should go through a long phase of supersoft X-ray emission. However, it is unclear whether there are enough sources of this emission to account for the observed SNIa rate [Di Stefano, 2010; Gilfanov & Bogdán, 2010; Hachisu et al., 2010]. Regarding the double-degenerate channel, it has long been thought that the merger would lead to a high-mass oxygen-neon white dwarf or to the collapse of the remnant to a neutron star, however, some recent studies find that the merger can resemble a SNIa-type explosion.

1.5 Binary population synthesis

The macroscopic properties of a specific population of binary systems are for example the distribution of periods and mass ratios as well as space densities. These properties show the imprint of the processes that govern the evolution of those binaries. However, the evolution of binaries is not clear-cut and several of the processes are quite uncertain. We can study these processes and the effect of the uncertainty of these processes on binary populations with a binary population synthesis (BPS) approach.

BPS codes enable the rapid calculation of the evolution of a binary system. At every timestep appropriate recipes for binary processes are taken into account. Examples of such processes are stellar winds, stability of mass transfer, mass- and angular momentum-loss, common-envelope evolution, tidal evolution, gravitational wave emission etc. As the calculation of a single system with a BPS code takes merely a fraction of a second, BPS codes are ideal for studying the most diverse properties of binary populations.

An important difference between BPS codes and detailed stellar evolution codes [such as *ev*, Eggleton, 1971] is that the latter codes do resolve the stellar structure. Instead, BPS codes use prescriptions that give the characteristics of a star as a function of time and initial mass, such as radius, core mass and mass lost in stellar winds. Although the additional information of a computationally resolved stellar structure is a significant advantage when modelling binary interactions, it is computationally too expensive to evolve a binary population from the main-sequence to remnant formation with a detailed stellar evolution code. For the evolution of an individual binary system, the assumptions made in

BPS codes are oversimplified, however, for the macroscopic properties of a population of binaries the BPS approach works well (see also chapter 6).

Much effort has been devoted to increase the observational sample of specific populations of binary systems to statistically significant levels, and to create homogeneously selected samples. As large scale surveys (e.g. the Sloan Digital Sky Survey, Gaia) are and will be providing us with an unprecedented number and a homogeneous set of observations, it is an great moment to conduct BPS studies.

1.6 This thesis

In this thesis we study the formation and evolution of binaries with white dwarf components. Starting from two zero-age main-sequence stars, we follow the evolution through the first mass transfer phase when the initially more massive and faster evolving star fills its Roche lobe and forms a white dwarf. In chapter 2 we study close detached systems consisting of a white dwarf and a main-sequence companion which have evolved through a common-envelope phase (see Fig. 1.2). From recent observations it has become clear that these systems have short periods ranging from a few hours to a few days [Nebot Gómez-Morán et al., 2011], however, BPS studies [de Kool & Ritter, 1993; Willems & Kolb, 2004; Politano & Weiler, 2007; Davis et al., 2010] predict the existence of a population of long period systems. In chapter 2 we study if the discrepancy is caused by observational selection effects (that have not been taken into account in BPS studies previously) or by a lack of understanding of binary evolution i.e. common-envelope evolution.

Further following the evolution of the binary, another mass transfer phase is initiated as the main-sequence star evolves (see Fig. 1.2 bottom row). When the mass transfer is dynamically and tidally stable, mass is transferred to the white dwarf. Under the right circumstances, the mass can also be retained by the white dwarf (see also Sect. 1.3.3). Accretion onto white dwarfs in a complicated process, but important because accreting WDs can give rise to a SNIa explosion in the single-degenerate channel. The predictions of the SNIa rate in the single-degenerate channel by different BPS studies vary strongly [see e.g. Nelemans et al., 2013]. In chapter 3 we investigate whether these differences can be explained by different assumptions for the mass retention efficiency of white dwarfs.

The mass retention efficiencies of white dwarf are calculated assuming constant mass transfer rates. However, there are indications that the mass transfer rates fluctuate on various timescales. In chapter 4 we investigate how this behaviour affects systems with accreting white dwarf. We find that long-term mass-transfer variability allows for enhanced mass retention of white dwarfs. If long-term mass-transfer variability is present, it is an important effect to take into account in calculations of the SNIa rate from the single-degenerate channel and the evolution of cataclysmic variables.

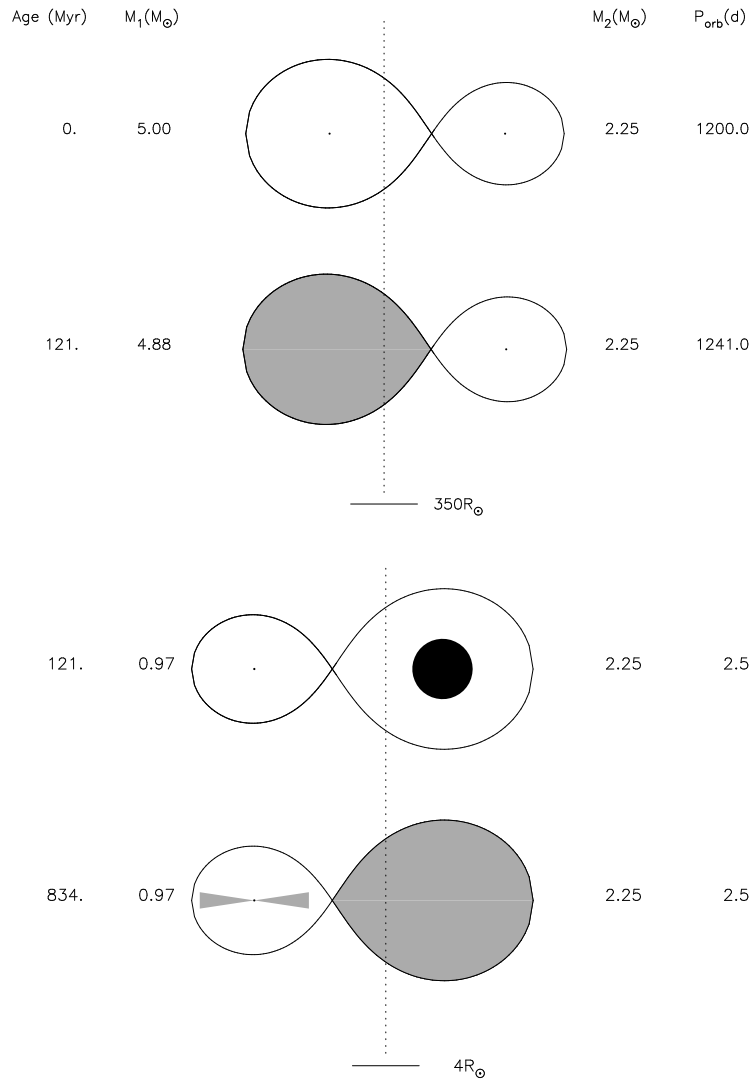


FIGURE 1.2: Schematic evolution of a binary system from the zero-age main-sequence (top row) to the formation of a semi-detached binary with a white dwarf and a main-sequence star component (bottom row). The different rows show the stars and their Roche lobes at different stages of their evolution. In this system the stars initially have a mass of $5M_{\odot}$ and $2.25M_{\odot}$ and are in an orbit with a period of 1200days. When the initially more massive star evolves off the main-sequence and fills its Roche lobe, a common-envelope phase commences (second row from the top). The binary orbit shrinks by a factor of about 100 (note the different scale in the top two and the bottom two rows). The third row from the top shows a detached system with a remnant and main-sequence component in a close orbit of 2.5days. After the CE-phase, the donor star becomes a carbon-oxygen white dwarf of mass $0.97M_{\odot}$. After 121Myr of hydrogen burning (bottom row), the initially less massive star has expanded sufficiently to fill its Roche lobe, that has been reduced greatly due to the CE-phase. Mass is transferred to the white dwarf which will grow in mass. This system is an example of a supernova type Ia progenitor in the single-degenerate channel.

On the other hand, if the mass transfer phase does not lead to a SNIa explosion and a merger can be avoided, a double white dwarf binary is formed. Figure 1.3 shows an example of the formation of a double white dwarf system. In this particular case, the first phase of mass transfer is unstable, as well as the second. In chapter 5 we predict SNIa rates from merging double white dwarfs in the double-degenerate channel with the additional constraint that our models reproduce the observed double white dwarf population well. As there are no double white dwarf binaries observed (yet!) that are SNIa progenitors unambiguously, BPS studies have not been able to constrain their SNIa models by comparing with observed progenitors. However, because the evolution of the observed double white dwarf population is similar to that of the SNIa progenitors, the former population can give important constraints to the SNIa models.

In the last chapter we compare four binary population synthesis codes and their predictions for the populations of binaries with one white dwarf and with two white dwarf components. The comparison is a complex process as BPS codes are often extended software packages that are based on many assumptions. The goal of this project is to assess the degree of consensus between the codes regarding the two binary populations, and to understand whether the differences are caused by numerical effects (e.g. a lack of accuracy) or by different assumptions in the physics of binary evolution.

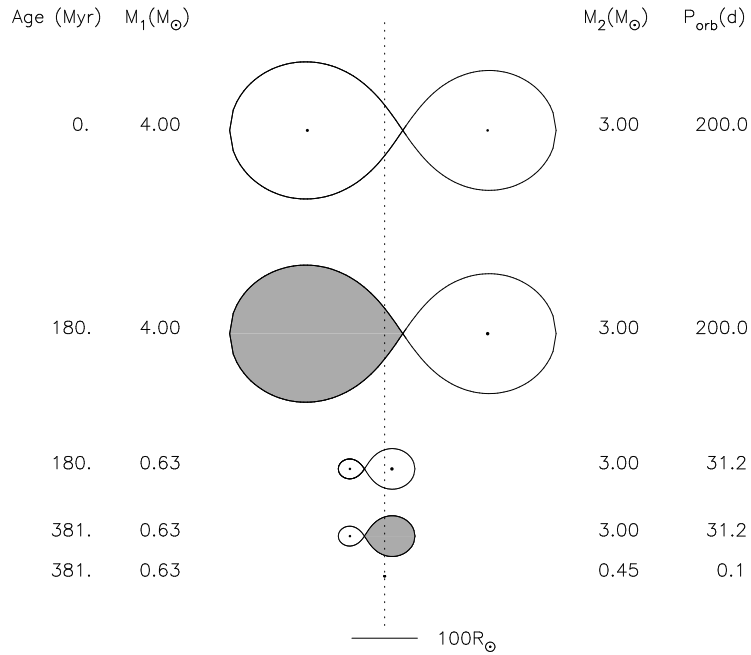


FIGURE 1.3: Schematic evolution of a binary system from the zero-age main-sequence (top row) to the formation of a close double white dwarf system (bottom row). The different rows show the stars and their Roche lobes at different stages of their evolution. In this system the binary initially contains two stars of mass $4M_\odot$ and $3M_\odot$ in an orbit of 200days. The initially more massive star evolves off the main-sequence first and fills its Roche lobe in an unstable way 180Myr after the formation of the binary system (second row from the top). The donor star loses its envelope and becomes a carbon-oxygen white dwarf of $0.63M_\odot$ (third row from the top). When the initially less massive star evolves off the main-sequence and fills its corresponding Roche lobe, a second CE-phase commences (fourth row from the top). Due to the loss of its envelope, the donor star will turn into a white dwarf prematurely. The last row shows the formation of a compact double white dwarf binary, however, in the figure the binary stars are not resolved.

THE EFFECT OF COMMON-ENVELOPE EVOLUTION ON THE VISIBLE POPULATION OF POST-COMMON-ENVELOPE BINARIES

S. Toonen, G. Nelemans

Accepted by Astronomy and Astrophysics

Abstract

An important ingredient in binary evolution is the common-envelope (CE) phase. Although this phase is believed to be responsible for the formation of many close binaries, the process is not well understood. We investigate the characteristics of the population of post-common-envelope binaries (PCEB). As the evolution of these binaries and their stellar components are relatively simple, this population can be directly used to constrain CE evolution. We use the binary population synthesis code SeBa to simulate the current-day population of PCEBs in the Galaxy. We incorporate the selection effects in our model that are inherent to the general PCEB population and that are specific to the SDSS survey, which enables a direct comparison for the first time between the synthetic and observed population of visible PCEBs. We find that selection effects do not play a significant role on the period distribution of visible PCEBs. To explain the observed dearth of long-period systems, the α -CE efficiency of the main evolutionary channel must be low. In the main channel, the CE is initiated by a red giant as it fills its Roche lobe in a dynamically unstable way. Other evolutionary paths cannot be constrained more. Additionally our model reproduces well the observed space density, the fraction of visible PCEBs amongst

white dwarf (WD)-main sequence (MS) binaries, and the WD mass versus MS mass distribution, but overestimates the fraction of PCEBs with helium WD companions.



2.1 Introduction

Many close binaries are believed to have encountered an unstable phase of mass transfer leading to a common-envelope (CE) phase [Paczynski, 1976]. The CE phase is a short-lived phase in which the envelope of the donor star engulfs the companion star. Subsequently, the companion and the core of the donor star spiral inward through the envelope. If sufficient energy and angular momentum is transferred to the envelope, it can be expelled, and the spiral-in phase can be halted before the companion merges with the core of the donor star. The CE phase plays an essential role in binary star evolution and, in particular, in the formation of short-period systems that contain compact objects, such as post-common-envelope binaries (PCEBs), cataclysmic variables (CVs), the progenitors of Type Ia supernovae, and gravitational wave sources, such as double white dwarfs.

Despite of the importance of the CE phase and the enormous efforts of the community, all effort so far have not been successful in understanding the phenomenon in detail. Much of the uncertainty in the CE phase comes from the discussion of which and how efficient certain energy sources can be used to expel the envelope [e.g. orbital energy and recombination energy, Iben & Livio, 1993; Han et al., 1995; Webbink, 2008], or if angular momentum can be used [Nelemans et al., 2000; van der Sluys et al., 2006]. Even though hydrodynamical simulations of parts of the CE phase [Ricker & Taam, 2008, 2012; Passy et al., 2012] have become possible, simulations of the full CE phase are not feasible yet due to the wide range in time and length scales that are involved [see Taam & Sandquist, 2000; Taam & Ricker, 2010; Ivanova et al., 2013, for reviews].

In this study, a binary population synthesis (BPS) approach is used to study CE evolution in a statistical way. BPS is an effective tool to study mechanisms that govern the formation and evolution of binary systems and the effect of a mechanism on a binary population. Particularly interesting for CE research is the population of PCEBs (defined here as close, detached WDMS-binaries with periods of less than 100d that underwent a CE phase) for which the evolution of the binary and its stellar components is relatively simple. Much effort has been devoted to increase the observational sample and to create a homogeneously selected sample of PCEBs [e.g. Schreiber & Gänsicke, 2003; Rebassa-Mansergas et al., 2007; Nebot Gómez-Morán et al., 2011].

In recent years, it has become clear that there is a discrepancy between PCEB observations and BPS results. BPS studies [de Kool & Ritter, 1993; Willems & Kolb, 2004; Politano & Weiler, 2007; Davis et al., 2010] predict the existence of a population of long period PCEBs (>10 d) that have not been observed [e.g. Nebot Gómez-Morán et al., 2011]. It is unclear if the discrepancy is caused by a lack of understanding of binary formation and evolution or by observational biases. This study aims to clarify this by considering the observational selection effects that are inherent to the PCEB sample into the BPS study. Using the BPS code SeBa, a population of binary stars is simulated with a realistic model of the Galaxy and magnitudes and colors of the stellar components. In Sect. 2.2, we describe the BPS models, and in Sect. 2.3, we present the synthetic PCEB populations generated by the models. In Sect. 2.3.1, we incorporate the selection effects in our models that are specific to the population of PCEBs found by the SDSS. Comparing this to the observed PCEB sample [Nebot Gómez-Morán et al., 2011; Zorotovic et al., 2011a] leads to a constraint on CE evolution, which will be discussed in Sect. 2.4.

2.2 Method

2.2.1 SeBa - a fast stellar and binary evolution code

We employ the binary population synthesis code SeBa [Portegies Zwart & Verbunt, 1996; Nelemans et al., 2001c; Toonen et al., 2012] to simulate a large amount of binaries. We use SeBa to evolve stars from the zero-age main sequence until remnant formation. At every timestep, processes as stellar winds, mass transfer, angular momentum loss, common envelope, magnetic braking, and gravitational radiation are considered with appropriate recipes. Magnetic braking [Verbunt & Zwaan, 1981] is based on Rappaport et al. [1983]. A number of updates to the code has been made since Toonen et al. [2012], which are described in Appendix 2.A. The most important update concerns the tidal instability [Darwin, 1879; Hut, 1980] in which a star is unable to extract sufficient angular momentum from the orbit to remain in synchronized rotation, leading to orbital decay and a CE phase. Instead of checking at RLOF, we assume that a tidal instability leads to a CE phase instantaneously when tidal forces become affective i.e. when the stellar radius is less than one-fifth of the periastron distance.

SeBa is incorporated in the Astrophysics Multipurpose Software Environment (AMUSE). This is a component library with a homogeneous interface structure and can be downloaded for free at amusecode.org [Portegies Zwart et al., 2009].

2.2.2 The initial stellar population

The initial stellar population is generated on a Monte Carlo based approach, according to appropriate distribution functions. These are

$$\begin{aligned}
 \text{Prob}(M_i) &= \text{KTG93} && \text{for } 0.95M_\odot \leq M_i \leq 10M_\odot, \\
 \text{Prob}(q_i) &\propto \text{const} && \text{for } 0 < q_i \leq 1, \\
 \text{Prob}(a_i) &\propto a_i^{-1} \text{ (A83)} && \text{for } 0 \leq \log a_i/R_\odot \leq 6 \\
 \text{Prob}(e_i) &\propto 2e_i \text{ (H75)} && \text{for } 0 \leq e_i \leq 1,
 \end{aligned} \tag{2.1}$$

where M_i is the initial mass of the more massive star in a specific binary system, the initial mass ratio is defined as $q_i \equiv m_i/M_i$ with m_i the initial mass of the less massive star, a_i is the initial orbital separation and e_i the initial eccentricity. Furthermore, KTG93 represents Kroupa et al. [1993], A83 Abt [1983], and H75 Heggie [1975]. A binary fraction of 50% is assumed and for the metallicity solar values.

2.2.3 Common-envelope evolution

For CE evolution, two evolutionary models are adopted that differ in their treatment of the CE phase. The two models are based on a combination of different formalisms for the CE phase. The α -formalism [Tutukov & Yungelson, 1979] is based on the energy budget, whereas the γ -formalism [Nelemans et al., 2000] is based on the angular momentum balance. In model $\alpha\alpha$, the α -formalism is used to determine the outcome of the CE phase. For model $\gamma\alpha$, the γ -prescription is applied unless the CE is triggered by a tidal instability rather than dynamically unstable Roche lobe overflow [see Toonen et al., 2012].

In the α -formalism, the α -parameter describes the efficiency with which orbital energy is consumed to unbind the CE according to

$$E_{\text{gr}} = \alpha(E_{\text{orb,init}} - E_{\text{orb,final}}), \tag{2.2}$$

where E_{orb} is the orbital energy and E_{gr} is the binding energy of the envelope. The orbital and binding energy are as shown in Webbink [1984], where E_{gr} is approximated by

$$E_{\text{gr}} = \frac{GM_d M_{\text{d,env}}}{\lambda R}, \tag{2.3}$$

where M_d is the donor mass, $M_{\text{d,env}}$ is the envelope mass of the donor star, R is the radius of the donor star and in principle, λ depends on the structure of the donor [de Kool et al., 1987; Dewi & Tauris, 2000; Xu & Li, 2010; Loveridge et al., 2011].

In the γ -formalism, γ -parameter describes the efficiency with which orbital angular momentum is used to expel the CE according to

$$\frac{J_{\text{b,init}} - J_{\text{b,final}}}{J_{\text{b,init}}} = \gamma \frac{\Delta M_d}{M_d + M_a}, \tag{2.4}$$

TABLE 2.1: Common-envelope prescription and efficiencies for each model.

	γ	$\alpha\lambda$
Model $\gamma\alpha1$	1.75	2
Model $\alpha\alpha1$	-	2
Model $\gamma\alpha2$	1.75	0.25
Model $\alpha\alpha2$	-	0.25

where $J_{b,\text{init}}$ and $J_{b,\text{final}}$ are the orbital angular momentum of the pre- and post-mass transfer binary respectively, and M_a is the mass of the companion.

The motivation for the γ -formalism comes from the observed distribution of double WD systems that could not be explained by the α -formalism nor stable mass transfer for a Hertzsprung gap donor star [see Nelemans et al., 2000]. The idea is that angular momentum can be used for the expulsion of the envelope, when there is a large amount of angular momentum available such as in binaries with similar-mass objects. However, the physical mechanism remains unclear.

In the standard model in SeBa, we assume $\gamma = 1.75$ and $\alpha\lambda = 2$, based on the evolution of double WDs [Nelemans et al., 2000, 2001c]. However, lower CE efficiencies have been claimed [Zorotovic et al., 2010], and therefore, we construct a second set of models assuming $\alpha\lambda = 0.25$. See Table 2.1 for an overview of the models that are used in this paper.

2.2.4 Galactic model

When studying populations of stars that are several Gyr old on average, the star formation history of the Galaxy becomes important. We follow Nelemans et al. [2004] in taking a realistic model of the Galaxy based on Boissier & Prantzos [1999]. In this model, the star formation rate is a function of time and position in the Galaxy. It peaks early in the history of the Galaxy and has decreased substantially since then. We assume the Galactic scale height of our binary systems to be 300 pc [Roelofs et al., 2007b,a]. The resulting population of PCEBs at a time of 13.5 Gyr is analysed.

2.2.5 Magnitudes

For WDs, the absolute magnitudes are taken from the WD cooling curves of pure hydrogen atmosphere models [Holberg & Bergeron, 2006; Kowalski & Saumon, 2006; Tremblay et al., 2011, and references therein¹]. These models cover the range of effective temperatures of $T_{\text{eff}} = 1500 - 100000\text{K}$ and of surface gravities of $\log g = 7.0 - 9.0$ for WD masses between 0.2 and $1.2M_{\odot}$. For MS stars of spectral type A0-M9, we adopt the absolute magnitudes as given by Kraus & Hillenbrand [2007]. Overall the colours, correspond well to colours from other spectra, such as the observational spectra from Pickles [1998, with colors by

¹See also <http://www.astro.umontreal.ca/~bergeron/CoolingModels>.

Covey et al. [2007]] and synthetic spectra [Munari et al., 2005] from Kurucz’s code [Kurucz & Avrett, 1981; Kurucz, 1993]. For both the MS stars and WDs, we linearly interpolate between the brightness models. For MSs and WDs that are not included in the grids, the closest gridpoint is taken.

To convert absolute magnitudes to apparent magnitudes, the distance from the sun is used as given by the Galactic model. Furthermore, we adopt the total extinction in the V filter band from Nelemans et al. [2004], which is based on Sandage’s extinction law [Sandage, 1972]. We assume the Galactic scale height of the dust to be 120 pc [Jonker et al., 2011]. To evaluate the magnitude of extinction in the different bands of the ugriz-photometric system, we use the conversion of Schlegel et al. [1998], which are based on the extinction laws of Cardelli et al. [1989] and O’Donnell [1994] with $R_V = 3.1$.

2.2.6 Selection effects

We assume that WDMS binaries can be observed in the magnitude range 15-20 in the g-band. As WDs are inherently blue and MS are inherently red, we assume that WDMS binaries can be distinguished from single MS stars if

$$\Delta g \equiv g_{\text{WD}} - g_{\text{MS}} < 1, \quad (2.5)$$

where g_{WD} and g_{MS} are the magnitude in the g band of the WD and the MS respectively, and distinguished from single WDs if

$$\Delta z \equiv z_{\text{WD}} - z_{\text{MS}} > -1, \quad (2.6)$$

where z_{WD} and z_{MS} are the z band magnitudes of the WD and the MS respectively. The g-band is used instead of the u-band, because the u-g colours of late-type MS stars are fairly uncertain [Munari et al., 2005; Bochanski et al., 2007]. The effect of (varying) the cuts will be discussed in forthcoming sections.

2.3 Results

Figures 2.1 and 2.2 show the full and visible population of PCEBs in ugriz color-color space for model $\alpha\alpha 2$. The full population of PCEBs lies close to the unreddened MS. Most PCEB systems will be observed as apparent single MS stars. On the other hand, the visible population of PCEBs is by construction clearly distinguished from the MS in the u-g vs. g-r color-color diagram. In the r-i vs. i-z diagram and g-r vs. r-i diagram, most visible systems lie close to the MS indicating that the WD components are generally cold [see Augusteijn et al., 2008, Fig 2]. The u-g vs. g-r diagram also shows that the majority of systems is relatively red confirming that samples of PCEBs that are discovered by their blue colors [e.g. Schreiber & Gänsicke, 2003], are severely biased and incomplete. The

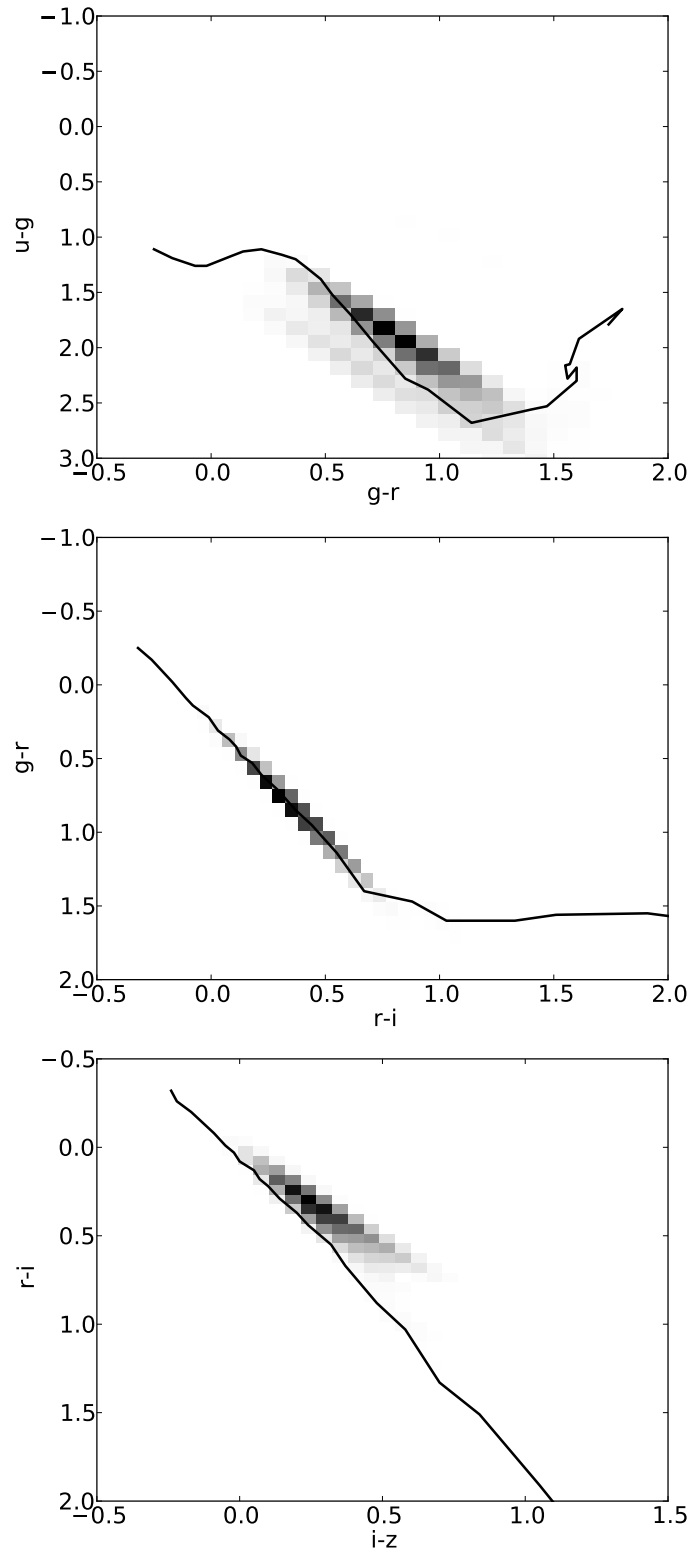


FIGURE 2.1: Color-color diagrams for the full population of PCEBs with orbital periods less than 100d and for a limiting magnitude of $g = 15 - 20$ for model $\alpha\alpha 2$. On the top, it shows the $u-g$ vs. $g-r$ diagram, in the middle, the $g-r$ vs. $r-i$ diagram, and on the bottom, the $r-i$ vs. $i-z$ diagram. The intensity of the grey scale corresponds to the density of objects on a linear scale. The solid line corresponds to the unreddened MS from A-type to M-type MS stars.

CHAPTER 2 : THE EFFECT OF CE EVOLUTION ON THE VISIBLE POPULATION OF PCEBs

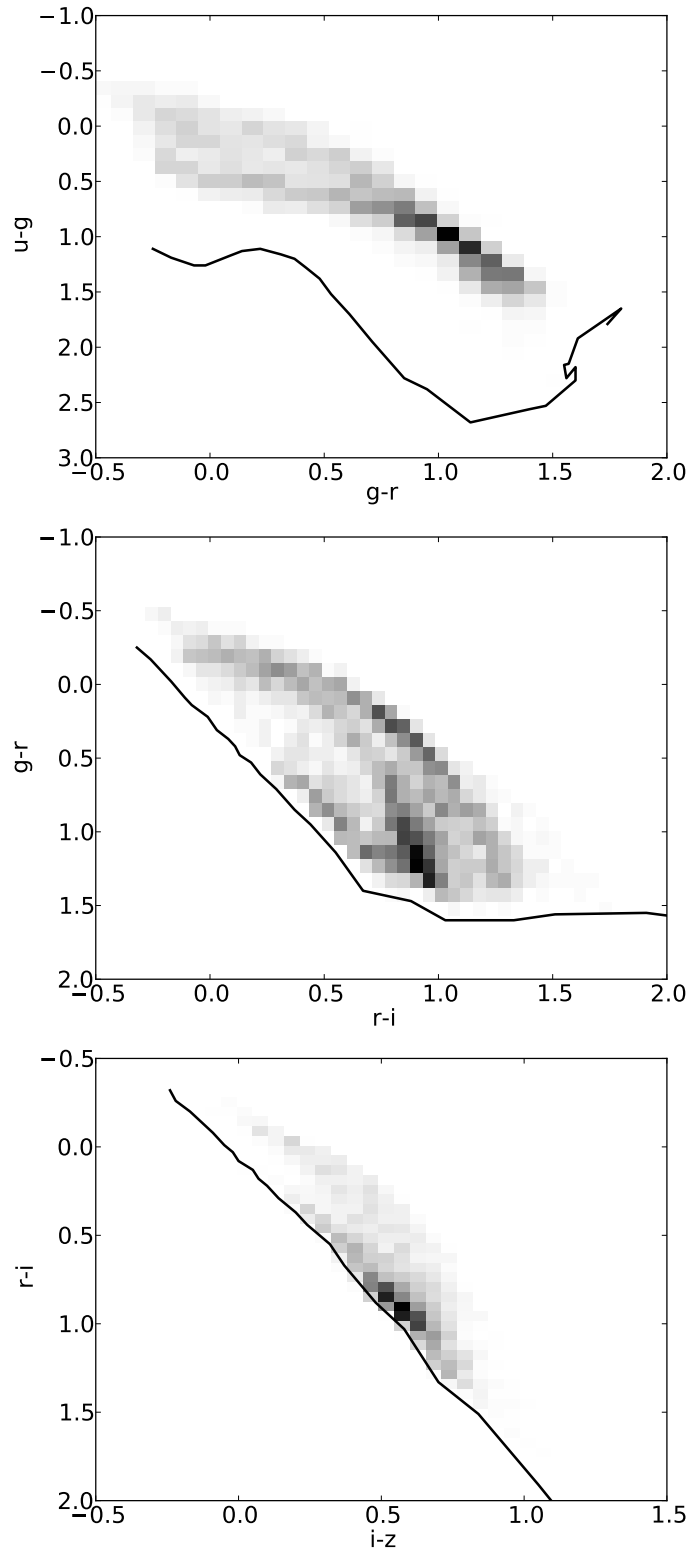


FIGURE 2.2: Color-color diagrams for the visible population of PCEBs for model $\alpha 2$. The order of the diagrams is as in Fig. 2.1. The intensity of the grey scale corresponds to the density of objects on a linear scale. The solid line corresponds to the unreddened MS from A-type to M-type MS stars.

TABLE 2.2: The space density of visible PCEBs within 200 and 500pc from the Sun in 10^{-6} pc^{-3} for different models of CE evolution.

	within 200pc	within 500 pc
Model $\gamma\alpha 1$	13	9.0
Model $\alpha\alpha 1$	15	12
Model $\gamma\alpha 2$	5.8	5.2
Model $\alpha\alpha 2$	4.9	4.0
Observed	6-30 ¹	

NOTES: ¹ Schreiber & Gänsicke [2003].

color-color diagrams for model $\alpha\alpha 1$, model $\gamma\alpha 1$, and model $\gamma\alpha 2$ are very comparable to those of model $\alpha\alpha 2$.

The space density of visible PCEBs follows directly from our models where the position of the PCEBs in the Galaxy is given by the Galactic model (see Sect. 2.2.4). The space density (see Table 2.2) is calculated in a cylindrical volume with height above the plane of 200pc and radii of 200pc and 500pc centred on the Sun. At small distances ($\lesssim 100$ pc) from the Sun, our data is noisy due to low number statistics, and at larger distances, the PCEB population is magnitude limited. The observed space density of PCEBs $(6 - 30) \cdot 10^{-6} \text{ pc}^{-3}$ [Schreiber & Gänsicke, 2003] is fairly uncertain and consistent with all BPS models.

Figures 2.3, 2.4, and 2.5 show the distribution of MS mass, WD mass, and orbital period of the visible population of PCEBs. Model $\gamma\alpha 1$, $\alpha\alpha 1$ and $\gamma\alpha 2$ show PCEB systems with periods between 0.05-100d, whereas model $\alpha\alpha 2$ shows a narrower period range of about 0.05-10d. Few PCEBs exist at periods of less than a few hours, as these systems come in contact and possibly evolve into CVs. Figure 2.4 shows a relation between MS and WD mass that is different for each model. The masses of WDs in visible PCEBs are roughly between 0.2 and $0.8M_{\odot}$; most WDs have either helium (He) or carbon-oxygen (CO) cores. Figure 2.5 shows that the model $\gamma\alpha 1$ and model $\gamma\alpha 2$ periods at a given WD mass can be longer than for model $\alpha\alpha 1$ and model $\alpha\alpha 2$. This is because the CE phase leads to a strong decrease in the orbital separation according to the α -prescription, while this is not necessarily true in the γ -prescription.

Varying the cuts that determine which PCEBs are visible (see Sect. 2.2.6), does not change our results much. The limiting magnitude of $g = 15 - 20$ does not affect the relations between WD mass, MS mass, and period, but it can effect the space density of visible PCEBs. If the sensitivity of the observations increases to $g = 21$, the space density within 200pc and 500pc increases by about 15-30% and 30-50% respectively.

The cut that distinguishes WDMS from apparent single WDs (see eq. 2.6) has a small effect on the population of PCEBs. If we assume a more conservative cut, less massive MS stars are visible at a given WD temperature. Varying the cut between $\Delta z > 0$ and

CHAPTER 2 : THE EFFECT OF CE EVOLUTION ON THE VISIBLE POPULATION OF PCEBs

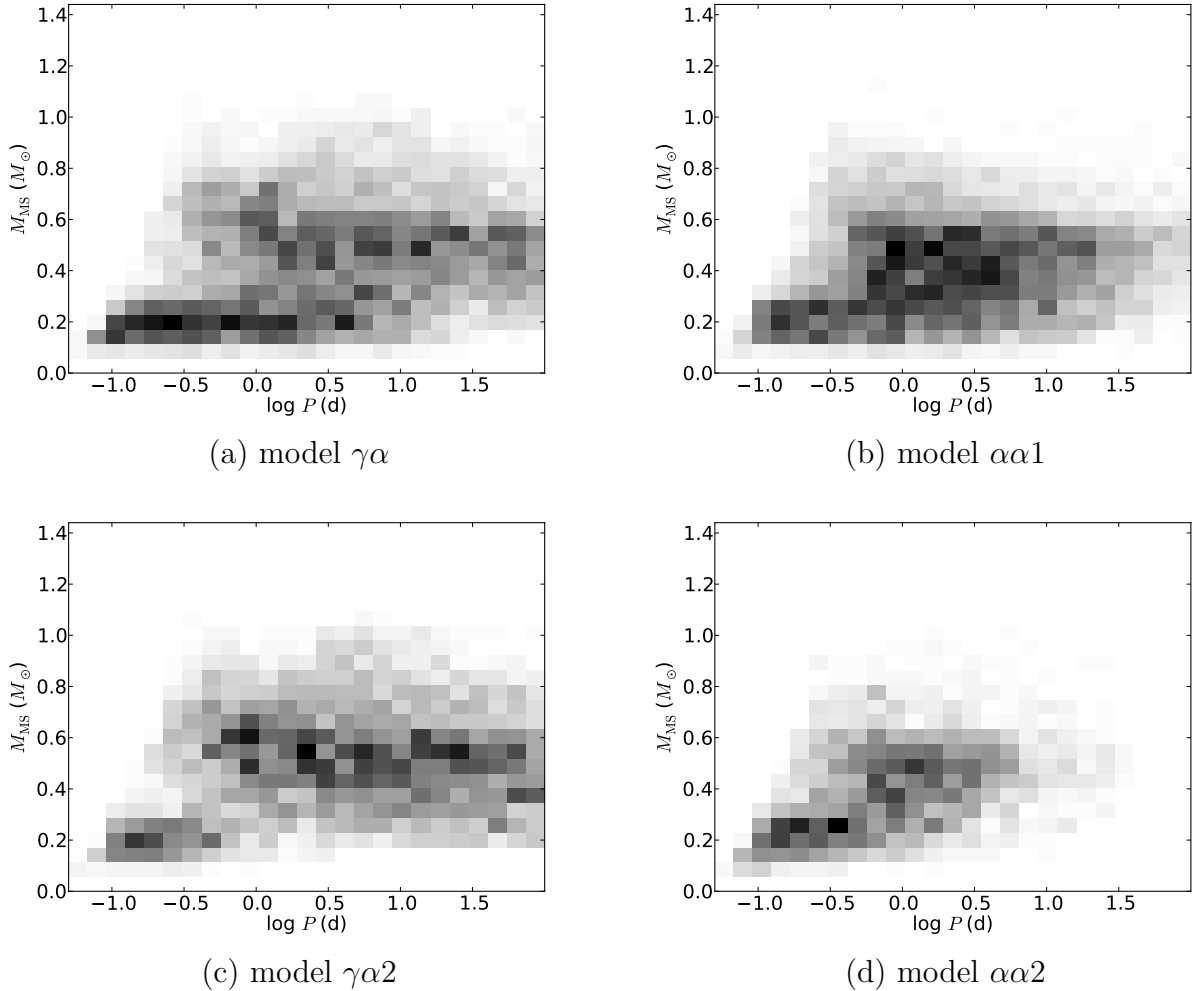


FIGURE 2.3: Visible population of PCEBs as a function of orbital period and mass of the MS star for all models. The intensity of the grey scale corresponds to the density of objects on a linear scale.

$\Delta z > -2$ does not affect the space density significantly. The distribution of periods is not affected. Making a cut in the i-band instead of the z-band has a similar effect on the visible PCEB population as varying Δz .

Varying the cut that distinguishes WDMS from apparent single MS stars (see eq. 2.5) is important for the space density and the MS mass distribution of PCEBs, as the WD is less bright than the secondary star for most systems. If a more conservative cut is appropriate i.e. $\Delta g > 0$, the space density decreases by about 30-40%, and the less massive MS stars are visible at a given WD temperature. The space density increases by 40-50% when assuming $\Delta g > 2$. Varying the cut between $\Delta g > 0$ and $\Delta g > 2$ affects the maximum MS mass in PCEBs by $\pm 0.1M_{\odot}$. Most importantly, the correlations of MS mass with WD mass and period are, however, not affected. The effect on the visible PCEB population of making a cut in the u-band is comparable to that in the g-band.

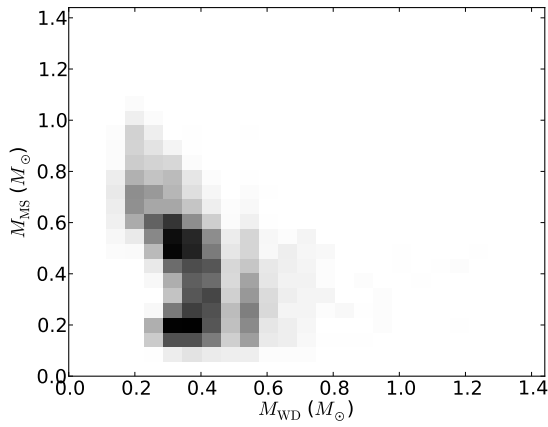
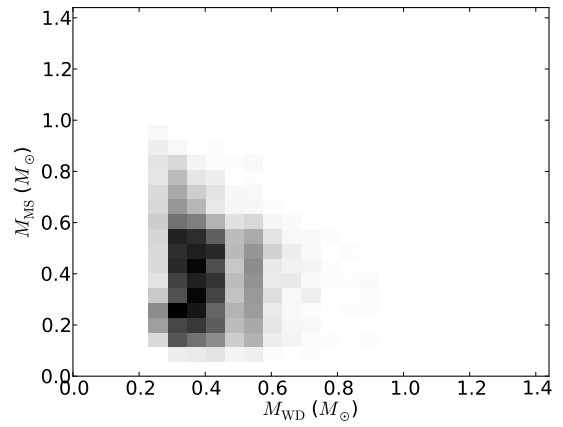
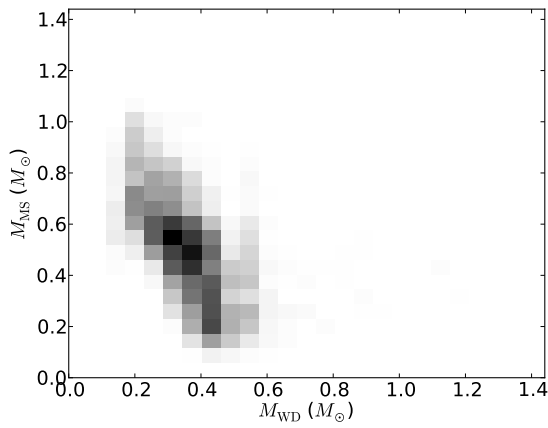
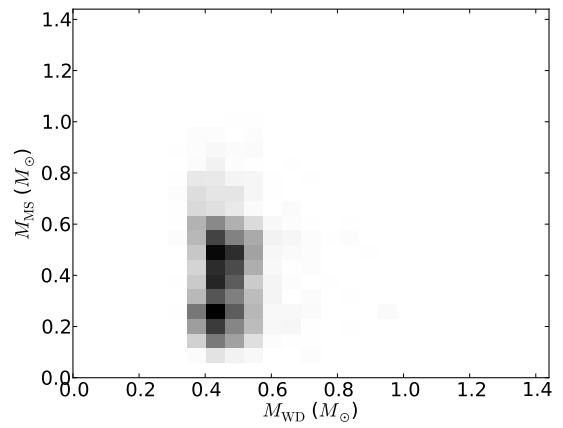
(a) model $\gamma\alpha$ (b) model $\alpha\alpha1$ (c) model $\gamma\alpha2$ (d) model $\alpha\alpha2$

FIGURE 2.4: Visible population of PCEBs as a function of mass of the WD and the MS star for all models. The intensity of the grey scale corresponds to the density of objects on a linear scale.

CHAPTER 2 : THE EFFECT OF CE EVOLUTION ON THE VISIBLE POPULATION OF PCEBs

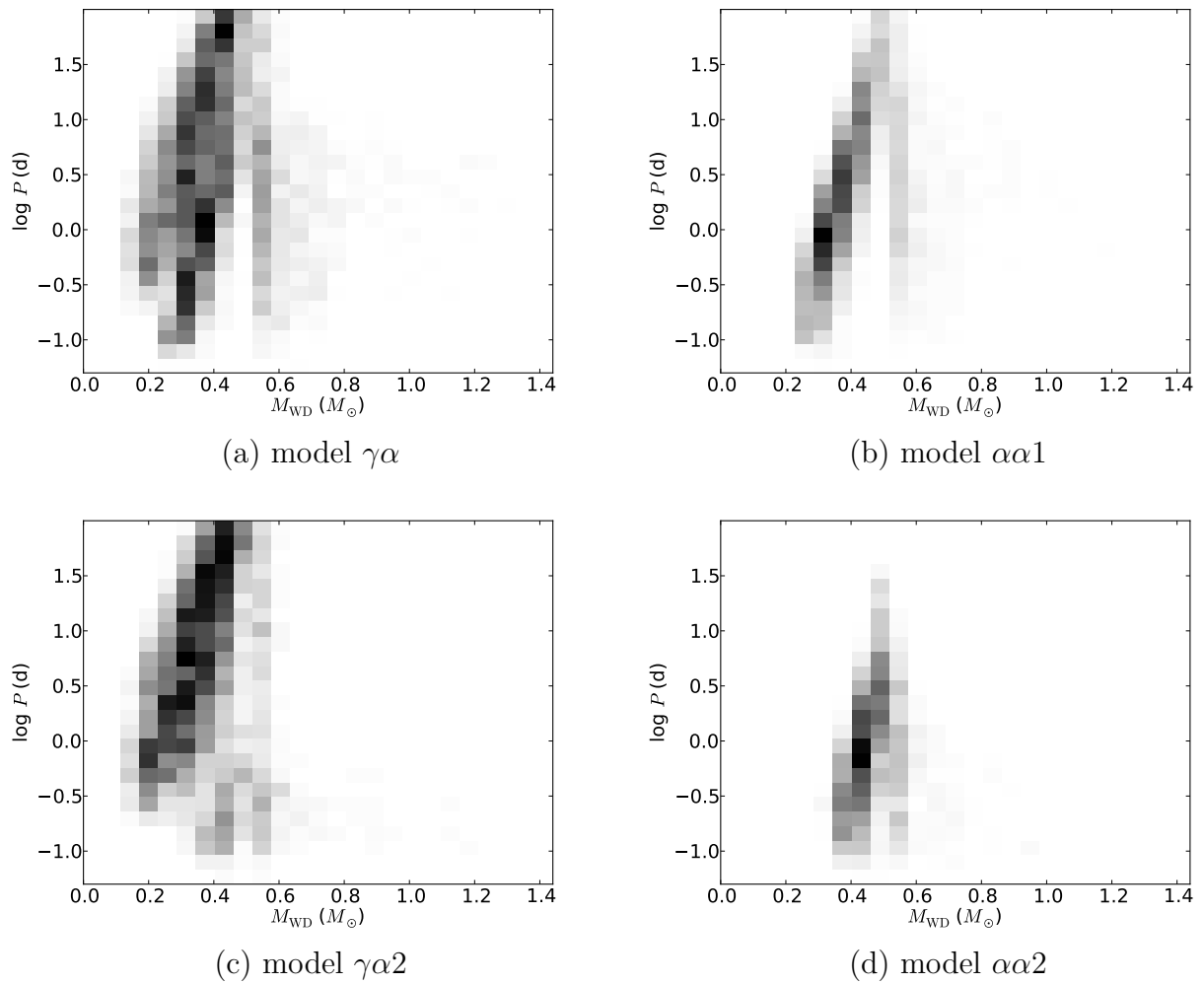


FIGURE 2.5: Visible population of PCEBs as a function of orbital period and WD mass for all models. The intensity of the grey scale corresponds to the density of objects on a linear scale.

2.3.1 The SDSS PCEB sample

To compare our models with the results of Nebot Gómez-Morán et al. [2011] and Zorotovic et al. [2011a], we place two additional constraints on the visible population of PCEBs in comparison to those described in Sect. 2.2.6. Following these authors, we only consider WDs that are hotter than 12000K and MS stars of the stellar classification M-type. However, there is a discrepancy in the relation between spectral type and stellar mass used in those papers and that of Kraus & Hillenbrand [2007] due to the uncertainty in stellar radii of low-mass stars. Where the former [based on Rebassa-Mansergas et al., 2007] finds that M-type stars have masses of less than $0.472M_{\odot}$, Kraus & Hillenbrand [2007] find that the M-dwarf mass range is extended to $0.59M_{\odot}$. To do a consistent comparison, we will adopt the relation between spectral type and stellar mass of Rebassa-Mansergas et al. [2007] and the relation between magnitudes and spectral types of Kraus & Hillenbrand [2007]. The effect of this discrepancy is further discussed in the Sect. 2.B.

Comparing the color-color diagrams of the visible PCEB population (see Fig. 2.2) with that of the fraction that is visible in the SDSS (see Fig. 2.6) shows that the observed population is biased toward late-type secondaries and hot WDs [see Augusteijn et al., 2008, Fig. 2]. The bias against systems containing early-type secondaries is in accordance with the findings of Rebassa-Mansergas et al. [2010] for the WDMS population from the SDSS.

Nebot Gómez-Morán et al. [2011] studied the observed period distribution of observed PCEBs. They find the distribution follows approximately a log-normal distribution that peaks at about 10.3h and ranges from 1.9h to 4.3d (see points in Fig. 2.7). They also find that the period distribution of the PCEBs found by the SDSS is very comparable to that of previously known PCEBs. However, Nebot Gómez-Morán et al. [2011] point out that the dearth of long-period systems is in contradiction with the results of binary population synthesis studies [see de Kool & Ritter, 1993; Willems & Kolb, 2004; Politano & Weiler, 2007; Davis et al., 2010] indicating a low α -CE efficiency, if selection effects do not play a role. Figure 2.7 shows that the selection effects do not cause a dearth of PCEBs with long periods in model $\alpha\alpha 1$, $\gamma\alpha 1$, and $\gamma\alpha 2$. Only the results of model $\alpha\alpha 2$ with a reduced α -CE efficiency are consistent with the observed period distribution.

Another observational constraint for our models can come from the relative population sizes. Although the space density of PCEBs is not known very accurately, it has become possible to determine the fraction of PCEBs amongst WDMS systems of all periods. From SDSS observations, Nebot Gómez-Morán et al. [2011] find that the fraction of PCEBs amongst unresolved WDMS with M-dwarf companions is $27\pm 2\%$. Wide WDMS that are blended or fully resolved are not included in their sample. To compensate for this effect, we exclude those WDMS systems from our WDMS sample for which the angular size of an object is larger than twice the seeing, where the size of the object is approximated by the orbital separation, and where the distance to the WDMS is given by the Galactic model

CHAPTER 2 : THE EFFECT OF CE EVOLUTION ON THE VISIBLE POPULATION OF PCEBs

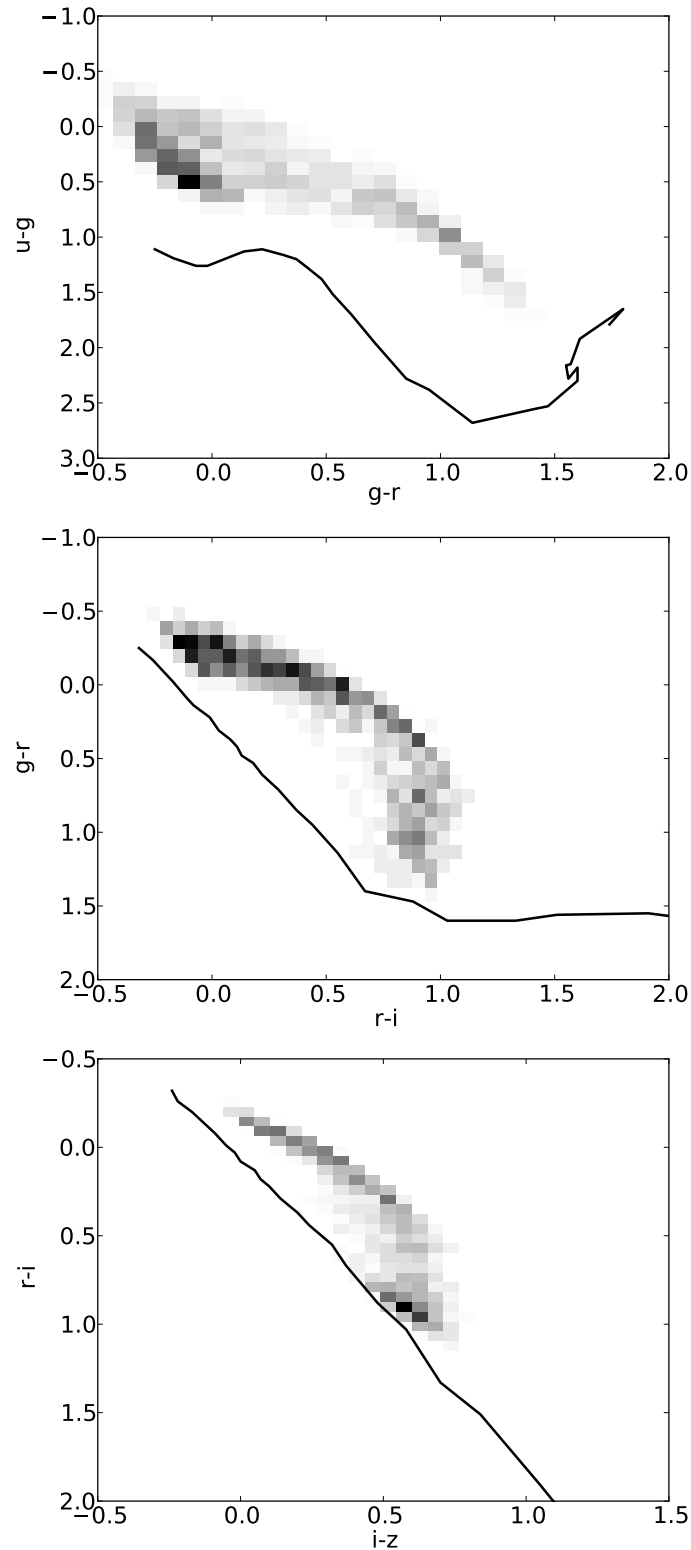


FIGURE 2.6: Color-color diagrams for the visible population of PCEBs in the SDSS for model $\alpha 2$. The order of the diagrams is as in Fig. 2.1. The intensity of the grey scale corresponds to the density of objects on a linear scale. The solid line corresponds to the unreddened MS from A-type to M-type MS stars. The color-color diagrams are very comparable to those of model $\alpha 1$, model $\gamma 1$, and model $\gamma 2$.

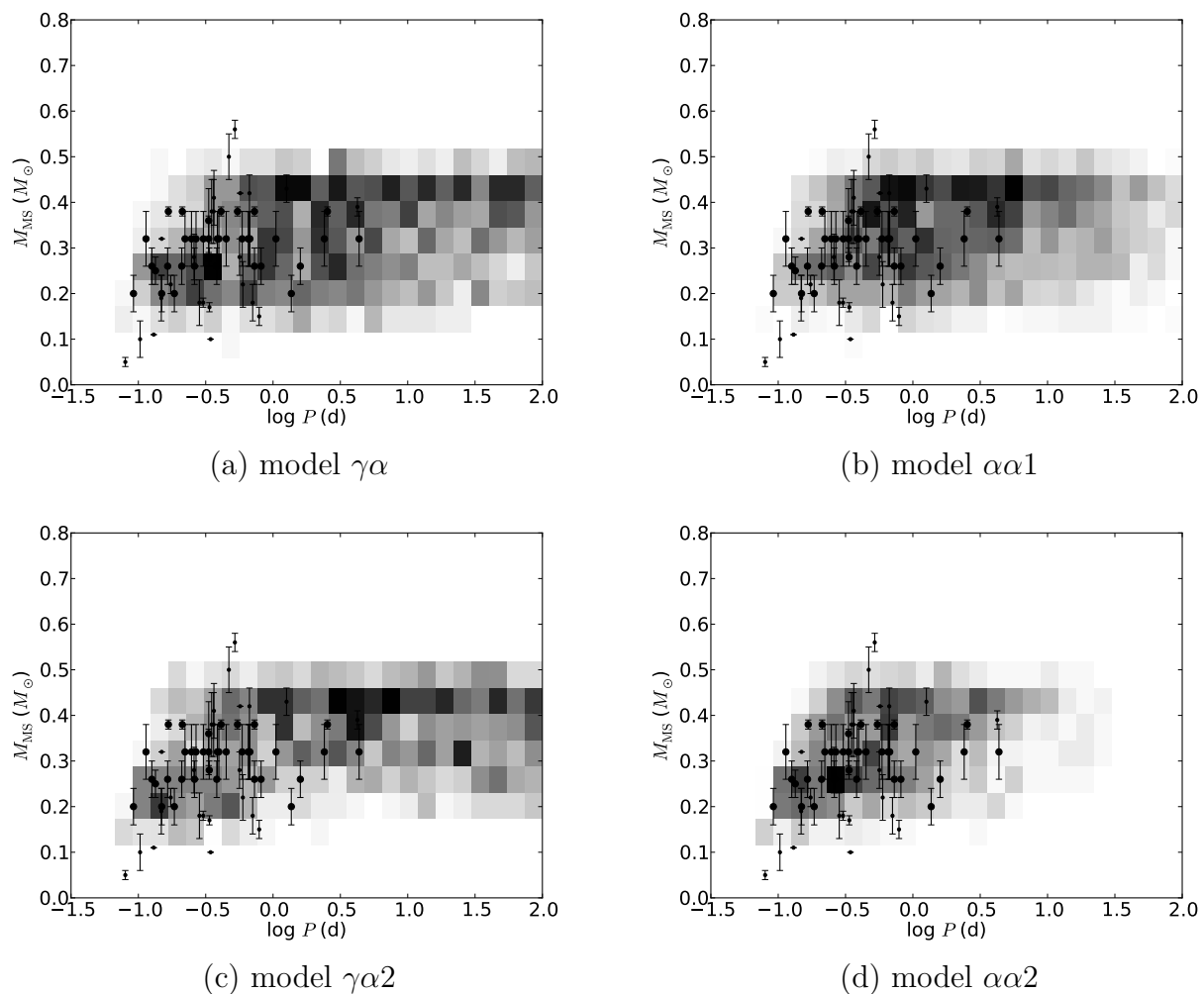


FIGURE 2.7: Visible population of PCEBs in the SDSS as a function of orbital period and mass of the MS star for all models. The intensity of the grey scale corresponds to the density of objects on a linear scale. Overplotted are the observed PCEBs taken from Zorotovic et al. [2011a]. Thick points represent systems that are found by the SDSS, and thin points represent previously known PCEBs with accurately measured parameters. The previously known sample of PCEBs is affected by other selection effects than the SDSS sample or the synthetic sample. Note that Ix Peg has been removed from the sample as its MS component is not an M-dwarf.

CHAPTER 2 : THE EFFECT OF CE EVOLUTION ON THE VISIBLE POPULATION OF PCEBs

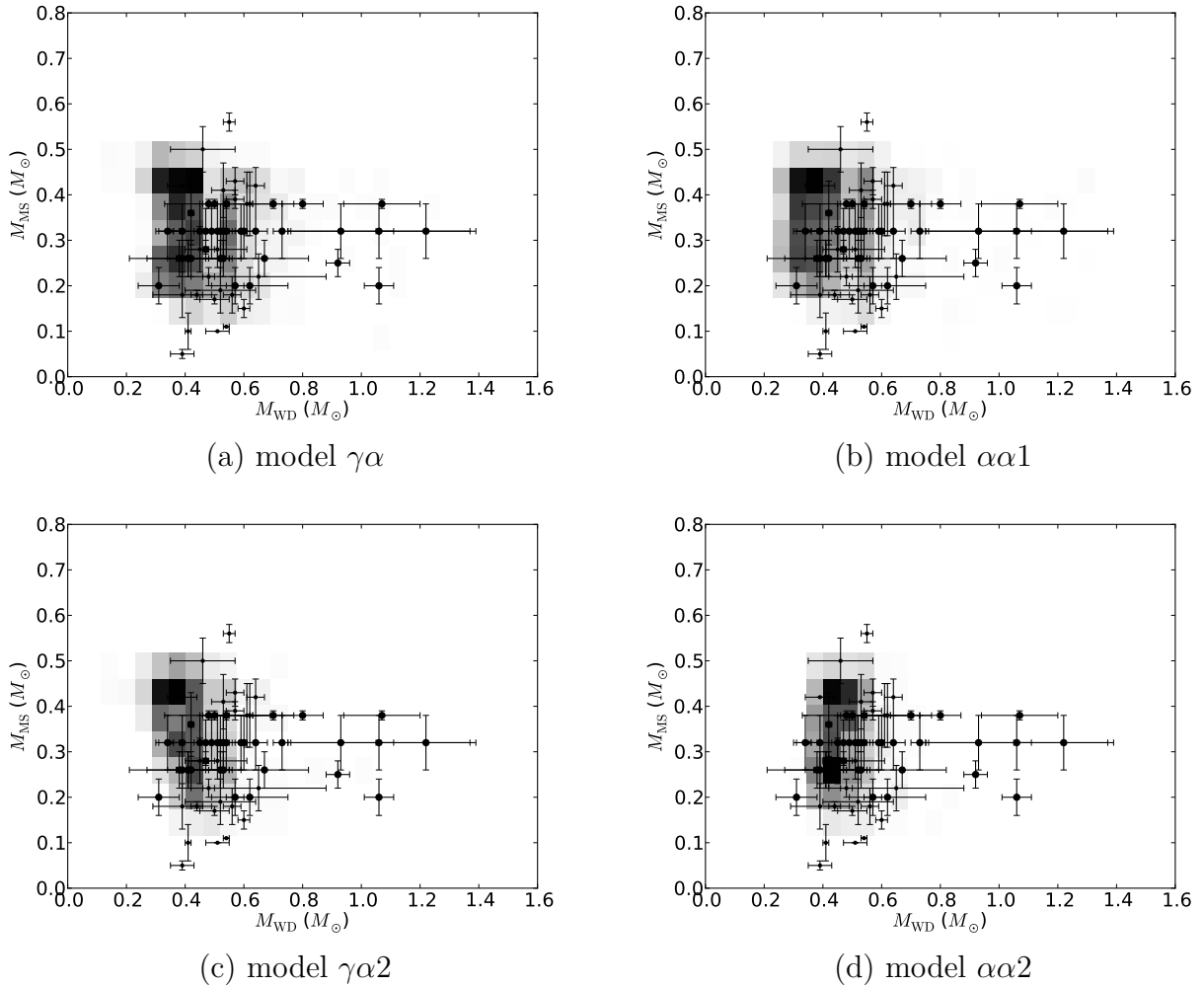


FIGURE 2.8: Visible population of PCEBs in the SDSS as a function of mass of the WD and the MS star for all models. The intensity of the grey scale corresponds to the density of objects on a linear scale. Overplotted are the observed PCEBs taken from Zorotovic et al. [2011a]. Thick points represent systems that are found by the SDSS, and thin points represent previously known PCEBs with accurately measured parameters. The previously known sample of PCEBs is affected by other selection effects than the SDSS sample or the synthetic sample. Note that Ikaros has been removed from the sample as its MS component is not an M-dwarf.

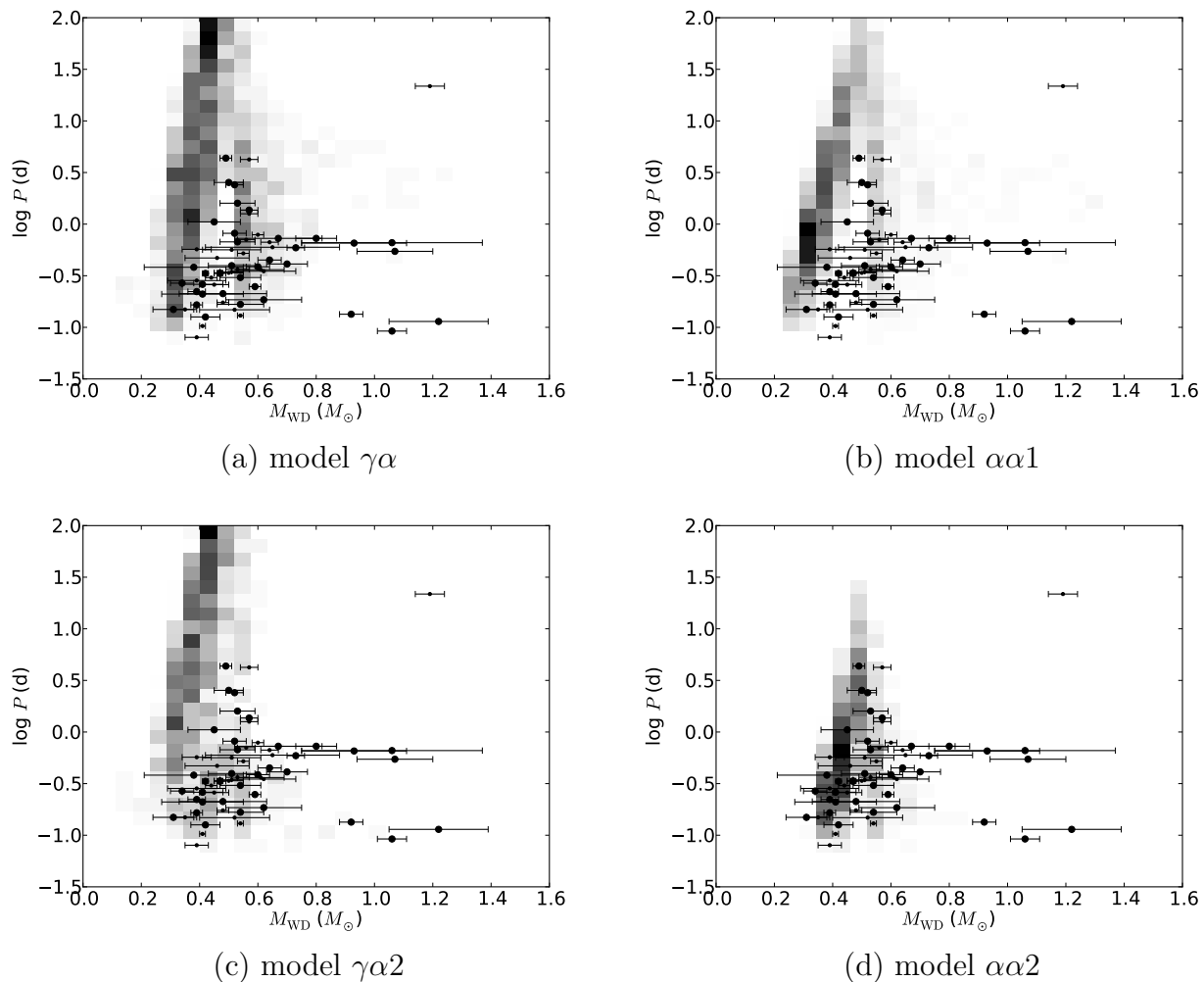


FIGURE 2.9: Visible population of PCEBs in the SDSS as a function of orbital period and WD mass for all models. The intensity of the grey scale corresponds to the density of objects on a linear scale. Overplotted are the observed PCEBs taken from Zorotovic et al. [2011a]. Thick points represent systems that are found by the SDSS, and thin points represent previously known PCEBs with accurately measured parameters. The previously known sample of PCEBs is affected by other selection effects than the SDSS sample or the synthetic sample. Note that Ix Peg has been removed from the sample as its MS component is not an M-dwarf.

TABLE 2.3: The fraction of visible PCEBs amongst unresolved WDMS for different models of CE evolution. The errors are not statistical errors but come from varying boundaries for the limiting period and seeing.

Model $\gamma\alpha 1$	0.17-0.23
Model $\alpha\alpha 1$	0.27-0.35
Model $\gamma\alpha 2$	0.10-0.14
Model $\alpha\alpha 2$	0.13-0.15
Observed	0.27 ± 0.02^1

NOTES: ¹Nebot Gómez-Morán et al. [2011]

(see Sect. 2.2.4). The seeing limit is varied between the median seeing of SDSS of $1.4''$ and an upper limit for over 90% of the SDSS data of $2''$. Furthermore, the SDSS PCEB identification method is based on radial velocity measurements, and, as such dependent on the number of spectra taken, the temporal sampling of the measurements and the accuracy of the radial velocity measurement. Nebot Gómez-Morán et al. [2011] find that their identification method is not sensitive to systems with periods of more than a few tens of days, however, the observed period distribution that cuts off at a few days is not strongly affected by this bias. In the calculation of the fraction of PCEBs amongst WDMS systems, we therefore exclude long-period PCEBs from the PCEB sample (but include them in the WDMS sample). As the sensitivity of the SDSS PCEB identification method depends on the orbital period of the system [see Fig. 10 of Nebot Gómez-Morán et al., 2011], the limiting period is varied between 10d and 50d. The fraction of visible PCEBs amongst unresolved WDMS for all models are consistent with the observed value within a factor of two (see Table 2.3). Based on a sample of WDs with near-infrared emission observed with the Hubble Space Telescope, Farihi et al. [2010] also found a ratio of about 25%.

Zorotovic et al. [2011a] studied the mass dependencies of the orbital period distribution and found that systems containing high-mass secondaries tend to have longer orbital periods. Figure 2.7 shows a similar trend in our models, however, model $\alpha\alpha 2$ reproduces the observations best due to the period distribution. The relation between WD and secondary mass cannot be used to differentiate between CE theories, because the models show very similar distributions (see Fig. 2.8), which is contrary to the complete visible PCEB sample (see Fig. 2.4). However, the models match well to the observed systems in Fig. 2.8 for WD masses less than about $0.7M_{\odot}$. The models show a lack of PCEBs with massive WD components (see Sect. 2.4 for a discussion). Disregarding WDs with masses more than about $0.8M_{\odot}$, Fig. 2.9 shows a good match between the observations and the predictions of model $\alpha\alpha 2$ regarding the distribution of orbital period versus WD mass. The discrepancy between the observed period distribution and the synthetic ones from model $\alpha\alpha 1$, model $\gamma\alpha 1$, and model $\gamma\alpha 2$ is mainly found in PCEBs with helium WD components. For He-core

TABLE 2.4: Percentage of helium WDs and carbon/oxygen (including oxygen/neon) WDs in visible PCEBs in the SDSS for different models of CE evolution.

	He WD	CO WD
Model $\gamma\alpha 1$	72	28
Model $\alpha\alpha 1$	75	25
Model $\gamma\alpha 2$	83	17
Model $\alpha\alpha 2$	68	32
Observed ¹	33-46	54-67

NOTES: ¹Zorotovic et al. [2011b]. The percentages in the PCEB population that is found by SDSS are similar to the percentages of the full sample of Zorotovic et al. [2011b] that is given here. The observed type of the WD is determined by its mass with a limiting mass of $0.5M_{\odot}$ for helium WDs, which is consistent with our models. The range in the observed percentages is caused by a few systems in which the stellar type could not be determined unambiguously.

WDs (i.e. $M_{\text{WD}} < 0.5M_{\odot}$), all models show an increase in orbital period with WD mass, however, statistical evidence of this relation in the current observed sample has not been found [Zorotovic et al., 2011a]. In addition, less than half of the observed systems contains a He WD, which is in contradiction with our models for which at least 70% of PCEB WDs are helium rich (see Table 2.4).

2.3.2 Variable CE efficiency

Next, we consider the possibility that CE evolution occurs differently for different types of donor stars or types of instabilities. We differentiate between red giant (RG) donors and asymptotic giant branch (AGB) donors and between dynamical (DY) and tidal (TI) instabilities. The majority of PCEBs is formed through a dynamical instability initiated by a RG (see Table 2.5, RG-DY). This evolutionary path is not much affected by processes other than the CE phase, as the evolution is relatively simple: For example, the donor stars do not suffer from superwinds as AGB stars. For this path, only the PCEBs from model $\alpha\alpha 2$ with a reduced CE efficiency of $\alpha\lambda = 0.25$ are consistent with the observed period distribution and its mass dependencies. Any other CE model produces a high number of PCEBs at periods larger than 10d.

Subsequently, we study CE evolution in the other evolutionary channels with two hypotheses. First, we assume that CE interactions with red giant donors suffer from a low CE efficiency and that those with AGB donors suffer from a high CE efficiency (RG-DY and RG-TI according to model $\alpha\alpha 2$, AGB-DY and AGB-TI according to model $\gamma\alpha 1$ or $\alpha\alpha 1$). However, the PCEB population from this hypothesis does not reproduce the observed period and mass distributions significantly better or worse than model $\alpha\alpha 2$. The percentage

TABLE 2.5: Percentage of visible PCEBs in the SDSS from different evolutionary paths for different models of CE evolution. The last column represents the total number of visible systems for each model in our simulations. RG and AGB represent systems in which the CE phase is initiated by a red giant and a AGB star respectively. DY and TI represent systems that evolve through a dynamical or tidal instability, respectively.

	RG-DY	RG-TI	AGB-DY	AGB-TI	Total
Model $\gamma\alpha 1$	55	18	5	23	1958
Model $\alpha\alpha 1$	64	11	11	14	2967
Model $\gamma\alpha 2$	77	7	8	9	1390
Model $\alpha\alpha 2$	61	7	24	8	1142

of systems containing a He WD improves slightly to about 60% and 50% for AGB-DY and AGB-TI according to model $\gamma\alpha 1$ and $\alpha\alpha 1$ respectively. The second hypothesis is that all systems evolving through dynamical instabilities suffer from low CE efficiency and that systems evolving through a tidal instability do not (RG-DY and AGB-DY according to model $\alpha\alpha 2$ and RG-TI and AGB-TI according to model $\alpha\alpha 1^2$). However, also this hypothesis does not lead to a significant improvement (or worsening) in the period and mass distributions compared to model $\alpha\alpha 2$. The percentage of systems containing a He WD is about 75%. Concluding, at current we cannot constrain the CE evolution or efficiencies of the evolutionary channels RG-TI, AGB-DY and AGB-TI, although the percentage of systems with helium WDs improves when assuming that the CE efficiency is lower when the CE phase is initiated by a RG star than for an AGB star.

2.4 Discussion and conclusion

We have studied common-envelope evolution by theoretical modelling of the formation and evolution of post-common-envelope binaries with constraints from observations. We have considered four models of CE evolution that differ in the CE prescription and CE efficiency. The SDSS has played an important role in providing the largest and most homogeneous sample of PCEBs, however, the visible population of PCEBs is still affected by strong selection effects. We presented here the first binary population models that consider the selection effects that are inherent to the population of visible PCEBs.

We find that although selection effects are important, e.g. for the secondary mass distribution, they do not lead to a dearth of long-period systems as is observed [e.g., Nebot Gómez-Morán et al., 2011]. Furthermore, we find that the main evolutionary path of visible PCEBs in the SDSS consists of a CE phase caused by a red giant that fills its Roche lobe in a dynamically unstable manner. Most importantly, we find that the efficiency for this

²Note that model $\gamma\alpha 1$ is identical to model $\alpha\alpha 1$ for systems evolving through a tidal instability.

channel at which orbital energy can be used to expel the envelope in the CE phase is low - to reproduce the observed period distribution with few systems at 10-100d. Secondary evolutionary paths cannot be constrained at present; low and high CE efficiencies for energy consumption or angular momentum consumption are consistent with observations.

Besides the distribution of orbital periods, the results from the model with the reduced α -CE efficiency are consistent with the observed space density, the fraction of PCEBs amongst WDMS, and the WD mass vs. MS mass distribution, however, the fraction of PCEBs containing He WDs is overestimated. When assuming that the CE efficiency is higher when the CE phase is initiated by an AGB star rather than a RG star, the fraction of He WDs in PCEBs is in better agreement with the observations. At face value, an overestimation of the fraction of He WDs companions in PCEBs exaggerates the importance of the RG-DY channel, however, the conclusion about the low CE efficiency for RG systems is based on the the short periods that are observed for PCEBs with He WD components.

The fraction of He WDs amongst PCEBs depends on the CE efficiency as shown by Table 2.4 [see also de Kool & Ritter, 1993; Willems & Kolb, 2004] and the initial distribution of mass ratios and orbital separations. Willems & Kolb [2004] showed that the effect of the CE efficiency and the initial mass ratios on the He-WD ratio for the *full* PCEB population cannot be distinguished, but that the effect of the initial mass ratio distribution for low CE efficiencies ($\alpha\lambda = 0.1$) becomes negligible. Furthermore the He WD fraction is affected by the cooling curves of WDs. We have adopted the cooling curves of Holberg & Bergeron [2006]; Kowalski & Saumon [2006]; Tremblay et al. [2011] that assume a carbon and carbon-oxygen composition of the core. However, He-core WDs for a given stellar mass have a longer cooling time as the specific heat is larger (Althaus, Miller Bertolami, priv. comm). If we systematically underestimated the brightness of He WDs compared to CO WDs, the synthetic fraction of He WDs in visible PCEBs would be even higher.

So far, we have studied the CE efficiency (α) assuming a constant envelope-structure parameter (λ). In other words we studied the combination $\alpha\lambda$. While the CE efficiency is not well known, the structure parameter has been calculated by several studies [Dewi & Tauris, 2000; Xu & Li, 2010; Loveridge et al., 2011]. For low mass stars of $M < 3M_{\odot}$, $\lambda \approx 1.1 - 1.3$ on the RG and $\lambda \approx 0.5 - 0.8$ on the AGB on average at the onset of the CE phase [van der Sluys et al., 2010, including internal energy in the envelope binding energy]. Therefore, our result of a small value for $\alpha\lambda$ is not due to a small value for λ ; the CE efficiency is low.

The SDSS has observed six (possibly eight) PCEBs with high WD masses of more than $0.8M_{\odot}$. The number of massive WDs is small, but they represent about 10% of the observed sample. Although our models do create massive WDs with M-dwarf companions, the relative number to other PCEB systems is not reproduced by our models. If the observed number of these systems increases to a statistical significant amount, it would be interesting to look in more detail in the evolution of these systems, because it is hard to envision how to form a high number of these systems with the current IMF and initial

mass ratio distribution . It is particularly interesting in the context of CV-progenitors, as WDs in CVs are on average significantly more massive than single WDs [e.g. Warner, 1995; Savoury et al., 2011].

Constraints on CE evolution other than this study have come from reconstruction methods of the evolution of observed binaries. From observed PCEBs, Zorotovic et al. [2010] deduces a value of $\alpha = 0.2 - 0.3$ for the CE efficiency when including the internal energy of the envelope into the energy balance equation. They find that the internal energy is important for CE evolution when the CE phase is initiated by AGB donors, but the effect is not significant for RG donors. We therefore conclude that our results are consistent with those of Zorotovic et al. [2010].

From reconstructing the evolution of post-CE binaries (mostly pre-SDSS PCEBs and some SdB+MS binaries), De Marco et al. [2011] found that the CE efficiency decreases with mass ratio ($q = \frac{M_a}{M_d}$). The effect, however, has not been observed in the SDSS PCEB population [Zorotovic et al., 2011b].

Portegies Zwart [2013] reconstructs the formation and evolution of the cataclysmic variable HU Aquarius. The two planets that orbit this CV play an important role in constraining the CE efficiency. Portegies Zwart [2013] find that the CE efficiency is low, $\alpha\lambda = 0.45 \pm 0.17$. This is consistent with our conclusion.

From reconstructing the evolution of double He WDs, Nelemans et al. [2000] deduces two constraints on CE evolution. First, CE evolution occurs very efficiently (i.e. $\alpha\lambda = 2$) in a binary system with a giant donor and a WD companion. The physical interpretation of this is that more energy sources than orbital energy are used to expel the envelope. An example of possible energy source is the internal energy of the envelope including recombination energy [e.g. Han et al., 1995; Webbink, 2008]. Second, neither the α -CE prescription nor stable mass transfer is able to explain the observations for the first phase of mass transfer in the evolution of progenitor systems of double He WDs, and therefore, Nelemans et al. [2000] proposed the γ -prescription. Furthermore, Nelemans et al. [2001c] showed in a BPS study that the population of Galactic double WDs is well modelled when assuming $\gamma = 1.75$ and $\alpha\lambda = 2$, whereas the standard α -prescription does not. Recently, Woods et al. [2012, see also Woods et al. 2010] suggested a new evolutionary model to create double WDs that involves stable, non-conservative mass transfer between a RG and a MS star. The effect on the orbit is a modest widening with a result alike to the γ -description.

Summarizing, the CE phase is a crucially important phase in the formation and evolution of binaries, however, it is not well understood. BPS and evolutionary reconstruction studies have lead to valuable constraints on CE evolution that contribute to the formation of a coherent picture of CE evolution over mass ratios and stellar types involved in the CE phase. In our option, the emerging picture of CE evolution with non-degenerate companions thus far is that:

- in approximately equal mass binaries that lead to the formation of double WDs, mass transfer leads to a modest widening of the orbit;
- in binaries with low mass ratios ($q \approx 0.2 - 0.5$) that lead to the formation of PCEBs, CE evolution leads to a strong contraction of the orbital separation;
- in binaries with extreme low mass ratios ($q \lesssim 0.2$) the CE phase is caused by a tidal instability rather than a dynamical instability and the CE phase might evolve differently for that reason.

Acknowledgements

We thank Kars Verbeek, Simo Scaringi, and Kevin Covey for very helpful discussions on colours and magnitudes of main-sequence stars. This work was supported by the Netherlands Research Council NWO (grant VIDI [# 639.042.813]) and by the Netherlands Research School for Astronomy (NOVA).

2.A Population synthesis code SeBa

We present here the most important changes that we made to the population synthesis code SeBa, since Toonen et al. [2012]. First, the method of modelling a tidal instability [Darwin, 1879] is updated. This instability takes place in systems of extreme mass ratios in which there is insufficient orbital angular momentum to keep the stars in synchronous rotation [Hut, 1980]. The tidal forces that are responsible for the orbital decay are strongly dependent on the ratio of the stellar radius and the distance between the stars [Zahn, 1977]. Instead of checking at RLOF, we assume tidal forces are effective if the stellar radius is less than one-fifth of the periastron distance between the stars and that the orbital decay proceeds instantaneously.

In addition, the winds of hydrogen-poor helium-burning stars are updated. We adopt the formalism of Hurley et al. [2000], which consists of the maximum of the wind-mass loss of Reimers [1975] and a Wolf-Rayet-like wind-mass loss.

Finally, the responses of the radius of helium stars to mass loss are updated. The adiabatic response ζ_{ad} and the thermal response ζ_{eq} [see Eq. A.14 and A.18 in Toonen et al., 2012] are used to determine the stability of Roche lobe overflow. For helium MS-stars and helium hertzsprung-gap stars, we assume $\zeta_{\text{ad}} = 4$. For helium giants, ζ_{ad} is based on the prescription of Hjellming & Webbink [1987]. For helium hertzsprung-gap stars and helium giants, we assume $\zeta_{\text{th}} = -2$.

2.B The spectral type - mass relation

In the last decade, it has become clear that there is a discrepancy between theoretical models of and observationally determined radii and masses of low-mass stars, challenging our understanding of stellar evolution, structure, and atmospheres [see e.g. Hillenbrand & White, 2004; Berger et al., 2006; López-Morales, 2007; Boyajian et al., 2012]. To exclude these uncertainties from the comparison with the SDSS observations (see Sect. 2.3.1), we have used the relation between spectral type and mass, as determined by Rebassa-Mansergas et al. [2007] and the relation between spectral type and magnitudes, as given by Kraus & Hillenbrand [2007]. There is a good agreement between the effective temperatures as a function of spectral type of Rebassa-Mansergas et al. [2007] and Kraus & Hillenbrand [2007]. For comparison, we show the synthetic populations of visible PCEBs in SDSS in Fig. 2.10 where we assume the relation between spectral type and mass from Kraus & Hillenbrand [2007]. The population is significantly extended to higher secondary masses when compared to those shown in Fig. 2.7 and 2.8.

2.B THE SPECTRAL TYPE - MASS RELATION

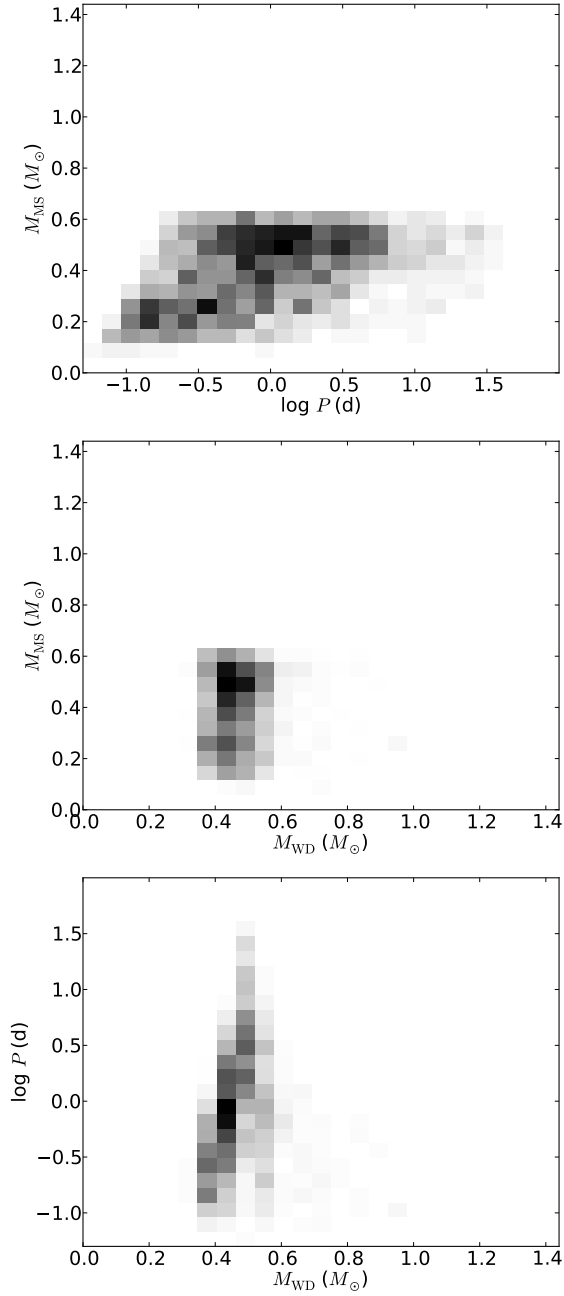


FIGURE 2.10: Visible population of PCEBs in the SDSS assuming the spectral type-mass relation of Kraus & Hillenbrand [2007] for model $\alpha\alpha 2$.

THE SINGLE DEGENERATE SUPERNOVA TYPE IA PROGENITORS: STUDYING THE INFLUENCE OF DIFFERENT MASS RETENTION EFFICIENCIES

M. Bours, S. Toonen, G. Nelemans

Astronomy and Astrophysics, 2013, 552, A24

Abstract

There is general agreement that supernovae Ia correspond to the thermonuclear runaway of a white dwarf that is part of a compact binary, but the details of the progenitor systems are still unknown and much debated. One of the proposed progenitor theories is the single-degenerate channel in which a white dwarf accretes from a companion, grows in mass, reaches a critical mass limit, and is then consumed after thermonuclear runaway sets in. However, there are major disagreements about the theoretical delay time distribution and the corresponding time-integrated supernova Ia rate from this channel. We investigate whether the differences are due to the uncertainty in the common envelope phase and the fraction of transferred mass that is retained by the white dwarf. This so-called retention efficiency may have a strong influence on the final amount and timing of supernovae Ia. Using the population synthesis code SeBa, we simulated large numbers of binaries for various assumptions on common envelopes and retention efficiencies. We compare the resulting supernova Ia rates and delay time distributions with each other and with those from the literature, including

observational data. For the three assumed retention efficiencies, the integrated rate varies by a factor 3-4 to even more than a factor 100, so in extreme cases, the retention efficiency strongly suppresses the single-degenerate channel. Our different assumptions for the common envelope phase change the integrated rate by a factor 2-3. Although our results do recover the trend in the theoretical predictions from different binary population synthesis codes, they do not fully explain the large disagreement among them.



3.1 Introduction

Supernova Ia (SNIa) light curves are scalable to one prototype light curve due to the consistent production of a certain peak luminosity [e.g. Phillips, 1993]. This characteristic makes it relatively easy to estimate distances to observed SNeIa, which is why they can be used as standard candles in cosmology [e.g. Leibundgut et al., 1991; Riess et al., 1998; Perlmutter et al., 1999]. SNeIa also strongly affect the Galactic chemical evolution through the expulsion of iron [e.g. van den Bergh & Tammann, 1991]. In addition, SNeIa play an important role in astroparticle physics, because the accompanying shocks are prime accelerator sites for galactic cosmic ray particles [Blandford & Ostriker, 1978]. Although they are part of many research fields, their origin and the details of the underlying physical processes are not fully understood.

It is generally accepted that SNIa events are caused by the thermonuclear explosions of carbon/oxygen (C/O) white dwarfs (WDs) with masses near the Chandrasekhar mass [Nomoto, 1982]. Of the two classical progenitor scenarios, we look at the single-degenerate (SD) channel [Whelan & Iben, 1973], in which a WD accretes from a companion. The double-degenerate (DD) channel describes the merger of two WDs [e.g. Iben & Tutukov, 1984; Webbink, 1984; Toonen et al., 2012]. Other channels are amongst others accreting WDs from helium-rich, non-degenerate companions [see e.g. Wang et al., 2009b], and mergers between a WD and the core of an asymptotic giant branch star [Kashi & Soker, 2011].

The progenitor theory should give a reliable description of the evolution of a SNIa progenitor binary. Beyond this, it should be able to explain and reproduce general features of the type Ia supernova class. Both the SD and DD scenarios have problems in matching observed features of the SNeIa events. We briefly mention the most important issues; however, see Livio [2000] and Wang & Han [2012] for reviews. Regarding the DD scenario, a serious concern is whether the collapse of the remnant would lead to a supernova or to a neutron star through accretion-induced collapse [see Nomoto & Iben, 1985; Saio & Nomoto,

1985; Piersanti et al., 2003; Yoon et al., 2007; Pakmor et al., 2010, 2012; Shen et al., 2012]. In the SD channel, a SNIa-like event is more easily reproduced in the simulations of the explosion process, although the explosion process needs to be fine-tuned to reproduce the observed spectra and lightcurves [see e.g. Hillebrandt & Niemeyer, 2000, for a review]. Another issue is the long phase of supersoft X-ray emission SNIa SD progenitors should go through. It is unclear whether there are enough of these sources to account for the SNIa rate [see Di Stefano, 2010; Gilfanov & Bogdán, 2010; Hachisu et al., 2010]. Archival data of known SNeIa have not shown this emission unambiguously, although there is possibly one case [see Voss & Nelemans, 2008; Roelofs et al., 2008; Nielsen et al., 2010]. Finally, several predictions for the SD rate have been made by different groups using binary population synthesis (BPS) simulations [Yungelson & Livio, 2000; Han & Podsiadlowski, 2004; Ruiter et al., 2009b; Meng et al., 2009; Mennekens et al., 2010; Wang et al., 2010; Yungelson, 2010; Claeys et al., 2011], time-integrated rates, as well as the distribution of rates over time, the so-called delay time distribution (DTD). For an overview, see Nelemans et al. [2013]. However, the results show a wide spread and do not agree with each other or with observational data. The exact origin of these differences is so far unclear.

In this paper we try to uncover the reason for these differences, and we focus in particular on the efficiency with which the WD accretes and retains matter from its companion and on the common envelope (CE) phase. There are several prescriptions [Nomoto et al., 2007; Ruiter et al., 2009b; Yungelson, 2010, hereafter NSKH07, RBF09 and Y10 respectively] in the literature for the efficiency of retaining matter by the WD. The retention efficiencies of NSKH07, RBF09 and Y10 differ strongly. We study how the retention efficiency influences the SNIa rate and the DTD. Furthermore we investigate if the differences in the assumed retention efficiencies can explain the differences in the predicted SNIa rate from different BPS codes.

Differences between the retention efficiencies arise from the uncertainty in the novae phase and the strength of the optically thick WD wind at high mass transfer rates [Kato & Hachisu, 1994]. The optically thick wind stabilises mass transfer such that a CE phase can be avoided. [Hachisu et al., 1999b, hereafter HKN99b] argues that the WD wind can interact with the envelope of the companion and strip some of the envelope mass from the donor, which stabilises the mass transfer further. The wind-stripping effect affects the retention efficiency moderately, but enlarges the parameter space for producing SNeIa effectively. However, for low metallicities the wind attenuates [e.g. Kobayashi et al., 1998; Kobayashi & Nomoto, 2009], but a low-metallicity threshold of SNeIa in comparison with SNe type II have not been found in observations [Prieto et al., 2008; Badenes et al., 2009]. Regarding the novae phase, despite much progress in the understanding of classical novae, they are still poorly understood e.g. the mixing between the accreted envelope and WD [e.g. Denissenkov et al., 2013]. Currently it is unclear if a cycle of novae outbursts removes more mass from the WD than the accreted envelope, effectively reducing the WD in mass [Prialnik, 1986; Prialnik & Kovetz, 1995; Townsley & Bildsten, 2004; Yaron et al., 2005].

In particular, the results from helium novae are different, which affects the chain of nuclear burning in the SD channel for which first hydrogen-rich material is burned into helium-rich material and consequently the helium-rich matter into carbon-rich material. The uncertainty in helium accretion creates the strongest difference between the assumed retention efficiencies.

In Sect. 3.2 the general evolution of a progenitor binary will be described. The CE phase and the growth in mass of the WD will be discussed in detail. To predict the distribution of SNIa rates for different assumptions we simulate the evolution for a large population of binaries using the population synthesis code SeBa, which is described in Sect. 3.3. Different methods for selecting those binaries that will evolve into a SNIa are also outlined. This includes a straightforward selection on binary parameters and an implementation in SeBa of the efficiency of mass retention on the WD. The resulting rates are presented in Sect. 3.4, and compared with theoretical predictions from different groups in Sect. 3.5.

3.2 Evolution of single degenerate SNIa progenitors

3.2.1 Global evolution

The evolution of most binaries starts with two zero-age main sequence (ZAMS) stars in orbit around their common centre of mass. This is shown as the first stage in Fig. 3.1, which shows the evolutionary stages a SD progenitor binary goes through. The initially more massive (hereafter primary) star has a mass of about $3-8M_{\odot}$ and evolves into a C/O WD of about $0.6-1.2M_{\odot}$. In order to form a compact system, binaries go through one or several mass transfer phases. The mass transfer can be stable or unstable, where the latter is described by the CE phase, the onset of which is shown in the second stage in Fig. 3.1. Here the primary has evolved off the main sequence (MS) and overfills its Roche lobe. In the following CE phase the envelope of the primary star engulfs the initially less massive star, hereafter secondary. The core of the primary and secondary spiral inward through the envelope and the envelope itself is expelled. After the CE phase the binary consists of a degenerate C/O WD and a MS star in a close binary, see the third stage in Fig. 3.1. Note that the evolutionary stages following the MS are relatively short, so that even an initially small mass difference can lead to a binary with a WD and a MS star. In spite of the importance of the CE phase for creating short period systems containing compact objects, the phenomenon is not yet well understood. In Sect. 3.2.2 we discuss two prescriptions for the CE phase.

If the orbital separation of the binary after the CE phase is small, the secondary will fill its Roche lobe when it evolves. Depending on the exact orbital distance this may occur when the secondary is a late MS star, a Hertzsprung gap star, or after it has evolved into a red giant.

3.2 EVOLUTION OF SINGLE DEGENERATE SNIa PROGENITORS

Mass from the outer layers of the secondary will be transferred through the first Lagrangian point onto the WD. The hydrogen-rich material accumulates in a layer on the surface of the WD. When the pressure and temperature are high enough, the hydrogen layer ignites. As a result (a fraction of the) mass can be expelled from the WD and (a fraction of the) mass can be retained by the WD to form a helium layer on the WD. If the helium layer ignites, carbon and oxygen will be formed. Under the right conditions this mass too can be retained by the WD. A favourable combination of these two stages is needed for the C/O WD to be able to grow significantly in mass. In Sect. 3.2.3 we will discuss in more detail the possible mechanisms of helium and hydrogen burning layers and expulsion efficiencies. As the mass of the WD approaches the critical mass limit of $M_{\text{SNIa}} = 1.38M_{\odot}$ ¹, carbon ignites. Due to the degenerate nature of the WD a thermonuclear runaway takes place, leading to a SNIa event.

3.2.2 Common envelope phase

The classical way to parametrise the CE phase is by the α -formalism [Paczynski, 1976; Webbink, 1984] which is based on conservation of energy:

$$\frac{GMM_e}{\lambda R} = \alpha \left(\frac{GM_c m}{2a_f} - \frac{GMm}{2a_i} \right), \quad (3.1)$$

where the left hand side represents the binding energy of the CE ΔE_{bind} and the right hand side a fraction α of the orbital energy ΔE_{orb} of the binary. M represents the mass of the donor star and the subscripts e and c refer to the envelope and core of the donor star. The secondary mass is denoted by m and is assumed not to vary during the CE phase. The a_i and a_f are the initial and final separation of the binary. R is the radius of the donor star and λ is a structural parameter of the envelope. All the uncertainty can be taken into one parameter, the product $\alpha\lambda$. For higher values of $\alpha\lambda$, the CE is expelled more efficiently and the change in orbital separation will be less dramatic. However, in all cases the orbital separation shrinks as a result of the CE phase. Contradicting this, observed double WD binaries seem to have mass ratios close to one [Maxted & Marsh, 1999]. To form a double WD pair the binary usually goes through two CE phases. One when the primary star evolves into a giant and subsequently a WD and one when the secondary evolves. In order for the mass of the WDs to be roughly equal, the conditions at the start of the first CE cannot differ much from those at the onset of the second CE. Therefore the orbital separation of these systems cannot shrink substantially during the first CE phase.

As a possible solution to this problem the γ -algorithm was introduced by Nelemans et al. [2000]. Based on the conservation of angular momentum, angular momentum is lost in a linear way with mass according to:

$$\frac{\Delta J}{J} = \gamma \frac{\Delta M_{\text{tot}}}{M_{\text{tot}}} = \gamma \frac{M_e}{M + m}, \quad (3.2)$$

¹In accordance with most of the cited papers.

CHAPTER 3 : THE SINGLE DEGENERATE SNIa PROGENITORS

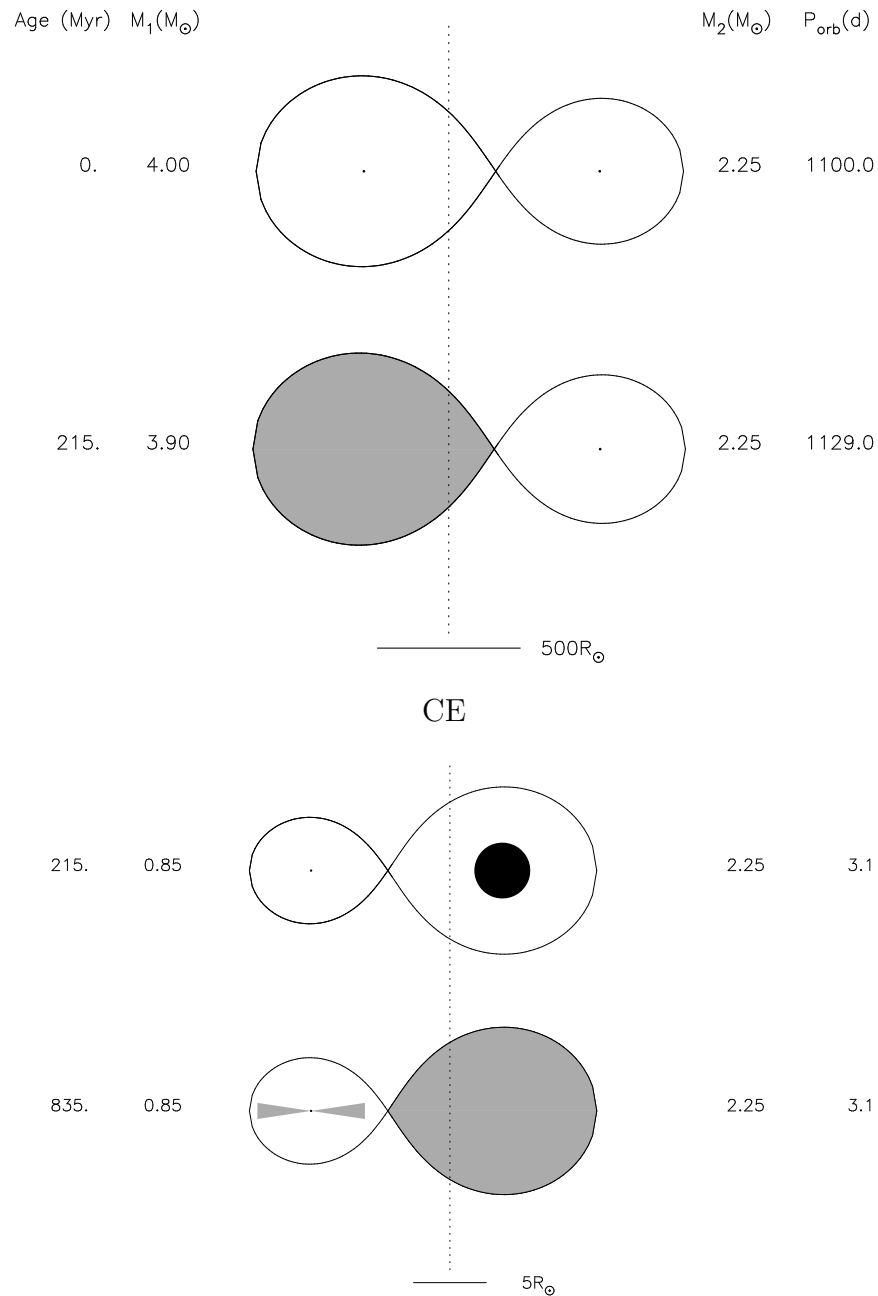


FIGURE 3.1: Binary evolution for a single-degenerate SNIa progenitor. In this case the donor is a MS star. The top and bottom parts of the figure have different scales due to the common envelope phase, denoted as CE in the figure.

where J represents the angular momentum of the binary, M_{tot} is the total mass of the binary and the other parameters have the same meaning as before. Depending on the mass ratio, the orbital separation will be unchanged or decreased due to the description of the CE phase. The physical mechanism behind the γ -description remains unclear. Interesting to note here is that recently Woods et al. [2012] suggested a new evolutionary model to create DWDs. These authors find that mass transfer between a red giant and a MS star can be stable and non-conservative. The effect on the orbit is a modest widening, with a result alike to the γ -description.

3.2.3 Growth of the white dwarf

How efficiently the WD grows in mass as a result of the accretion is described by the total retention efficiency η_{tot} . This represents the fraction of transferred hydrogen-rich matter from the companion that eventually burns into carbon-rich matter and stays on the WD. Therefore $\dot{M}_{WD} = \eta_{tot}|\dot{M}_{comp}|$, where \dot{M}_{WD} represents the mass growth rate of the WD and \dot{M}_{comp} the mass transfer rate of the companion. Note that $\dot{M}_{comp} < 0$, while $\dot{M}_{WD} > 0$. Ultimately the retention efficiency of the transferred mass determines in which systems a SNIa event takes place and therefore shapes the SNIa rate and delay time distribution.

3.2.3.1 Hydrogen-rich accretion

When hydrogen-rich material is transferred onto a WD, the evolution of the accreted layer depends on the mass transfer rate of the companion \dot{M}_{comp} and the WD mass M_{WD} . The evolution can be split into three distinct regimes, separated by a so-called steady and critical accretion rate $\dot{M}_{st}(M_{WD})$ and $\dot{M}_{cr}(M_{WD})$ [Nomoto, 1982; Hachisu & Kato, 2001]. These are both functions of the WD mass and are discussed in detail below.

For low mass transfer rates ($|\dot{M}_{comp}| < \dot{M}_{st}$) the hydrogen-rich matter is transferred to the WD conservatively, so that the mass transfer rate onto the WD is $\dot{M}_H = |\dot{M}_{comp}|$. The temperature in the accumulating hydrogen layer on the WD is too low to ignite the hydrogen immediately. The layer will gradually grow in mass, increasing the pressure and temperature until hydrogen ignition values are reached. Then nuclear burning will quickly spread through the layer, which starts expanding. The strength of these so-called novae [Starrfield et al., 1972] depends strongly on the amount of mass involved. This also determines how much of the processed layer is expelled from the binary and how much falls back onto the WD as helium. The accretion rate of the helium-rich matter will be denoted by \dot{M}_{He} . We define the hydrogen retention efficiency to be the fraction of transferred mass which is burned and retained by the WD:

$$\eta_H = \frac{\dot{M}_{He}}{\dot{M}_H}. \quad (3.3)$$

If none of the matter stays on the WD $\eta_H = 0$ and if all of the transferred matter is retained by the WD as helium $\eta_H = 1$. In the nova regime $\eta_H < 1$. For very strong novae

not only the complete layer but also some of the WD itself may be expelled. In these cases $\eta_H < 0$. However, note that there may be observational evidence suggesting that WDs in mass transferring cataclysmic variables grow in mass, even though these binaries have very low mass transfer rates and therefore undergo strong novae [Zorotovic et al., 2011a]

Intermediate mass transfer rates are those between the steady and critical value, so that $\dot{M}_{\text{st}} \leq |\dot{M}_{\text{comp}}| \leq \dot{M}_{\text{cr}}$. All of the mass lost by the companion star is transferred to the WD, so that $\dot{M}_H = |\dot{M}_{\text{comp}}|$. On the WD the hydrogen accumulates in such a way that the ignition values are reached at the bottom of the layer and the hydrogen stably burns into helium. No material is lost from the layer or the WD, therefore $\eta_H = 1$ and $\dot{M}_{\text{He}} = \dot{M}_H$.

For higher mass transfer rates exceeding the critical value ($|\dot{M}_{\text{comp}}| > \dot{M}_{\text{cr}}$) a hydrogen red-giant-like envelope forms around the WD. If the high accretion rate is maintained a CE phase will soon follow. However, hydrogen burning on top of the WD is strong enough for a wind to develop from the WD [Kato & Hachisu, 1994, HKN99b]. This attenuates the mass transfer rate \dot{M}_H and hydrogen retention efficiency η_H , and ensures that the CE phase is postponed. Part of the hydrogen-rich matter, corresponding to \dot{M}_{cr} , is burned into helium and stays on the WD. The remainder $\dot{M}_H - \dot{M}_{\text{cr}} = \dot{M}_{\text{wind}}$ is carried away by the wind. In this wind regime, $\dot{M}_{\text{He}} = \dot{M}_{\text{cr}} = \eta_H \dot{M}_H$ and so $\eta_H < 1$.

A possible second effect influencing the retention efficiency in this high mass transfer rate regime, results from the wind if it reaches the companion star. There it heats up the envelope of the companion, which expands and can then be stripped off by subsequent wind [HKN99b]. It is now no longer the case that all of the mass lost by the companion is transferred to the WD. The part that is transferred to the WD is equivalent to the amount lost by the companion minus the amount stripped away by the WD wind: $\dot{M}_H = |\dot{M}_{\text{comp}}| - |\dot{M}_{\text{strip}}|$, where $\dot{M}_{\text{strip}} < 0$. The strength of this stripping effect is represented by the stripping parameter c_1 , defined by

$$\dot{M}_{\text{strip}} = c_1 \dot{M}_{\text{wind}}. \quad (3.4)$$

Details on how and when this stripping effect is taken into account are described in Sect. 3.3 and appendix 3.A.

3.2.3.2 Helium-rich accretion

After a fraction of the hydrogen-rich matter is burned into helium-rich material, the helium-rich material accumulates in a layer on the surface of the WD. This layer sits in between the WD and the (still accumulating) hydrogen layer. For the helium-rich accretion similar regimes exist for low and medium helium accretion rates, resulting in helium novae and steady helium burning respectively. No helium wind regime exists because these high helium accretion rates cannot be reached by the hydrogen burning. The fraction of helium that is burned into carbon-rich material is represented by the helium retention efficiency η_{He} . The total retention efficiency is then given by:

$$\eta_{\text{tot}} = \eta_H(\dot{M}_{\text{comp}}) \cdot \eta_{\text{He}}(\dot{M}_{\text{He}}). \quad (3.5)$$

3.3 Method

To test the viability of SD SNIa theory a population of binary stars is simulated and the corresponding theoretical SNIa rate is compared to observational results. We employ the binary population synthesis code SeBa [Portegies Zwart & Verbunt, 1996; Nelemans et al., 2001c; Toonen et al., 2012] for fast stellar and binary evolution computations. In SeBa stars are evolved from the ZAMS until remnant formation. At every timestep, processes as stellar winds, mass transfer, angular momentum loss, magnetic braking and gravitational radiation are taken into account with appropriate recipes. SeBa is a Monte Carlo based code in which the initial binary parameters are generated randomly according to appropriate distribution functions. The initial mass of the primary stars is drawn from a Kroupa Initial Mass Function [Kroupa et al., 1993] which ranges from $0.1-100M_{\odot}$ and the initial mass of the secondary from a flat mass ratio distribution with values between 0 and 1. We assume that a complete stellar population consists of 50% binary stars and 50% single stars. The semi-major axis of the binary is drawn from a power law distribution with an exponent of -1 [Abt, 1983], ranging from 0 to 10^6R_{\odot} and the eccentricity from a thermal distribution, ranging from 0 to 1 [Heggie, 1975]. For the metallicity solar values are assumed.

In this research we differentiate between four ways to determine which binaries will give rise to a SNIa event. For the first method (model NSKH07) we adopt the retention efficiencies given by NSKH07, including updates from Hachisu et al. [2008, hereafter HKN08]. Using SeBa in combination with these retention efficiencies, a population of binaries is simulated and those systems in which a C/O WD reaches the critical mass limit are selected as SNIa progenitors. For the second approach (model RBF09) we utilise the retention efficiencies used in RBF09 and for the third approach (model Y10) the efficiencies based on Y10. The assumed retention efficiencies differ strongly. For the final method (model Islands) the phase of stable mass transfer onto the WD is not modelled by SeBa. Instead we select those systems that at the formation of the C/O WD lie in specific regions of the parameter space of orbital period, WD mass and companion mass ($P_{\text{orb}} - M_{\text{WD}} - M_{\text{comp}}$). Systems in these specific regions, hereafter islands, are determined to lead to SNeIa [HKN08; HKN99b, and references therein].

In order to compare our simulated rates to the results of research groups that use the same retention efficiencies, the prescription of the CE is varied to match different BPS codes. We distinguish between two models. The first model is based on the α -prescription assuming a value of $\alpha = 1$ and $\lambda = 0.5$ as in accordance with RBF09. The second model assumes the γ -formalism with a value of $\gamma = 1.75$ [see Nelemans et al., 2001c].²

In this section we describe the three prescriptions for the hydrogen and helium retention efficiencies as given by NSKH07 RBF09 and Y10. The total retention efficiency is a combination of the hydrogen and helium one as described by eq. 3.5. The retention effi-

²The γ -formalism is applied, unless the binary contains a compact object or the CE is triggered by a tidal instability [Darwin, 1879] for which the α -formalism is used.

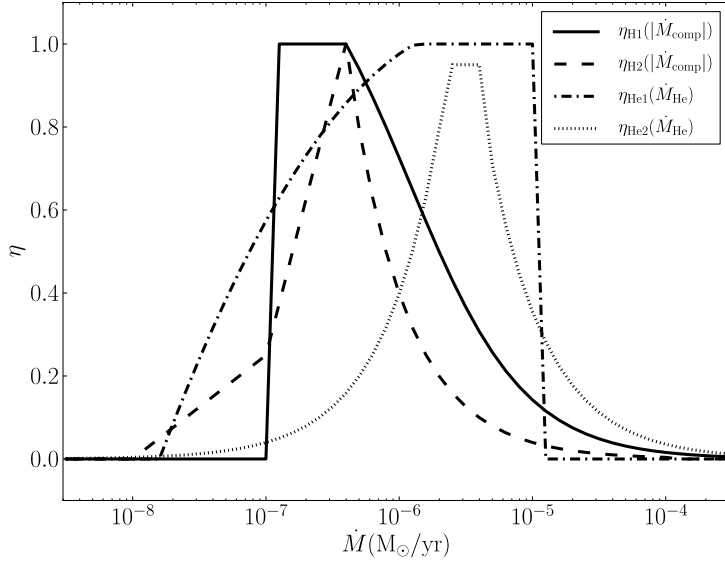


FIGURE 3.2: Examples of hydrogen and helium retention efficiencies as a function of the mass transfer rate for a WD of $1M_{\odot}$. The prescriptions for the hydrogen retention efficiency η_{H1} [solid line - NSKH07; HKN08] & η_{H2} [dashed line - RBF09; Y10] and the helium retention efficiency η_{He1} [dot-dashed line - Hachisu et al., 1999; Kato & Hachisu, 1999] & η_{He2} [dotted line - Iben & Tutukov, 1996] are shown in Appendix 3.A. Note that the position of the peak of η_{H2} is dependent on the exact prescription for \dot{M}_{cr} . The mass transfer rate for hydrogen accretion is given by $|\dot{M}_{\text{comp}}|$. For helium accretion this is \dot{M}_{He} .

ciency used in NSKH07, including updates from HKN08, is a combination of the hydrogen retention efficiency η_{H1} and the helium retention efficiency η_{He1} , see Fig. 3.2. For η_{H1} the region of steady burning occurs at mass transfer rates between

$$\dot{M}_{\text{st}} = 3.1 \cdot 10^{-7} (M_{\text{WD}} - 0.54) M_{\odot} \text{yr}^{-1} \text{ and} \quad (3.6)$$

$$\dot{M}_{\text{cr}} = 7.5 \cdot 10^{-7} (M_{\text{WD}} - 0.40) M_{\odot} \text{yr}^{-1}, \quad (3.7)$$

which are the updated formulae from HKN08 with M_{WD} in units of M_{\odot} . This region is visible in Fig. 3.2 as the plateau at intermediate mass transfer rates. In the wind regime $|\dot{M}_{\text{comp}}| > \dot{M}_{\text{cr}}$, the wind-stripping effect is included with $c_1 = 3$ (see eq. 3.4). For the prescription of η_{He1} see Appendix 3.A [Kato & Hachisu, 1999; HKN99b].

3.3.1 Retention efficiencies

The retention efficiency based on RBF09 combines η_{He1} with η_{H2} , see Fig. 3.2. In this model there is no region of steady hydrogen burning. Instead the nova regime immediately borders the wind regime. The critical mass transfer rate \dot{M}_{cr} is given by eq. 3.7. The stripping effect is not taken into account, hence $c_1 = 0$ (see eq. 3.4). The retention efficiency in the nova

regime ($|\dot{M}_{\text{comp}}| < \dot{M}_{\text{cr}}$) is based on an interpolation of results from Prialnik & Kovetz [1995]. Our own fit to these results is included in Appendix 3.A. For lower (higher) M_{WD} than assumed in Fig. 3.2, the retention efficiency in the nova regime stays the same between $10^{-8} < |\dot{M}_{\text{comp}}| < 10^{-7}$ and shifts with the peak in the regime $10^{-7} < |\dot{M}_{\text{comp}}| < \dot{M}_{\text{cr}}$.

The retention efficiency based on Y10 combines η_{H2} with η_{He2} , see Fig. 3.2. The critical rate for the hydrogen accretion is given by

$$\dot{M}_{\text{cr}} = 10^{-9.31+4.12M_{\text{WD}}-1.42M_{\text{WD}}^2} M_{\odot}\text{yr}^{-1}, \quad (3.8)$$

with M_{WD} in units of M_{\odot} . For the retention efficiency in the hydrogen nova regime the same interpolation from Prialnik & Kovetz [1995] is used as for the efficiency of RBF09, see Appendix 3.A. Again there is no region of steady hydrogen burning, the wind is taken into account but the stripping effect is not. Due to the different prescription for \dot{M}_{cr} the position of the peak is slightly different from the example curve. Using eq. 3.8 as the border to the wind regime for hydrogen accretion, the peak occurs at smaller values of $|\dot{M}_{\text{comp}}|$ for a given M_{WD} , as compared to eq. 3.7. This reduces the total retention efficiency η_{tot} substantially, as we will see in Fig. 3.3. Following Y10, the prescription for η_{He2} was taken from Iben & Tutukov [1996].

The exact prescriptions of the hydrogen and helium retention efficiencies for NSKH07, RBF09 and Y10 are detailed in Appendix 3.A. Figure 3.3 shows the large variety in the total retention efficiency for the three prescriptions as a function of mass transfer rate of the companion. The most optimistic retention efficiency is that of NSKH07 and the most pessimistic that of Y10. Note that in the regime with strong novae the retention efficiency $\eta_{\text{tot}} \leq 0$. Here we have set $\eta_{\text{tot}} = 0$ in this regime for simplicity as these systems are not part of the SD channel.

A complication of this method is that the instantaneous mass transfer rates in binary population synthesis codes, such as SeBa, is only an approximation to the one derived from detailed stellar evolution codes. Therefore, we also implemented a hybrid method in which progenitors are selected from binary population synthesis according to results from the literature based on more detailed mass transfer tracks. These tracks can be calculated by an analytical approach e.g. HKN99b or by a detailed binary evolution code e.g. Li & van den Heuvel [1997], Li & van den Heuvel [2002], Han & Podsiadlowski [2004] and HKN08.

3.3.2 Islands

In this method, the progenitor binaries are selected on P_{orb} , M_{WD} , and M_{comp} at the time of WD birth (third stage in Fig. 3.1). The parameter regions used are shown at the right hand side in Fig. 3.4 for binaries containing a WD and a MS star or Hertzsprung gap star (WD+MS binaries) and Fig. 3.5 for those containing a WD and a red giant star (WD+RG binaries). They are made to match the islands in HKN08 and HKN99b respectively, which are shown on the left hand side in these figures. For the WD+MS channels a moderate wind-stripping parameter of $c_1 = 3$ is taken (see eq. 3.4).

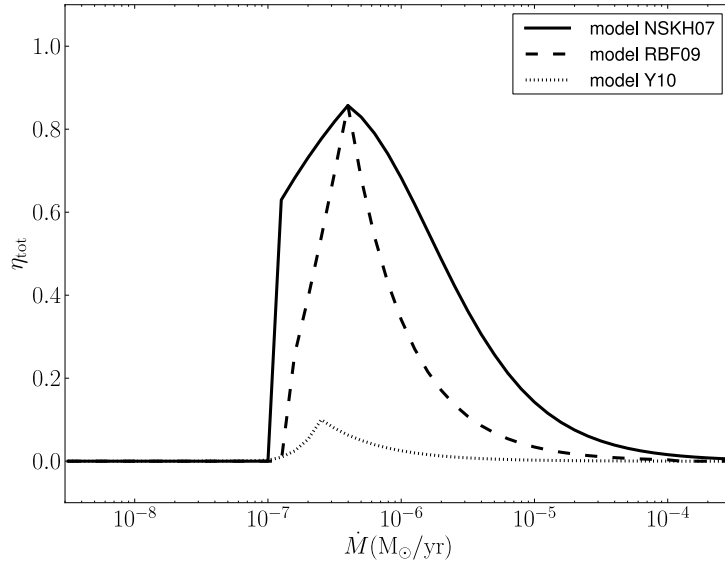


FIGURE 3.3: Total retention efficiencies, resulting from different combinations of the hydrogen and helium retention efficiencies. In this figure we have assumed $M_{\text{WD}} = 1M_{\odot}$ as an example. The mass transfer rate $\dot{M} = |\dot{M}_{\text{comp}}|$. For lower (higher) M_{WD} the maximum retention efficiency shift to lower (higher) $|\dot{M}_{\text{comp}}|$. For a more detailed explanation of the retention efficiencies see Sect. 3.3.1.

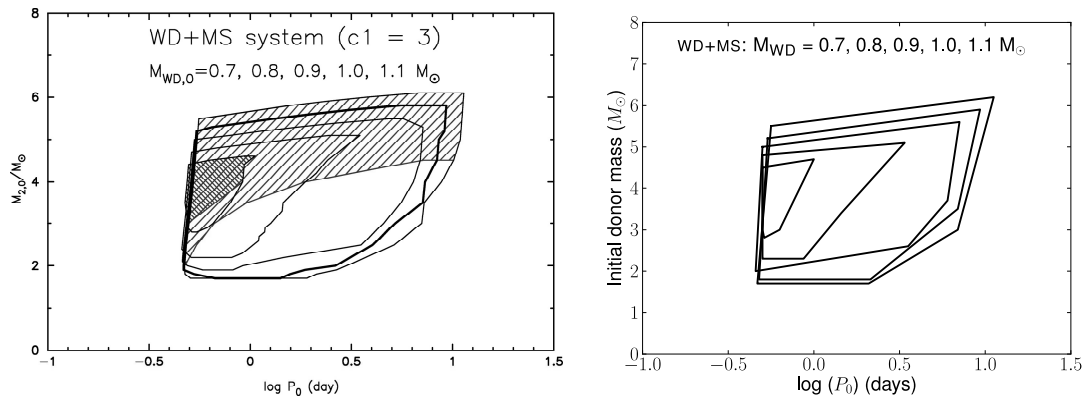


FIGURE 3.4: Initial parameter regions for the WD+MS track to SNIa. The different contours are for different WD masses (increasing in size with increasing mass) and the stripping parameter $c_1 = 3$. Left: from HKN08. The hatched regions indicate SNIa explosions with short delay times of $t < 100\text{Myr}$ for masses of $M = 0.7M_{\odot}$ and $M = 1.1M_{\odot}$. Right: initial parameter regions as used in this work.

3.4 RESULTS: SNIa RATES AND DELAY TIMES

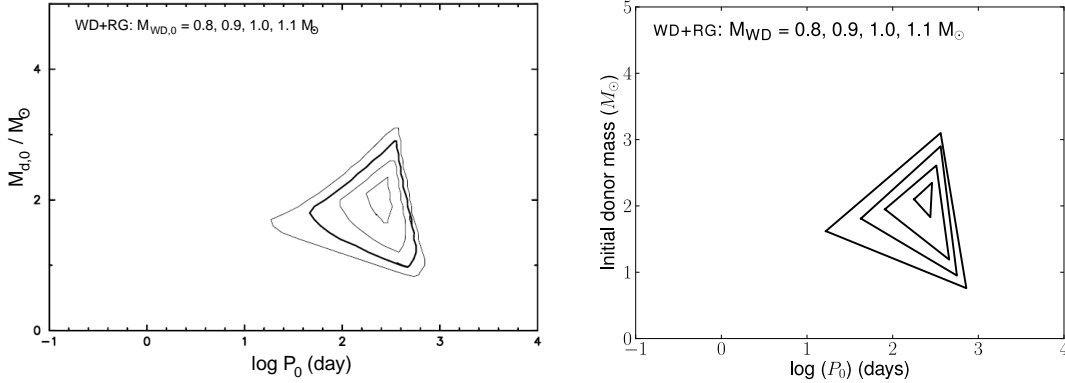


FIGURE 3.5: Initial parameter regions for the WD+RG track to SNeIa. The different contours are for different WD masses (increasing in size with increasing mass) and the stripping parameter $c_1 = 1$. Left: from HKN99b. Right: initial parameter regions as used in this work.

3.4 Results: SNIa rates and delay times

We have simulated a population of SD SNIa progenitors for the four approaches described in Sect.3.3 assuming our model for the γ -prescription or the α -prescription. The delay time distributions for the γ -prescription simulations can be seen in Fig.3.6 and for the α -prescription in Fig.3.7. The delay time t is the time at which a SNIa occurs, where $t = 0$ is the time when the binary is born as a double ZAMS-star binary. A DTD shows the distribution of delay times after a single starburst involving a large number of binaries. For model Islands, we assume the phase between the onset of mass transfer and the SNIa explosion is short compared to the lifetime of the binary.

The progenitor islands are based on the work of NSKH07 and HKN08, as is our model NSKH07 that uses the retention efficiencies directly. If we compare the DTD resulting from model Islands with model NSKH07, there is a noticeable difference at early delay times. The DTD of model Islands peaks earlier and higher. The reason is the extend of the Islands to high donor masses of about $6M_{\odot}$ for WD+MS progenitors. These massive companions fill their Roche lobes soon and therefore the SNIa explosion occurs at earlier delay times ($t < 1\text{Gyr}$). In SeBa, binaries with such high mass ratios undergo unstable mass transfer and a CE phase. They do not develop a SNIa explosion, resulting in less SNeIa at early delay times from the retention efficiencies method.

Our progenitor regions in model Island consist of adjacent slices that increase in size for increasing M_{WD} , for both WD+MS and WD+RG progenitors. These slices have a thickness of $0.1M_{\odot}$ around the values $M_{WD} = 0.7, 0.8, 0.9, 1.0$ and $1.1M_{\odot}$ for WD+MS binaries and $M_{WD} = 0.8, 0.9, 1.0$ and $1.1M_{\odot}$ for WD+RG binaries. Ideally the volume enclosing the progenitor binaries has smooth edges in all three dimensions. Since this is not the case in our approach we explored the resulting inaccuracy by increasing our resolution. We double

TABLE 3.1: Time-integrated SNIa rates in the SD channel for different combinations of the retention efficiency and the common envelope prescription in units of $10^{-4}M_{\odot}^{-1}$.

Model	Approach used	γ -prescription	α -prescription
Model NSKH07	Retention efficiency of NSKH07 ¹	0.59	1.3
Model RBF09	Retention efficiency of RBF09 ²	0.19	0.35
Model Y10	Retention efficiency of Y10 ³	<0.001	<0.001
Model Islands	Islands of HKN08 ⁴ , HKN99b ⁵	0.73	1.5

REFERENCES: ¹ Nomoto et al. [2007]; ² Ruiter et al. [2009b]; ³ Yungelson [2010]; ⁴ Hachisu et al. [2008]; ⁵ Hachisu et al. [1999b];

the amount of islands covering the same range of WD mass, so the thickness of each island slice is now $0.05M_{\odot}$. We found that the change in the final integrated SNIa rate is 3-4% and the DTD is barely affected.

The SNIa DTD and integrated rate are strongly influenced by the prescription of the retention efficiency, as shown in Fig. 3.6 and 3.7, and Table 3.1. For more pessimistic values of the total retention efficiency the rates and overall height of the DTD decreases. Note that the total retention efficiency of model Y10 is so small that no SNeIa developed and only an upper limit is given in Table 3.1. Model NSKH07 and RBF09 give rise to DTDs that differ most strongly at short delay times. This is due to high donor masses that transfer mass at a high rates, where the total retention efficiencies differ significantly, see Fig. 3.3. This results from the inclusion of the wind stripping effect in NSKH07.

Changing the prescription used for the CE phase modifies the integrated SNIa rate by a factor of about two. When the γ -prescription is applied, less (very) close binaries are created as the binary orbits do not shrink as effectively as for the α -prescription. An exception to this is when the mass ratio of the binary is extreme at the moment of Roche lobe overflow. These systems merge at short delay times $t < 0.1$ Gyr. Therefore the DTD when the γ -prescription is assumed declines faster with time than when the α -prescription is assumed. The classical evolution path towards a SD binary as depicted in Fig. 3.1, is less common in the BPS model using the γ -prescription. Assuming the α -prescription 80% of the SD binaries evolve through this channel, where as for the γ -prescription this has decreased to 30-40% (depending on the retention efficiency). In the most common evolution path for the model assuming the γ -prescription, the first phase of mass transfer is stable.

3.4 RESULTS: SNIa RATES AND DELAY TIMES

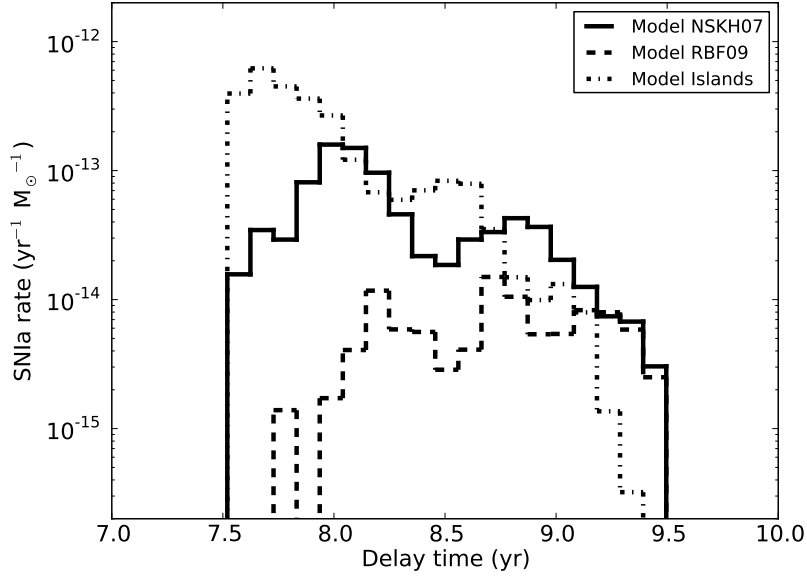


FIGURE 3.6: Delay time distribution assuming the γ -algorithm for the CE with $\gamma = 1.75$. Different lines correspond to the delay time distributions that result from four different approaches described in Sect 3.3, all for the γ -prescription. The dot-dashed line shows the result of the Islands selection method, the three other linestyles correspond to the retention efficiencies as in Fig. 3.3. Note that for the retention efficiency of Y10 no SD binaries evolve into a SNeIa.

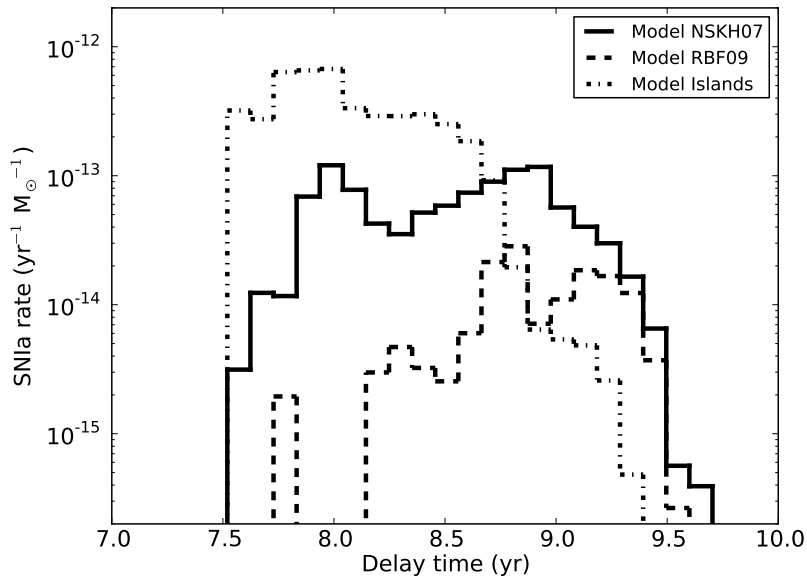


FIGURE 3.7: Same as in Fig. 3.6 but assuming the α -formalism with $\alpha\lambda = 0.5$. Again no SD binaries evolve into a SNeIa for the retention efficiency of Y10.

3.5 Discussion

The theoretical SD SNIa rates that follow from SeBa in this study can be compared to the results of various other BPS research groups [e.g. RBF09; Y10; Mennekens et al., 2010; Wang et al., 2010; Claeys et al., 2011]. Table 3.2 shows the time-integrated SNIa rates of these groups taken from Nelemans et al. [2013]. The disagreement in the rates is large up to a factor of about 600, but so far no explanation has been found. Note that Nelemans et al. [2013] rescaled the results (if needed) to the same initial distribution of parameters as discussed in Sect. 3.3. Assumptions and simplifications vary between the different BPS codes [See Toonen et al. in prep. for a study on this] causing differences in their predictions. An important assumption for the BPS simulations is the assumed CE-prescription, which is also given in in Table 3.2. The effect of different values for α has been studied by several groups, e.g. the effect on the DTD [Wang et al., 2010; Ruiter et al., 2009b; Mennekens et al., 2010; Claeys et al., 2011]. The effect on the integrated rate of a small change in α is of the order of a factor 0.7-3 [Ruiter et al., 2009b; Mennekens et al., 2010], however, the effect can be up to an order of magnitude for larger changes in α (Claeys et al. in prep.).

The entries in Table 3.2 are ordered to increase in rate. The smallest rate is from the work of Yungelson [Y10]. Similarly we find the lowest rate for model Y10, however, we find an even lower rate than Yungelson. The preliminary rate of Claeys et al. [2011] is significantly lower than our corresponding model. However, Claeys et al. [2011] does not take wind stripping into account, as in Ruiter et al. [2009b]. The integrated rates of Ruiter et al. [2009b] is a factor of about two lower than the rates of our best corresponding model. The rates of Mennekens et al. [2010] and Wang et al. [2010] are a factor of a about seven and two higher respectively. So although our results do recover the trend in the theoretical predictions from different binary population synthesis codes, they do not fully explain the large disagreement among them.

The integrated rates based on observations are given in Table 3.2. The most recent measurements are based on field galaxies and generally show lower rates, while earlier estimates based on galaxy clusters are higher. At this moment it is unclear if the different observed integrated rates are due to systematic effects or if there is a real enhancement of SNeIa in cluster galaxies. See also Maoz et al. [2012] for a discussion. Even though the different retention efficiency models affect the SNIa rates with a factor $> 10^3$, none of the integrated rates comfortably matches the observed rates, especially those from galaxy clusters. In addition, the DTD reconstructed from observations typically show a continuation to longer delay times, which are absent in all our SD DTDs. We conclude from this, that in the current model of SD SNIa theory, the main contribution to the SNIa rate comes from other evolution channels. One possible channel involves semi-detached binaries in which a WD accretes from a hydrogen-poor helium-rich donor, such as sdB stars. Wang et al. [2009a], Ruiter et al. [2009b] and Claeys et al. [2011] showed that in this channel the DTD peaks at delay times of about 100Myr, although rates at this delay time vary

TABLE 3.2: Time-integrated SNIa rates in the SD channel for the assumptions of different research groups in units of $10^{-4}M_{\odot}^{-1}$. Columns 3 and 5 shows the integrated rate predicted by SeBa and the BPS group in question respectively. The assumption of the BPS group for the CE-evolution is shown in column 6 and the best corresponding CE-model in SeBa is shown in column 4.

BPS	WD accretion	SNIa rate	CE	SNIa rate	CE
Yungelson ¹	Y10	<0.001	$\gamma = 1.5$	0.006	$\gamma = 1.5$
Claeys ²	HKN99b	1.3	$\alpha\lambda = 0.5$	0.13	$\alpha = 1, \lambda = \text{variable}$
Ruiter ³	RBF09	0.35	$\alpha\lambda = 0.5$	0.17	$\alpha\lambda = 0.5$
Wang/Han ⁴	HKN99b	1.3	$\alpha\lambda = 0.5$	2.8	$\alpha\lambda = 0.5$
Mennekens ⁵	HKN99b, HKN08	0.55	$\alpha\lambda = 1$	3.7	$\alpha\lambda = 1$
Observed ⁶		4-26			

REFERENCES: ¹ Y10; ² Claeys et al. [2011] (preliminary results); ³ RBF09; ⁴ Wang et al. [2010]; ⁵ Mennekens et al. [2010]; ⁶ Maoz & Mannucci [2012a]; Perrett & et al. [2012]; Maoz et al. [2012]; Graur & Maoz [2012];

between $10^{-4} - 10^{-2}\text{yr}^{-1}(10^{10}M_{\odot})^{-1}$. The contribution from binaries of the DD channel is debated heavily. Explosion models favour accretion-induced collapse to a neutron star over a SNIa event [see e.g. Hillebrandt & Niemeyer, 2000, for a review]. However, BPS codes find more SNIa events from the standard DD channel than the SD channel [RBF09; Y10; Mennekens et al., 2010; Toonen et al., 2012]³. Toonen et al. [2012] study the contribution from the double-degenerate channel with SeBa comparing the α - and γ -prescription for the CE. They find that even though the DD DTDs fit the observed DTD beautifully, the normalisation does not by a factor of about 7-12 compared to the cluster rates. Taking into account the new rates from field galaxies, the factor becomes about 1.2-12. Other contributions to the SNIa rate can possibly come from e.g. core-degenerate mergers [Kashi & Soker, 2011], double detonating sub-Chandrasekhar accretors [see e.g. Kromer et al., 2010] or Kozai oscillations in triple systems [Shappee & Thompson, 2012; Hamers et al., 2013].

3.6 Conclusions

In this work we have studied the effect of the poorly understood phase of WD accretion in the context of supernova type Ia rates. We employed the binary population synthesis code SeBa [Portegies Zwart & Verbunt, 1996; Nelemans et al., 2001c; Toonen et al., 2012] to study the SNIa rates and progenitors for different CE prescriptions. We differentiated

³Note that the integrated rate from the violent merger model for double WDs [Pakmor et al., 2010, 2011, 2012; Röpke et al., 2012] can be much lower [Toonen et al., 2012; Chen et al., 2012; Ruiter et al., 2012]

between four models assuming either one of three retention efficiencies of NSKH07, RBF09 and Y10 or making a selection of SNIa progenitors based on binary parameters at the time of WD formation [HKN08; HKN99b]. The three retention efficiencies assumed by different binary population synthesis codes differ strongly. The difference comes from a lack of understanding at low mass transfer rates where novae occur, and mass transfer rates higher than the rate for stable burning. This is true for the accretion of hydrogen that is transferred to the WD by the companion, as well as the accretion of helium that has been burned from hydrogen on the WD. The efficiency with which a C/O WD grows in mass is strongly affected by the combination of the efficiency of hydrogen and helium accretion. For example the hydrogen and helium retention efficiencies of Y10 are maximal at different ranges of the mass transfer rate resulting in a low total retention efficiency.

The total number of SNIa progenitors is significantly influenced by the choice of the model. The integrated SNIa rate vary between $< 1 \cdot 10^{-7} - 1.5 \cdot 10^{-4} M_{\odot}^{-1}$, where the rates are highest for the model that assume the retention efficiencies of NSKH07 and only an upper limit can be given for Y10. Our method based on the parameter space of binaries at WD birth of HKN08 and HKN99b consists of a discrete set of islands in the space spanned by P_{orb} , M_{WD} and M_{comp} . The discretisation introduces an error of 3-4% on the integrated rates. We showed in this paper that independent of the WD accretion model the SNIa rate approximately doubles when the α -prescription is assumed with $\alpha\lambda = 0.5$ as compared to the γ -formalism with $\gamma = 1.75$. The effect of different values for α on the SD SNIa rate is a factor of 0.7-3 [Ruiter et al., 2009b; Mennekens et al., 2010] for small changes in the CE-efficiency and up to an order of magnitude for larger changes in the CE-efficiency (Claeys et al. in prep.). Also note that throughout this work we have assumed solar values for the stellar metallicities. Using a broad range of metallicities in the BPS code might influence the SNIa rates and DTDs, both in the Islands and retention efficiency approach. See Kobayashi et al. [1998] for a study on how the progenitor islands depend on metallicity.

Several predictions for the SD rate have been made by different groups using binary population synthesis simulations. The results show a wide spread and do not agree with each other or with observational data. The integrated rates vary between values of $6 \cdot 10^{-7} M_{\odot}^{-1}$ and $3.7 \cdot 10^{-4} M_{\odot}^{-1}$. In this study we find that also the model for the WD accretion is a major source of uncertainty on the SNIa rates. The different prescriptions for the retention efficiency introduce a source of uncertainty with an effect on the integrated rates by a factor of about 3-4 (comparing our models that assume the retention efficiencies of NSKH07 with RBF09) or even larger up to a factor of a few hundred (comparing with the efficiency of Y10). Although our results do recover the trend in the theoretical predictions from different binary population synthesis codes, they do not fully explain the large disagreement among them. As the exact origin of the differences in the SD rate remains unclear, Toonen et al. in prep. study the results of four different binary population synthesis codes and investigate the importance of the different assumptions and numerical approaches in these codes.

Acknowledgements

We thank Zhanwen Han for useful comments which helped us to improve the manuscript. This work was supported by the Netherlands Research Council NWO (grant VIDI [#639.042.813]) and by the Netherlands Research School for Astronomy (NOVA).

3.A Retention efficiencies

The total retention efficiency is the product of the hydrogen and helium retention efficiencies. In the equations in this appendix, all \dot{M} are in units of M_{\odot}/yr .

3.A.1 Retention efficiencies based on NSKH07

The hydrogen retention efficiency is a strong function of the mass transfer rate of the companion \dot{M}_{comp} . Three regimes can be distinguished, separated by the stable and critical mass transfer rates (\dot{M}_{st} and \dot{M}_{cr}), see Table 3.3. In the nova and stable burning regime all the mass lost by the companion is transferred onto the WD. In the stable regime all hydrogen-rich matter is burned into helium-rich matter and all stays on the WD, so that $\eta_{\text{H}} = 1$. The nova regime is linearly interpolated between the lower boundary at $|\dot{M}_{\text{comp}}| = 10^{-7}$ and the start of the stable regime at \dot{M}_{st} . In the third regime the nuclear hydrogen burning on top of the white dwarf is so strong that a wind is produced which not only attenuates the mass transfer rate but can also strip the companion's outer envelope. It is no longer the case that all the mass lost by the companion accretes onto the white dwarf. The maximum that the white dwarf can accrete is \dot{M}_{cr} , which is a fraction η_{H} of the mass transferred to the white dwarf \dot{M}_{H} . All the excess is blown off by the wind. The amount of matter that is stripped from the companion is defined by eq. 3.4 and the stripping parameter is taken to be $c_1 = 3$.

TABLE 3.3: The three regimes for different mass transfer rates of the companion star, as in NSKH07.

	\dot{M}_{comp} range
Nova regime	$ \dot{M}_{\text{comp}} < \dot{M}_{\text{st}}$
Stable burning regime	$\dot{M}_{\text{st}} \leq \dot{M}_{\text{comp}} \leq \dot{M}_{\text{cr}}$
Wind and stripping regime	$ \dot{M}_{\text{comp}} > \dot{M}_{\text{cr}}$

The exact prescriptions for the stable and critical mass transfer rates are:

$$\dot{M}_{\text{st}} = 3.1 \cdot 10^{-7} \left(\frac{M_{\text{WD}}}{M_{\odot}} - 0.54 \right) \text{ and} \quad (3.9)$$

$$\dot{M}_{\text{cr}} = 7.5 \cdot 10^{-7} \left(\frac{M_{\text{WD}}}{M_{\odot}} - 0.40 \right). \quad (3.10)$$

For the hydrogen retention efficiency we arrive at the following:

$$\eta_{\text{H}} = \begin{cases} 0 & \text{if } |\dot{M}_{\text{comp}}| < 10^{-7} \\ (\log(|\dot{M}_{\text{comp}}|) + 7)/((\log(\dot{M}_{\text{st}}) + 7)) & \text{if } 10^{-7} < |\dot{M}_{\text{comp}}| < \dot{M}_{\text{st}} \\ 1 & \text{if } \dot{M}_{\text{st}} < |\dot{M}_{\text{comp}}| < \dot{M}_{\text{cr}} \\ \dot{M}_{\text{cr}}/\dot{M}_{\text{H}} & \text{if } \dot{M}_{\text{cr}} < |\dot{M}_{\text{comp}}| < 10^{-4} \end{cases} \quad (3.11)$$

with, for the wind and stripping regime,

$$\frac{\dot{M}_{\text{cr}}}{\dot{M}_{\text{H}}} = \frac{(c_1 + 1)\dot{M}_{\text{cr}}}{c_1\dot{M}_{\text{cr}} + |\dot{M}_{\text{comp}}|}. \quad (3.12)$$

This last equation follows from eq. 3.4. Furthermore, we take into account that \dot{M}_{comp} , \dot{M}_{wind} and $\dot{M}_{\text{strip}} < 0$, because they describe matter travelling away from one of the stars. For the helium retention efficiency the following prescriptions were used:

$$\eta_{\text{He}} = \begin{cases} 0 & \text{if } \dot{M}_{\text{He}} < 10^{-7.8} \\ -0.175(\log(\dot{M}_{\text{He}}) + 5.35)^2 + 1.05 & \text{if } 10^{-7.8} < \dot{M}_{\text{He}} < 10^{-5.9} \\ 1 & \text{if } 10^{-5.9} < \dot{M}_{\text{He}} < 10^{-5.0} \\ 0 & \text{if } \dot{M}_{\text{He}} > 10^{-5.0} \end{cases} \quad (3.13)$$

where $\dot{M}_{\text{He}} = \eta_{\text{H}}\dot{M}_{\text{comp}}$.

3.A.2 Retention efficiencies based on RBF09

For the hydrogen retention efficiency two regimes can be distinguished, the nova regime and the wind regime, see Table 3.4. The stripping effect is not taken into account ($c_1 = 0$). In the hydrogen nova regime an interpolation of the results from Prialnik & Kovetz [1995] is used for η_{H} . The amount of mass transferred to the white dwarf is always equal to the amount of mass lost by the companion, $|\dot{M}_{\text{H}}| = |\dot{M}_{\text{comp}}|$.

TABLE 3.4: The two regimes for different mass transfer rates of the companion star, as in RBF09.

	\dot{M}_{comp} range
Nova regime	$ \dot{M}_{\text{comp}} < \dot{M}_{\text{cr}}$
Wind regime	$ \dot{M}_{\text{comp}} > \dot{M}_{\text{cr}}$

The critical mass transfer rate is given by:

$$\dot{M}_{\text{cr}} = 7.5 \cdot 10^{-7} \left(\frac{M_{\text{WD}}}{M_{\odot}} - 0.40 \right). \quad (3.14)$$

The hydrogen retention efficiency is:

$$\eta_{\text{H}} = \begin{cases} 0 & \text{if } |\dot{M}_{\text{comp}}| < 10^{-8} \\ 0.25(\log(|\dot{M}_{\text{comp}}|) + 8) & \text{if } 10^{-8} < |\dot{M}_{\text{comp}}| < 10^{-7} \\ 0.25 + 0.75(\log(|\dot{M}_{\text{comp}}|) + 7)/(\log(\dot{M}_{\text{cr}}) + 7) & \text{if } 10^{-7} < |\dot{M}_{\text{comp}}| < \dot{M}_{\text{cr}} \\ \dot{M}_{\text{cr}}/\dot{M}_{\text{H}} & \text{if } \dot{M}_{\text{cr}} < |\dot{M}_{\text{comp}}| < 10^{-4} \end{cases} \quad (3.15)$$

where

$$\frac{\dot{M}_{\text{cr}}}{\dot{M}_{\text{H}}} = \frac{\dot{M}_{\text{cr}}}{|\dot{M}_{\text{comp}}|}. \quad (3.16)$$

The helium retention efficiency is given by

$$\eta_{\text{He}} = \begin{cases} 0 & \text{if } \dot{M}_{\text{He}} < 10^{-7.3} \\ -0.175(\log(\dot{M}_{\text{He}}) + 5.35)^2 + 1.05 & \text{if } 10^{-7.3} < \dot{M}_{\text{He}} < 10^{-5.9} \\ 1 & \text{if } 10^{-5.9} < \dot{M}_{\text{He}} < 10^{-5.0} \\ 0 & \text{if } \dot{M}_{\text{He}} > 10^{-5.0} \end{cases} \quad (3.17)$$

where $\dot{M}_{\text{He}} = \eta_{\text{H}}\dot{M}_{\text{comp}}$. Note the similarity with the helium retention efficiency of NSK07, except for the lower limit of the mass transfer rate of the stable burning regime.

3.A.3 Retention efficiencies based on Y10

Two regimes can be distinguished for the hydrogen retention efficiency, the nova and wind regimes, see Table 3.5. The same interpolation from Prialnik & Kovetz [1995] is used for the hydrogen nova regime. The stripping effect is not taken into account ($c_1 = 0$). In all cases the amount of mass transferred to the white dwarf is equal to the amount of mass lost by the companion, $|\dot{M}_{\text{H}}| = |\dot{M}_{\text{comp}}|$. It is very similar to the retention efficiencies in Sect. 3.A.2, except that the prescription for \dot{M}_{cr} is different.

TABLE 3.5: The two regimes for different mass transfer rates of the companion star, as in Y10.

	\dot{M}_{comp} range
Nova regime	$ \dot{M}_{\text{comp}} < \dot{M}_{\text{cr}}$
Wind regime	$ \dot{M}_{\text{comp}} > \dot{M}_{\text{cr}}$

The prescription for the critical mass transfer rate is:

$$\dot{M}_{\text{cr}} = 10^{-9.31+4.12M_{\text{WD}}-1.42M_{\text{WD}}^2}. \quad (3.18)$$

The hydrogen retention efficiency is given by:

$$\eta_{\text{H}} = \begin{cases} 0 & \text{if } |\dot{M}_{\text{comp}}| < 10^{-8} \\ 0.25(\log(|\dot{M}_{\text{comp}}|) + 8) & \text{if } 10^{-8} < |\dot{M}_{\text{comp}}| < 10^{-7} \\ 0.25 + 0.75(\log(|\dot{M}_{\text{comp}}|) + 7)/(\log(\dot{M}_{\text{cr}}) + 7) & \text{if } 10^{-7} < |\dot{M}_{\text{comp}}| < \dot{M}_{\text{cr}} \\ \dot{M}_{\text{cr}}/\dot{M}_{\text{H}} & \text{if } \dot{M}_{\text{cr}} < |\dot{M}_{\text{comp}}| < 10^{-4} \end{cases} \quad (3.19)$$

with

$$\frac{\dot{M}_{\text{cr}}}{\dot{M}_{\text{H}}} = \frac{\dot{M}_{\text{cr}}}{|\dot{M}_{\text{comp}}|}. \quad (3.20)$$

The helium retention efficiency is:

$$\eta_{\text{He}} = \begin{cases} 0 & \text{if } \dot{M}_{\text{He}} < 10^{-7.5} \\ \frac{\dot{M}_{\text{He}}}{10^{-5.75}} & \text{if } 10^{-7.5} < \dot{M}_{\text{He}} < 10^{-5.7} \\ 0.95 & \text{if } 10^{-5.7} < \dot{M}_{\text{He}} < 10^{-5.4} \\ \frac{10^{-5.45}}{\dot{M}_{\text{He}}} & \text{if } 10^{-5.4} < \dot{M}_{\text{He}} < 10^{-4.0} \\ 0 & \text{if } \dot{M}_{\text{He}} > 10^{-4.0} \end{cases} \quad (3.21)$$

where $\dot{M}_{\text{He}} = \eta_{\text{H}}\dot{M}_{\text{comp}}$.

THE INFLUENCE OF MASS-TRANSFER VARIABILITY ON THE GROWTH OF THE MASS OF WHITE DWARFS IN ACCRETING SYSTEMS

S. Toonen, R. Voss, C. Knigge
will be submitted to MNRAS

Abstract

White dwarfs can increase their mass by accretion from companion stars, provided the mass accretion rate is high enough to avoid unstable nuclear burning. Unstable burning manifests itself in nova eruptions, in which most or all of the accreted mass is lost from the binary. The accretion regimes that allow growth of the white dwarfs are usually calculated assuming constant mass-transfer rates. However, it is possible that the type Ia supernova progenitor systems are influenced by effects that cause the mass-transfer rate to fluctuate on various timescales. We investigate how long-term mass-transfer variability affects accreting white dwarfs systems. We show that, if such variability is present, it expands the parameter space of binaries where the white dwarf can effectively increase its mass through accretion. The variability allows binaries with lower average accretion rates to grow compared to the standard scenario without variability, because the variability allows them to spend part of the time at accretion rates where hydrogen burns stably on their surface. As an example, we study the effect of mass-transfer variability on the rate of

type Ia supernovae (SNIa) in the single-degenerate channel. We find that the SNIa rate is enhanced by a factor 2-3 to a rate that is comparable with the lower limit of the observed rates. Due to the enhancement in the effective mass retention efficiency, the parameter space of white dwarf binaries that evolve to SNIa significantly widens, however, few initial binaries evolve into this parameter space. The changes in the delay time distribution allow for more type Ia supernovae from the single degenerate channel in stellar populations with ages of a few Gyr. Mass-transfer variability is also likely to affect other binary populations through enhanced growth of the white dwarf. For example, it may explain why white dwarfs in cataclysmic variables are observed to be more massive than single white dwarfs, on average.



4.1 introduction

White dwarfs (WDs) in binaries can accrete from their companion stars. Such binaries are called cataclysmic variables (CVs) if the donor stars are low-mass main-sequence stars, symbiotic binaries (SBs) if they are evolved red giants, or AM CVNs if the donor stars are low-mass Helium WDs or Helium stars. For CVs and SBs, the matter accreted by the WD consists mainly of hydrogen. As the matter piles up on the surface of the WD, it eventually reaches temperatures and densities high enough for nuclear burning.

The burning can proceed in two ways, depending on the accretion rate and the mass of the WD. For high accretion rates and WD masses, the hydrogen burning on the surface of the WD is continuous [Whelan & Iben, 1973; Nomoto, 1982], whereas for low accretion rates and WD masses the hydrogen is burned in thermo-nuclear runaway novae [Schatzman, 1950; Starrfield et al., 1974]. In general, the high mass-transfer rates needed for continuous surface hydrogen burning can only be reached by SBs, where high mass-transfer rates can be driven by the expansion of the evolved star and by systems with main-sequence donors more massive than the accreting WDs [Nomoto et al., 2000]. The masses of WDs with high accretion rates can grow effectively, but at very high accretion rates close to the Eddington limit, the growth of the white dwarf is limited. At these rates a hydrogen red-giant-like envelope forms around the WD and hydrogen burning on top of the WD is strong enough for a wind to develop from the WD [Kato & Hachisu, 1994; Hachisu et al., 1996]. On the other hand, at low accretion rates mass accretion onto the WD is not very efficient either, as the nova eruptions ejects some or all of the accreted matter from the binary system, possibly along with some of the surface material of the WD itself [e.g. Prialnik

& Kovetz, 1995]. The average mass-transfer rate allowing growth of the white dwarf is therefore limited to a relatively narrow range ($\sim 10^{-7} - 10^{-6} M_{\odot} \text{ yr}^{-1}$).

The growth of WD masses can have important consequences. In the single-degenerate (SD) scenario for type Ia supernova (SNIa) progenitors [Whelan & Iben, 1973; Nomoto, 1982] the accretion onto a carbon-oxygen WD pushes the mass above the critical mass limit for WDs (close but not equal to the Chandrasekhar limit) which then explodes as a SNIa. In this scenario, it is necessary for the WD to retain several tenths of solar masses of accreted material. It is not possible to achieve such mass growth for the majority of systems with mass-transfer rates in the nova regime, even if some of the accreted matter is retained. Following this theory, the rate and delay time distribution (DTD, evolution of the rate as a function of time after a single star formation episode) can be estimated using population synthesis models [e.g. Yungelson et al., 1994; Han et al., 1995; Han & Podsiadlowski, 2004; Yungelson, 2005; Bogomazov & Tutukov, 2009; Ruiter et al., 2009b; Mennekens et al., 2010; Wang et al., 2010; Meng et al., 2011; Toonen et al., 2012; Bours et al., 2013] While there currently is no consensus between the models as to the shape of the DTD [Nelemans et al., 2013; Bours et al., 2013], the majority of models agree on two problems: 1) There are not enough systems with high mass-transfer rates to account for all the observed SNeIa, and 2) after an age of $\sim 6 - 7$ Gyr, it is not possible to create SNIa explosions through this scenario, as only low-mass donors remain.

The considerations above apply to systems where the mass-transfer rate is given by the evolutionary state of the system, i.e. two binaries with the same parameters will have the same mass-transfer rate. Observations of accreting WD systems indicates that the long-term average mass-transfer rates do indeed follow the expectations [e.g. Knigge et al., 2011]. However, it is possible that the mass-transfer rates are highly variable on intermediate timescales [Patterson, 1984; Verbunt, 1984; Warner, 1987; Hameury et al., 1989]. In this paper, we discuss such variability and show that it affects the evolution of accreting WD systems. In particular, the effects can be of high importance for understanding SD SNIa progenitors, as it increases the volume of the parameter space of systems that can explode as SNeIa.

4.2 Mass-transfer variability

Over the past decades there have been many studies discussing the theoretical and observational aspects of mass-transfer variability in WD binaries. Below we shortly review the current knowledge in order to construct models that capture the main effects of the possible variability. For a thorough review, see Knigge et al. [2011], section 4.

4.2.1 Theoretical considerations

In the majority of accreting WD binaries (excepting strongly magnetic WDs with low accretion rates), hydrogen rich matter is accreted through an accretion disk that deposits the matter onto the surface of the white dwarf. The matter quickly spreads over the surface of the white dwarf. What then happens depends on the rate of accretion and the resulting temperature and density structure near the surface of the white dwarf [Nomoto, 1982; Nomoto et al., 2007; Shen & Bildsten, 2007]. At low accretion rates the temperature of the white dwarf surface remains low and the accreted hydrogen burns in an unstable manner, leading to nova eruptions that eject most (if not all) of the accreted matter. At high accretion rates the hydrogen burning is stable and the matter remains on the WD, except if the accretion rate is so high (\sim the Eddington limit) that most of the matter cannot be retained by the WD.

For the fate of the accreted matter in a system with mass-transfer variability to be different for a similar system without variability, the timescale must neither be too long, nor too short. If it is too long, it will affect binary properties, such as the radius of the donor star, that depend on the average long-term mass-transfer rate. This would be observable and would also change the whole evolution of the binary [see e.g. Knigge et al., 2011]. On the other hand, if the timescale of the variability is too short, the surface temperature of the white dwarf will not adjust to the instantaneous mass-transfer rate, which is necessary for the burning to be affected.

For example, in the accretion disk instability model [e.g. Osaki, 1996; Lasota, 2001], the mass transfer rate is increased by a factor of $\sim 10^3 - 10^5$ during outbursts (observed as dwarf novae), and this model has been invoked to stabilize the hydrogen burning [King et al., 2003; Alexander et al., 2011]. However, in this model, the accretion rate is only high for a very short time, and the heat and density of the accreted layer is not raised enough during the outburst to ignite [Tout, 2005], as also evidenced by the lack of hydrogen burning events triggered by dwarf novae. The layer will therefore build up without a significant temperature increase, and when burning eventually is ignited, it will be unstable and therefore lead to a nova eruption¹.

Another example regards nova outbursts. After the eruption, the temperature of the white dwarf will be increased, and it is possible that for some time the burning can be stable. Such short-lived stable surface burning triggered by nova eruptions is seen in some systems [see Schaefer & Collazzi, 2010, and Sect.4.2.2], but radiation losses during the quiescent periods will quickly cool the WD down into the unstable burning regime.

Therefore, if mass-transfer variability is to significantly change the surface burning, the

¹The effect of the instability of accretion discs on the SNIa rate has been studied by Wang et al. [2010] with a model similar to our model CONST. If stable burning can be maintained, the SNIa rate is increased by a factor 2-3 compared to a model without mass-transfer variability. Note that while the effect on the SNIa rate is similar to our findings, the model that we assume (model NORM-MAX) is different.

timescale of the mass-transfer fluctuations must at least be longer than the timescale of the nova and dwarf novae eruptions. In this case a continuous high accretion rate after an eruption ensures that the temperature on the surface of the WD is sufficient such that the nuclear burning continues. Therefore only the variability of the rate of matter being transferred from the companion star to the WD accretion disk can be of importance to the growth of the WD (and not the variability of the transfer from the disk to the WD). Such a variability can be achieved in two ways, either through the change in the radius of the companion star, or through a change in the size of its Roche-lobe [see e.g. Knigge et al., 2011].

One way that long-term variability can be induced is through irradiation of the donor star from the accreting WD that heats the envelope of the donor star and causes it to expand slightly. An increase in the mass-transfer rate leads to stronger irradiation and therefore expansion of the donor star, whereas a decrease leads to weaker irradiation and contraction. If the effects are strong enough, the mass transfer becomes unstable on long timescales, and the system will go through so-called irradiation-induced mass-transfer cycles [IMC, Podsiadlowski, 1991; Hameury et al., 1993; King et al., 1996; Büning & Ritter, 2004]. In this theory, the mass-transfer rate is through a series of cycles on Myr timescales, with an “off” state where there is little or no accretion, and an “on” state, where the mass-transfer rate slowly increases towards a peak, and then decreases until returning to the “off” state. Büning & Ritter [2004] find that the parameter space of WD binaries that are susceptible to IMCs is highly uncertain. CVs that are most likely to be affected have relatively massive ($\sim 1M_{\odot}$) main-sequence or somewhat evolved donors with convective envelopes. Giant donors are unlikely to be affected significantly because the radius variations caused by the irradiation are small compared to the radial evolution of the envelope and the reaction to mass loss.

Another way to achieve long term mass-transfer variability is from episodic mass loss from the binary which can cause cyclic variations of the Roche-lobe radius. CVs naturally experience such mass loss events when they erupt as novae [Shara et al., 1986; MacDonald, 1986]. If the angular momentum loss is high compared to the mass loss, the orbit will contract in response to the nova eruption, whereas the orbit will widen if the angular momentum loss is low compared to the mass loss. The effects of this process are therefore most likely stronger in systems with extreme mass ratios, where the specific angular momentum of the two stars is very different.

4.2.2 Observations

The mass-transfer cycles discussed above are difficult to study observationally, as the timescales are longer than the time we have been able to monitor CVs. A useful method is by comparing systems with similar properties, as they would be expected to also have similar mass-transfer rates. Townsley & Gänsicke [2009] used the effective temperatures of

the WDs to trace the mass accretion rates. The seven non-magnetic CVs above the period gap show a large scatter in WD effective temperature and inferred mass-transfer rate, and this might be evidence for mass-transfer variability. Below the period gap, the mass transfer differences found by Townsley & Gänsicke [2009] are much smaller, and a similar result is found by Patterson [2009] using time-averaged accretion disk luminosities. The co-existence of dwarf novae and novae-likes at the same orbital periods adds to the case of weak mass-transfer variability below the period gap, but the evidence is not compelling.

The recurrent nova T Pyx might provide evidence for mass-transfer variability on its own. At a period of 1.83 h [Patterson et al., 1998; Uthas et al., 2010] it is clearly below the period-gap and should therefore be faint with a low mass accretion rate. However, it is observed as a recurrent nova with a very high quiescent temperature, luminosity and change in orbital period, implying an accretion rate $> 10^{-8} M_{\odot} \text{ yr}^{-1}$, two orders of magnitude above ordinary CVs at this period. Most likely the system is in a transient evolutionary state. Schaefer & Collazzi [2010] suggest that it was an ordinary CV until it erupted as a nova in 1866. This eruption triggered a wind-driven supersoft X-ray phase, resulting in an unusually high luminosity and accretion rate [Knigge et al., 2000]. The recurrence time of the nova eruptions of T Pyx has increased, and Schaefer & Collazzi [2010] argue that the state is not self-sustaining. According to them the mass-transfer rate has decreased from about $10^{-7} M_{\odot} \text{ yr}^{-1}$ after the first nova eruption in 1866 to the current rate of about $10^{-8} M_{\odot} \text{ yr}^{-1}$. It is therefore likely that it will cease being a recurrent nova in the near future and return to the population of faint CVs.

The mass distribution of the white dwarf components in CVs may indicate at mass transfer variability as well. Contradicting the standard model of CV evolution [see also Zorotovic et al., 2011b], white dwarfs in CVs are significantly more massive than single white dwarfs [e.g. Warner, 1995; Savoury et al., 2011]. If long-term mass-transfer cycles occur in CVs, the masses of the white dwarf components could be significantly enhanced.

4.3 Model

4.3.1 Mass-transfer variability

From Sect. 4.2 we conclude that there are both theoretical and observational support for long-term mass-transfer variability in accreting WD binaries. To understand the effects of the mass-transfer variability on the growth of white dwarfs we need to model it. However, the observational evidence hardly constrain the theoretical models which rely on highly uncertain parameters [e.g. Büning & Ritter, 2004]. Here our main goal is to understand whether the effects of the variability are important, should such variability exist, rather than studying in detail the effects of a particular theoretical model. We therefore set up a number of toy models according to the following considerations: The mass-transfer rate cycles between two separate states, “on” and “off”, with a duty cycle $\alpha < 1$ representing

the fraction of the time the source spends in the “on” state. In mathematical terms, $\bar{R}_{\text{MT}} = \alpha \bar{R}_{\text{on}} + (1 - \alpha) \bar{R}_{\text{off}}$, where \bar{R}_{MT} is the average long-term mass-transfer rate, \bar{R}_{on} the average mass transfer rate in the “on” state, and \bar{R}_{off} the average mass transfer rate in the “off” state.

In most variability models, the stars do not fill their Roche-lobe in the “off”-state, either because the stars shrink, or the orbit expands, and binary models show dramatic drops in the mass-transfer rate when this happens. We therefore assume that all of the accretion takes place in the “on” state. Even if mass transfer in the “off” state only drops by a factor of $f \approx 10$ below the average mass-transfer rate (i.e. $\bar{R}_{\text{off}} = \bar{R}_{\text{MT}}/f$), the fraction of mass transferred in this state will be $(1 - \alpha)/f$ and will therefore only change our results at the percentage level.

The behaviour in the “on” state is probably different from system to system, but to retain the *average* long-term mass-transfer rate \bar{R}_{MT} , the average mass transfer rate in the “on” state must be $\bar{R}_{\text{on}} = \frac{\bar{R}_{\text{MT}}}{\alpha} \cdot (1 - \frac{1-\alpha}{f}) \simeq \bar{R}_{\text{MT}}/\alpha$. We employ two model types: (model CONST) a constant mass-transfer rate, representing systems that quickly attain and keep their peak rate, and (model NORM) a lognormal probability distribution (with a standard deviation σ_e given in base e), representing systems with a gradual increase (or decrease) of the mass transfer rate, as is typically seen in the IMC scenario. Examples of these models are shown in Fig. 4.1, showing the fraction of time that a system with an average mass-transfer rate of $\bar{R}_{\text{MT}} = 2.0 \times 10^{-9} M_{\odot} \text{ yr}^{-1}$ will spend at different accretion rates.

Also shown in Fig. 4.1 is a model (model NORM-MAX), in which there is a maximum accretion rate that the systems can reach. The reason for this is that the models for hydrogen surface burning have a critical mass \dot{M}_{crit} , above which mass is accreted too fast. The luminosity of the hydrogen burning at \dot{M}_{crit} is similar to the Eddington luminosity, and it is normally assumed that the surplus is ejected in the form of a wind [Hachisu et al., 1996] or at very high accretion rates it piles up as “red giant” envelope. The wind density will be high enough to obscure the X-rays from the hydrogen burning. As this irradiation is necessary to keep the mass-transfer rate high in the IMC scenario, the rate is unlikely to exceed \dot{M}_{crit} for long. For our lognormal model we therefore redistribute the parts of the probability density function above \dot{M}_{crit} to lower mass-transfer rates, modifying the function to retain the average mass-transfer rate. For model NORM-MAX it is per definition not possible to construct models with $\alpha \leq \bar{R}_{\text{MT}}/\dot{M}_{\text{crit}}$ as too much time is spent at low accretion rates to reach \bar{R}_{MT} . For these models we therefore gradually increase the duty cycle so $\alpha = \bar{R}_{\text{MT}}/\dot{M}_{\text{crit}}$ when necessary.

We furthermore assume that for mean mass-transfer rates in the classical hydrogen burning regime ($> \text{few times } 10^{-7} M_{\odot} \text{ yr}^{-1}$) the variability disappears. In almost all systems with such high mass transfer rates, the mass transfer is transferred on the thermal timescale of the donor star, which is shorter or comparable to the timescale of the mass-transfer cycles (i.e. the star does not have the time to adjust to the heating before the heated layers are lost).

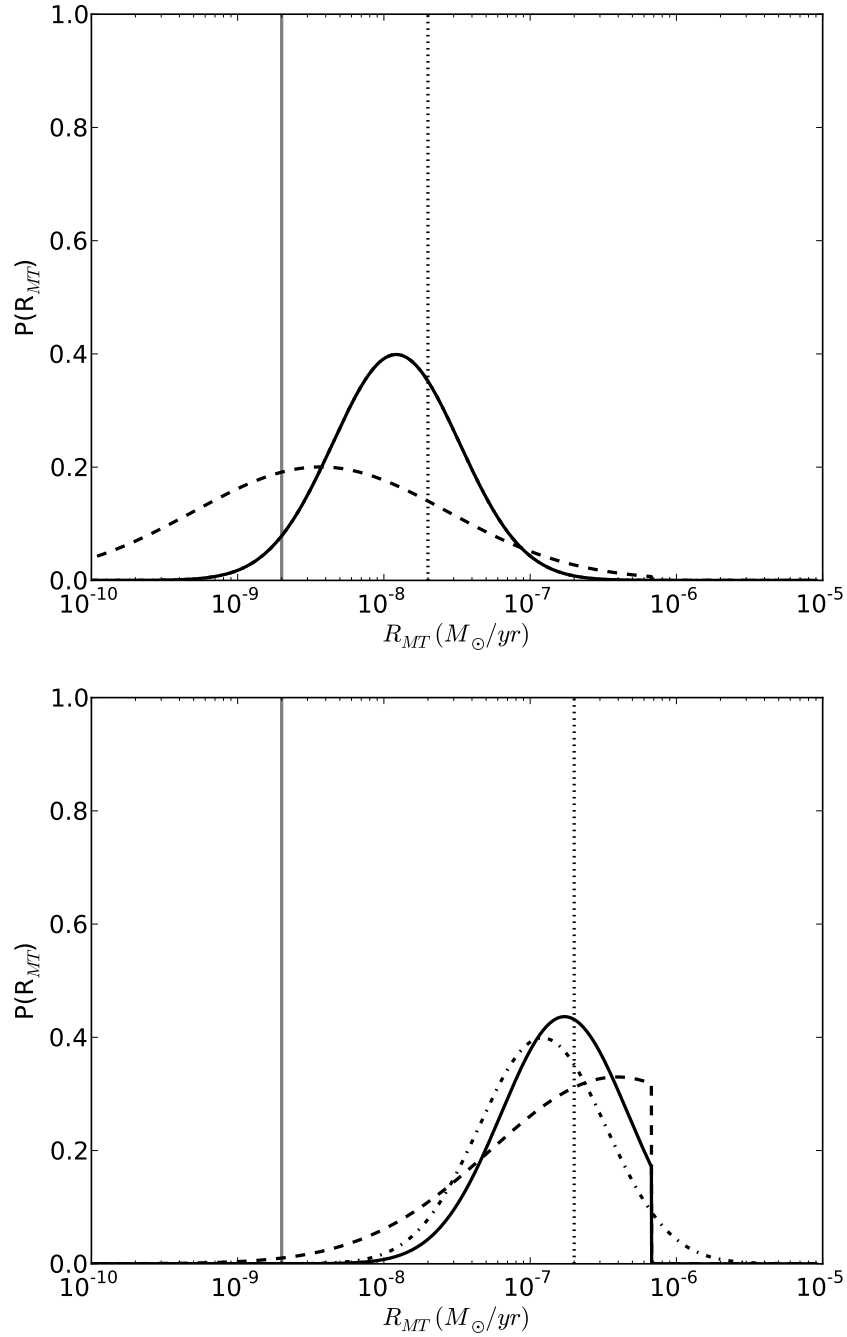


FIGURE 4.1: Example of the mass-transfer variability models, for an average mass-transfer rate of $\bar{R}_{MT} = 2.0 \times 10^{-9} M_{\odot} \text{ yr}^{-1}$ (grey line). The lines show the fraction of time that the system will stay at a given mass-transfer rate in the “on” state for each of the models. The black lines indicate models with duty cycles of $\alpha = 0.1$ on the top and $\alpha = 0.01$ on the bottom. The dotted line is model CONST, the dash-dotted line is model NORM with $\sigma_e = 1$, and the solid line model NORM-MAX with $\sigma_e = 1$. The dashed line is also model NORM-MAX with with a larger spread $\sigma_e = 2$.

4.3.2 Integrated retention efficiency

The retention efficiency η is the fraction of mass transferred that is retained by the WD. This is the fraction of hydrogen that is burned stably into helium *and* where the helium is also burned stably. The fraction of mass η that is retained depends on the mass of the WD and on the accretion rate. We estimate η based on Nomoto [1982]; Nomoto et al. [1984, 2007]; Hachisu et al. [2008]. These estimates takes a wind driven from the white dwarf and the stripping effect on the companion star into account. We assume that for low accretion rates the retention factor is $\eta \leq 0$, corresponding to a net loss of mass from the white dwarf, with values estimated from Prialnik & Kovetz [1995]. The model is shown in Fig. 4.2, where the final retention efficiency as a function of the mass-transfer rate is shown as the grey line. We use this model in the following analysis, but we caution that the theoretical models that this is based on are calculated assuming constant accretion rates. As discussed above, the properties of the WD (in particular the temperature) depend on the accretion history, therefore it is not clear if these models are accurate for systems with variable accretion rates. However, we note that in the irradiation-induced mass-transfer scenario, the change in the mass-transfer rate is slow enough (timescales of Myr) that the assumption of a constant mass-transfer rate is likely to be justified.

If we know the retention efficiency as a function of the mass-transfer rate, R_{MT} , we can find the effective retention factor for a given *mean* mass-transfer rate \bar{R}_{MT} for each of the models:

$$\eta_{\text{eff}} = \frac{\int_0^\infty p(R_{\text{MT}}) \cdot R_{\text{MT}} \cdot \eta(R_{\text{MT}}) dR_{\text{MT}}}{\bar{R}_{\text{MT}}} \quad (4.1)$$

where $p(R_{\text{MT}})$ is the model probability of a given mass-transfer rate R_{MT} .

Figure 4.2 shows the results of applying Eq. 4.1 to the examples of the mass-transfer models. By construction, all of the models conform to the shape given in by the grey line in Fig. 4.2 in the stable burning regime (with mass-transfer rates of a few times $10^{-7} M_\odot$ to \dot{M}_{crit}), where we assume that there is no variability. Below this range the models with mass-transfer cycles clearly distinguish themselves from the model without, as they are able to retain a significant fraction of the accreted mass at much lower mean accretion rates $\sim \alpha \cdot 10^{-7} M_\odot \text{yr}^{-1}$, irrespective of the details of the model. The differences between the models are easily understood: model CONST corresponds to a simple shift of the average mass-transfer rate by a factor $1/\alpha$, and the retention curve is therefore keeping its narrow shape, whereas model NORM both shifts the curve and broadens it due to the lognormal variability. The maximum is shifted slightly downwards for this model, due to the difference between the mean and the median of a lognormal model. Both curves display local minima in the retention curves near $\bar{R}_{\text{MT}} \sim 10^{-7} M_\odot \text{yr}^{-1}$, because above this value the peaks of the mass-transfer cycles are located above \dot{M}_{crit} . As we argue above, this is probably not realistic due to the obscuration of the X-rays from the white dwarf surface at these high accretion rates. Most likely the systems that have accretion rates in this range ($\sim 10^{-8}$ to $\sim 10^{-7}$ in Fig. 4.2) will either have higher duty cycles (the depressions only appear for

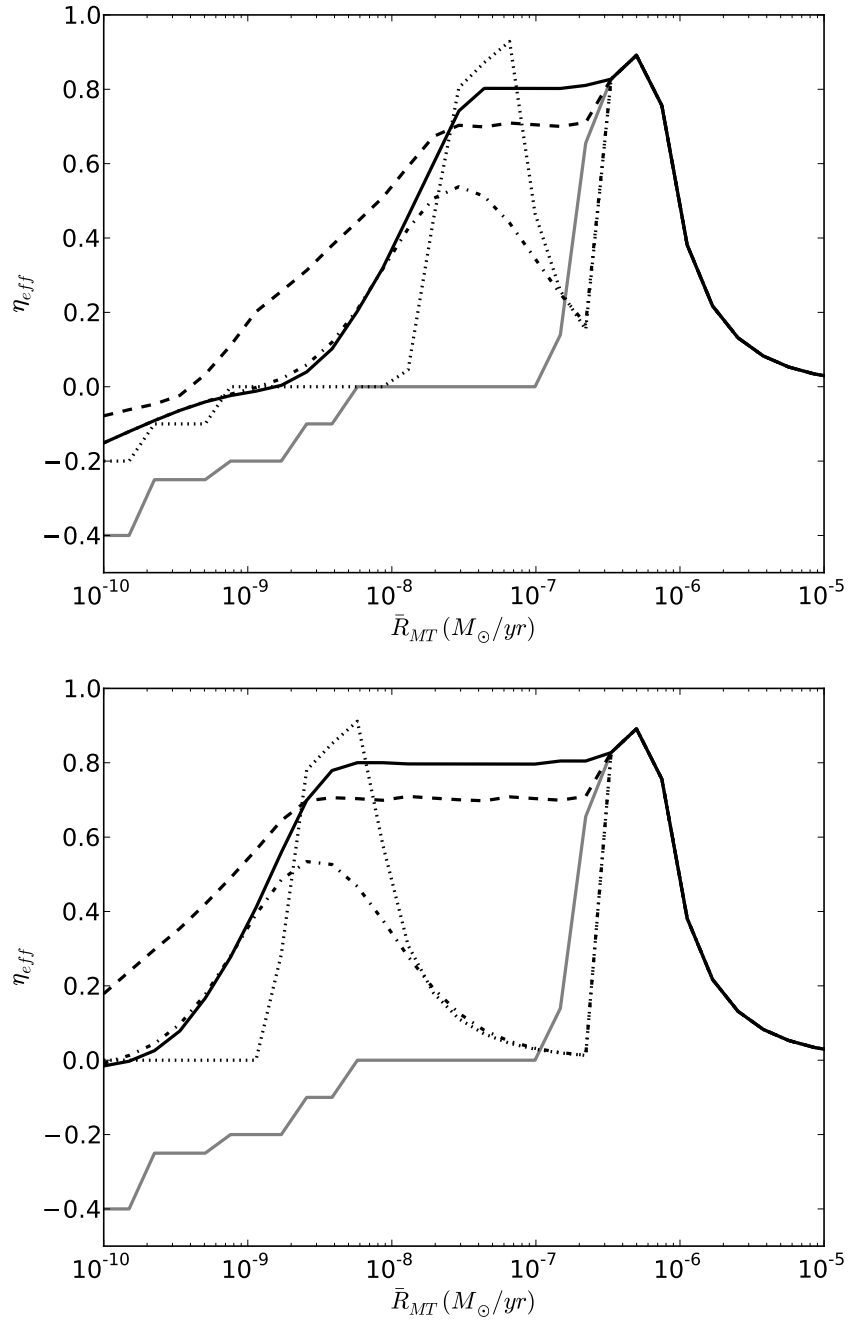


FIGURE 4.2: Effective retention efficiency as a function of average mass-transfer rate for different variability models (black lines) for a $1.3M_{\odot}$ WD accretor. Model CONST is shown as a dotted line and model NORM with $\sigma_e = 1$ is shown as the dash-dotted line. The solid and dashed lines are model NORM-MAX with $\sigma_e = 1$ and $\sigma_e = 2$ respectively. On the top models with a duty cycle of $\alpha = 0.1$ and on the bottom $\alpha = 0.01$. The grey line shows a model without mass-transfer variability.

duty cycles $\alpha \lesssim 0.1$) and/or lower peak accretion rates than assumed, and will therefore also retain much of the accreted mass. Indeed in model NORM-MAX where accretion is not allowed to exceed \dot{M}_{crit} , the retention efficiency stays high in this accretion range.

For models NORM and NORM-MAX the retention efficiency stays above zero well below $\bar{R}_{\text{MT}} = 10^{-9} M_{\odot} \text{ yr}^{-1}$, despite the systems spending more time in accretion states with negative retention efficiencies, because even if they only spend a short time at high R_{MT} , the fraction of mass accreted in this regime is still considerable. We believe that model NORM-MAX captures the behaviour of IMCs best, such as the ones modelled by Büning & Ritter [2004], because the formation of a WD envelope at high mass transfer rates is likely to quench the irradiation process (see also Sect. 4.3). We conclude that for all of the models the WDs can effectively grow down to average mass-transfer rates a factor of α lower than in the standard scenario without variability, irrespective of the specific shape of the variability (assuming that the mass-transfer rate does not exceed \dot{M}_{crit}).

4.4 Application to binary stellar evolution

Our models of mass-transfer cycles from Sect. 4.3 significantly modify and enhance the mass retention efficiency of accreting white dwarfs (see Fig. 4.2). This can have a significant effect on the characteristics of the population of accreting white dwarf binaries, e.g. the distribution of WD masses in cataclysmic variables. Furthermore, the growth of carbon-oxygen white dwarfs is important for understanding the rate of SNIa and their delay time distribution in the single-degenerate channel, which we study here as an example of the implications of mass-transfer variability.

In the traditional picture without variability, the systems that can become type Ia supernovae are distributed in two regions (“islands”) in the plane of the two parameters - orbital period and secondary mass - just after the formation of the WD [Li & van den Heuvel, 1997; Hachisu et al., 1999b; Li & van den Heuvel, 2002; Han & Podsiadlowski, 2004; Hachisu et al., 2008]. One of the islands consists of progenitors where the companion has evolved to a giant before commencing the mass transfer. As mentioned above, these systems are not likely to be susceptible to IMCs [Büning & Ritter, 2004]. The other island consists of main-sequence or slightly evolved donors. If the mass of the donor star is much higher than the white dwarf mass, the mass transfer will be dynamically or tidally unstable, leading to a merger of the two stars, leading to a natural upper mass limit to the island. The lower mass limit is determined by the fact that when the mass of the donor star comes near to the mass of the white dwarf, the mass transfer rate drops below the stable surface hydrogen burning limit. This typically happens around $1.5M_{\odot}$, and since the vast majority of CO WDs are born below $1M_{\odot}$, the initial mass of the donor star must be above $\sim 2M_{\odot}$.

In the models with mass-transfer variability it is possible to retain the matter accreted at lower mass-transfer rates. This will not affect the upper limit to the donor mass, since

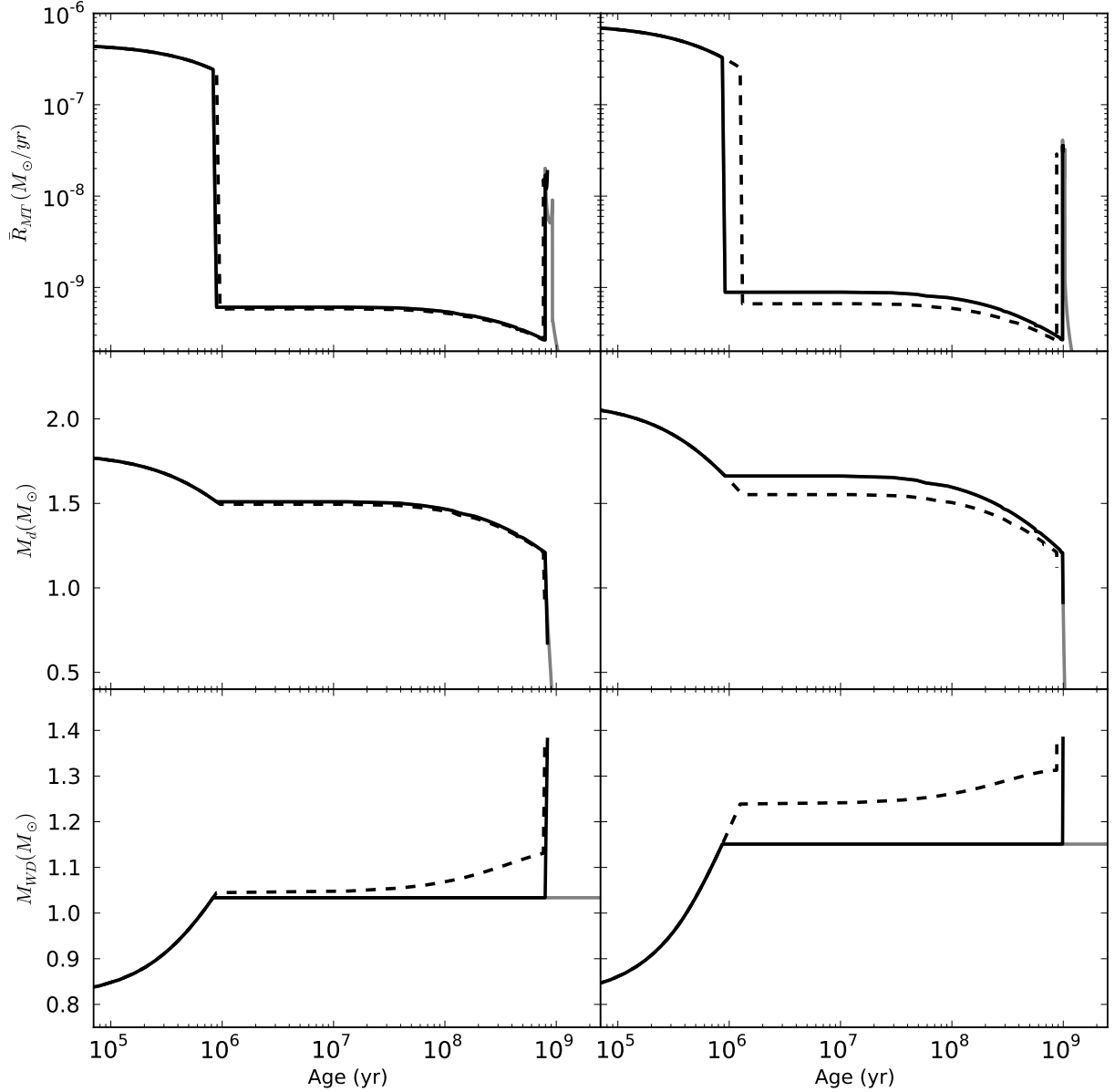


FIGURE 4.3: Binary tracks for two WD binaries starting mass transfer while the donor star is on the main sequence. The initial mass of the WD is $0.8M_{\odot}$, the initial orbital separation is $4.5R_{\odot}$, and the initial mass of the donor star is $1.8M_{\odot}$ (left) and $2.1M_{\odot}$ (right). The panels show the evolution of the (time-averaged) mass-transfer rate \bar{R}_{MT} (upper), the donor mass M_d (middle) and the WD mass M_{WD} (lower), for three different models: SeBa standard (grey solid), model NORM-MAX with $\alpha = 0.1, \sigma_e = 1$ (black solid) and model NORM-MAX with $\alpha = 0.01, \sigma_e = 1$ (black dashed).

4.4 APPLICATION TO BINARY STELLAR EVOLUTION

this limit is determined by the stability of mass transfer at high rates. However, the lower mass limit of the donor star is likely to be affected. Therefore an increased retention at low mass-transfer rates allows WDs in binaries with lower donor masses to grow, and therefore allows systems with lower initial donor masses to become type Ia supernovae.

The limits depend on the strengths and shape of the mass-transfer variability, but also on the evolution of the donor star and its reaction to the mass loss. To better understand what our results mean for the evolution of binaries with WDs, we have calculated binary evolutionary sequences with the binary population synthesis code SeBa [Portegies Zwart & Verbunt, 1996; Nelemans et al., 2001c; Toonen et al., 2012, Toonen & Nelemans, submitted]. Our goal is to understand how the possible long-term variability affects the evolution of accreting WD binaries that might become type Ia supernovae. We therefore compare evolutionary tracks computed with a standard SeBa model to tracks where the accretion efficiency has been modified by variability. The standard retention efficiency in SeBa is based on Nomoto [1982]; Nomoto et al. [1984, 2007]; Hachisu et al. [2008] [see the grey line in Fig. 4.2 and Bours et al., 2013, Eq. 5, A1-A5]. In the nova regime

$$\bar{R}_{\text{MT}} < \dot{M}_{\text{st}} = 3.1 \cdot 10^{-7} \left(\frac{M_{\text{WD}}}{M_{\odot}} - 0.54 \right) \quad (4.2)$$

with \dot{M}_{st} as given by Hachisu et al. [2008], the retention efficiency η of model NORM-MAX is additionally modified to:

$$\eta = \begin{cases} 0.8 & \text{if } \alpha \dot{M}_{\text{ST}} < \bar{R}_{\text{MT}} < \dot{M}_{\text{ST}} \\ 0.8(\log(\bar{R}_{\text{MT}}) - \log(\alpha \dot{M}_{\text{ST}})) & \text{if } 0.1\alpha \dot{M}_{\text{ST}} < \bar{R}_{\text{MT}} < \alpha \dot{M}_{\text{ST}} \\ 0 & \text{if } \bar{R}_{\text{MT}} < 0.1\alpha \dot{M}_{\text{ST}} \end{cases} \quad (4.3)$$

As can be seen from Fig. 4.2, other variability models might give somewhat smaller effects if the peak accretion rate is not limited. For each model, we make the simplifying assumption that the effective retention η_{eff} only depends on \bar{R}_{MT} and the mass of the WD, i.e. that the shape and strength of the IMCs are the same irrespective of the properties of the donor star. This is clearly unrealistic. However, the goal of our study is to understand *if* the variability is likely to impact the SNIa population properties, and to indicate what the possible effects might be, and the assumption is sufficient for this.

In Fig. 4.3 we show the results of evolving two WD binaries with close main-sequence companions according to the standard SeBa model (grey solid lines) and model NORM-MAX with $\sigma_e = 1$, and $\alpha = 0.1$ (black solid lines) and $\alpha = 0.01$ (black dashed lines). The systems behave similarly after the initial contact, when the mass-transfer rate is high. When it drops below the standard surface burning regime, differences appear, not just in the WD growth (bottom panel), but also in the time-averaged mass-transfer rate itself (top panel). This is because the matter ejected from the system carries angular momentum, which can strongly affect the evolution of the binary orbit. Note that this is the only way

in which we allow the time-averaged mass transfer rate to vary in our models. Furthermore we assume that the matter that can not be accreted by the WD leaves the system with the specific orbital angular momentum of the WD.

The main point of Fig. 4.3 is that for both systems of the standard model the mass of the WD never reaches the critical explosion mass ($\sim 1.4M_{\odot}$, for this model the initial companion mass must be about $2.3M_{\odot}$ for the WD to reach this mass), whereas the variability models do reach the explosion mass.

4.5 Binary population Synthesis

In the previous sections we have shown that mass-transfer variability has the potential to significantly change the parameter space of initial WD binaries that can become type Ia supernovae, towards both lower-mass donor stars as well as lower-mass white dwarfs. To understand how this can affect the population of type Ia supernovae, we use the binary population synthesis (BPS) code SeBa [Portegies Zwart & Verbunt, 1996; Nelemans et al., 2001c; Toonen et al., 2012, Toonen & Nelemans, submitted] to model the evolution of SNIa progenitors according to different mass-transfer variability models.

In SeBa, stars are evolved from the zero-age main sequence (ZAMS) until remnant formation, and, at every timestep, processes such as stellar winds, mass transfer, angular momentum loss, magnetic braking and gravitational radiation are taken into account with appropriate recipes. The initial stellar population is generated with a Monte-Carlo approach according to appropriate distribution functions. Initial primary masses are drawn from $0.95\text{-}10M_{\odot}$ from a Kroupa IMF [Kroupa et al., 1993] and secondary masses from a flat mass ratio distribution between 0 and 1. The semi-major axis of the binary is drawn from a power law distribution with an exponent of -1 [Abt, 1983], ranging from 0 to 10^6R_{\odot} and the eccentricity from a thermal distribution, ranging from 0 to 1 [Heggie, 1975]. Furthermore, solar metallicities and a binary fraction of 50% are assumed.

The CE-phase [Paczynski, 1976] plays an essential role in binary evolution in the formation of close binaries with compact objects. Despite of the importance of the CE-phase and the enormous efforts of the community, we still do not understand the phenomenon in detail. To take into account the uncertainty in the CE-phase in our models, we differentiate between two CE-models. The canonical CE-formalism is the α_{CE} -formalism [Tutukov & Yungelson, 1979; Webbink, 1984] that is based on the energy budget of the binary system. The α_{CE} -parameter describes the efficiency with which orbital energy E_{orb} is consumed to unbind the CE, i.e.

$$\frac{GM_1M_{1,e}}{\lambda R} = \alpha_{\text{CE}}(E_{\text{orb,init}} - E_{\text{orb,final}}), \quad (4.4)$$

where M_1 , $M_{1,\text{env}}$ and R are the mass, envelope mass and radius of the donor star and λ is the envelope structure parameter [de Kool et al., 1987]. Based on the evolution of double WDs, [Nelemans et al., 2000] derives a value of $\alpha_{\text{CE}}\lambda = 2$, which we have assumed here.

TABLE 4.1: Time-integrated SNIa rates in the SD channel for different mass-transfer variability models and the common envelope prescriptions in units of $10^{-4}M_{\odot}^{-1}$.

	γ -prescription	α_{CE} -prescription
No variability	0.82	1.4
Model NORM-MAX ($\alpha = 0.1$)	1.6	3.2
Model NORM-MAX ($\alpha = 0.01$)	1.9	4.1
Observed	4– > 34 ¹	

NOTES: ¹ Maoz & Mannucci [2012b]; Perrett & et al. [2012]; Maoz et al. [2012]; Graur & Maoz [2013]

An alternative CE-prescription was introduced by Nelemans et al. [2000] in order to explain the observed distribution of double WDs systems. The γ -formalism of CE-evolution is based on the angular momentum balance. The γ -parameter describes the efficiency with which orbital angular momentum is used to expel the CE according to:

$$\frac{J_{\text{b,init}} - J_{\text{b,final}}}{J_{\text{b,init}}} = \gamma \frac{\Delta M_1}{M_1 + M_2}, \quad (4.5)$$

where J_{b} is the orbital angular momentum of the binary, and M_2 is the mass of the companion. We assume $\gamma = 1.75$ [Nelemans et al., 2001c]. Although assuming the γ -prescription in BPS codes leads to a significant improvement in the synthetic double WD population, the physical mechanism remains unclear. Recently Woods et al. [2010, 2012] proposed that double WDs can be formed by stable, non-conservative mass transfer between a red giant and a main-sequence star. The effect on the orbit is a modest widening, with a result not unlike the γ -description.

4.6 Results and discussion

Figure 4.4 and 4.5 shows the systems that become type Ia supernovae in the diagram of orbital period - donor mass at the birth of the WD. The solid line marks the theoretical region for the classical SD SNIa progenitors for a $1.1M_{\odot}$ WD [Hachisu et al., 2008, as approximated by Bours et al. 2013]. Taking into account the formation and evolution of the binary prior to the formation of the WD, Fig. 4.4a and 4.5a shows the distribution of classical SD SNIa progenitors according to SeBa. Most systems have low-mass donor stars and relatively long periods. Furthermore most systems lie in or close to the marked region of Hachisu et al. [2008], where differences occur by different assumptions for the mass-transfer rate and the (dynamical) stability of mass transfer. Figure 4.4b and 4.5b show how the parameter space of systems that can become type Ia supernovae is extended for model NORM-MAX with a duty cycle of $\alpha = 0.1$, and Fig. 4.4c and 4.5c for a lower duty

cycle of $\alpha = 0.01$. These four figures show that the parameter space of SNIa progenitors extends to lower donor masses when mass-transfer cycles are taken into account.

The time-integrated number of SNIa events is about $10^{-4} M_{\odot}^{-1}$, see Table 4.1. When taking into account mass-transfer variability according to model NORM-MAX, the rate is increased by a factor of 2-2.3 and 2.3-2.9 for $\alpha = 0.1$ and $\alpha = 0.01$ respectively, compared to the standard model of non-variable mass-transfer rates. The DTDs (assuming a single burst of star formation at $t=0$) from all models show a strong decline with time (see Fig. 4.6). When mass-transfer variability is included in our simulations, the DTDs are affected at delay times from about 100Myr to a Hubble time. However, the shape of the DTDs has not changed significantly.

The effect of including mass-transfer variability on the SNIa rate is mild, even though the retention efficiency of WD accretion is greatly enhanced in our models. The extra number of systems that become SNeIa due to mass-transfer variability is limited, compared to the extra number of ZAMS systems that are born with secondaries in the extended mass range. Our study shows that the reason for this is that, as the mass of the secondary decreases, it becomes harder to create close binaries with massive WDs. As the initial binary mass ratio is higher for these systems, the orbital separation is decreased more during the first mass-transfer episode from the WD progenitor to the secondary star, and most of the lower-mass secondaries end up being too close to survive until the formation of the WD. Most of the systems that do survive experience Roche-lobe overflow from the WD progenitor (primary) when it has become a helium star, which significantly increases their donor mass and therefore decreases the evolutionary timescale. This speed-up means that they cannot explode as the very delayed supernovae that could be expected of low-mass secondaries, but rather on relatively short timescales below 1 Gyr.

From galaxy cluster measurements and cluster iron abundances, Maoz & Mannucci [2012b] and Maoz et al. [2010] find an observed integrated rate of $(18 - 29) \cdot 10^{-4} M_{\odot}^{-1}$ and $> 34 \cdot 10^{-4} M_{\odot}^{-1}$. Furthermore Maoz & Mannucci [2012b] finds that the delay time distribution that roughly follows a $\sim t^{-1}$ power-law shape. Neither the integrated rate and DTD from the standard model nor from the variability models are consistent with these observations. Recent measurements in volumetric surveys, however, have shown lower rates; $(4.4 \pm 0.2) - (5.0 \pm 0.2) \cdot 10^{-4} M_{\odot}^{-1}$ by Perrett & et al. [2012] [$(6 - 10) \cdot 10^{-4} M_{\odot}^{-1}$ when rescaling the Salpeter IMF to a diet-Salpeter IMF to account for the reduced number of low-mass stars Maoz et al., 2012], $(13 \pm 1.5) \cdot 10^{-4} M_{\odot}^{-1}$ by Maoz et al. [2012] and $(4 - 12) \cdot 10^{-4} M_{\odot}^{-1}$ by Graur & Maoz [2013]. It is unclear if the different observed integrated rates are due to systematic effects (for example overestimation of the cosmic star formation history or over-correction of dust extinction) or if there is a real enhancement of SNeIa in cluster galaxies [see also Maoz et al., 2012]. With these recent observations of the integrated rate, the long-standing problem of BPS studies predicting too low SNIa rates has diminished. The SNIa rates of our most optimistic models of low duty cycles are consistent with the lowest observed integrated rates, but the corresponding synthetic DTD shows a stronger

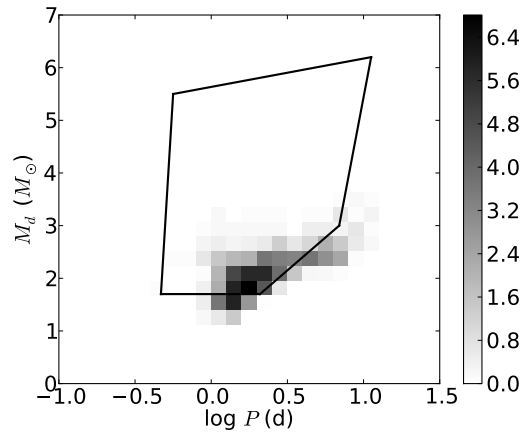
decline with time than the observed DTDs.

The increase in the SNIa rate in the mass-transfer variability models compared to the standard model is limited by the formation of close binaries with low mass companions, which is dependent on our understanding of binary evolution. A comprehensive comparison of four BPS codes (including SeBa, see Toonen et al. submitted) showed that differences between the predictions of BPS codes for low- and intermediate-mass stars are not caused by numerical effects in the codes, but by different assumptions for phases in stellar and binary evolution that are not understood well. When these assumptions are equalized, the synthetic populations of the four BPS codes are similar. Important assumptions (or uncertain processes) for the SD channel are the retention efficiency for WD accretion and common-envelope (CE) evolution [Bours et al., 2013, Toonen et al. submitted, Claeys et al. in prep.]. Bours et al. [2013] shows that the effect of different retention efficiencies can effect the SNIa rate by a factor 3-4 to even more than a factor 100, which explains for a large degree the large disagreement in the predictions of the SD SNIa rate by different BPS studies. Regarding the poorly understood common-envelope phase, we have shown that mass-transfer variability can effect the SNIa rate to a comparable degree as CE-evolution. Especially now that the gap between observed and synthetic SNIa rates has decreased, it is important to take uncertainties in binary evolution such as CE-evolution and mass-transfer variability into account.

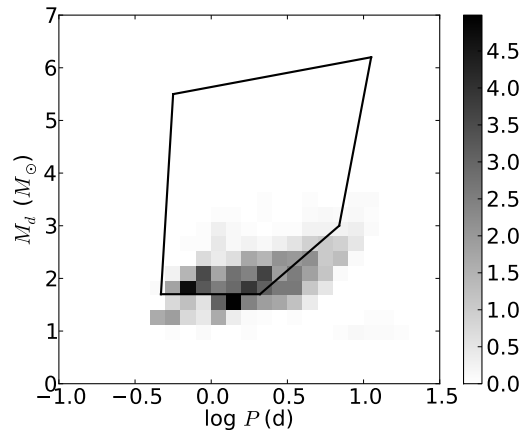
4.7 Conclusions

We have studied the effect of mass-transfer variability on accreting WDs in binary companion stars. Long-term mass-transfer variability can be induced by e.g. irradiation of the donor star by the accreting WD or by cyclic variations of the Roche lobe from mass loss episodes [Knigge et al., 2011]. The timescale of the variability should be longer than the thermal timescale of the non-degenerate surface layer of the WD so that the surface burning is affected. On the other hand, the timescale of the mass-transfer cycles should not be too long, such that the binary is not affected in any observable way (e.g. strong bloating of donor stars by irradiation). Currently observations hardly constrain the theoretical models of mass-transfer variability [e.g. Büning & Ritter, 2004] and therefore we have constructed a number of toy models rather than studying the details of a particular mass-transfer variability model. We show that long-term mass-transfer variability can significantly affect the accretion process and retention efficiency of mass-transfer towards WDs.

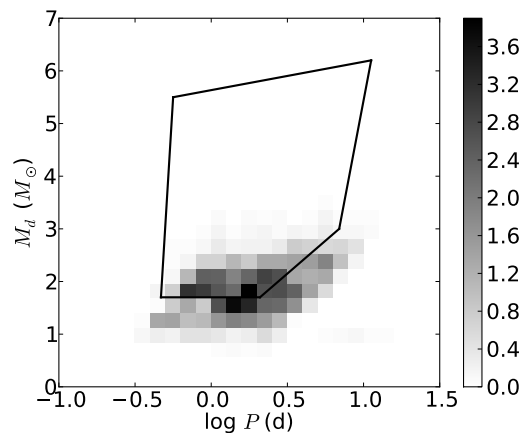
Mass-transfer variability and accompanying enhanced retention efficiencies is likely to impact the properties of accreting WD binaries. As an example, we study the evolution of SNIa progenitors from the single-degenerate channel. We find that if mass-transfer cycles take place, the parameter space of systems that become SNIa events is increased towards low mass donor stars. Furthermore we find that the integrated SNIa rate increases by a



(a)

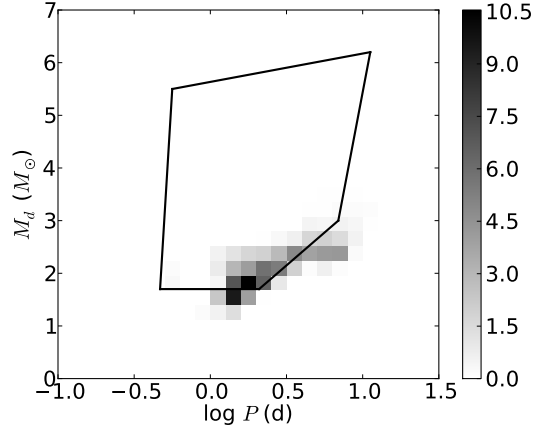


(b)

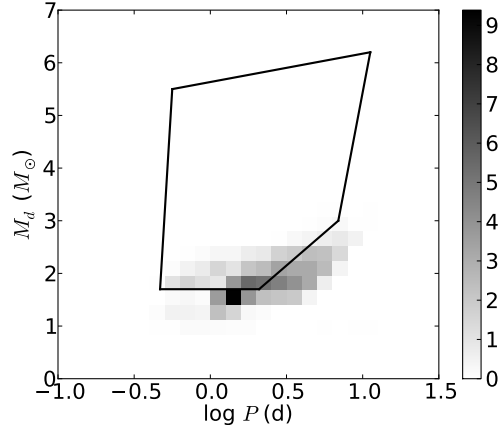


(c)

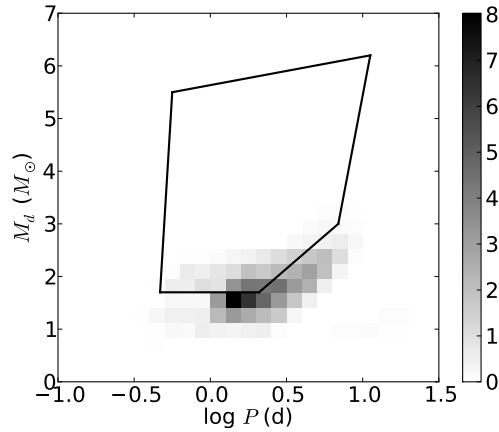
FIGURE 4.4: Donor mass vs. orbital period at WD formation for the SD SNIa progenitors assuming the γ -algorithm with $\gamma = 1.75$ for three different mass-transfer models. On the top a model without mass-transfer variability, in the middle model NORM-MAX with $\alpha = 0.1$ and on the bottom model iii with a duty cycle of $\alpha = 0.01$. The intensity of the grey scale corresponds to the density of objects on a linear scale. The solid lines mark the theoretical parameter region [Hachisu et al., 2008] for main-sequence and slightly evolved donor stars that transfer mass to a WD of $1.1M_{\odot}$.



(a)



(b)



(c)

FIGURE 4.5: Donor mass vs. orbital period at WD formation for the SD SNIa progenitors assuming the α_{CE} -algorithm with $\alpha_{\text{CE}}\lambda = 2$. On the top a model without mass-transfer variability, in the middle model NORM-MAX with $\alpha = 0.1$ and on the bottom model NORM-MAX with a duty cycle of $\alpha = 0.01$. The intensity of the grey scale corresponds to the density of objects on a linear scale. The solid lines mark the theoretical parameter region [Hachisu et al., 2008] for main-sequence and slightly evolved donor stars for a WD of $1.1M_{\odot}$.

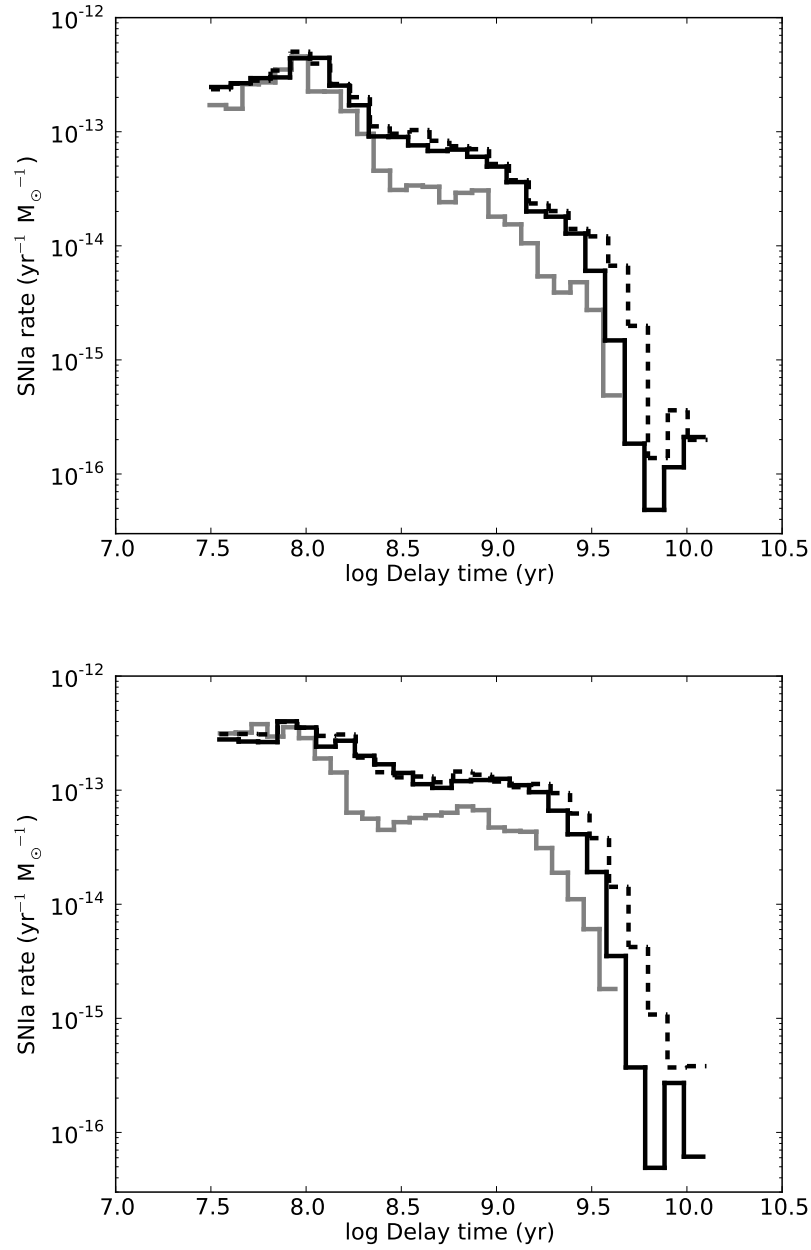


FIGURE 4.6: Delay time distribution of SNIa events from the SD channel for three different mass-transfer models. The black lines indicate model NORM-MAX with $\alpha = 0.1$ (solid) and $\alpha = 0.01$ (dashed). The grey line shows a model without mass-transfer variability. On the top assuming the γ -algorithm with $\gamma = 1.75$ and on the bottom assuming the α_{CE} -algorithm with $\alpha_{\text{CE}}\lambda = 2$.

factor of about 2-3, which is comparable with the lower limit of the observed rates [see Maoz & Mannucci, 2012b; Perrett & et al., 2012; Maoz et al., 2012; Graur & Maoz, 2013]. Variability models in which the maximum mass-transfer rate is not limited will affect the SNIa rate less.

Acknowledgements

We thank Gijs Nelemans for useful comments which helped us to improve the manuscript. This work was supported by the Netherlands Research Council NWO (VIDI grant number [#016.093.305] and [# 639.042.813]) and by the Netherlands Research School for Astronomy (NOVA).

SUPERNOVA TYPE IA PROGENITORS FROM MERGING DOUBLE WHITE DWARFS: USING A NEW POPULATION SYNTHESIS MODEL

S. Toonen, G. Nelemans, S. Portegies Zwart
Astronomy and Astrophysics, 2012, 546, A70

Abstract

The study of Type Ia supernovae (SNIa) has led to greatly improved insights into many fields in astrophysics, e.g. cosmology, and also into the metal enrichment of the universe. Although a theoretical explanation of the origin of these events is still lacking, there is a general consensus that SNIa are caused by the thermonuclear explosions of carbon/oxygen white dwarfs with masses near the Chandrasekhar mass. We investigate the potential contribution to the supernova Type Ia rate from the population of merging double carbon-oxygen white dwarfs. We aim to develop a model that fits the observed SNIa progenitors as well as the observed close double white dwarf population. We differentiate between two scenarios for the common-envelope (CE) evolution; the α -formalism based on the energy equation and the γ -formalism that is based on the angular momentum equation. In one model we apply the α -formalism always. In the second model the γ -formalism is applied, unless the binary contains a compact object or the CE is triggered by a tidal instability for which the α -formalism is used. The binary population synthesis code SeBa was used to evolve binary systems from the zero-age main sequence to the formation of double white dwarfs and subsequent mergers. SeBa has been thoroughly updated since the

last publication of the content of the code. The limited sample of observed double white dwarfs is better represented by the simulated population using the γ -formalism for the first CE phase than the α -formalism. For both CE formalisms, we find that although the morphology of the simulated delay time distribution matches that of the observations within the errors, the normalisation and time-integrated rate per stellar mass are a factor of about 7-12 lower than observed. Furthermore, the characteristics of the simulated populations of merging double carbon-oxygen white dwarfs are discussed and put in the context of alternative SNIa models for merging double white dwarfs.



5.1 Introduction

Type Ia supernovae (SNIa) are one of the most energetic explosive events known. They have been of great importance in many fields, most notably as a tool in observational cosmology. They have been used very successfully as standard candles on cosmological distance scales [e.g. Riess et al., 1998; Perlmutter et al., 1999], owing to the special property of great uniformity in the light curves [e.g. Phillips, 1993]. The SNIa also strongly affect the Galactic chemical evolution through the expulsion of iron [e.g. van den Bergh & Tammann, 1991]. Despite their significance Type Ia supernovae are still poorly understood theoretically.

Supernovae Type Ia are generally thought to be caused by thermonuclear explosions of carbon/oxygen (CO) white dwarfs (WDs) with masses near the Chandrasekhar mass $M_{\text{ch}} \approx 1.4M_{\odot}$ [e.g. Nomoto, 1982]. Various progenitor scenarios have been proposed. The standard scenarios can be divided into two schools of thoughts: the single-degenerate (SD) [Whelan & Iben, 1973] and double-degenerate (DD) scenario [Webbink, 1984; Iben & Tutukov, 1984]. In the SD scenario, a CO WD explodes as an SNIa if its mass approaches M_{ch} through accretion from a non-degenerate companion. In the DD scenario, two CO WDs can produce an SN Ia while merging if their combined mass is larger than M_{ch} .

However, observationally as well as theoretically, the exact nature of the SNIa progenitors remains unclear. The explosion mechanism is complex due to the interaction of hydrodynamics and nuclear reactions. Several models exist that vary for example between a detonation or deflagration disruption or vary between explosions at the Chandrasekhar mass or sub-Chandrasekhar masses [see e.g. Hillebrandt & Niemeyer, 2000, for a review]. It also remains unclear whether the DD and SD scenario both contribute to the SNIa rate or if one of the scenarios dominates. Both scenarios have problems in matching theories with observations. A serious concern about the DD scenario is whether the collapse of the remnant would lead to a supernova or to a neutron star through accretion-induced collapse

[see Nomoto & Iben, 1985; Saio & Nomoto, 1985; Piersanti et al., 2003; Yoon et al., 2007; Pakmor et al., 2010, 2012; Shen et al., 2012]. Although in the SD channel the models for the explosion process need to be fine-tuned to reproduce the observed spectra and light curves, an SNIa like event is more easily reproduced in the simulations of the explosion process. One problem with the SD scenario is that the white dwarfs should go through a long phase of supersoft X-ray emission, although it is unclear if there are enough of these sources to account for the SNIa rate [see Di Stefano, 2010; Gilfanov & Bogdán, 2010; Hachisu et al., 2010]. Moreover archival data of known SNIa have not shown this emission unambiguously, but there is may be one case [see Voss & Nelemans, 2008; Roelofs et al., 2008; Nielsen et al., 2010]. Furthermore, SNIa that take place more than a few 10^9 years after the starburst [see e.g. Maoz et al., 2010] are hard to create in this channel [e.g. Yungelson & Livio, 2000; Han & Podsiadlowski, 2004].

To use SNIa as proper standard candles, we need to know what SNIa are, when they happen and what their progenitors are. Therefore, we study the binary evolution of low- and intermediate mass stars. In a forthcoming paper (Bours, Toonen & Nelemans, in preparation) we study the SD-scenario by looking into the poorly understood physics of accretion onto white dwarfs. In this paper we focus on the DD scenario and the effect of the as yet very uncertain phases of common-envelope (CE) evolution on the double white dwarf (DWD) population. These DWD systems are interesting sources for studying various phases of stellar evolution, in our case the CE evolution. Gravitational wave emission is also important as this affects the binary system by decreasing the orbital period and eventually leading to a merger [Kraft et al., 1962; Peters, 1964], or possible a SNIa. The DWDs are expected to be the dominant source [Evans et al., 1987; Nelemans et al., 2001a] of gravitational waves for the future space-born gravitational wave observatories such as eLISA [Amaro-Seoane et al., 2012a,b].

We study the population of merging DWDs that might lead to a SNIa from a theoretical point of view. We incorporated results from observations where possible. We use the population synthesis code SeBa for simulating the stellar and binary evolution of stellar systems that leads to close DWDs. In Sect. 5.2 we describe the code and the updates since the last publication of SeBa. A major influence on the merging double-degenerate population is the poorly understood CE phase [Paczynski, 1976; Webbink, 1984; Nelemans et al., 2000]. We adopt two different models for the CE. In Sect. 5.3 we describe these models and their implications for the observations of close DWDs. In Sect. 5.4 we discuss the binary paths leading to SNIa for each model. The SNIa rates and time-integrated numbers are derived in Sect. 5.5. The properties of the population of merging DWDs are discussed in the context of the classical and alternative sub- and super-Chandrasekhar SNIa explosion models in Sect. 5.6. A discussion and conclusion follows in Sect. 5.7.

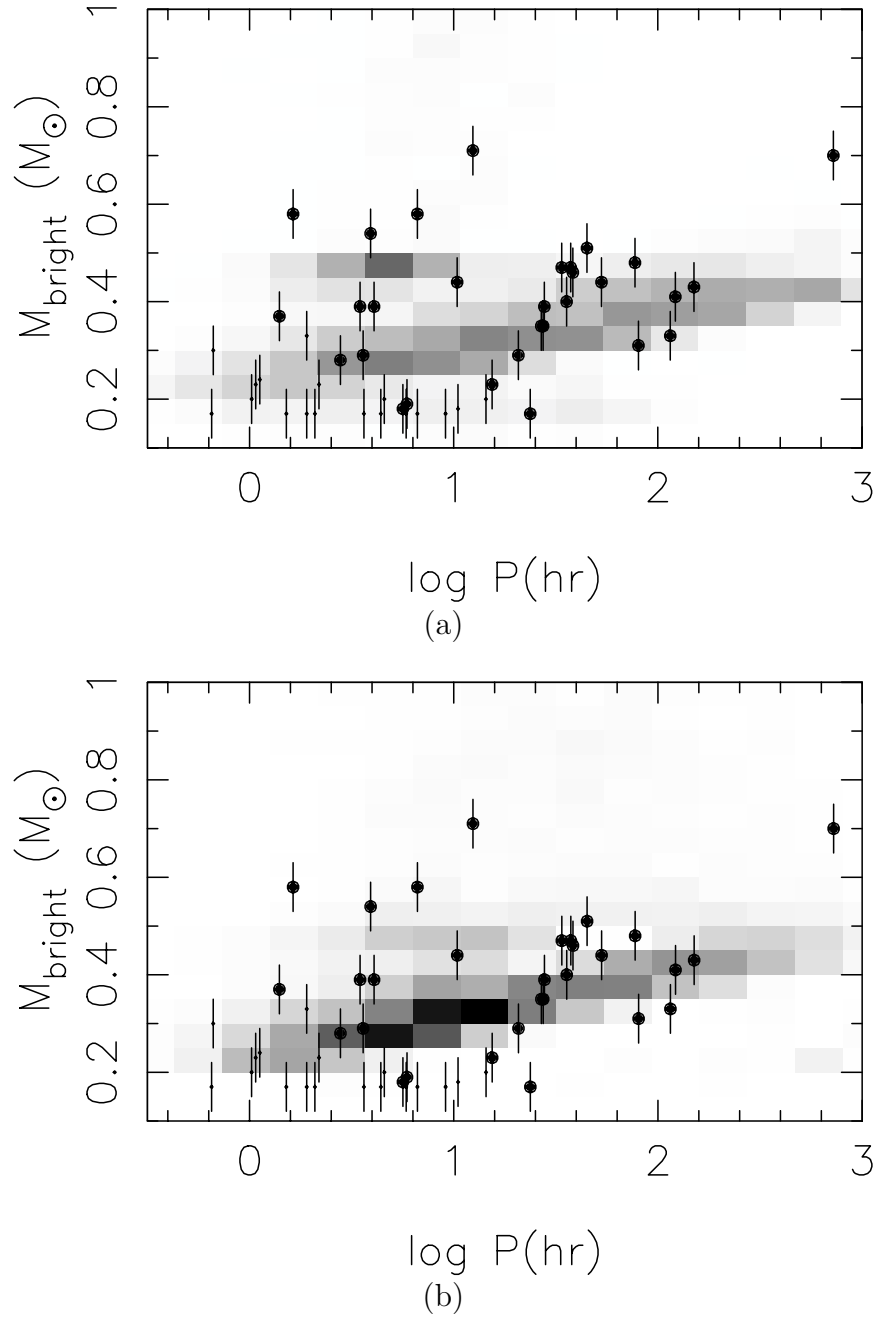


FIGURE 5.1: Simulated population of visible double white dwarfs as a function of orbital period and mass of the brighter white dwarf. Top: the stellar evolution tracks according to EFT are used; bottom: HPT (using model $\gamma\alpha$, see Sect. 5.3). The intensity of the grey scale corresponds to the density of objects on a linear scale. The same grey scale is used for both plots. Observed binary white dwarfs are overplotted with filled circles. Thick points taken are from Marsh et al. [2011], thinner points from Tovmassian et al. [2004]; Napiwotzki et al. [2005]; Kulkarni & van Kerkwijk [2010]; Brown et al. [2010, 2011]; Marsh et al. [2011]; Kilic et al. [2011a,c,b], see Sect. 5.2.1 for a discussion.

5.2 SeBa - a fast stellar and binary evolution code

We present an update to the software package SeBa [Portegies Zwart & Verbunt, 1996; Nelemans et al., 2001c] for fast stellar and binary evolution computations. Stars are evolved from the zero-age main sequence (ZAMS) until remnant formation and beyond. Stars are parametrised by mass, radius, luminosity, core mass, etc. as functions of time and initial mass. Mass loss from winds, which is substantial e.g. for massive stars and post main-sequence stars, is included. Binary interactions such as mass loss, mass transfer, angular momentum loss, CE, magnetic braking, and gravitational radiation are taken into account with appropriate recipes at every timestep [Portegies Zwart & Verbunt, 1996; Portegies Zwart & Yungelson, 1998]. Following mass transfer in a binary, the donor may turn into a helium-burning star without hydrogen envelope. When the mass transfer leads to a merger between the binary stars, we estimate the resulting stellar product and follow the evolution further. Note that we do not solve the equations of stellar structure. The stellar tracks instead assume stellar models in hydrostatic equilibrium. When this is not the case, however the gas envelope surrounding the core may puff outward (see Appendix 5.A.2 for details on the formalism). In our simulation the mass transfer rate is calculated from the relevant timescales (see Appendix 5.A.3) and not from than the stellar radii. Therefore binary evolution is not critically dependent on out-of-equilibrium parameter values.

The philosophy of SeBa is to not a priori define the binary's evolution, but rather to determine this at runtime depending on the parameters of the stellar system. When more sophisticated models become available of processes that influence stellar evolution, these can be included, and the effect can be studied without altering the formalism of binary interactions. An example is the accretion efficiency onto the accretor star during mass transfer. Instead of prescribing a specific constant percentage of the transferred matter to be accreted (and the rest to be lost from the system), the efficiency depends on the properties of the accreting star, such as the thermal timescale, the radius and the Roche lobe of the accretor (see Appendix 5.A.2 for details). Another example is the stability of mass transfer. In our simulations the stability and rate of mass transfer are dependent on the reaction to mass change of the stellar radii and the corresponding Roche lobes. The advantage of this is that the (de)stabilising effect of non-conservativeness of stable mass transfer [see Soberman et al., 1997] is taken into account automatically. There is no need to make the assumption in the stability calculation that stable mass transfer is conservative, as with methods that depend on the mass ratio [Hjellming & Webbink, 1987; Tout et al., 1997; Hurley et al., 2002].

Since the last publication of the code content, many changes have been made. We briefly discuss the most important changes below, and provide more detail in Appendix 5.A. First, the wind mass loss prescriptions that we implemented are mostly based on the recommendations by Hurley et al. [2000]. The specific prescriptions for different types of stars are described in Appendix 5.A.1. Second, a summary of the treatment of accretion

onto different stars can be found in Appendix 5.A.2. The accretion procedure previously used in SeBa is complemented with a procedure for accretion from a hydrogen-poor star. We assume that for ordinary stars, helium-rich matter is accreted directly to the core of the star. The mass accretion process onto white dwarfs is updated with new efficiencies of mass retention on the surface of the white dwarf. For hydrogen accretion we have the option to choose between the efficiencies of Hachisu et al. [2008] and Prialnik & Kovetz [1995]. Helium retention can be modelled according to Kato & Hachisu [1999] [with updates from Hachisu et al., 1999] or Iben & Tutukov [1996]. In this research we used the efficiencies of Hachisu et al. [2008], Kato & Hachisu [1999], and Hachisu et al. [1999]. For a study of different retention efficiencies and the effect on the Supernova Type Ia rate using the new version of SeBa, see Bours, Toonen & Nelemans, in preparation. Third, the stability of mass transfer is based on the adiabatic and thermal response of the donor star to mass loss and the response of the Roche lobe. The adjustment of the Roche lobe is dependent on the mass transfer rate, which in turn sets the efficiency of accretion onto the accretor star, see Appendix 5.A.3. Fourth, regarding the stellar tracks, previously, stellar evolution has been based on evolutionary tracks described by analytic formulae given by Eggleton et al. [1989, hereafter EFT] with updates from Tout et al. [1997] and helium star evolution as described by Portegies Zwart & Verbunt [1996] based on Iben & Tutukov [1985]. In the new version, the evolution of ordinary stars and hydrogen-poor stars is based on Hurley et al. [2000, hereafter HPT]. We do not adopt the HPT tracks for remnants, instead we maintain our prescription [Portegies Zwart & Verbunt, 1996; Nelemans et al., 2001c], which includes processes such as natal kick velocities to compact objects in supernovae explosions.

5.2.1 Impact on the population of double white dwarfs

Figure 5.1 shows the visible close DWD population simulated by SeBa. On the left a simulation is shown of the previous version of SeBa that a.o. uses the EFT tracks and on the right we show the current version using the HPT tracks. Initial parameters are distributed according to the distributions described in Table 5.1. Primary masses are drawn from $0.96M_{\odot}$ to $11M_{\odot}$ to include all stars that evolve into a white dwarf in a Hubble time. For the mass ratio and eccentricity we cover the full range 0-1, and the orbital separation out to 10^6R_{\odot} . We assumed solar metallicity, unless specified otherwise. In the normalisation of the simulation we assumed that primary masses lie in the range $0.1-100M_{\odot}$. Our method to estimate the visible population of DWDs is described in Nelemans et al. [2004], in which the Galactic star formation history is based on Boissier & Prantzos [1999] and WD cooling according to Hansen [1999]. We assume a magnitude limit of 21. In Fig. 5.1, the observed DWDs are overplotted with filled circles. The systems are described by Marsh [2011] and references therein, as well as Tovmassian et al. [2004] and Rodríguez-Gil et al. [2010]. Additionally, we included 19 newly discovered DWDs from Kulkarni & van Kerkwijk [2010]; Brown et al. [2010, 2011]; Marsh et al. [2011]; Kilic et al. [2011a,c] and Kilic et al. [2011b].

TABLE 5.1: Distributions of the initial binary parameter mass, mass ratio, orbital separation and eccentricity.

Parameter	Distribution
Mass of single stars	Kroupa IMF ⁽¹⁾
Mass of binary primaries	Kroupa IMF ⁽¹⁾
Mass ratio	Flat distribution
Orbital separation	$N(a)da \propto a^{-1}da$ ⁽²⁾
Eccentricity	Thermal distribution ⁽³⁾

REFERENCES: ⁽¹⁾ Kroupa et al. [1993]; ⁽²⁾ Abt [1983]; ⁽³⁾ Heggie [1975];

These new systems are displayed with smaller circles and thinner lines to separate them from the previously found systems. We did this because the observational biases are very different. The previously found systems were selected from a magnitude-limited sample down to 16-17 magnitude. The new systems are much fainter at about 20 magnitude. Moreover, most of the new systems are discovered as part of the ELM survey [Brown et al., 2010]. This survey focuses on finding extremely low-mass white dwarfs from follow-up observations of spectroscopically selected objects from the Sloan Digital Sky Survey. Therefore, the set of new systems is biased to lower masses. One should take this bias into account while comparing with the simulations and not take the combined set of observed systems as a representative sample of the DWD population. Kilic et al. [2011a] showed in their Fig. 12 a visualisation of the population of visible DWDs simulated by SeBa, where this selection effect has been taken into account.

The locations of the observed DWDs in Fig. 5.1 correspond reasonably well to the predictions of both models. The overall structure of the simulated populations from both models are similar. At masses of about $0.5M_{\odot}$ and periods of 1 – 10 hr, there is a very pronounced region in the plot from the EFT tracks that seems to be missing in the HPT plot. However, this is not really the case. These systems mainly consist of one helium (He) WD and one CO WD. Masses of CO WDs span a wider range of values in the HPT tracks, which distributes the pronounced region in EFT over a larger region in mass and period in HPT.

For a single burst of star formation the number of created DWDs within 13.5 Gyr and with an orbital period $P < 1000\text{hr}$ for the HPT and EFT stellar tracks is very similar; $6.9 \cdot 10^{-3}$ per M_{\odot} of created stars for both models. The time-integrated merger rate is $2.4 \cdot 10^{-3}M_{\odot}^{-1}$ for HPT and $3.2 \cdot 10^{-3}M_{\odot}^{-1}$ for EFT. The current merger rate in the Milky Way according to the HPT and EFT stellar tracks is very similar; $1.4 \cdot 10^{-2}\text{yr}^{-1}$ for HPT and $1.2 \cdot 10^{-2}\text{yr}^{-1}$ for EFT, for which we have assumed a star formation history as in Nelemans et al. [2004] based on Boissier & Prantzos [1999].

Classically, the population of double He dwarfs is thought to dominate in number over the other types of close DWDs. Using the EFT tracks for a single burst of star formation, we

predict a percentage of [He-He, He-CO, CO-CO] = [60%, 17%, 21%] and a negligible number of DWDs containing oxygen/neon (ONe) dwarfs. For the HPT tracks, the percentage of double He dwarfs decreases to 38%. The population consists of [He-He, He-CO, CO-CO]=[38%, 27%, 33%] and 2% CO - ONe dwarfs. The decrease in number of He WDs is caused by a difference in the stellar tracks related to helium ignition under degenerate conditions. As shown by Han et al. [2002], degenerate stars do not ignite helium at a fixed core mass, but instead the core mass at helium ignition is a decreasing function of the ZAMS mass of the star. Taking this into account, more WDs in close binaries are labelled CO WDs.

5.3 Two models for common-envelope evolution

Close DWDs are believed to encounter at least two phases of mass transfer in which one of the stars loses its hydrogen envelope. In at least one of these phases mass transfer from the evolving more massive star to the less massive companion is dynamically unstable [Paczynski, 1976; Webbink, 1984] which leads to a common-envelope phase. The core of the donor and companion spiral inward through the envelope, expelling the gaseous envelope around them. Because of the loss of significant amounts of mass and angular momentum, the CE phase plays an essential role in binary star evolution in particular the formation of short-period systems that contain a compact object.

Despite of the importance of the CE phase and the enormous efforts of the community, all effort so far have not been successful in understanding the phenomenon. Several prescriptions for CE evolution have been proposed. The α -formalism [Webbink, 1984] is based on the conservation of orbital energy. The α -parameter describes the efficiency with which orbital energy is consumed to unbind the CE according to

$$E_{\text{gr}} = \alpha(E_{\text{orb,init}} - E_{\text{orb,final}}), \quad (5.1)$$

where E_{orb} is the orbital energy and E_{gr} is the binding energy between the envelope mass M_{env} and the mass of the donor M . E_{gr} is often approximated by

$$E_{\text{gr}} = \frac{GMM_{\text{env}}}{\lambda R}, \quad (5.2)$$

where R is the radius of the donor star and λ depends on the structure of the donor. We assume $\alpha\lambda = 2$. Nelemans et al. [2000] deduced this value from reconstructing the last phase of mass transfer for 10 known DWDs using the unique core-mass – radius relation for giants.

To explain the observed distribution of DWDs, Nelemans et al. [2000] proposed an alternative formalism. According to this γ -formalism, mass transfer is unstable and non-conservative. The mass-loss reduces the angular momentum of the system in a linear way according to

$$\frac{J_{\text{init}} - J_{\text{final}}}{J_{\text{init}}} = \gamma \frac{\Delta M}{M + m}, \quad (5.3)$$

5.3 TWO MODELS FOR COMMON-ENVELOPE EVOLUTION

where J_{init} resp. J_{final} is the angular momentum of the pre- and post-mass transfer binary respectively, and m is the mass of the companion. We assumed $\gamma = 1.75$, see Nelemans et al. [2001c].

We adopt two evolutionary models that differ in their treatment of the CE phase. In model $\alpha\alpha$ the α -formalism is used to determine the outcome of every CE. For model $\gamma\alpha$ the γ -prescription is applied unless the binary contains a compact object or the CE is triggered by a tidal instability (rather than dynamically unstable Roche lobe overflow, see Appendix 5.A.3). Typically, the second CE (with a giant donor and white dwarf companion) is described by the α -formalism, which gives consistent results when compared with the observations [Nelemans et al., 2000]. If the first phase of mass transfer is unstable, it typically evolves through a γ -CE. In model $\gamma\alpha$ and $\alpha\alpha$, if both stars are evolved when the CE develops, we assumed that both cores spiral-in [see Nelemans et al., 2001c]. The envelopes are expelled according to

$$E_{\text{gr},*\text{don}} + E_{\text{gr},*\text{comp}} = \alpha(E_{\text{orb,init}} - E_{\text{orb,final}}), \quad (5.4)$$

analogous to Eq.5.1, where $E_{\text{gr},*\text{don}}$ represents the binding energy of the envelope of the donor star and $E_{\text{gr},*\text{comp}}$ of the companion star.

The motivation for the alternative formalism is the large amount of angular momentum available in binaries with similar-mass objects. The physical mechanism behind the formalism remains unclear however. Interesting to note here is that recently Woods et al. [2010, 2012] suggested a new evolutionary model to create DWDs. It differs from standard assumptions in the first phase of mass transfer. These authors find that mass transfer between a red giant and a main-sequence star can be stable and nonconservative. The effect on the orbit is a modest widening, with a result alike to the γ -description.

5.3.1 Impact on the population of double white dwarfs and type Ia supernova progenitors

Figure 5.2 shows the mass ratio of the visible population (see Sect. 5.2.1) of DWDs versus the orbital period according to model $\gamma\alpha$ and $\alpha\alpha$. Overlaid with filled circles are the observed populations. For systems for which only a lower limit to the mass of the companion is known, we show a plausible range of mass ratios of that system with an arrow. The arrow is drawn starting from the maximum mass ratio, which corresponds to an inclination of 90 degrees. It extends to a companion mass that corresponds to an inclination of 41 degrees. Within this range of inclinations there is a 75% probability that the actual mass ratio lies along the arrow. The filled circles overplotted on the arrow indicate the mass ratio for the median for random orientations, i.e., 60 degrees.

Using model $\alpha\alpha$, the DWDs cluster around a mass ratio of $q \approx 0.5$, while model $\gamma\alpha$ shows a wider range in mass ratio. This agrees better with the observed binaries. The different mass ratio distributions are inherent to the models and only slightly dependent

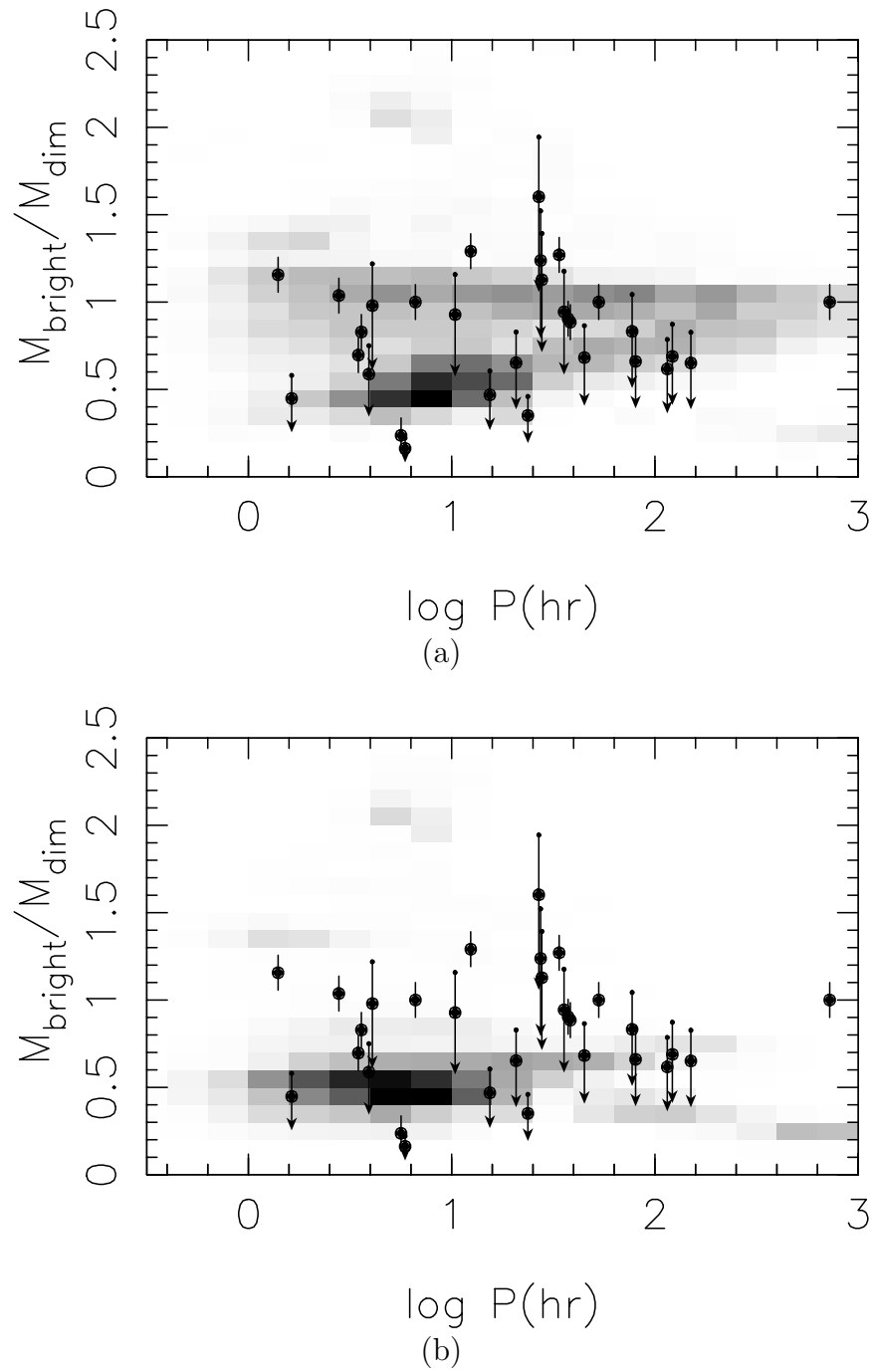


FIGURE 5.2: Simulated population of visible double white dwarfs as a function of orbital period and mass ratio, where mass ratio is defined as the mass of the brighter white dwarf divided by that of the dimmer white dwarf. In the top model $\gamma\alpha$ is used, in the bottom model $\alpha\alpha$. The intensity of the grey scale corresponds to the density of objects on a linear scale. The same grey scale is used for both plots. Observed binary white dwarfs are overplotted with filled circles, see Fig. 5.1 for references.

on the CE efficiency. This is because in the first CE phase, the γ -CE allows for widening or very mild shrinkage of the orbit, whereas in the α -prescription the orbit will always shrink. The resulting orbital separation determines when the secondary will fill its Roche lobe, and the corresponding core mass of the secondary, which determines the mass ratio distribution of the prospective DWD.

In Fig. 5.3 the population of observed and simulated DWDs are shown as a function of combined mass of the two WDs for the two models of CE evolution. The left upper corner bounded by the dotted and dashed lines contains SNIa progenitors. In Fig. 5.3 there are two systems that have a probability to fall in this region. These systems are the planetary nebulae nuclei with WD companions TS 01 (PN G135.9+55.9) [Tovmassian et al., 2004; Napiwotzki et al., 2005; Tovmassian et al., 2010] and V458 Vul [Rodríguez-Gil et al., 2010]. An immediate precursor of a DWD that is possibly a progenitor candidate for a SN Ia via the DD channel has also been observed; a subdwarf with a white dwarf companion, KPD 1930+2752 [Maxted et al., 2000; Geier et al., 2007].

In our model of the visible population of DWDs (see Sect. 5.2.1), the percentage of merging DWDs with a total mass exceeding the Chandrasekhar is 1.2% for model $\gamma\alpha$ and 4.3% for model $\alpha\alpha$. Including only double CO WDs, the percentage is 0.9 and 2.9%, respectively. Because the number of observed close DWDs until today is low, we do not expect to observe many SNIa progenitors [see also Nelemans et al., 2001c]. Therefore a comparison of the SNIa progenitors with population synthesis by a statistical approach is unfortunately not yet possible. We find it important to compare the observed close DWD population with the simulated one, since these systems go through similar evolutions and are strongly influenced by the same processes. Although the observed population mostly consists of He DWDs and He - CO DWDs instead of CO DWDs required for SNIa progenitors, at this time the population of all close DWDs are the closest related systems that are visible in bulk.

5.4 Evolutionary paths to supernova type Ia from the double degenerate channel

In this section we discuss the most common binary scenarios that leads to a potential supernova type Ia in the DD channel. We assume that every merger of two carbon/oxygen white dwarf with a mass exceeding $1.4M_{\odot}$ will lead to a supernova. The contribution of merging systems that contains a helium white dwarf that surpasses the Chandrasekhar mass is negligible. In the canonical scenario a DWD is formed through two consecutive CEs. This we label the 'common-envelope channel'. In accordance with Mennekens et al. [2010], we find that there are other channels that can lead to a SNIa as well. We find that the common-envelope scenario can account for less than half of the supernova progenitors in a single burst of star formation, 34% for model $\gamma\alpha$ and 45% for model $\alpha\alpha$. We distinguish

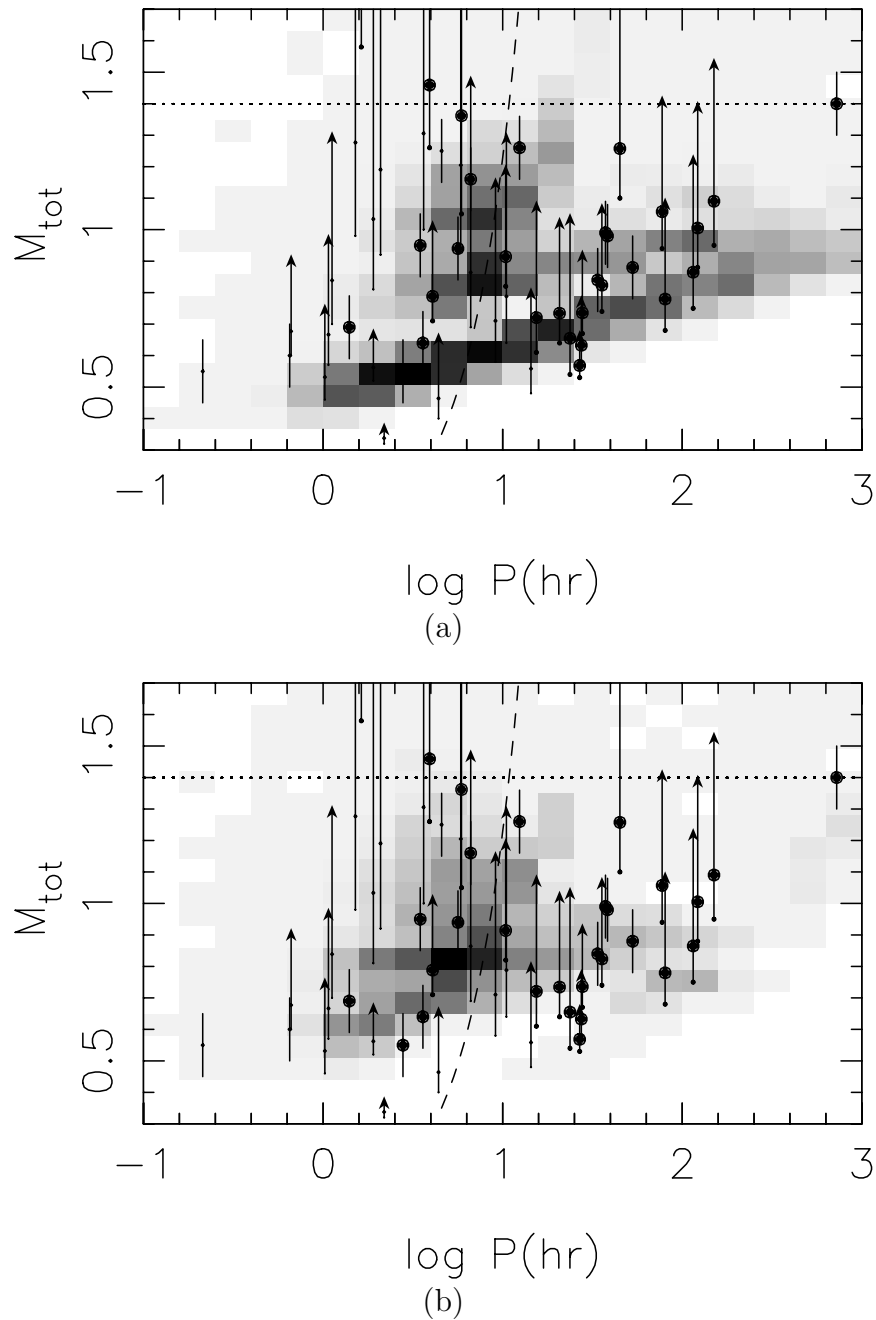


FIGURE 5.3: Simulated population of visible double white dwarfs as a function of orbital period and the combined mass of the two dwarfs. On the top the common-envelope phase is parametrised according to model $\gamma\alpha$, on the bottom according to model $\alpha\alpha$ (see Sect. 5.3). The intensity of the grey scale corresponds to the density of objects on a linear scale. The same grey scale is used for both plots. Observed binary white dwarfs are overplotted with filled circles, see Fig. 5.1 for references. The Chandrasekhar mass limit is indicated with the dotted line. The dashed line roughly demarks the region in which systems merge within a Hubble time. Systems located to the left of the dashed line and above the dotted line are supernova type Ia progenitors in the standard picture.

between three scenarios labelled 'common-envelope', 'stable mass transfer' and 'formation reversal'. The names of the first two tracks refer to the first phase of mass transfer, whereas 'formation reversal' applies to the reversed order in which the two white dwarf are formed, see Sect. 5.4.3). The stable mass transfer channel accounts for 52% and 32% assuming model $\gamma\alpha$ and $\alpha\alpha$, respectively, for a single burst of star formation. The formation reversal channel accounts for a lower percentage of all SNIa, 14% for model $\gamma\alpha$ and 23% for model $\alpha\alpha$ for a single starburst. Note that the importance of the stable mass transfer channel strongly depends on the assumed amount of mass loss and angular momentum loss.

In population synthesis studies all known information about binary evolution is combined, and different evolutionary paths emerge out of these quite naturally. As noted by Mennekens et al. [2010], the significant contribution to the SNIa rate from other channels than the common-envelope channel complicates the use of analytical formalisms for determining the distribution of SNIa delay times. The SNIa delay time of a binary is the time of the SNIa since the formation of the system. This is commonly used to compare observational and synthetic rates to constrain different physical scenarios [e.g. Yungelson & Livio, 2000; Ruiter et al., 2009b; Mennekens et al., 2010, see also Sect. 5.5 in this paper]. During a CE phase the companion is assumed to be hardly affected e.g. by accretion. If this is not the case, as in stable mass transfer, the assumption that the formation timescale of the DWD is approximately the main-sequence lifetime of the least massive component is not valid any more. Furthermore, the in-spiral timescale from DWD formation to merger due to gravitational waves is strongly dependent on the orbital separation at DWD formation. This can be very different for systems that undergo stable mass transfer instead of a CE evolution. Concluding, the delay time, which is the sum of the DWD formation and in-spiral timescale can be significantly different when these tracks are not properly taken into account.

5.4.1 common-envelope channel

In the canonical path, both stars lose their hydrogen envelopes through two consecutive common-envelope phases. An example of a typical evolution is shown in Fig. 5.4. In this example two zero-age main-sequence stars of $6M_{\odot}$ and $4M_{\odot}$ are in an orbit of 125 days. When the initially more massive star (hereafter primary) ascends the giant branch, it fills its Roche lobe and a CE commences. The primary loses its hydrogen envelope, but does not become a WD immediately and a helium star is born. The primary becomes a white dwarf of about solar mass. When the initially less massive star (hereafter secondary) evolves off the main sequence and its radius significantly increases, another common-envelope phase occurs. As a result, the orbit shrinks. The secondary evolves further as a helium star without a hydrogen envelope until it eventually turns into a white dwarf. For model $\alpha\alpha$ the orbit decreases more severely in the first phase of mass transfer. Therefore the initial periods in this channel are higher, by a factor of about 1.5-3 and the primaries are typically

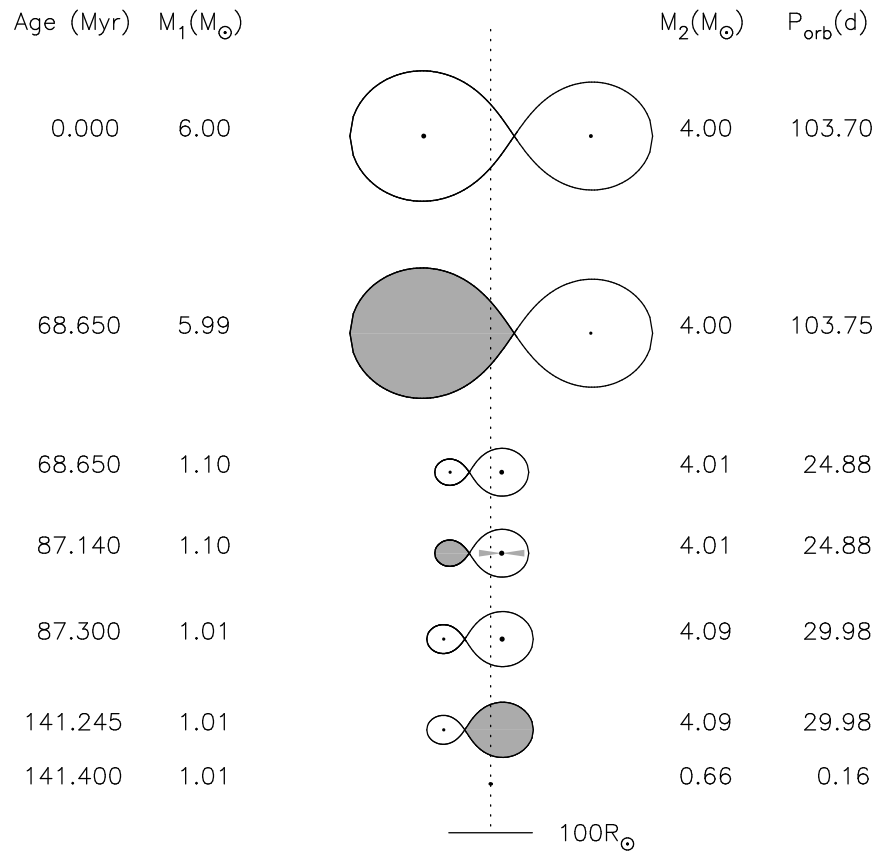


FIGURE 5.4: Evolutionary track for the merger of two carbon/oxygen white dwarfs of a combined mass that exceeds the Chandrasekhar mass. In this scenario the first phase of mass transfer is dynamically unstable which results in a common-envelope phase. In this figure we show a representative example of model $\gamma\alpha$, see Sect. 5.3.

more evolved giants when the donors fill their Roche lobes. In this evolution channel both the primary and secondary can fill their Roche lobes as helium giants. If this happens, mass transfer is usually dynamically stable, but the effect on the orbit is small.

A variation of this evolution can occur when the secondary has reached the giant stages of its evolution when the primary fills its Roche lobe. This happens for systems of nearly equal masses. We assume both stars lose their envelope in the CE phase according to Eq. 5.4, in which the orbit is severely decreased. This variation contributes 23% of the systems in the common-envelope channel for model $\gamma\alpha$ and 10% for model $\alpha\alpha$.

With the α -CE prescription it is likely to have another variation on the evolution, in which the primary becomes a white dwarf immediately after the first phase of mass transfer. This can happen when the primary fills its Roche lobe very late on the asymptotic giant branch when the star experiences thermal pulses. These systems have initial periods that are a factor 5 larger than in the standard CE channel using model $\alpha\alpha$. This subchannel contributes 43% to the CE channel for model $\alpha\alpha$. When using the $\gamma\alpha$ -model for the CE, the contribution from this subchannel is 20%. However, these systems are not formed through a standard γ -CE because the orbit does not shrink severely enough to obtain a significant contribution. Instead these systems are formed through a double-CE as described by Eq. 5.4. For model $\alpha\alpha$ the double-CE mechanism is important in only 18% of the 43%.

5.4.2 Stable mass transfer channel

In this channel the initial masses of the stars and the initial orbits are smaller than for the common-envelope channel. Typical values are a primary mass of $5M_{\odot}$, a secondary mass of $3M_{\odot}$ and an orbital separation of $40R_{\odot}$ (assuming a circular orbit). The primary fills the Roche lobe as a Hertzsprung gap star and mass transfer occurs stably. Which fraction of transferred mass is actually accreted by the secondary and how much is lost from the system depends on the mass and radius of the secondary and the secondary's Roche lobe (see Appendix 5.A.2 for more details). In Fig. 5.5 an example of a typical evolution is shown. When the secondary fills its Roche lobe, a CE commences. In this channel the tidal instability (see Appendix 5.A.3) is important. In one third of the systems the CE occurs because of a tidal instability, the other part is caused by a dynamical instability. The secondary turns into a hydrogen-deficient helium-burning star in a system in which the period has decreased by one or two orders of magnitude. As in the previous channel, the primary and secondary can fill their Roche lobe as helium giants. If the primary fills its Roche lobe, mass transfer is usually dynamically stable and has little effect on the orbit. If the secondary fills its Roche lobe, mass transfer can be stable or unstable. In the example of Fig. 5.5 when the secondary fills its Roche lobe again as it ascends the helium giant branch, the mass transfer is unstable and the orbital separation decreases by a factor of about 5.

CHAPTER 5 : SNIA PROGENITORS FROM MERGING DOUBLE WHITE DWARFS

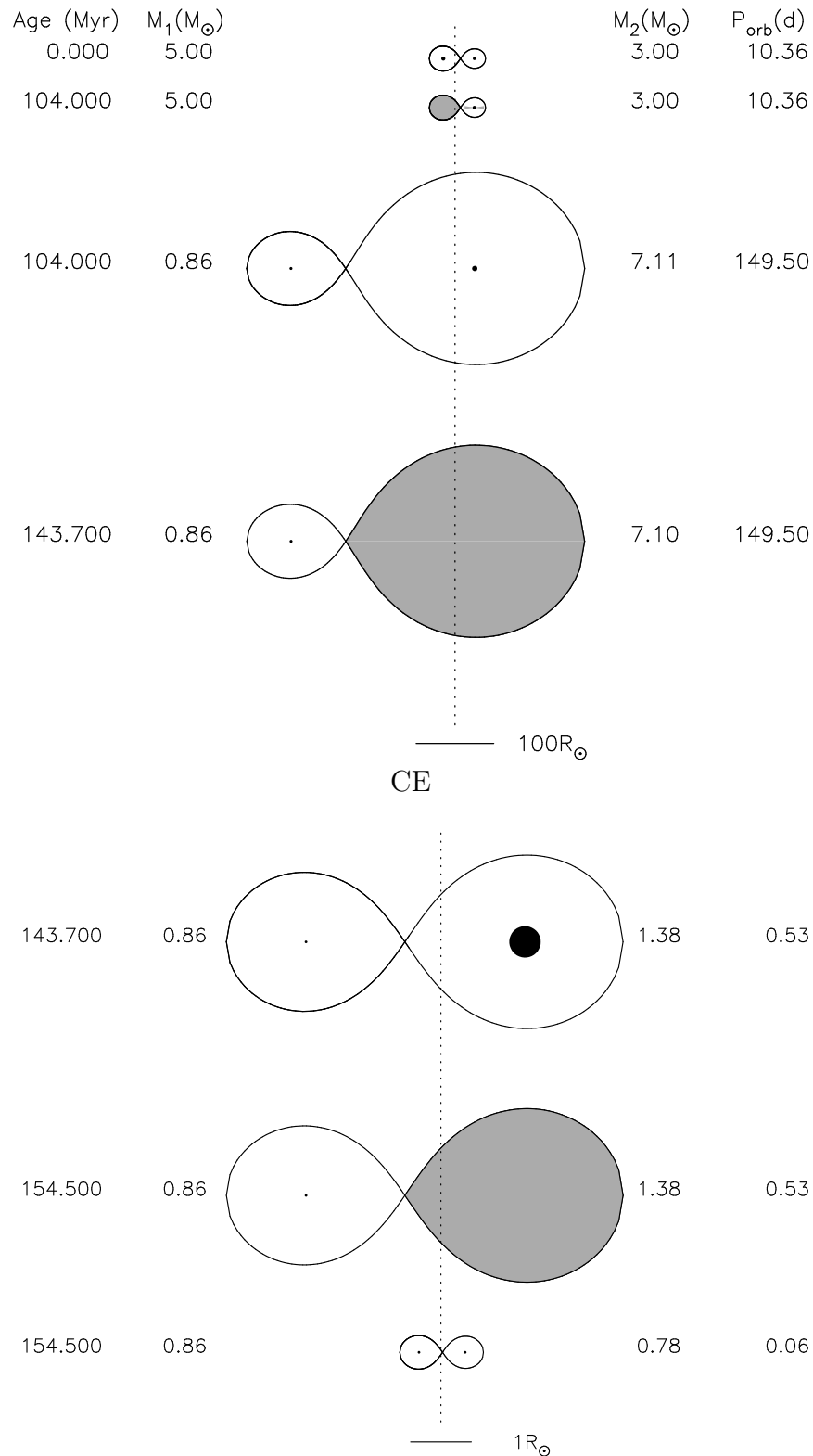


FIGURE 5.5: Evolutionary tracks for the merger of two carbon/oxygen white dwarfs of a combined mass exceeding the Chandrasekhar mass in the stable mass transfer channel. In this scenario the first phase of mass transfer is dynamically stable. The top and bottom parts of the figure have different scales due to a common-envelope phase, denoted as CE in the figure.

5.4.3 Formation reversal channel

We present a scenario¹ in which in the first mass transfer a helium star (sdB star) is formed that becomes a white dwarf only after the companion has become a white dwarf. A typical example of an evolution like this is shown in Fig. 5.6. The first phase of mass transfer is stable, like the stable mass transfer track. However, the resulting helium stars in this channel have low masses in the range of $0.5\text{-}0.8M_{\odot}$ and long lifetimes of about 10^8 yr. The first mass transfer occurs approximately conservatively. As a consequence, the subsequent evolution of the high-mass secondary ($5\text{-}8M_{\odot}$) accelerates. When the secondary fills its Roche lobe, mass transfer is tidally unstable (see Appendix 5.A.3). The secondary loses its hydrogen and helium envelope in two consecutive CEs and becomes a white dwarf. Subsequently, the original primary evolves off the helium main-sequence and becomes a white dwarf.

To our knowledge, this track has not been studied in detail before. Therefore we evaluated this track by performing detailed numerical calculations using the `ev` binary stellar-evolution code originally developed by Eggleton [Eggleton, 1971, 1972; Yakut & Eggleton, 2005, and references therein] and updated as described in Pols et al. [1995] and Glebbeek et al. [2008]. The code solves the equations of stellar structure and evolution for the two components of a binary simultaneously. The simulation showed that indeed the evolution of the secondary can be accelerated through accretion so that the secondary can stop helium burning prior to the primary.

5.5 Delay time distribution

One way to constrain the population of SNIa progenitors is through the delay time distribution (DTD), where the delay times is the time between the formation of the binary system and the SNIa event. In a simulation of a single burst of star formation the DTD gives the SNIa rate as a function of time after the starburst. The DTD is linked to the nuclear timescales of the progenitors and the binary evolution timescales up to the merger. We assumed a 50% binary fraction and initial parameters are distributed according to the distributions described in Table 5.1.

In Fig. 5.7a we compare the delay time distribution for the two different models of CE evolution. The sharp cut-off near 13.5 Gyr is artificial, because evolution was only allowed to proceed for 13.5 Gyr. The delay time distribution shows that these mergers are expected to take place in young as well as old populations. The peak in the supernova Ia rate is

¹This track is a close analogy of the track proposed by Sipior et al. [2004] regarding recycled pulsars. In the scenario proposed by these authors the end states of the two components are reversed, resulting in a neutron star that forms prior to a black hole. However, in our scenario the name 'formation reversal' applies to the evolutionary timescales of the primary and secondary. Although the primary first evolves off the main sequence, the secondary becomes a remnant first.

CHAPTER 5 : SNIA PROGENITORS FROM MERGING DOUBLE WHITE DWARFS

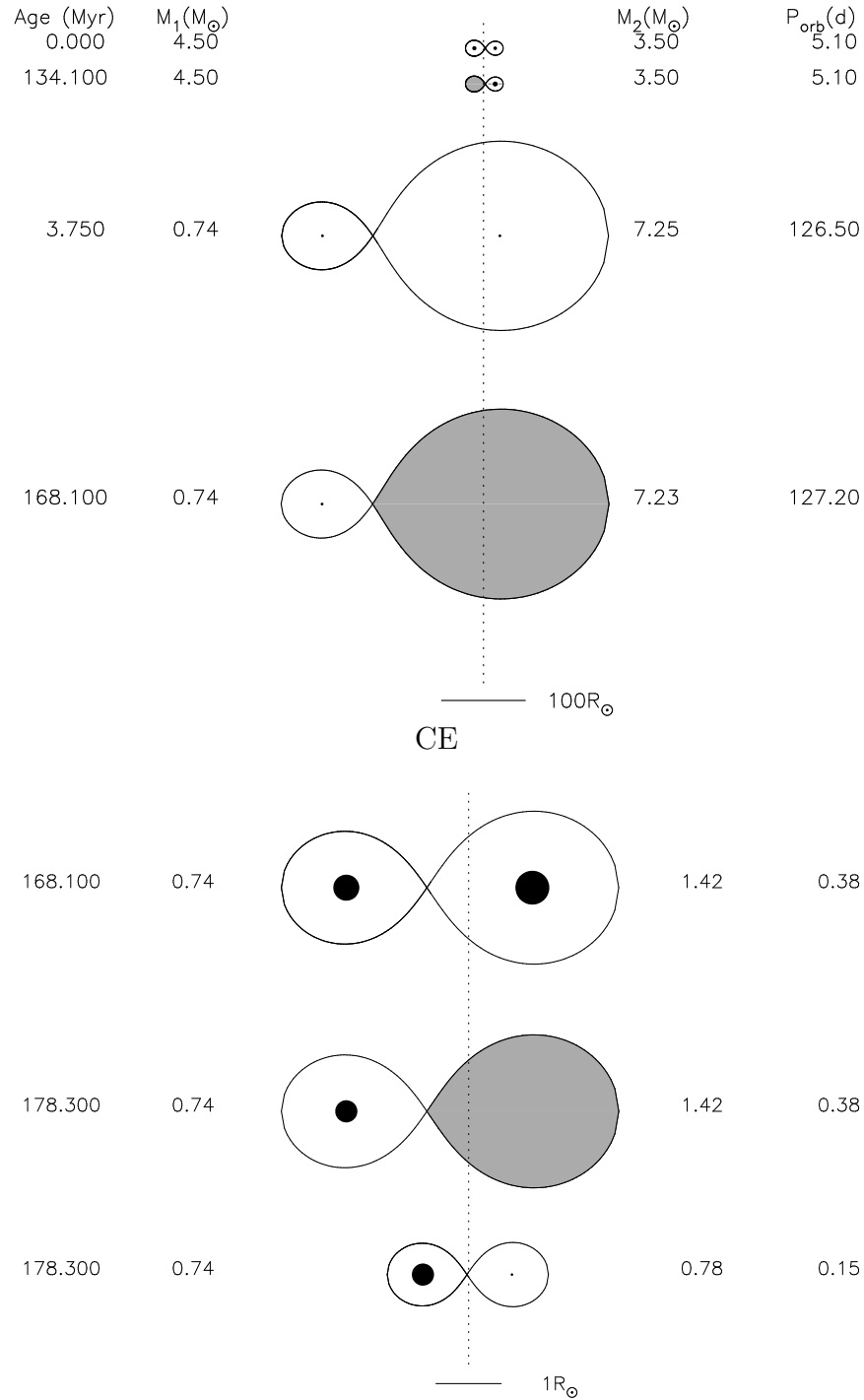
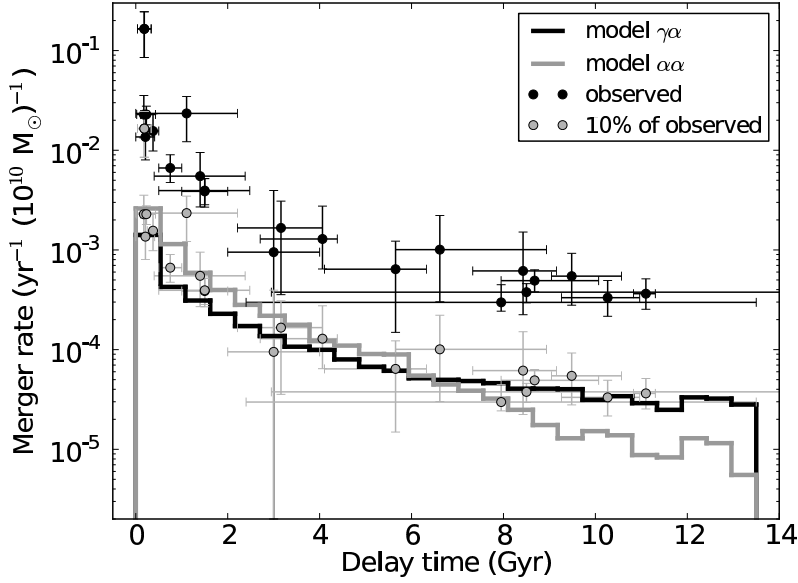
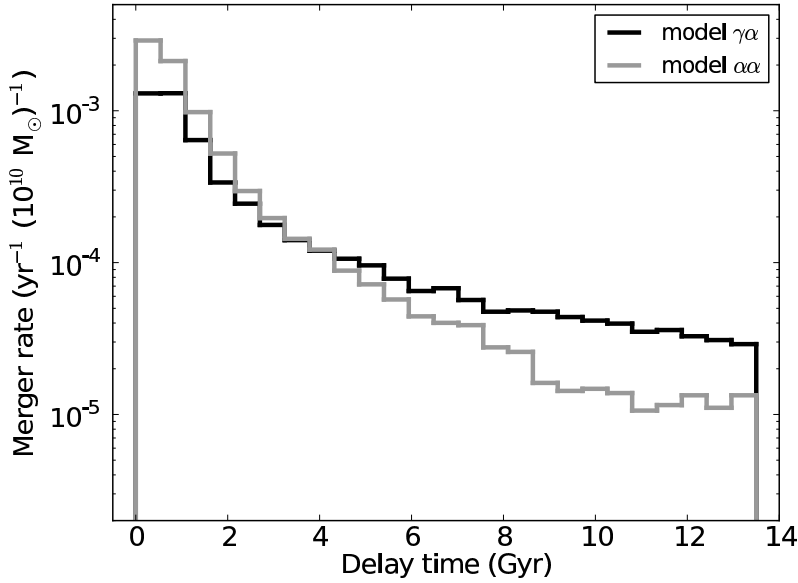


FIGURE 5.6: Evolutionary tracks for the merger of two carbon/oxygen white dwarfs of a combined mass exceeding the Chandrasekhar mass in the formation reversal channel. In this scenario the first phase of mass transfer is dynamically stable which results in a low-mass helium-star with a long lifetime. The initially less massive star becomes the first formed white dwarf. The top and bottom parts of the figure have different scales due to a common-envelope phase, denoted as CE in the figure.



(a)



(b)

FIGURE 5.7: Merger rate of double carbon/oxygen white dwarfs with a total mass above the Chandrasekhar mass as a function of delay time. Rates are in yr^{-1} per $10^{10} M_{\odot}$ formed stellar mass of the parent galaxy. Delay times are shown for two different prescriptions of the CE phase. In black we plot model $\gamma\alpha$ and in grey model $\alpha\alpha$, see Sect. 5.3. Top: Solar metallicity ($Z = 0.02$) is assumed. Overplotted with black circles are the observed values of the SNIa rate of Totani et al. [2008], Maoz et al. [2010], Maoz & Badenes [2010] and Maoz et al. [2011] [see Maoz & Mannucci, 2012a, for a review]. For comparison the grey circles show the observations scaled down by a factor 10. Bottom: A metallicity of 0.001 is assumed.

at about 150 Myr for both models. The median delay time is 0.7 Gyr for model $\alpha\alpha$ and 1.0 Gyr for model $\gamma\alpha$. The normalisations of the delay time distribution of model $\alpha\alpha$ and $\gamma\alpha$ are comparable. The time-integrated number of SNe Ia per unit formed stellar mass is $2.0 \cdot 10^{-4} M_{\odot}^{-1}$ and $3.3 \cdot 10^{-4} M_{\odot}^{-1}$ for model $\gamma\alpha$ and $\alpha\alpha$, respectively. From the Lick Observatory Supernova Search, Maoz et al. [2011] inferred a value of $2.3 \pm 0.6 \cdot 10^{-3} M_{\odot}^{-1}$, which is a factor 7-12 higher than the predictions from our models.

The morphologies of the DTD of model $\gamma\alpha$ and $\alpha\alpha$ resemble each other in that they show a strong decline with delay time, although with a slightly different slope. Model $\alpha\alpha$ shows higher rates at short delay times, whereas the rate for model $\gamma\alpha$ shows higher rates at long delay times. This is because the α -CE causes a stronger decrease of the orbital separation than the γ -CE in the first phase of mass transfer. The observed rates from Totani et al. [2008], Maoz et al. [2010], Maoz & Badenes [2010], and Maoz et al. [2011] [see Maoz & Mannucci, 2012a, for a review], shown in Fig. 5.7a, are much higher than the predicted rates from both models. To compare the morphological shapes of the DTDs more easily, we scaled down the observations by a factor 10 in Fig. 5.7a in light grey. The shape of the observed DTD fits the synthetic DTDs well. At long delay times > 6 Gyr, the flattening of the DTD is better reproduced by the $\gamma\alpha$ -model.

We have a last remark about Fig. 5.7a, about the datapoint from Maoz et al. [2010] at 185 Myr and a rate of $0.165 \text{ yr}^{-1} (10^{10} M_{\odot})^{-1}$. If this datapoint is true, it could indicate a steep rise of the delay time distribution at the shortest delay times. Neither model $\gamma\alpha$, or $\alpha\alpha$ reproduces the steep rise indicated by this point. At short delay times the contribution to the SNIa rate from other channels might be significant, for instance the contribution from helium donors in the SD channel. Wang et al. [2009a], Ruiter et al. [2009b] and Claeys et al. [2011] showed that at delay times of about 100 Myr, the DTD from helium donors in the SD channel peaks, although rates at this delay time vary between $10^{-4} - 10^{-2} \text{ yr}^{-1} (10^{10} M_{\odot})^{-1}$. Hydrogen donors in the SD channel are a possible contributor to the SNIa rate as well, but there is a strong disagreement over the DTD from this channel, [see for example Nelemans et al., 2013, for an overview]. In that paper it was shown that the simulated peaks of the DTDs lie anywhere between 0.1 to 3 Gyr and the peak rates vary between $10^{-6} - 10^{-2} \text{ yr}^{-1} (10^{10} M_{\odot})^{-1}$.

If we do not assume an instantaneous burst of star formation, but instead convolve the DTD with a star formation rate, we can estimate the SNIa rate from double degenerates for spiral galaxies like the Milky Way. If we assume a Galactic star formation rate as in Nelemans et al. [2004] based on Boissier & Prantzos [1999], model $\alpha\alpha$ gives $8.3 \cdot 10^{-4}$ SNIa yr^{-1} . Model $\gamma\alpha$ gives a Galactic rate of $5.8 \cdot 10^{-4}$ SNIa yr^{-1} . The reason for the relatively high Galactic rate for model $\gamma\alpha$ in comparison with model $\alpha\alpha$ relative to the integrated rates is that the peak of star formation occurs at long delay times where the DTD of model $\gamma\alpha$ dominates over model $\alpha\alpha$. The empirical SN Ia rate from Sbc-type galaxies like our own [Cappellaro & Turatto, 2001] is $4 \pm 2 \cdot 10^{-3} \text{ yr}^{-1}$, which is a factor of about 5-7 higher than the simulated rates.

When convolving the DTD with a star formation history, one should also take into account a metallicity dependence of the stars. To study the effect of metallicity on the SNIa rate, we simulated a delay time distribution from a single burst of stars of metallicity $Z = 0.001$. The important part of the DTDs in this respect are the long delay times because this is where the fraction of metal poor stars is highest. The DTD of model $\gamma\alpha$ for $Z = 0.001$ is lower at long delay times and higher at short delay times than the same CE model for solar metallicities. The time-integrated number of SNe Ia per unit formed stellar mass is $2.8 \cdot 10^{-4} M_{\odot}^{-1}$ for model $\gamma\alpha$. This is an increase of about 60% with respect to $Z = 0.02$. The integrated rate for model $\alpha\alpha$ for $Z = 0.001$ is $4.2 \cdot 10^{-4} M_{\odot}^{-1}$, which is an increase of about 30% with respect to $Z = 0.02$. The DTD for $Z = 0.001$ is roughly similar in morphological shape to that for $Z = 0.02$, see Fig. 5.7b. The DTDs of both metallicities for model $\alpha\alpha$ are similar at long delay times, and consequently the effect on the Galactic SNIa rate is expected to be marginal.

5.6 Population of merging double white dwarfs

In this section we discuss the properties of the population of SNIa progenitors from merging DWD and place it in the context of recent studies of the SNIa explosion itself. Figure 5.8 shows the combined mass of the system as a function of delay time for merging CO DWDs. It shows that for classical SNIa progenitors, the number of merging events decreases with time and that the number decreases faster with time for model $\alpha\alpha$ than for model $\gamma\alpha$, as discussed in Sect. 5.5. Moreover, the figure shows that mergers near the Chandrasekhar mass are most common, independent of delay time.

Fryer et al. [2010] showed that if super-Chandrasekhar mergers of CO DWDs of about $2M_{\odot}$ produce thermonuclear explosions, the light curves are broader than the observed SNIa sample. These authors argued that these mergers cannot dominate the current SNIa sample. We find indeed in both models that mergers with combined masses of about $2M_{\odot}$ are much less common than mergers in systems with a combined mass near the Chandrasekhar mass limit.

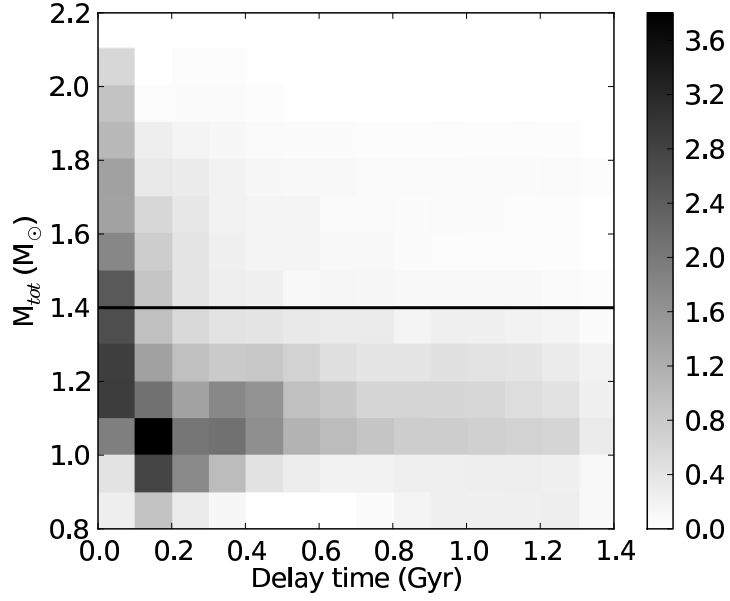
Where Fryer et al. [2010] studied a merger of a $1.2M_{\odot}$ CO WD with a $0.9M_{\odot}$ CO WD, Pakmor et al. [2010] focused on mergers of nearly equal mass WDs. In their scenario both WDs are distorted in the merger process and the internal structure of the merger remnant is quite different. Pakmor et al. [2010] argued that these mergers become hot enough to ignite carbon burning if the WD masses exceed $M \gtrsim 0.9M_{\odot}$. They found that these systems resemble subluminal SNIa such as SN 1991bg. Li et al. [2001] found 1991bg-like supernovae account for $16 \pm 6\%$ of all SNIa. From an improved sample Li et al. [2011] found a percentage of $15.2_{5.9}^{6.8}$. If we assume that 1991bg-like events account for 15% of all SNIa and the time-integrated of all SNIa types is If we assume in a simplistic way that all CO DWD mergers of $q = M_2/M_1 > 0.92$ and $M_1 > 0.9$ (where M_1 is the most massive WD and

M_2 the least massive WD) would lead to a 1991bg-like event, the time-integrated number of events is $2.3 \cdot 10^{-5} M_{\odot}^{-1}$ according to model $\gamma\alpha$ and $1.8 \cdot 10^{-5} M_{\odot}^{-1}$ assuming model $\alpha\alpha$. While the SNIa rate from the classical progenitors from model $\gamma\alpha$ is comparable to that of model $\alpha\alpha$, the population of DWDs is very different. In Sect. 5.3.1 we showed that the type of CE parametrisation introduces a bias in the mass ratio distribution of observed DWDs, which mostly consist of (double) He DWDs and He-CO DWDs. In Fig. 5.9 we show that this is also the case for the population of merging CO DWDs. Although the mass ratio distribution is not important for the standard DD scenario, it is important for the scenario proposed by Pakmor et al. [2010]. If the standard scenario and the scenario proposed by Pakmor et al. [2010] hold, SN 1991bg-like events are more common in model $\gamma\alpha$. We have to make a side remark on the expected delay times of this scenario. The median delay times are 180 Myr for model $\gamma\alpha$ and 150 Myr for model $\alpha\alpha$. The timescales are short because generally, more massive WDs have more massive progenitor stars, whose evolutionary timescales are short compared to those of less massive stars. Observations show, however, that subluminous SNIa are associated with old stellar populations of about 5-12Gyr [Howell, 2001].

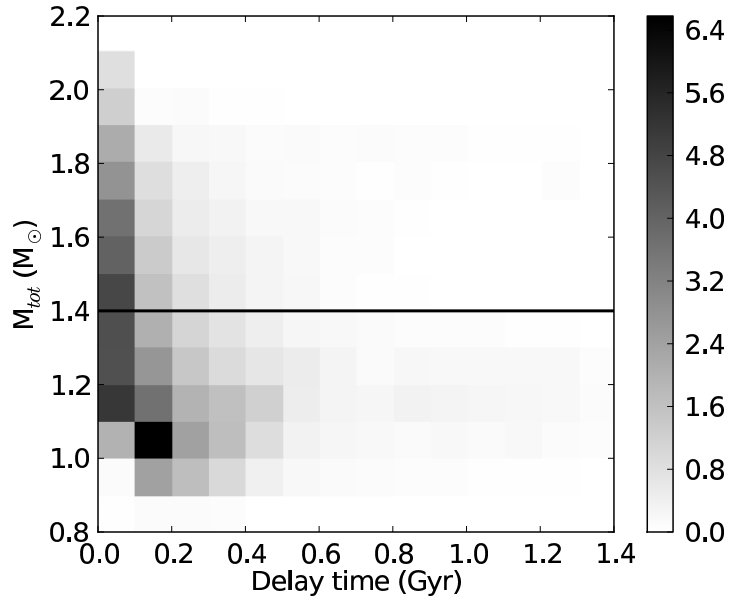
In our simulations the majority of merging CO DWDs have combined masses below the Chandrasekhar mass, see Fig. 5.8. Sub-Chandrasekhar models have long been proposed in order to raise total number of SNIa to match observations. Sim et al. [2010] found that if sub-Chandrasekhar WDs can be detonated, especially in the range $1.0 - 1.2 M_{\odot}$, the explosions match several observed properties of SNIa reasonably well. In the hypothetical situation that all double CO WDs that merge lead to an SNIa event, the integrated rate is $8.3 \cdot 10^{-4} M_{\odot}^{-1}$ for model $\gamma\alpha$ and $9.3 \cdot 10^{-4} M_{\odot}^{-1}$ for model $\alpha\alpha$. This is still a factor 3 lower than the observed rate of $2.3 \pm 0.6 \cdot 10^{-3} M_{\odot}^{-1}$ [Maoz et al., 2011]. Only if we assume that all mergers between a CO WD and a CO or He WD lead to an SNIa, the rates of $1.6 \cdot 10^{-3} M_{\odot}^{-1}$ and $2.1 \cdot 10^{-3} M_{\odot}^{-1}$ for model $\gamma\alpha$ and $\alpha\alpha$, respectively, match the observed rate.

The challenge for sub-Chandrasekhar models is how to detonate the white dwarf. A scenario for this was recently suggested by van Kerkwijk et al. [2010]. In this scenario two CO WDs with nearly equal masses merge. The merger remnant itself is too cold and insufficiently dense to produce an SNIa by itself, as noted by Pakmor et al. [2010]. van Kerkwijk et al. [2010] proposed that accretion of the thick disk that surrounds the remnant leads to an SNIa through compressional heating. If we simplistically assume that every merger of a double CO DWD with $q > 0.8$ and $M_1 + M_2 < 1.4$ leads to an SNIa, the time-integrated number per unit formed mass is $1.3 \cdot 10^{-4} M_{\odot}^{-1}$ for model $\gamma\alpha$ and $8.8 \cdot 10^{-5} M_{\odot}^{-1}$ for model $\alpha\alpha$. Relaxing the condition of $M_1 + M_2 < 1.4$ to all masses, $2.3 \cdot 10^{-4} M_{\odot}^{-1}$ for model $\gamma\alpha$ and $1.9 \cdot 10^{-4} M_{\odot}^{-1}$ for model $\alpha\alpha$. As in the scenario proposed by Pakmor et al. [2010], when a scenario is biased to merging systems of high-mass ratio, the relative contribution from this scenario in the $\gamma\alpha$ model is higher than the $\alpha\alpha$ model.

5.6 POPULATION OF MERGING DOUBLE WHITE DWARFS



(a)



(b)

FIGURE 5.8: Simulated distribution of the population of merging double CO white dwarfs from a single burst of star formation as a function of delay time and total mass of the system. On the top model $\gamma\alpha$ is used for the common-envelope parametrisation, on the bottom model $\alpha\alpha$ (see Sect. 5.3). The intensity of the grey scale corresponds to the density of objects on a linear scale in units of number of systems per $10^5 M_{\odot}$. The black line corresponds to a combined mass of $1.4 M_{\odot}$.

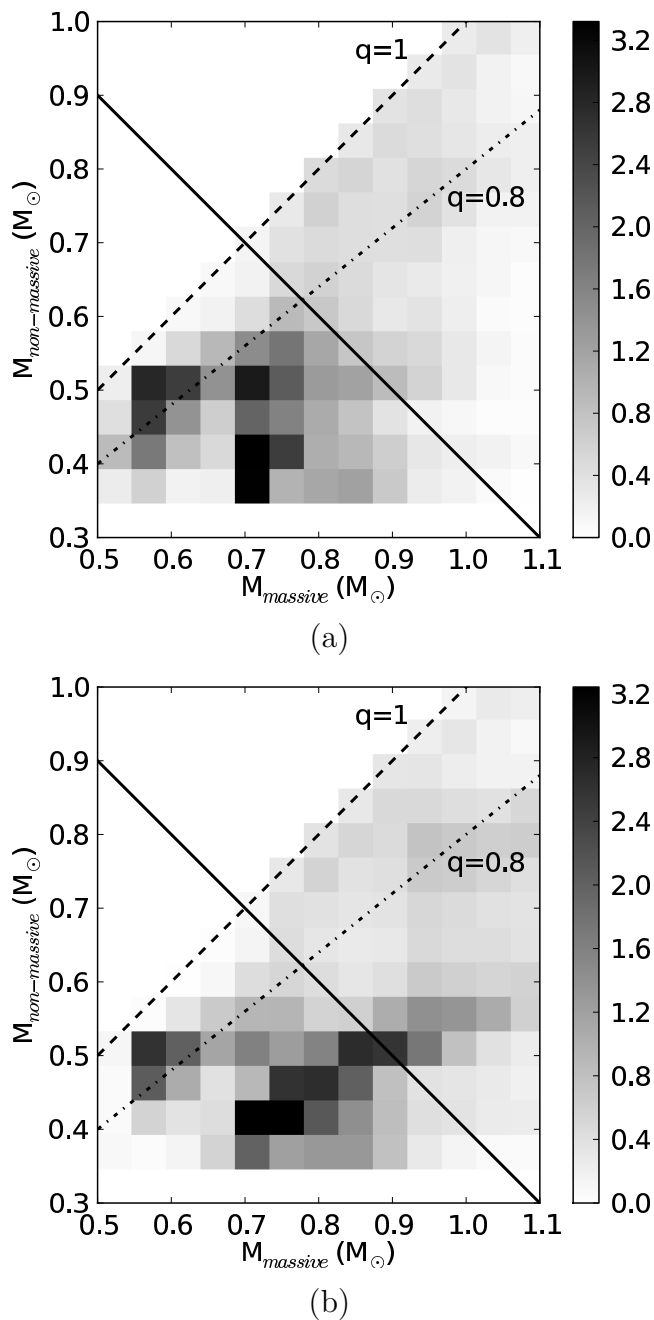


FIGURE 5.9: Simulated population of merging double CO white dwarfs from a single burst of star formation as a function of the masses of the two white dwarfs. M_{massive} is the mass of the most massive white dwarf, $M_{\text{non-massive}}$ corresponds to the least massive white dwarf. On the top model $\gamma\alpha$ is used for the common-envelope parametrisation, on the bottom model $\alpha\alpha$ (see Sect. 5.3). The intensity of the grey scale corresponds to the density of objects on a linear scale in units of number of systems per $10^5 M_{\odot}$. To increase the contrast, we placed an upper limit on the intensity, which effects only one bin for model $\gamma\alpha$ and two bins for model $\alpha\alpha$. The black solid line corresponds to a combined mass of $1.4M_{\odot}$. The dashed and dashed-dotted line correspond to a mass ratio $q = m/M$ of 1 and 0.8, respectively.

5.7 Conclusion and discussion

We studied the population of SNIa progenitors from merging double CO WDs with a combined mass exceeding the Chandrasekhar mass, the so-called DD progenitors. We considered two prescriptions of the CE phase. The CE evolution is a crucial ingredient in the formation of close double degenerate compact objects, but the process itself is still poorly understood. The first model assumes the α -formalism for all CE. The second model is a combination of the α -formalism and the γ -formalism (see Sect. 5.3). Typically, the first CE is described by the γ -scenario and the second by the α -formalism, if mass transfer is unstable.

We applied the updated version of the population synthesis code SeBa to simulate the population of DWDs and SNIa progenitors. At present, close DWDs (of all WD types) are the closest related systems to the DD SNIa progenitors that are visible in bulk. The mass ratio distribution of the DWDs in model $\alpha\alpha$ is inconsistent with the observations. Using model $\gamma\alpha$ the simulated population of DWDs compares well with observations, nevertheless, this is what the γ -formalism was designed to do.

Recently, Webbink [2008] and Zorotovic et al. [2010] claimed that the predictive power of the γ -scenario is more restricted. They suggested that the α -scenario is valid when sources of an energy other than the binding energy of the envelope is available, such as, the energy released by recombination in the common envelope. This could explain the high value of α found by Nelemans et al. [2000] for the second CE, but certainly does not solve the problem for the first CE for which Nelemans et al. [2000] found a value of $\alpha < 0$.

The delay time distributions from our two models show the characteristic shape of a strong decay with time. This strong decay is expected when the delay time is dominated by the gravitational wave timescale ($t_{gr} \propto a^4$) and the distribution of orbital separations at DWD formation is similar to the initial (ZAMS) distribution of $N(a)da \propto a^{-1}da$ [Abt, 1983]. The DTD from model $\gamma\alpha$ fits the shape of the observed DTD best. Mennekens et al. [2010] also showed a DTD using the γ -scenario for the CE phase. They found that the DD DTD lies almost an order of magnitude lower in absolute rate than when using the α -scenario. However, they used the γ -formalism for all CE phases. In our prescription (see Sect. 5.3) the γ -formalism is typically used in the first CE phase only. The reason for this is that in equal mass systems there is more angular momentum compared to unequal mass systems with similar orbits. Mennekens et al. [2010] and also Yungelson & Livio [2000]; Ruiter et al. [2009b] and Claeys et al. [2011] showed DD DTDs using the α -scenario (however their CE-prescriptions may differ slightly from Eq.5.2). Surprisingly, but as realised before, even though different groups used different binary evolution codes with different versions of the α -CE and CE efficiencies, the DTDs of the DD channel are very uniform in that they show a strong decline with time [see for example Nelemans et al., 2013, for an overview].

Usually in synthetic DTD studies, the shape and normalisation of the DTD are discussed

separately. This might not be valid any more, as more and more observed rates are available and the conversion from observational units to synthetic units (e.g. the star formation history (SFH) and rate in per K-band luminosity instead of per M_{\odot} of created stars) is better understood. For example, the SFH is often convolved with the DTD to estimate the SNIa rate in spiral galaxies like our Milky Way. The problem with this is that different assumptions for the Galactic SFH can significantly alter the theoretical Galactic SNIa rate. Since the SNIa rate follows the SFH with typical delay times of a few Gyr, the synthetic Galactic SNIa rate is very sensitive to the assumed SFH at recent times. When a constant SFH (of $\gtrsim 3M_{\odot} \text{ yr}^{-1}$) is assumed, the SNIa rate is artificially enhanced compared with detailed SFHs that show a peak in the star formation at a few Gyr and a decline to $1M_{\odot} \text{ yr}^{-1}$ at recent times, see e.g. Nelemans et al. [2004]. In the observed SNIa rates of Maoz & Badenes [2010] and Maoz et al. [2011] the detailed SFH of every individual galaxy or galaxy subunit was taken into account to reconstruct the DTD. Therefore it is no longer necessary to convolve the theoretical SNIa rate from a burst of star formation with an approximate SFH. The theoretical calculations of the SNIa rate from a single starburst can directly be compared with observations.

We found that the normalisation of the DTD of model $\alpha\alpha$ and $\gamma\alpha$ do not differ much, even though the CE evolution is very different. The time-integrated number of SNIa in model $\alpha\alpha$ ($3.3 \cdot 10^{-4} M_{\odot}^{-1}$) is 70% larger as in model $\gamma\alpha$ ($2.0 \cdot 10^{-4} M_{\odot}^{-1}$). But most importantly, the simulated time-integrated numbers do not match the observed number of $2.3 \pm 0.6 \cdot 10^{-3} M_{\odot}^{-1}$ by [Maoz et al., 2011] by a factor of about 7-12. If our understanding of binary evolution and initial parameter distributions is correct, the standard DD channel is not a major contributor to the SNIa rate.

For the SNIa model proposed by Pakmor et al. [2010], in which carbon burning is ignited in the merger process of two massive white dwarfs of nearly equal mass, we found an SNIa rate of $2.3 \cdot 10^{-5} M_{\odot}^{-1}$ for model $\gamma\alpha$ and $1.8 \cdot 10^{-5} M_{\odot}^{-1}$ for model $\alpha\alpha$. Pakmor et al. [2010] finds that these systems resemble subluminous SNIa such as SN 1991bg. Assuming the fraction of 1991bg-like events to all SNIa events is $15 \pm 6\%$ [Li et al., 2001, 2011], the observed event rate is $3.5 \pm 1.6 \cdot 10^{-4} M_{\odot}^{-1}$. van Kerkwijk et al. [2010] proposed a model in which sub-Chandrasekhar WDs can explode as an SNIa. In this scenario two white dwarfs of nearly equal mass merge, though carbon ignition occurs only after the merger when the thick disk surrounding the remnant is accreted onto it. The event rate is $2.3 \cdot 10^{-4} M_{\odot}^{-1}$ for model $\gamma\alpha$ and $1.9 \cdot 10^{-4} M_{\odot}^{-1}$ for model $\alpha\alpha$. When only taking into account systems with a combined mass below $1.4M_{\odot}$, the rates are $1.3 \cdot 10^{-4} M_{\odot}^{-1}$ and $8.8 \cdot 10^{-5} M_{\odot}^{-1}$, respectively. In the scenario proposed by Pakmor et al. [2010] and in the scenario by van Kerkwijk et al. [2010], systems are required to have high mass ratios. We showed that the mass ratio distribution of DWDs depends on the prescription for the CE. When the γ -scenario is used, the average mass ratio of DWDs lies closer to one, which increases the SNIa rate in the above described scenario with respect to the α -scenario. The rates of the channel proposed by van Kerkwijk et al. [2010] for systems with sub-Chandrasekhar masses are on the same

order of magnitude as the rates of the standard DWD channel. Therefore the combination of the two models is not sufficient to explain the observed rates. For our synthetic rates of the DD scenario to match the observed SNIa rates, within our current model of binary evolution, the parameter space of the DD progenitors has to be increased severely, e.g. to include all CO-CO and CO-He mergers, which seems unlikely.

Alternatively (and if contributions from channels other than the DD are minor), our model underpredicts the fraction of standard DD SNIa progenitors in the entire DWD population. Our model of the visible population of DWDs predicts 0.9-2.9% of the visible DWDs (depending on the model) to be SNIa progenitors. To match the observed rate of Maoz et al. [2011], 10-30% (excluding any errors on the observed and synthetic values) of the observed DWDs should lie in the SNIa progenitor region (upper left corner of Fig. 5.3). With 46 observed DWDs so far, 4-15 SNIa progenitors are expected without taking non-uniform selection effects into account. So far, only two systems have been found that possibly are SNIa progenitors, which makes it improbable, but not impossible, that our model underpredicts the number of DD SNIa progenitors. When the population of observed DWDs is increased, the fraction of SNIa progenitors amongst DWDs will give more insight into the validity of our knowledge of binary evolution of massive DWDs.

Concluding, although the shape of the DD DTD fits the observed DTD beautifully, the normalisation does not. An important point is that we did not optimise our model to fit the observed DTD in shape or number. We showed that the normalisation can be influenced by the metallicity; about 30-60% depending on the model for $Z = 0.001$ with respect to $Z = 0.02$. Furthermore, the normalisation depends on the initial mass function, the percentage of single stars, and the initial distribution of mass ratios and orbital periods. In this paper and in Nelemans et al. [2013] we assumed the percentage of single stars to be 50%. Results from e.g. Kouwenhoven et al. [2007, see also Raghavan et al. 2010] showed that the binary fraction might be as high as 70% or more for A- and B-type stars, potentially raising the synthetic SNIa rate by a factor < 2 . Preliminary results show that the initial distribution of mass ratio and orbital separation affects the slope of the DTD, still the strong decline with time remains. Moreover, the integrated rates are not affected by factors sufficient to match the observed rate. Additional research is needed to study if the normalisation can be raised sufficiently to match the observed rate. If not, the main contribution to the SNIa rate comes from other channels, such as the SD scenario (e.g. supersoft sources), double detonating sub-Chandrasekhar accretors [see e.g. Kromer et al., 2010], or Kozai oscillations in triple systems (Shappee & Thompson 2012; Hamers et al. in prep.).

Acknowledgements

We thank Haili Hu, Marc van der Sluys and Lev Yungelson for providing results from their detailed stellar and binary evolution models. We also thank Dan Maoz for providing us his data of the observed SNIa rate and Frank Verbunt for his software to make the Roche

lobe plots. This work was supported by the Netherlands Research Council NWO (grants VIDI [# 639.042.813], VICI [# 639.073.803], AMUSE [# 614.061.608] and Little Green Machine) and by the Netherlands Research School for Astronomy (NOVA).

5.A Most important changes to the population synthesis code SeBa

5.A.1 Treatment of wind mass-loss

Each star may lose mass in the form of a stellar wind. In a binary system the stellar wind matter from a binary component can be accreted by the companion star or lost from the system (see Appendix 5.A.2). This influences the binary parameters via the loss of mass and angular momentum from the system. We assume that the matter that is lost from the system carries a specific angular momentum equal to that of the star from which it originates. Furthermore, we assume that wind accretion onto the binary companion is Bondi-Hoyle accretion [Bondi & Hoyle, 1944], as re-formulated by Livio & Warner [1984]. The wind mass loss prescriptions for different types of stars used in SeBa are updated e.g. to include metallicity dependency where possible. The prescriptions correspond to some degree to the recommendations by Hurley et al. [2000]. If multiple mass loss predictions are applicable to a star, we take the one that predicts the maximum mass loss rate.

- For all types of luminous stars ($L > 4000L_{\odot}$) from the main sequence (MS) to the asymptotic giant branch (AGB) we apply the empirical mass loss rate by Nieuwenhuijzen & de Jager [1990] given by

$$\dot{M} = 9.631 \cdot 10^{-15} R^{0.81} L^{1.24} M^{0.16} M_{\odot} \text{ yr}^{-1}, \quad (5.5)$$

where \dot{M} is the mass accretion rate, R the stellar radius in R_{\odot} , L the luminosity in L_{\odot} and M the stellar mass in M_{\odot} . We assume that the formalism of Nieuwenhuijzen & de Jager [1990] is dependent on the initial metallicity as $\dot{M}(z) = (z/z_{\odot})^{1/2} \dot{M}(z_{\odot})$ [see Kudritzki et al., 1987].

- For a massive MS star we give preference to the rates of Vink et al. [2000, 2001]. Where they do not apply, the rates of Nieuwenhuijzen & de Jager [1990] are used. Massive MS suffer from strong winds driven by radiation pressure in lines and in the continuum. Vink et al. [2000, 2001] take into account multiple scattering effects of photons. They find good agreement between observations and theoretical mass-loss rates.
- For stars in giant phases we adopt the empirical relation found by Reimers [1975],

$$\dot{M} = 4 \cdot 10^{-13} \frac{\eta RL}{M} M_{\odot} \text{ yr}^{-1}. \quad (5.6)$$

5.A MOST IMPORTANT CHANGES TO THE POPULATION SYNTHESIS CODE SEBA

We assume a numerical prefactor of $\eta = 0.5$, see Maeder & Meynet [1989] and Hurley et al. [2000].

- AGB stars can experience severe mass-loss caused by radiation pressure on dust that condensates in the upper atmosphere of the stars. Empirically, the mass-loss rate has been coupled to the period of large-amplitude radial pulsations P_{puls} [Vassiliadis & Wood, 1993]:

$$\log P_{\text{puls}} \text{ (days)} = -2.07 + 1.94 \cdot \log(R) - 0.9 \cdot \log(M). \quad (5.7)$$

We apply mass-loss to the envelope according to the prescription of Vassiliadis & Wood [1993]. During the superwind phase the radiation pressure driven wind is modelled by

$$\dot{M} = \frac{L}{cv_{\text{exp}}}, \quad (5.8)$$

where c represents the speed of light and v_{exp} the stellar wind expansion velocity. The latter is given by:

$$v_{\text{exp}}(\text{km s}^{-1}) = -13.5 + 0.056P_{\text{puls}}(\text{days}). \quad (5.9)$$

Furthermore, v_{exp} is constrained to the range 3.0-15.0 km s⁻¹.

Before the superwind phase, the mass loss rate increases exponentially with P_{puls} as

$$\log \dot{M} (M_{\odot} \text{ yr}^{-1}) = \begin{cases} -11.4 + 0.0123 \cdot P_{\text{puls}} & \text{if } M \leq 2.5, \\ -11.4 + 0.0125 \cdot (P_{\text{puls}} - 100 \cdot (M - 2.5)) & \text{if } M > 2.5. \end{cases} \quad (5.10)$$

The mass loss rate of Vassiliadis & Wood [1993] is given by the minimum of Eq. 5.8 and Eq. 5.10.

- Luminous blue variables (LBVs) are extremely massive and luminous stars near the Humphreys-Davidson limit [Humphreys & Davidson, 1994] with enormous mass-loss rates. We use the LBV mass loss prescription and implementation suggested by Hurley et al. [2000]:

$$\dot{M} = 0.1 \times \left(10^{-5}RL^{1/2} - 1.0\right)^3 \left(\frac{L}{6.0 \cdot 10^5} - 1.0\right) M_{\odot} \text{ yr}^{-1}, \quad (5.11)$$

if $L > 6.0 \cdot 10^5 L_{\odot}$ and $10^{-5}RL^{1/2} > 1.0$.

- Wolf-Rayet stars are stars in a stage of evolution following the LBV phase where weak or no hydrogen lines are observed in their spectra. Like Hurley et al. [2000]

we include a Wolf-Rayet-like mass-loss for stars with a small hydrogen-envelope mass ($\mu < 1.0$ from their Eq. 97). The prescription itself, however, is different. We model it according to Nelemans & van den Heuvel [2001]:

$$\dot{M} = 1.38 \cdot 10^{-8} M^{2.87} M_{\odot} \text{ yr}^{-1}. \quad (5.12)$$

This is a fit to observed mass-loss rates from Nugis & Lamers [2000]. We multiply with a factor $(1 - \mu)$ to smoothly switch on mass loss.

- In addition to the evolution of ordinary hydrogen rich stars, the evolution of helium burning stars with hydrogen poor envelopes is simulated as well. For helium main-sequence stars with a mass $M > 2.5M_{\odot}$ we assume the same relation as for Wolf-Rayet-like stars. For helium giants, either on the equivalent of the Hertzsprung or giant branch, we describe mass loss in a very general way similar to Nelemans et al. [2001c]. We presume 30% of the mass of the envelope M_{env} will be lost during the naked helium giant phase with a rate that increases in time according to

$$\Delta M_{\text{wind}} = 0.3M_{\text{env}} \left[\left(\frac{t + \Delta t}{t_f} \right)^{6.8} - \left(\frac{t}{t_f} \right)^{6.8} \right], \quad (5.13)$$

where ΔM_{wind} is the amount of mass lost in the wind in M_{\odot} in a timestep Δt , t_f is the duration of the helium giant phase and t the time since the beginning of the phase.

Special attention has been given to prevent large wind mass losses in single timesteps because the mass loss prescriptions are very dependent on the stellar parameters of that timestep. For this reason we implemented an adaptive timestep in situations where strong winds are expected, e.g. at the tip of the giant branch. This procedure is accurate to differences in stellar mass of less than 4% for masses below $12M_{\odot}$.

5.A.2 Accretion onto stellar objects

Roche lobe overflow mass transfer and subsequent accretion can substantially alter the stars and the binary orbit. Mass accretion can affect the structure of the receiver star and its subsequent evolution. When more mass is transferred than the accretor can accrete, we assume that the non-accreted matter leaves the system with an angular momentum of 2.5 times the specific angular momentum of the binary [Portegies Zwart & Verbunt, 1996; Nelemans et al., 2001c]. For compact accretors we assume the matter leaves the system with the specific angular momentum of the compact remnant. In this section we discuss the limiting accretion rate, the response of the accretor to regain equilibrium, and the subsequent evolution of the new object for different types of accretors.

5.A.2.1 Accretion onto ordinary stars

For ordinary stars from MS to AGB stars, we distinguish between two types of accretion; accretion from a hydrogen-rich or a helium-rich envelope. Hydrogen-rich accretion can occur for example when a donor star ascends the giant branch and fills its Roche lobe. After it loses its hydrogen envelope, it can become a helium-burning core. When this helium star ascends the helium equivalent of the giant branch, a fraction of the helium-rich envelope can be transferred onto the accretor. We name this type of accretion 'helium accretion'. We assume that the accreted helium settles and sinks to the core instantaneously. The helium accretion rate is limited by the Eddington limit. Hydrogen is accreted onto the envelope of the receiver star. The accretion rate is bounded by the star's thermal timescale times a factor that is dependent of the ratio of Roche lobe radius of the receivers to its effective radius, as described by Portegies Zwart & Verbunt [1996]. The formalism is proposed by Pols & Marinus [1994], which is based on Kippenhahn & Meyer-Hofmeister [1977]; Neo et al. [1977] and Packet & De Greve [1979]. If the mass transfer rate is higher than the maximum mass accretion rate, the excess material is assumed to leave the binary system.

Because of the accretion, the star falls temporarily out of thermal equilibrium. While regaining equilibrium, the gas envelope surrounding the core puffs outward. Because we do not solve the equations of stellar structure and the stellar evolution tracks describe single stars in equilibrium, we add a procedure to account for a temporal increase in radius as in Portegies Zwart & Verbunt [1996]. This is important for example to determine if an accretor star fills its Roche lobe. It also affects the magnetic braking process and the Darwin-Riemann instability through the increased stellar angular momentum. Note that the mass transfer rate is not dependent on the stellar radius in our simulations, so that the binary evolution is not critically dependent on out-of-equilibrium parameter values.

Accretion can also affect the structure of the receiver star and its subsequent evolution. It is modelled by changing the stellar track and moving along the track. The former is described by the track mass, which is equivalent to the zero-age main-sequence mass that the star would have had without interaction. The latter is described by the relative age t_{rel} of the star. We distinguish two cases:

- Rejuvenation of an MS star

Accretion onto an MS star rejuvenates the star. The star evolves similarly to a younger star of its new mass and its MS lifetime can be extended. It would show up in a Hertzsprung-Russell diagram as a blue straggler. For hydrogen accretion the track mass is always updated and the renewed relative age of the star

$$t'_{\text{rel}} = t_{\text{rel}} \frac{t'_{\text{ms}}}{t_{\text{ms}}} \frac{M}{M'}, \quad (5.14)$$

where primes denote quantities after a small amount of mass accretion, t_{ms} the main-sequence lifetime, and M the mass of the star.

For helium accretion we assume the mass accretes to the core instantaneously and the track mass is increased accordingly. These stars appear older than for hydrogen accretion because more hydrogen has been burned previously. The rejuvenation process is described by

$$t'_{\text{rel}} = t_{\text{rel}} \frac{t'_{\text{ms}}}{t_{\text{ms}}} \frac{M}{M'} + \frac{\delta M t'_{\text{ms}}}{0.1 M'}, \quad (5.15)$$

where we assume 10% of the mass of the star will be burned during the MS phase.

- Rejuvenation of a giant

During the giant phases the envelope is decoupled from the core in terms of stellar structure. The evolution of the star will therefore not be influenced directly by small amounts of hydrogen accretion to the envelope. The track is only updated when the new mass is larger than the track mass to account for severe hydrogen accretion. The mass before accretion can be much lower than the track mass because of wind mass loss, which can be strong for giants. For helium accretion to the core, the track is always updated. An exception to this is the early AGB where the helium core does not grow. In this stage there is a one-to-one relation between the helium core mass and the track mass [Eq.66 in Hurley et al., 2000].

When a giant accretor star moves to a new evolutionary track, we need to determine the location of the star along this track. In a more physical picture this means determining the relative age of the star t_{rel} . For a giant its evolution is mainly determined by its core. Therefore for a given evolutionary track and core mass, the relative age is effectively constrained. For both types of accretion, we insist that the star stays in its same evolutionary state after its mass increase. When no solution can be found for t_{rel} , the relative age is set to the beginning or end of the current evolutionary state and the track mass is varied to find a fitting track that ensures mass conservation.

5.A.2.2 Accretion onto helium-burning cores

For accretion onto helium-burning stars that have lost their hydrogen envelopes, accretion is limited by the Eddington limit. Helium accretion onto a helium main-sequence star is similar as hydrogen accretion onto normal main-sequences stars. We assume that the star evolves similarly to a younger star of its new mass according to Eq. 5.14 where t_{ms} should be replaced by the helium main-sequence life time. We assume that for helium giants the envelope is decoupled from the core in terms of stellar structure, as with hydrogen-rich giants. Therefore we assume that the evolution of the giant is not affected and only update the track when the new mass is larger than the track mass.

The effect of hydrogen accretion onto helium stars is more complicated. If the hydrogen layer is sufficiently thick, the layer can ignite. This can significantly increase the radius of

the star and essentially turn it into a born-again star on the horizontal or asymptotic giant branch. We studied the effect of hydrogen accretion to helium stars with stellar models simulated by the stellar evolution code STARS. This code models stellar structure and evolution in detail by solving the stellar structure equations. The code is based on Eggleton [1971] and includes updated input physics as described in Hu et al. [2010]. The models do not include atomic diffusion. For mass accretion rates at ten percent of the Eddington rate of the accretor for about $10^4 - 10^5$ yr, the accreted hydrogen layer ignites. Helium stars that are more massive than about $0.55M_{\odot}$ resemble horizontal branch stars after accretion, but most of the luminosity still comes from helium burning. For lower mass helium stars this is not the case, because the corresponding horizontal branch stars ($< 3.5M_{\odot}$) can have ignited helium in a degenerate core, which strongly affects the characteristics of the star. For both mass ranges, the accretor expands by a factor of about 10-100 compared to the original helium star. Because hydrogen accretion to helium stars is not very likely, we model this very simply. When more than 5% of the total mass is accreted, the radius of the star is increased by a factor 50. With few exceptions, this leads to a merger of the two components.

The effect of hydrogen accretion to helium giants is not known very well and additional research is necessary. For now, because it is very unlikely to happen, we treat it in the same way as helium accretion onto the envelope of the giant.

5.A.2.3 Accretion onto remnants

White dwarf, neutron star and black hole accretors can accrete with a maximum rate of the Eddington limit. If more mass is transferred, the surplus material leaves the system with the specific angular momentum of the compact remnant. For neutron stars and black holes we assume that the transferred mass is temporarily stored in a disk. From this disk, mass will flow onto the surface of the remnant with ten percent of the Eddington limit. We assume that a neutron star collapses onto a black hole when its mass exceeds $1.5M_{\odot}$.

For white dwarfs, the accretion process is more complicated because of possible thermonuclear runaways in the accreted material on the surface of the white dwarf. In SeBa there are several options to model the effectiveness of the white dwarf to retain the transferred material. For hydrogen accretion we can choose between the efficiencies of Hachisu et al. [2008] and Prialnik & Kovetz [1995]. For helium retention, the option is between Kato & Hachisu [1999] [with updates from Hachisu et al., 1999] and Iben & Tutukov [1996].

5.A.3 Stability of mass transfer

A semi-detached system can become unstable in two ways. In a mass transfer instability, the Roche-lobe-filling star expands faster than the Roche lobe itself on the relevant timescale. In the other case tidal interactions lead to an instability [Darwin, 1879].

5.A.3.1 Tidal instability

A tidal instability can take place in systems of extreme mass ratios. When there is insufficient orbital angular momentum J_b that can be transferred onto the most massive star, the star cannot stay in synchronous rotation. Tidal forces will cause the companion to spiral into the envelope of the donor star. The tidal instability occurs when the angular momentum of the star $J_\star > \frac{1}{3}J_b$, where

$$J_b = Mm\sqrt{\frac{Ga}{M+m}}, \quad (5.16)$$

where J_b is the orbital angular momentum of the circularised binary, a is the orbital separation, M the mass of the donor star and m the mass of the accretor star. The angular momentum J_\star of a star with radius R is given by

$$J_\star = k^2 MR^2\omega, \quad (5.17)$$

where k^2 is the gyration radius described by Nelemans et al. [2001c] and ω is the angular velocity of the donor star, which is assumed to be synchronised with the orbit. It is given by $\omega = 2\pi/P_b$, where P_b is the orbital period. We model the inspiral according to the standard α -CE (see Sect. 5.3). Owing to the expulsion of the envelope, the binary may evolve to a more stable configuration or merge. If the mass-losing star is a main-sequence star, we assume that the instability always leads to a merger.

5.A.3.2 Mass transfer instability

The stability of mass transfer from Roche lobe overflow and its consequences on the binary depend on the response of the radius and the Roche lobe of the donor star to the imposed mass loss (e.g. Webbink 1985; Hjellming & Webbink 1987 (hereafter HW87); Pols & Marinus 1994; Soberman et al. 1997). We distinguish four modes of mass transfer; on the dynamical, thermal, nuclear timescale of the donor or on the angular-momentum-loss timescale. The response of the accretor star to the mass that is transferred onto it and the effect of this on the orbit is described in Appendix 5.A.2. The response of the donor star to mass loss is to readjust its structure to recover hydrostatic and thermal equilibrium. The dynamical timescale to recover hydrostatic equilibrium is short compared to the thermal timescale. For mass transfer to be dynamically stable, the dynamical timescale of the star is important. The change in radius due to adiabatic adjustment of hydrostatic equilibrium is expressed as a logarithmic derivative of the radius with respect of mass,

$$\zeta_{\text{ad}} = \left(\frac{d \ln R}{d \ln M} \right)_{\text{ad}}, \quad (5.18)$$

where M and R are the mass and radius of the donor star. The assumed values of ζ_{ad} are shown in Table 5.2.

The response of the Roche lobe R_L of the donor star is expressed as the logarithmic derivative of the Roche lobe radius with respect to mass:

$$\zeta_L = \frac{d \ln R_L}{d \ln M}. \quad (5.19)$$

The value of ζ_L is calculated numerically by transferring a test mass of $10^{-5} M_\odot$. Because $\zeta_L = \zeta_L(M_1, M_2, a)$, ζ_L is dependent on the mass accretion efficiency of the secondary, and therefore on the mass accretion rate of the test mass. For instance, for high mass ratios $q \gg 1$ the loss of some mass and corresponding angular momentum can have a stabilising effect on the mass-transferring binary. To determine the dynamical stability of mass transfer, we assume that the mass transfer rate of the test mass is on the thermal timescale of the donor star:

$$\tau_{\text{th}} = \frac{GM^2}{RL}. \quad (5.20)$$

1. When $\zeta_L > \zeta_{\text{ad}}$, mass transfer is dynamically unstable. We model this as a CE phase², as described in Sect. 5.3.

When $\zeta_L < \zeta_{\text{ad}}$ mass transfer is dynamically stable. The donor star is able to regain hydrostatic equilibrium and shrinks within its Roche lobe on a dynamical timescale. To determine if the donor star is also able to regain thermal equilibrium during mass transfer, we calculate the change in the radius of the star as it adjusts to the new thermal equilibrium:

$$\zeta_{\text{eq}} = \left(\frac{d \ln R}{d \ln M} \right)_{\text{th}}. \quad (5.21)$$

The assumed values for ζ_{eq} are described in Table 5.2.

To calculate the response of the Roche lobe $\zeta_{L,\text{eq}}$, we assume that the mass transfer rate of the test mass is on the nuclear evolution timescale:

$$\tau_{\text{nuc}} = dt \frac{R}{dR_{\text{eq}}}, \quad (5.22)$$

where R represents the equilibrium radius of the star according to the single-star tracks. dR_{eq} is the change in R in a short timestep dt without binary interactions.

2. When $\zeta_{L,\text{eq}} < \min(\zeta_{\text{eq}}, \zeta_{\text{ad}})$ mass transfer is driven by the expansion of the stellar radius due to its internal evolution.

² When the timescale of the CE phase becomes relevant, we assume that it proceeds on a time scale τ given by the geometric mean of the thermal τ_{th} and dynamical τ_{d} timescales of the donor [see Paczyński & Sienkiewicz, 1972]:

$$\tau = \sqrt{\tau_{\text{d}}\tau_{\text{th}}}; \quad \tau_{\text{d}} = \sqrt{\frac{R^3}{GM}}.$$

3. When $\zeta_{L,\text{eq}} > \min(\zeta_{\text{eq}}, \zeta_{\text{ad}})$, the mass transfer is thermally unstable and proceeds on the thermal time scale of the donor.
4. The previous modes of mass transfer are caused by an expanding donor star. The final mode is caused by shrinking of the orbit caused by angular momentum loss. We assume that this mode takes place when the corresponding timescale τ_J is shorter than the timescales at which the other three modes of mass transfer take place. Angular momentum loss can happen due to gravitational wave radiation \dot{J}_{gr} [Kraft et al., 1962] and magnetic braking \dot{J}_{mb} [Schatzman, 1962; Huang, 1966; Skumanich, 1972; Verbunt & Zwaan, 1981]. Mass transfer proceeds on the time scale on which these processes occur:

$$\tau_J = \frac{J_b}{\dot{J}_{\text{gr}} + \dot{J}_{\text{mb}}}, \quad (5.23)$$

where J_b is the angular momentum of the circularized binary given by Eq. 5.16. Next we discuss the assumptions and implications of \dot{J}_{gr} and \dot{J}_{mb} .

Gravitational wave radiation most strongly influences close binaries since it is a strong function of orbital separation. The change in orbital separation \dot{a} averaged over a full orbit is given by [Peters, 1964]

$$\dot{a}_{\text{gr}} = -\frac{64}{5} \frac{G^3 M m (M + m)}{c^5 a^3 (1 - e^2)^{7.2}} \left(1 + \frac{73}{24} e^2 + \frac{37}{96} e^4 \right), \quad (5.24)$$

where $\dot{J}_{\text{gr}}/J_b = \dot{a}_{\text{gr}}/(2a)$.

Magnetic braking affects stars within the mass range of $0.6 \lesssim M/M_\odot \lesssim 1.5$. These stars suffer from winds that are magnetically coupled to the star. Although the mass loss in this process is negligible, the associated angular momentum loss can be severe [Rappaport et al., 1983]:

$$\frac{\dot{J}_{\text{mb}}}{J_b} = -\frac{3.8 \cdot 10^{-30} R_\odot^{4-\beta} (M + m) R^\beta \omega^2}{m a^2}, \quad (5.25)$$

where β is a parameter that represents the dependence of the braking on the radius of the donor star. We take $\beta = 2.5$.

5.A MOST IMPORTANT CHANGES TO THE POPULATION SYNTHESIS CODE SEBA

TABLE 5.2: Values of the adiabatic ζ_{ad} and thermal ζ_{eq} response of the radius to mass loss for different types of stars.

k	Evolutionary state	ζ_{ad}	ζ_{eq}
0,1	Main-sequence:		
	$M_o < 0.4$	$-1/3$	0
	$0.4 < M_o < 1.5$	2	0.9
	$M_o > 1.5$	4	0.55
2	Hertzsprung gap:		
	$M_o < 0.4$	4	0
	$M_o > 0.4$	4	-2
3	First giant branch:		
	· shallow convective layer	4	0
	· deep convective layer	HW87	0
4	Horizontal branch:		
	$M_o < M_{\text{Hef}}$	4	4
	$M_{\text{Hef}} < M_o < M_{\text{FGB}}$:	as $k = 3$	0
	· decent along GB	4	4
	· blue phase	4	4
$M_o > M_{\text{FGB}}$:	· blue phase	4	-2
	· ascent to AGB	HW87	0
5,6	Asymptotic giant branch	HW87	0
7	Helium main-sequence:		
	$M < 0.2$	15	-0.19
	$M > 0.2$	15	1
8,9	Helium giant:		
	$M_c < 0.4$	HW87	$-1/3$
	$M_c > 0.4$	HW87	-2
10,11,12	White dwarf	$-1/3$	$-1/3$

NOTES: The types of stars correspond to the definition by Hurley et al. [2000] expressed by their integer k . The stellar tracks are distinguished by the mass M_o , which is equivalent to the ZAMS mass the star would have had without interaction. M_{Hef} and M_{FGB} are defined by Eq. 2 and 3 from Hurley et al. [2000]. M_{Hef} represents the maximum initial mass for which helium ignites degenerately in a helium flash, which is about $2M_{\odot}$ for solar metallicities. M_{FGB} is the maximum initial mass for which helium ignites on the first giant branch, which is about $13M_{\odot}$ for solar metallicities. M is the total mass of the star and M_c the mass of the core. HW87 represents Hjellming & Webbink [1987]. For stars on the first giant branch there are two prescriptions of ζ_{ad} . If the convective zone in the upper layers of the envelope is shallow [fits from Yungelson, private communication], we assumed the envelope responds to mass loss in a similar manner as radiative envelopes.

POPCORN: HUNTING DOWN THE DIFFERENCES BETWEEN BINARY POPULATION SYNTHESIS CODES

S. Toonen, J. S. W. Claeys, N. Mennekens, A. J. Ruiter

Submitted to Astronomy and Astrophysics

Abstract

Binary population synthesis (BPS) modelling is a very effective tool to study the evolution and properties of various types of close binary systems. The uncertainty in the parameters of the model and their effect on a population can be tested in a statistical way, which then leads to a deeper understanding of the underlying (sometimes poorly understood) physical processes involved. Several BPS codes exist that have been developed with different philosophies and aims. Although BPS has been very successful for studies of many populations of binary stars, in the particular case of the study of the progenitors of supernovae Type Ia, the predicted rates and ZAMS progenitors vary substantially between different BPS codes. To understand the predictive power of BPS codes, we study the similarities and differences in the predictions of four different BPS codes for low- and intermediate-mass binaries. We investigate the differences in the characteristics of the predicted populations, and whether they are caused by different assumptions made in the BPS codes or by numerical effects, e.g. a lack of accuracy in BPS codes. We compare a large number of evolutionary sequences for binary stars, starting with the same initial conditions following the evolution until the first (and when applicable, the second) white dwarf (WD) is formed.

To simplify the complex problem of comparing BPS codes that are based on many (often different) assumptions, we equalise the assumptions as much as possible to examine the inherent differences of the four BPS codes. We find that the simulated populations are similar between the codes. Regarding the population of binaries with one WD, there is very good agreement between the physical characteristics, the evolutionary channels that lead to the birth of these systems, and their birthrates. Regarding the double WD population, there is a good agreement on which evolutionary channels exist to create double WDs and a rough agreement on the characteristics of the double WD population. Regarding which progenitor systems lead to a single and double WD system and which systems do not, the four codes agree well. Most importantly, we find that for these two populations, the differences in the predictions from the four codes are not due to numerical differences, but because of different inherent assumptions. We identify critical assumptions for BPS studies that need to be studied in more detail.



6.1 Introduction

Binary population synthesis codes (hereafter BPS codes) enable the rapid calculation of the evolution of a large number of binary stars over the course of the binary lifetime. With such models, we can study the contribution of binary stars to an environment, e.g. the chemical enrichment of a region, or the frequency of an astrophysical event. We can learn about and study the formation and evolution of stellar systems that are important for a wide range of astronomical topics: novae, X-ray binaries, symbiotics, subdwarf B stars, gamma ray bursts, R Coronae Borealis stars, AM CVn stars, Type Ia and Type Ib/c supernovae, runaway stars, binary pulsars, blue stragglers, etc.

To carefully study binary populations, in principle it is necessary to follow the evolution of every binary system in detail. However, it is not feasible to evolve a population of binary stars from the zero-age main-sequence (ZAMS) to remnant formation with a detailed stellar evolution code. Such a task is computationally expensive as there are many physical processes which must be taken into account over large physical and temporal scales: tidal evolution, Roche lobe Overflow (RLOF), mass transfer. Moreover not all processes can be modelled with detailed codes, e.g. common envelope evolution, contact phases. Therefore, simplifying assumptions are made about the binary evolution process and many of its facets are modelled by the use of parameters. This process is generally known as binary population synthesis. Examples of such parametrisation are straightforward descriptions

for the stability of mass transfer, the accretion efficiency during mass transfer, the angular momentum loss during non-conservative mass transfer, etc. For the evolution of an individual system, the above can of course be an oversimplification. However, for the treatment of the general characteristics of a large population of binaries this process works very well [e.g. Eggleton et al., 1989].

The use of BPS codes dates back several decades [see e.g. Iben & Tutukov, 1984; Melnick et al., 1985; Eggleton et al., 1989; Meurs & van den Heuvel, 1989; Yungelson et al., 1993, for some early examples] and they were used to calculate the most diverse properties of binary populations [for a very thorough review, see Han et al., 2001]. A number of BPS codes are being used in the field, and (sometimes large) differences exist in the way the codes are designed to treat various stages of binary evolution. The physics of binary star evolution is not clear-cut, since many mechanisms that govern important processes are quite uncertain (e.g. mass transfer and transport of angular momentum in and from the binary). In all BPS codes, certain physical processes are modelled in some detail, while others are modelled using simple approximations, to e.g. save computational time. To some degree, the effects that are most important for the problem being studied will be more elaborately included in the corresponding BPS codes.

Recently, several BPS codes have been used to study the progenitors of Type Ia supernovae [e.g. Yungelson et al., 1994; Han et al., 1995; Jorgensen et al., 1997; Yungelson & Livio, 2000; Nelemans et al., 2001c; Han & Podsiadlowski, 2004; De Donder & Vanbeveren, 2004; Yungelson, 2005; Lipunov et al., 2009; Ruiter et al., 2009b, 2011; Mennekens et al., 2010; Wang et al., 2010; Meng et al., 2011; Bogomazov & Tutukov, 2009, 2011; Ruiter et al., 2013; Toonen et al., 2012; Mennekens et al., 2012, Claeys et al. in prep.]. From these recent studies, it has become evident that the various codes show different results in terms of the SNe Ia rate [Nelemans et al., 2013], in particular for the single degenerate channel in which binary systems can produce a SNe Ia by accretion from a non-degenerate companion to a WD. The differences in the predicted SNIa rate are largely, but not completely, due to differences in the assumed retention efficiency of the accretion onto the WD [Bours et al., 2013]. While it has long been expected by groups working on population synthesis that the differences in the BPS results were the result of different assumptions being made in these various studies rather than numerical in nature, it became ever more clear that a quantitative study of the nature and causes of these differences is necessary.

This paper aims to do this by clarifying, for four different BPS codes, the respective ingredients and assumptions included in the population codes and comparing models of several simulated populations for which all assumptions have been made the same as much as possible. We discuss the similarities and differences in the predicted populations and examine the causes for the differences that remain. The causes for differences are valuable information for interpreting binary population synthesis results, and as input for the astronomical community to increase our understanding of binary evolution. The project is known as PopCORN - Population synthesis of Compact Objects Research Network. It is

not the purpose of this paper to discuss the advantages or shortcomings of the respective methods used in BPS codes, nor to judge which assumptions made for binary evolutionary aspects are the most desirable.

The paper focuses on low and intermediate mass close binaries, i.e. those with initial stellar masses below $10 M_{\odot}$. The reason for this is twofold: firstly, as the project originates from differences in the predictions of SNe Ia rates, the systems that produce white dwarfs are the main focus. Secondly, since the evolution of massive stars is even less straightforward, and its modelling includes even more uncertainties, comparing massive star population synthesis will be a whole new project.

In Sect. 6.2 we give an overview of the relevant processes for the evolution of low- and intermediate-mass binaries. Section 6.3 describes the codes involved in this project. The method we use to conduct the BPS comparison is described in Sect. 6.4. We compare the simulated populations of systems containing one WD in Sect. 6.5.1 and two WDs in Sect. 6.5.2. Both sections start with a comparison of all systems and their progenitors and present the main results of the paper. A more detailed comparison follows in subsequent subsections of Sect. 6.5.1 and 6.5.2. In Sect. 6.6 we summarise and discuss the causes for differences that were found in Sect. 6.5. Our conclusions are given in Sect. 6.7. An overview of the inherent and typical assumptions of each code can be found in Appendix 6.A and 6.B respectively.

6.2 Binary evolution

In this section we will give a rough outline of binary evolution and the most important processes that take place in low and intermediate mass binaries. The actual implementation in the four BPS codes under consideration in this study is described in Appendix 6.A and 6.B.

6.2.1 Roche lobe overflow

Low-and intermediate-mass systems with initial periods less than approximately 10 years and primary masses above approximately $0.8M_{\odot}$, will come into Roche lobe contact within a Hubble time. The stars in a binary system evolve effectively as single stars, slowly increasing in radius and luminosity, until one or both of the stars fills its Roche lobe. At this point mass from the outer layers of the star can flow through the first Lagrangian point leaving the donor star.

Depending on the reaction of the star upon mass loss and the reaction of the Roche lobe upon the rearrangement of mass and angular momentum in the system, mass transfer can be stable or unstable. When mass transfer becomes unstable, the loss of mass from the donor star will cause it to overfill its Roche lobe further. In turn this increases the mass loss rate leading to a runaway process. In comparison, when mass transfer is stable, the donor star will stay approximately within the Roche lobe. Mass transfer is maintained by the

expansion of the donor star, or the contraction of the Roche lobe from the rearrangement of mass and angular momentum in the binary system.

RLOF influences the evolution of the donor star by the decrease in mass. The evolution of the companion star is affected too if some or all of the mass lost by the donor is accreted. This is particularly true if some of the accreted (hydrogen-rich) matter makes its way to the core through internal mixing, where it will thus lead to replenishment of hydrogen, a process known as rejuvenation [see e.g. Vanbeveren & De Loore, 1994].

Orbits of close binaries are affected by angular momentum loss (AML) from gravitational wave emission [e.g. Peters, 1964], possibly magnetic braking [Verbunt & Zwaan, 1981; Knigge et al., 2011] and tidal interaction. Magnetic braking extracts angular momentum from a rotating star by a stellar wind that is magnetically coupled to the star. If the star is in corotation with the orbit, angular momentum is essentially also removed from the binary orbit. Tidal interaction plays a crucial role in circularising binaries and will strive to synchronise the rotational period of each star with the orbital period. While it is known that tidal effects will eventually achieve tidal locking of both components, the strength of tidal effects is still subject to debate [see e.g. Zahn, 1977; Hut, 1981].

6.2.1.1 Stable mass transfer

In the case of conservative RLOF the variation in the orbital separation a during the mass transfer phase is dictated solely by the masses. If the gainer star accretes mass non-conservatively, there is a loss of matter and angular momentum from the system. We define the accretion efficiency:

$$\beta = \left| \dot{M}_a / \dot{M}_d \right|, \quad (6.1)$$

where M_d is the mass of the donor star and M_a is the mass of the accreting companion. If $\beta < 1$, it is also necessary to make an assumption about how much angular momentum J is carried away with it. We define this with a parameter η such that:

$$\frac{\dot{J}}{J} = \eta \frac{\dot{M}}{M_d + M_a} (1 - \beta). \quad (6.2)$$

The amount of angular momentum that is lost from the system due to mass loss has a large influence on the evolution of the binary. Several prescriptions for AML exist. They can be divided in four modes of AML or combinations of these modes [see e.g. Soberman et al., 1997, for an overview of the effect of the different prescriptions on the stability of the system].

- Orbital angular momentum loss mode;
In this mode the mass is assumed to leave the binary system, with (a multiple of) the specific orbital angular momentum of the binary, i.e $\eta = \text{constant}$.
- Jeans mode;
Mass is assumed to leave the system from the vicinity of the donor star in a fast

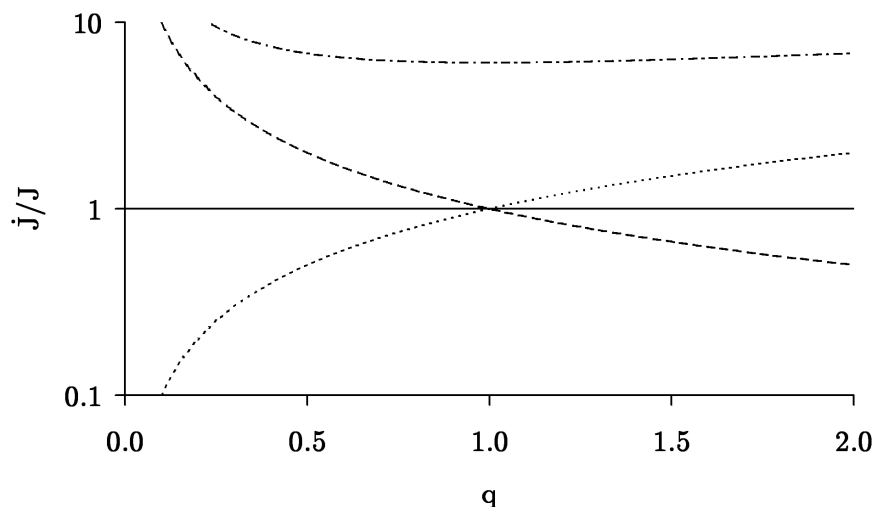


FIGURE 6.1: Angular momentum loss (in terms of $\frac{\dot{M}(1-\beta)}{M_d+M_a}$) as a function of mass ratio for four modes: specific angular momentum loss mode (solid, for $\eta = 1$), Jeans mode (dotted), isotropic re-emission mode (dashed) and in the case of a circumbinary ring (dashed-dotted, for $a_{ring}/a = 2.3$). See text for definition and explication of modes.

spherically symmetric wind. In this mode, the wind matter does not interact with the system. It takes with it the specific orbital angular momentum of the donor in its relative orbit around the centre of mass. Making the assumption that the donor star can be approximated by a point mass, the specific angular momentum loss is as in eq. 6.2 with:

$$\eta = \frac{M_a}{M_d}. \quad (6.3)$$

- Isotropic re-emission;

In this case mass is assumed to leave the system from the position of the gainer in a spherically symmetric way (or at least symmetric with respect to the equatorial plane of the star). Possible scenarios are an enhanced stellar wind or bipolar jets. Further assumptions are as in the previous case, resulting in:

$$\eta = \frac{M_d}{M_a}. \quad (6.4)$$

- Circumbinary ring;

Finally, it is possible to assume that the matter will leave the binary through the formation of a non-corotating circumbinary ring, after passing through the second Lagrangian point L_2 . The amount of angular momentum lost then depends on the radius of this ring a_{ring} compared to the orbital separation a :

$$\eta = \sqrt{\frac{a_{ring}}{a}} \frac{(M_d + M_a)^2}{M_d M_a}. \quad (6.5)$$

While an absolute minimum for a_{ring} is the distance from the center of mass to L_2 (which can be shown to vary only very slightly during a mass transfer episode), it was shown by Soberman et al. [1997] that a more realistic value is 2.3 times the orbital separation.

Figure 6.1 shows, for the four different AML modes, the angular momentum loss \dot{J}/J as a function of mass ratio $q = M_a/M_d$. It is clear that the assumption of AML from a circumbinary ring always leads to the largest AML. The Jeans mode causes the least AML for systems with low mass ratios $q < 1$, because the donor is then close to the center of mass of the system. As the mass ratio increases during mass transfer, the AML increases as well since the donor recedes from the center of mass. Conversely, the isotropic re-emission mode causes a large AML for low mass ratio systems, as the gainer is far from the center of mass. As the mass ratio rises, the gainer closes in on the center of mass and AML decreases. The orbital AML assumption results in an intermediate case between the two.

The choice of AML mode is critical for both the stability and the orbital evolution of mass transfer. To illustrate, in the case of the circumbinary ring mode (extracting the most angular momentum), a given amount of mass loss will lead to much more AML than in the case of Jeans mode AML. The former mode will thus result in a far greater number of systems that merge than the latter.

Matter and angular momentum can also be lost through stellar winds. As these are usually assumed to be spherically symmetric, they will extract the specific orbital angular momentum of the donor star i.e. Jeans mode, and result in an increase in the orbital period. If, however, the wind is allowed to interact with the orbit of the binary, the result is entirely dependent on this interaction.

6.2.1.2 Unstable mass transfer

During unstable mass transfer, the envelope of the donor star engulfs the companion star. Therefore this phase is often called the common envelope (CE) phase [Paczynski, 1976]. A merger of the companion and the core of the donor star can be avoided, if the gaseous envelope surrounding them is expelled e.g. by viscous friction that heats the envelope. Because of the loss of significant amounts of mass and angular momentum the CE-phase can have a very strong effect on the binary orbit. In particular it plays an essential role in the formation of short period systems containing at least one compact object. Despite this, the phenomenon is not yet well understood, see Ivanova et al. [2013] for an overview.

There are several formalisms available to treat the orbital evolution during CE-evolution. The most popular formalisms are the α -formalism [Tutukov & Yungelson, 1979] and the γ -formalism [Nelemans et al., 2000]. The first considers the energy budget of the initial and final configuration, while the latter is based on the angular momentum balance. Both prescriptions include a parameter after which they are named, which determines the efficiency to remove the envelope. Because such an unstable mass transfer phase occurs on

a short timescale, it is often assumed that the gainer does not have the time to gain an appreciable amount of mass during a CE-phase.

The α -parameter describes the efficiency of which orbital energy is consumed to unbind the common envelope according to:

$$E_{\text{gr}} = \alpha_{\text{ce}}(E_{\text{orb},i} - E_{\text{orb},f}), \quad (6.6)$$

where E_{orb} is the orbital energy, E_{gr} is the binding energy of the envelope and α_{ce} is the efficiency of the energy conversion. The subscript *i* and *f* represent the parameter before and after the CE-phase respectively. Several prescriptions for the quantities $E_{\text{orb},i}$ and E_{gr} have been proposed [Webbink, 1984; Iben & Livio, 1993; Hurley et al., 2002] resulting in de facto different α -formalisms. We assume $E_{\text{orb},i}$ and E_{gr} as given in the α -formalism of Webbink [1984], such that

$$E_{\text{orb},i} = \frac{GM_{\text{d}}M_{\text{a}}}{2a_i}, \quad (6.7)$$

and

$$E_{\text{gr}} = \frac{GM_{\text{d}}M_{\text{d,env}}}{\lambda_{\text{ce}}R}, \quad (6.8)$$

where R is the radius of the donor star, $M_{\text{d,env}}$ is the envelope mass of the donor and λ_{ce} depends on the structure of the donor [de Kool et al., 1987; Dewi & Tauris, 2000; Xu & Li, 2010; Loveridge et al., 2011].

In the case of mass transfer between two giants with loosely bound envelopes, some codes employ a formalism different from the canonical CE-descriptions. The envelopes are expelled according to

$$E_{\text{gr},\text{d1}} + E_{\text{gr},\text{d2}} = \alpha(E_{\text{orb},i} - E_{\text{orb},f}), \quad (6.9)$$

analogous to eq. 6.6, where $E_{\text{gr},\text{d1}}$ and $E_{\text{gr},\text{d2}}$ represents the binding energy of the envelope of the two donor stars. This mechanism is termed a double common envelope phase [Brown, 1995].

6.3 Binary population synthesis codes

In this paper we compare the results of the simulations of four different BPS codes. These codes have been developed throughout the years with different scientific aims and philosophies, which has resulted in different numerical treatments and assumptions to describe binary evolution. An overview of the methods that are inherent to and the typical assumptions in the four BPS codes can be found in Appendix 6.A and 6.B. Below a short description is given of each code in alphabetical order:

6.3.1 `binary_c/nucsyn`

`Binary_c/nucsyn` (`binary_c` for future reference) is a rapid single star and binary population synthesis code with binary evolution based on Hurley et al. [2000, 2002]. Updates

and relevant additions are continuously made [Izzard et al., 2004, 2006, 2009, Claeys et al., in prep.] to improve the code and to compare the effects of different prescriptions for ill-constrained physical processes. The most recent updates (Claeys et al., in prep.) that are relevant for this paper are a new formulation to determine the mass transfer rate, the accretion efficiency of WDs and the stability criteria for helium star donors and accreting WDs. The code uses analytical formulae based on detailed single star tracks at different metallicities [based on Pols et al., 1998; Karakas et al., 2002], with integration of different binary features [based on BSE, Hurley et al., 2002]. In addition, the code includes nucleosynthesis to follow the chemical evolution of binary systems and their output to the environment [Izzard et al., 2004, 2006, 2009].

The code is used for different purposes, from the evolution of low-mass stars to high-mass stars. This includes the study of carbon- or nitrogen-enhanced metal-poor stars [CEMP/NEMP-stars, Izzard et al., 2009; Pols et al., 2012; Abate et al., 2013], the evolution of Barium stars [Bonačić Marinović et al., 2006; Izzard et al., 2010], progenitor studies of SNe Ia (Claeys et al. in prep.), the study of rotation of massive stars [de Mink et al., 2013] and recently the evolution of triple systems [Hamers et al., 2013]. Although the code has different purposes, the main strength of the code is the combination of a binary evolution code with nucleosynthesis which enables the study of not only the binary effects on populations, but also the chemical evolution of populations and its output to the environment.

6.3.2 The Brussels code

The Brussels binary evolution population number synthesis code has been under development for the better part of two decades, primarily to study the influence of binary star evolution on the chemical evolution of galaxies. A thorough review of the Brussels PNS code is given by De Donder & Vanbeveren [2004].

The population code uses actual binary evolution calculations (not analytical formulae) performed with the Paczyński-based Brussels binary evolution code, developed over more than three decades at the Astrophysical Institute of the Vrije Universiteit Brussel. An important feature is that the effects of accretion on the further evolution of the secondary star are taken into account. The population code interpolates between the results of several thousands of actual binary evolution models, calculated under the assumption of the “snowfall model” by Neo et al. [1977] in the case of direct impact, and assuming accretion induced full mixing [see Vanbeveren & De Loore, 1994] if accretion occurs through a disk. The actual evolution models have been published by Vanbeveren et al. [1998]. The research done with the Brussels code mainly focuses on the chemical enrichment of galaxies caused by intermediate mass and massive binaries. Therefore the interpolations contained in the population code do not allow for the detailed evolution of stars with initial masses below $3 M_{\odot}$.

In recent years, the code was mainly used to study the progenitors of Type Ia supernovae [Mennekens et al., 2010, 2012], the contribution of binaries to the chemical evolution of globular clusters [Vanbeveren et al., 2012] and the influence of merging massive close binaries on Type II supernova progenitors [Vanbeveren et al., 2013].

6.3.3 SeBa

SeBa is a fast binary population synthesis code that is originally developed by Portegies Zwart & Verbunt [1996] with substantial updates from Nelemans et al. [2001c] and Toonen et al. [2012]. Recent updates include the metallicity dependent single stellar evolution tracks of Hurley et al. [2000] for non-degenerate stars, updated wind mass loss prescriptions and improved prescriptions for hydrogen and helium accretion, and the stability of mass transfer.

The philosophy of SeBa is to not a priori define evolution of the binary, but rather to determine this at runtime depending on the parameters of the stellar system. When more sophisticated models become available of processes that influence stellar evolution, these can be included, and the effect can be studied without altering the formalism of binary interactions. An example of this is the stability criterion of mass transfer and the mass accretion efficiency.

SeBa has been used to study a large range of stellar populations: high mass binaries [Portegies Zwart & Verbunt, 1996], double neutron stars [Portegies Zwart & Yungelson, 1998], gravitational wave sources [Portegies Zwart & Spreeuw, 1996; Nelemans et al., 2001b], double white dwarfs [Nelemans et al., 2001c], AM CVn systems [Nelemans & van den Heuvel, 2001], sdB stars [Nelemans, 2010], SNIa progenitors [Toonen et al., 2012; Bours et al., 2013] and ultracompact X-ray binaries van Haaften et al. [2013].

As part of the software package Starlab, it has been used to simulate the evolution of dense stellar systems [Portegies Zwart et al., 2001, 2004]. Recently, SeBa is incorporated in the Astrophysics Multipurpose Software Environment, or AMUSE. This is a component library with a homogeneous interface structure, and can be downloaded for free at amusecode.org [Portegies Zwart et al., 2009].

6.3.4 StarTrack

StarTrack is a Monte Carlo-based single and binary star rapid evolution code. Stars are evolved at a given metallicity (range: $Z = 0.0001 - 0.03$) by adopting analytical fitting formulae from evolutionary tracks of detailed single stellar models [Hurley et al., 2000], and modified over the years in order to incorporate the most important physics for binary evolution. The orbital parameters (separation, eccentricity and stellar spins) a, e, ω_1 and ω_2 are solved numerically as the system evolves, and re-distribution of angular momentum determines how the orbit behaves. As physical insights regarding various aspects of

stellar and binary evolution become available in the literature, new input physics can be implemented into the code, and thus the code is continuously being updated and improved.

The StarTrack code was originally used to predict physical properties of compact objects such as single and double black holes and neutron stars, as well as gamma ray bursts and compact object mergers in context of gravitational wave detection with *LIGO* [Belczynski et al., 2002b,a; Abbott et al., 2004]. In more recent years, studies with the code have grown to include compact binaries in globular clusters [Ivanova et al., 2005], X-ray binary populations [Belczynski et al., 2004; Ruiter et al., 2006], sources of gravitational wave radiation for ground-based and space-based gravitational wave detectors [Ruiter et al., 2009a, 2010; Belczynski et al., 2010a,c], gamma ray bursts [Belczynski et al., 2007; O’Shaughnessy et al., 2008; Belczynski et al., 2008b], Type Ia supernovae progenitors [Belczynski et al., 2005; Ruiter et al., 2009b, 2011, 2013] and core-collapse supernova explosion mechanisms [Belczynski et al., 2012]. The most comprehensive description of the code to date can be found in Belczynski et al. [2008a], with some updates described in Ruiter et al. [2009b] (SNe Ia), Belczynski et al. [2010b] (stellar winds), and Dominik et al. [2012] (wind mass-loss rates, CE).

6.4 Method

To examine the inherent differences between four BPS codes, we compare the results of a simulation made by these codes in which the assumptions are equalised as far as possible (see Sect. 6.4.1). We consider two populations of binaries:

- Single WDs with a non-degenerate companion (hydrogen-rich or helium-rich star) (SWDs)
- Double WD systems (DWDs)

Of both populations we investigate the initial distributions and the distributions at the moment that the SWD or DWD system forms. At these specific times we distinguish the different evolutionary paths, including (possibly several) phases of mass transfer. We establish the similarities between the results of the different BPS codes. If we notice differences between the results, we analyse these in greater detail by comparing e.g. individual systems, their evolutionary path, but also the mass transfer rate and/or wind mass loss rate; or the stability criteria of a group of systems.

We assume the initial primary mass $M_{1,\text{zams}}$ is between $M_{1,\text{zams},\text{min}} = 0.8M_{\odot}$ and $M_{1,\text{zams},\text{max}} = 10M_{\odot}$, an initial mass ratio $q_{\text{zams}} = M_{2,\text{zams}}/M_{1,\text{zams}}$ where the mass ratio is between $q_{\text{zams},\text{min}} = 0.1M_{\odot}/M_{1,\text{zams}}$ and $q_{\text{zams},\text{max}} = 1$, and an initial semi-major axis a_{zams} between $a_{\text{zams},\text{min}} = 5R_{\odot}$ and $a_{\text{zams},\text{max}} = 10^4R_{\odot}$ (see also Table 6.1). Furthermore we assume an initial eccentricity e_{zams} of zero. We consider SWDs and DWDs that are formed within a Hubble time, more specifically 13.7 Gyr. The initial distribution of the

primary masses follows Kroupa et al. [1993], the initial mass ratio distribution is flat¹, and the initial distribution of the semi-major axis is flat in a logarithmic scale.

Not every BPS research group focuses on the full range of stellar masses. Consequently in their codes there are no (valid) prescriptions available for all stellar masses. The research group that uses the Brussels code, mainly focuses on the chemical enrichment of galaxies and therefore is not interested in the evolution of stars with a mass lower than $3M_{\odot}$ (see Sect. 6.3.2). Consequently, in order to make the comparison with the results of the Brussels code we only compare with a subset of the SWD and DWD populations. We define this subset as the ‘intermediate mass range’, while the entire populations is considered as the ‘full mass range’. The ‘intermediate mass range’ is defined in the two populations as follows:

- for the *SWD population* we only consider WDs originating from initial primary masses higher than $3M_{\odot}$.
- for the *DWD population* we only consider WDs originating from initial primary and secondary masses both higher than $3M_{\odot}$.

In addition, we refer to the ‘low mass range’ or ‘low mass primaries’ which encompasses the systems with an initial primary mass lower than $3M_{\odot}$.

BPS codes are ideal to investigate the effect of different assumptions on populations, since a different assumption can cause a shift in e.g. the mass or separation of the population under investigation. We do not have to agree on the exact evolution of individual systems. As long as the shift is small the characteristics of the population do not change. Keeping this in mind when comparing the results of the different BPS codes we define them to agree when similar evolutionary paths are recovered at the same regions in the mass and separation space.

6.4.1 Assumptions for this project

In order to compare the codes we make the most simple assumptions. These are not necessarily believed to be realistic, but are taken to make the comparison feasible. The assumptions for this project are discussed below and shown in Table 6.1. The typical assumptions taken by the authors in the corresponding BPS codes in their previous research projects are summarised in Table 6.5 in Appendix 6.B. For simplicity and brevity, we do not study the effect of different assumptions on the characteristics of SWD and DWD populations in this project.

¹Note that the initially imposed constraint on the mass ratio (i.e. $q_{\text{zams},\text{min}} = 0.1M_{\odot}/M_{1,\text{zams}}$) affects the overall shape of the resulting q_0 -distribution. Even though the probability of drawing a mass ratio anywhere is equal, this is strictly only true between $q_{\text{zams}} \approx 0.1 - 1$. Mass ratios lower than approximately 0.1 are drawn less often, since the primary masses cluster around $1M_{\odot}$ due to the IMF, and the lower mass limit of the secondary is assumed to be $0.1M_{\odot}$.

TABLE 6.1: Equalised initial distribution and range of binary parameters

Parameter	Initial distribution
$M_{1,zams} (M_{\odot})$	KTG93
$a_{zams} (R_{\odot})$	$\propto a^{-1}$ (A83)
q_{zams}	Flat
Parameter	Value
$M_{1,zams,min}$	0.8 (0.1) ⁽¹⁾
$M_{1,zams,max}$	10 (100) ⁽¹⁾
$a_{zams,min}$	5
$a_{zams,max}$	1e4 (1e6) ⁽¹⁾
$q_{zams,min}$	0.1/ $M_{1,zams}$
$q_{zams,max}$	1
e_{zams}	0
Max time (Gyr)	13.7
Binary fraction (%)	100
β (RLOF)	1
$\alpha_{ce}\lambda_{ce}$	1
Physics	Assumption
AML (RLOF)	Orbit ($\eta = 1$)
CE	$\alpha^{(2)}$
Wind accretion	No
Tides	No
Magn. braking	No

NOTES:

References in the table: KTG93 = Kroupa et al. [1993], A83 = Abt [1983].

(1) The values outside and inside the brackets represent the values for the simulated and entire stellar population, respectively.

(2) The prescription is based on Webbink [1984].

- Mass transfer is assumed to be conservative ($\beta = 1$) during stable RLOF towards all types of objects. We emphasise that this is not a realistic assumption, especially in the case of a WD accretor. During the CE-phase no material is assumed to be accreted by the companion star ($\beta = 0$).

In the Brussels code a constant accretion efficiency of a WD-accretor cannot be implemented and therefore for this study mass transfer to all compact objects is assumed to be unstable and evolve into a common envelope in this code.

- We assume that during mass transfer the angular momentum lost is specific orbital angular momentum of the binary (with $\eta = 1$, see eq. 6.2).

It is not possible to equalise the assumptions for AML during wind mass loss between the codes (for an overview of the assumptions see Sect. 6.A.5).

- We use the α -prescription of Webbink [1984] to describe the CE-phase (see eq. 6.6 to eq. 6.8). We assume that the parameters α_{ce} and λ_{ce} are equal to one, mainly for simplicity, but also because the prevalence of this choice in the literature allows for comparison between this and other studies.
- We assume that matter lost through winds cannot be accreted by the companion star.
- Due to the diversity of the prescriptions for magnetic braking and tides, we do not consider these effects and they are turned off for this paper. However, in StarTrack, spin-orbit coupling is still taken into account, as it is firmly integrated with the binary evolution equations.

6.4.2 Normalisation

When calculating birthrates of evolutionary channels, the simulation has to be normalised to an entire stellar population (see Table 6.1). For this work the initial distribution and ranges of $M_{1,zams}$, q_{zams} and a_{zams} are as discussed in Sect. 6.4 with the exception of the initial primary masses of a stellar population to vary between 0.1 and $100M_{\odot}$, and the semi-major axis between 5 and $10^6 R_{\odot}$. We assume a binary fraction of 100%.

If the star formation rate S in $M_{\odot} \text{ yr}^{-1}$ is independent of time, the birthrate of an evolutionary channel X is given by:

$$\text{Birthrate}(X) = S \frac{\phi(X)}{M_{\text{tot}}}, \quad (6.10)$$

with $\phi(X)$ the total number of systems evolving through evolutionary channel X in the simulation, and M_{tot} the total mass of all stellar systems in the entire stellar population. More specifically,

$$\phi(X) = \int_{0.1}^{100} \int_{0.1/M_{1,zams}}^1 \int_5^{1e6} x \Psi dM_{1,zams} dq da, \quad (6.11)$$

with $x = x(M_{1,zams}, q, a)$ equals 1 for the binary systems evolving through evolutionary channel X, and zero otherwise and Ψ is the initial distribution function of $M_{1,zams}$, q_{zams} and a_{zams} . Note that in this project we assume that the initial distribution for $M_{1,zams}$, q_{zams} and a_{zams} are independent (see Table 6.1), such that Ψ is separable:

$$\Psi(M_{1,zams}, q_{zams}, a_{zams}) = \psi(M_{1,zams})\varphi(q_{zams})\chi(a_{zams}). \quad (6.12)$$

The total mass of all stellar systems assuming a 100% binary fraction is:

$$M_{tot} = \int_{0.1}^{100} \int_{0.1/M_{1,zams}}^1 \int_5^{1e6} M_{t,zams} \Psi dM_{1,zams} dq da, \quad (6.13)$$

where $M_{t,zams} = M_{1,zams} + M_{2,zams}$.

For this project a constant star formation rate of $1M_{\odot} \text{ yr}^{-1}$ is assumed. This simple star formation rate is chosen to make the comparison with other codes easier.

6.5 Results

6.5.1 Single white dwarf systems

Systems containing a WD and a non-degenerate companion have typically undergone a one-directional mass transfer event i.e. one star has lost mass and possibly the other gained mass. The mass transfer event may consist of one or two episodes, either of which may have been stable or unstable. The characteristics of the population of SWD systems show the imprint of the mass transfer episodes. Figure 6.2 and 6.3 show the orbital separation a_{swd} as a function of primary mass $M_{1,swd}$ at the moment of WD formation for the full and intermediate mass range respectively. Likewise Fig. 6.4 and 6.5 show the secondary mass $M_{2,swd}$ as a function of primary mass at WD formation for the full and intermediate mass range. These figures show that in general the codes find very similar SWD systems.

In more detail, at large separations ($a_{swd} \gtrsim 500R_{\odot}$ for the full mass range, and for the intermediate mass range $a_{swd} \gtrsim 2000R_{\odot}$) all codes find systems in which the stars do not interact. The population of SWDs with WD masses in the low mass range is very comparable in orbital separation, primary and secondary mass between the codes `binary_c`, `SeBa` and `StarTrack`. Intermediate mass systems can be divided in two groups, either in separation and/or in secondary mass. According to all codes, intermediate mass systems that undergo a CE-phase (for the first mass transfer episode) are compact with $a_{swd} \lesssim 200R_{\odot}$ and have secondary masses up to $10M_{\odot}$. Furthermore, the codes agree that in the intermediate mass range, systems for which the first phase of mass transfer is stable are in general more compact than non-interacting systems and less compact than the systems undergoing a CE-phase. The secondary mass is between 3 and $18M_{\odot}$ as it accretes conservatively during stable mass transfer.

TABLE 6.2: Birthrates in yr^{-1} for different evolutionary channels (described in Sect. 6.5) of single and double white dwarf systems for the three BPS codes for the full mass range and the intermediate mass range.

Evolutionary channels	Full mass range			Intermediate mass range			
	binary_c	SeBa	StarTrack	binary_c	Brussels code	SeBa	StarTrack
SWD systems	0.048	0.052	0.048	5.1e-3	7.8e-3	5.2e-3	4.4e-3
Channel 1	0.026	0.026	0.026	2.2e-3	1.9e-3	2.5e-3	2.3e-3
Channel 2a	6.9e-3	6.5e-3	6.8e-3	1.1e-3	2.6e-3	1.1e-3	1.1e-3
Channel 2b	5.7e-4	5.8e-4	5.0e-4	5.7e-4	-	5.8e-4	4.8e-4
Channel 3a	1.4e-3	4.2e-3	9.8e-4	4.0e-4	1.0e-3	2.9e-4	8.7e-5
Channel 3b	5.7e-4	4.6e-4	1.3e-4	5.7e-4	8.2e-4	4.6e-4	1.3e-4
Channel 4a	0.012	0.012	0.012	1.8e-6	3.6e-6	2.4e-6	1.6e-6
Channel 4b	1.8e-4	8.9e-5	1.8e-4	1.8e-4	1.8e-4	8.9e-5	1.8e-4
Channel 5	2.4e-4	5.6e-4	3.6e-4	9.1e-6	1.2e-3	5.4e-5	2.9e-5
DWD systems	0.012	0.014	0.015	8.4e-4	1.1e-3	8.7e-4	6.6e-4
Channel I	8.4e-3	8.8e-3	8.4e-3	4.9e-4	5.5e-4	5.5e-4	5.1e-4
Channel II	2.0e-3	1.3e-3	4.5e-3	4.5e-5	7.6e-5	3.5e-5	7.8e-5
Channel III	1.3e-3	3.0e-3	9.9e-4	2.5e-4	4.9e-4	1.8e-4	8.1e-7
Channel IV	1.6e-4	5.5e-5	$\lesssim 4e-7$	$\lesssim 4e-7$	-	$\lesssim 4e-7$	$\lesssim 4e-7$

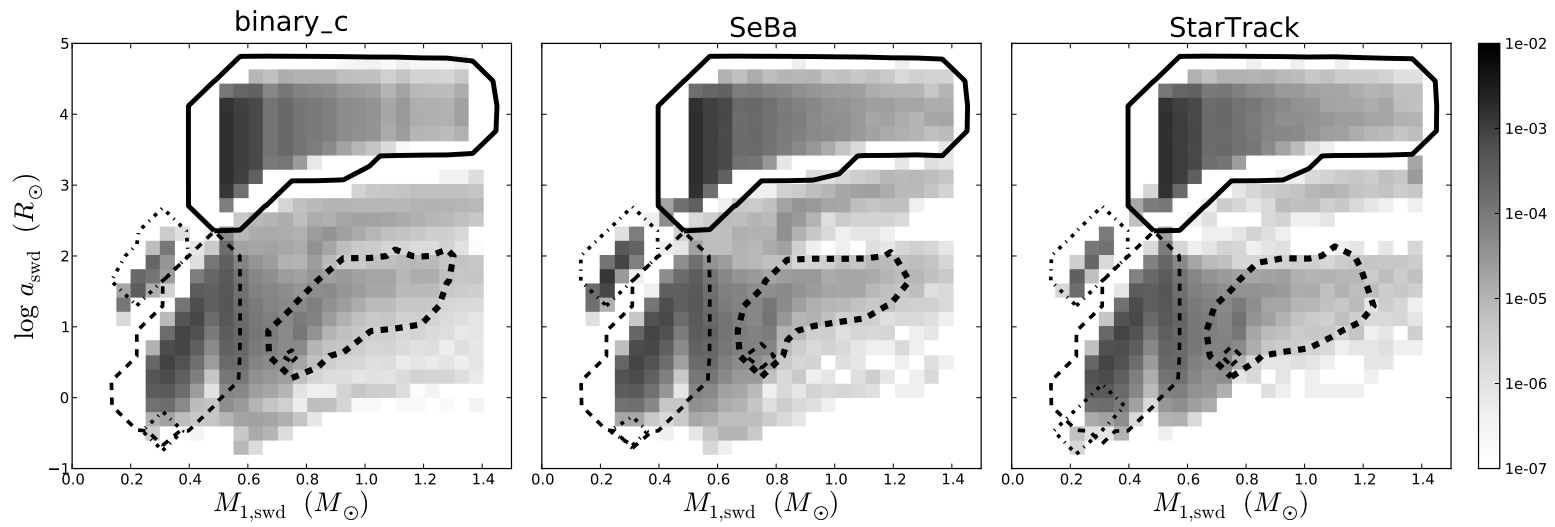


FIGURE 6.2: Orbital separation versus WD mass for all SWDs in the full mass range at the time of SWD formation. The contours represent the SWD population from a specific channel: channel 1 (solid line), channel 4a (thin dashed line), channel 4b (thick dashed line) and channel 5 (dash-dotted line).

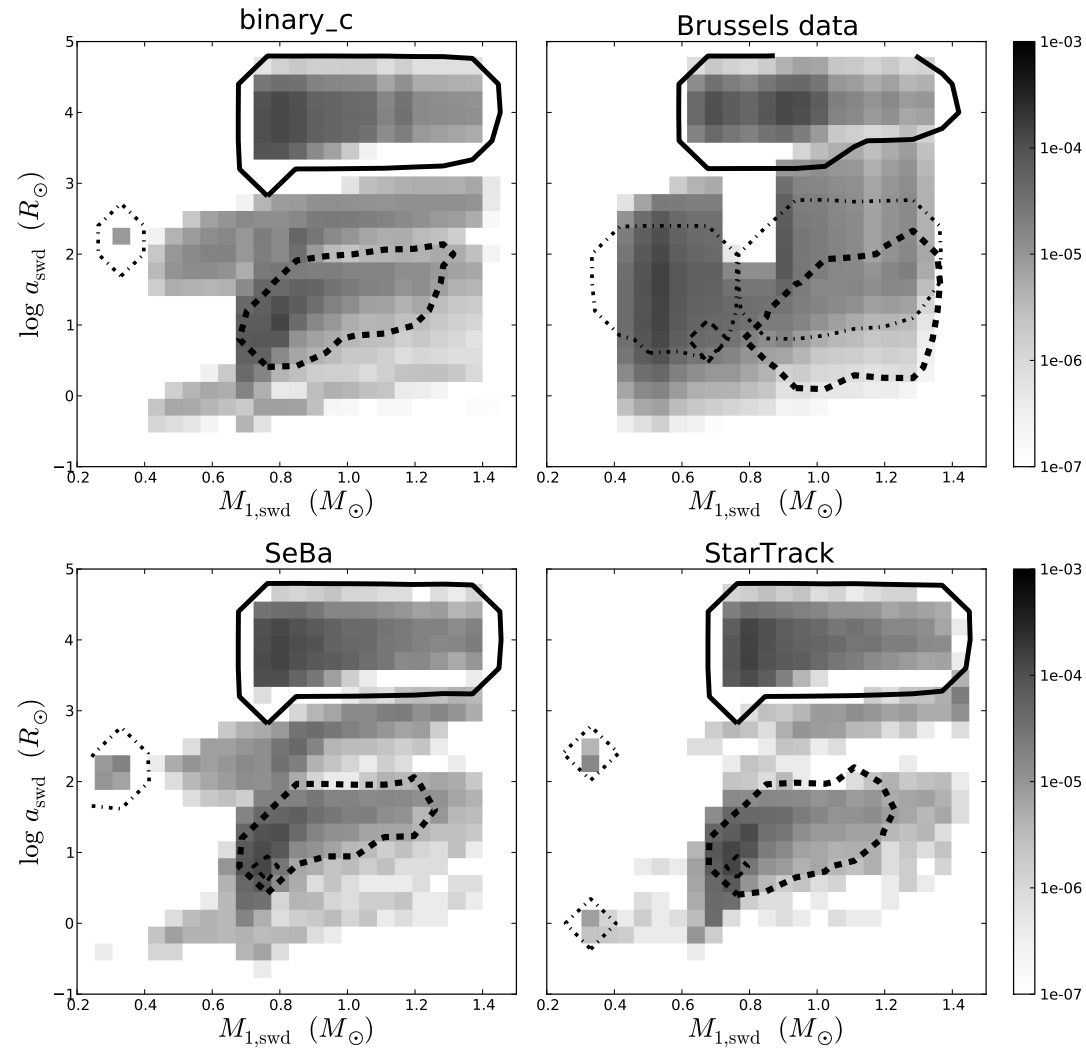


FIGURE 6.3: Orbital separation versus WD mass for all SWDs in the intermediate mass range at the time of SWD formation. The contours represent the SWD population from a specific channel: channel 1 (solid line), channel 4a (thin dashed line), channel 4b (thick dashed line) and channel 5 (dash-dotted line).

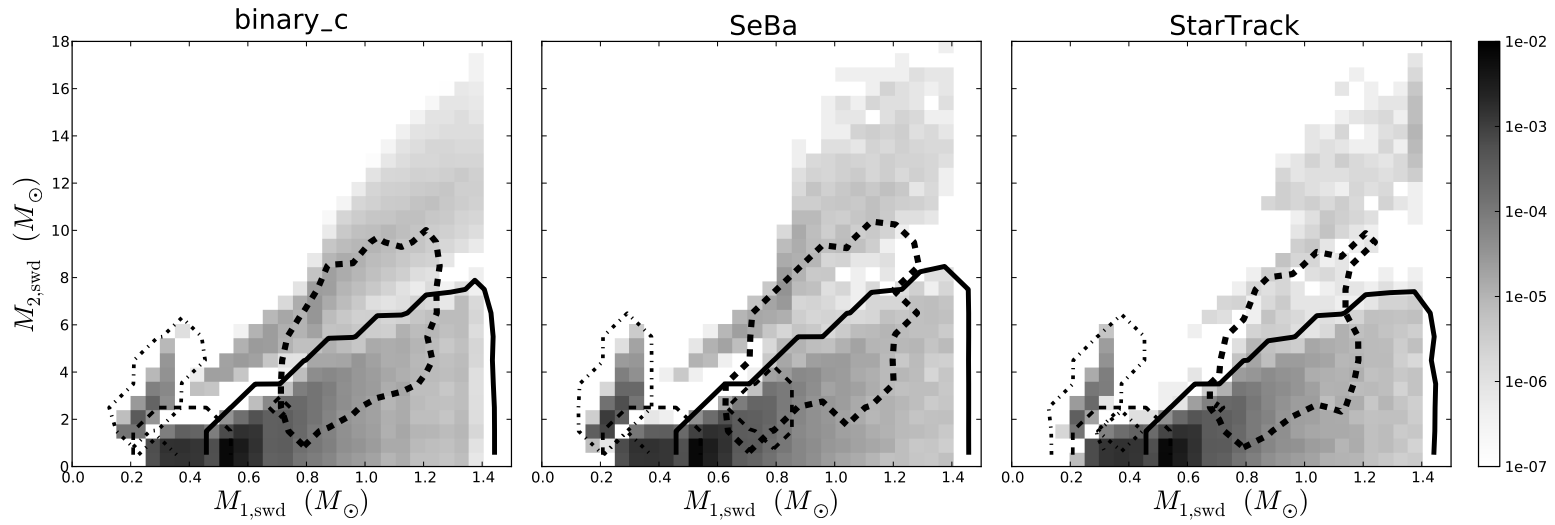


FIGURE 6.4: Secondary mass versus WD mass for all SWDs in the full mass range at the time of SWD formation. The contours represent the SWD population from a specific channel: channel 1 (solid line), channel 4a (thin dashed line), channel 4b (thick dashed line) and channel 5 (dash-dotted line).

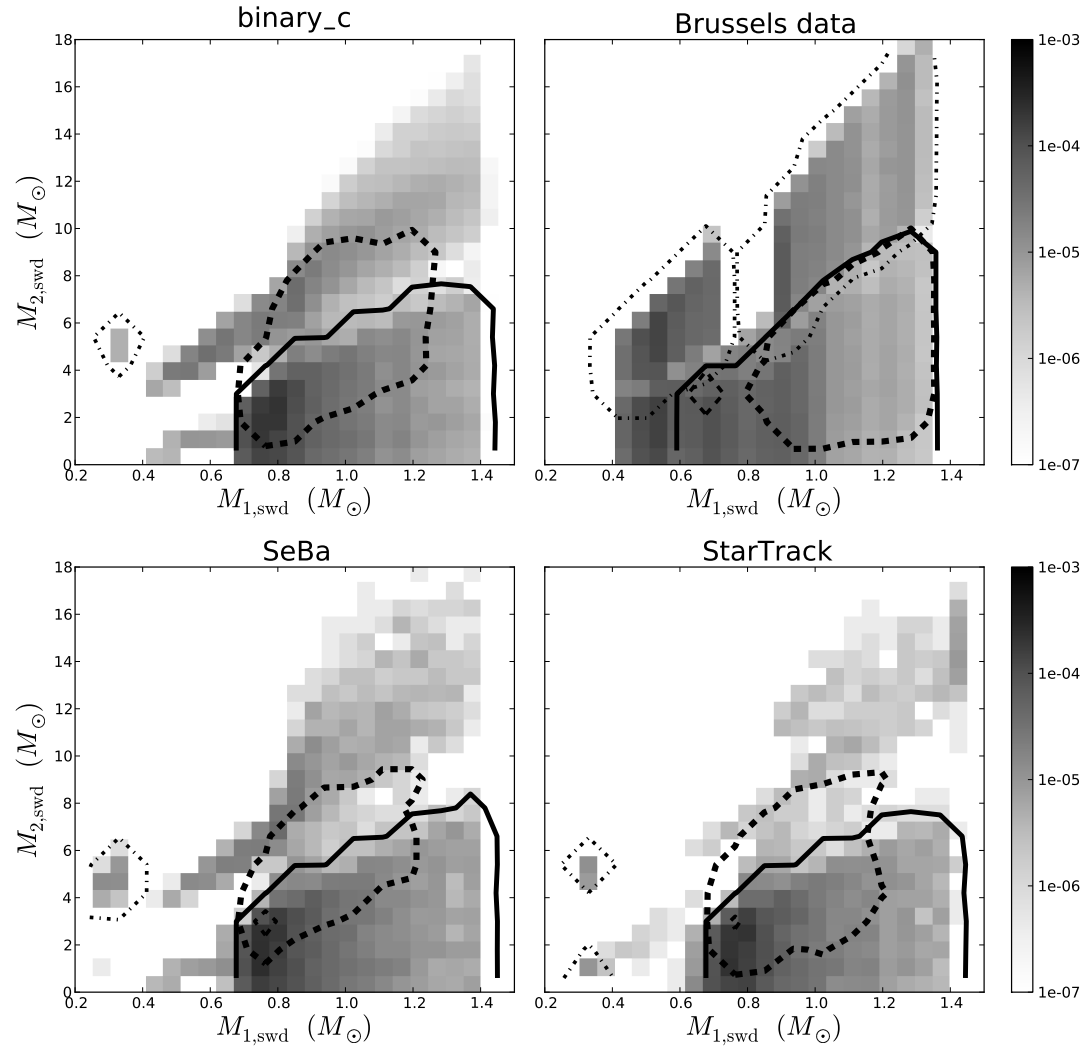


FIGURE 6.5: Secondary mass versus WD mass for all SWDs in the intermediate mass range at the time of SWD formation. The contours represent the SWD population from a specific channel: channel 1 (solid line), channel 4a (thin dashed line), channel 4b (thick dashed line) and channel 5 (dash-dotted line).

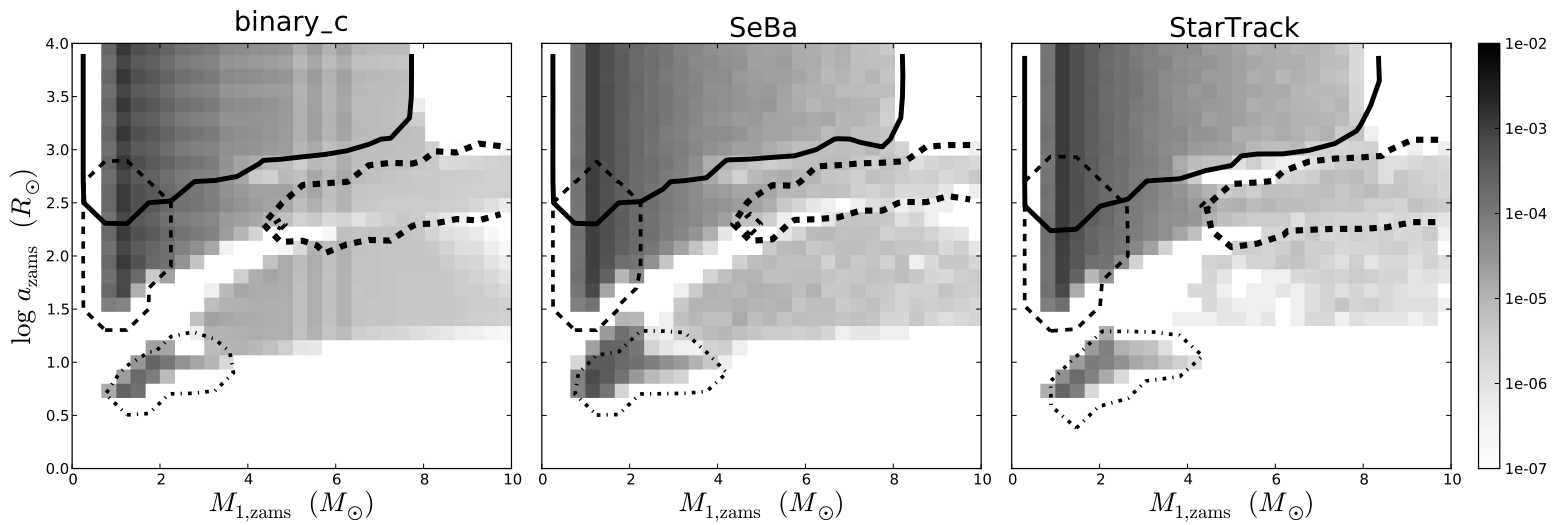


FIGURE 6.6: Initial orbital separation versus initial primary mass for all SWDs in the full mass range. The contours represent the SWD population from a specific channel: channel 1 (solid line), channel 4a (thin dashed line), channel 4b (thick dashed line) and channel 5 (dash-dotted line).

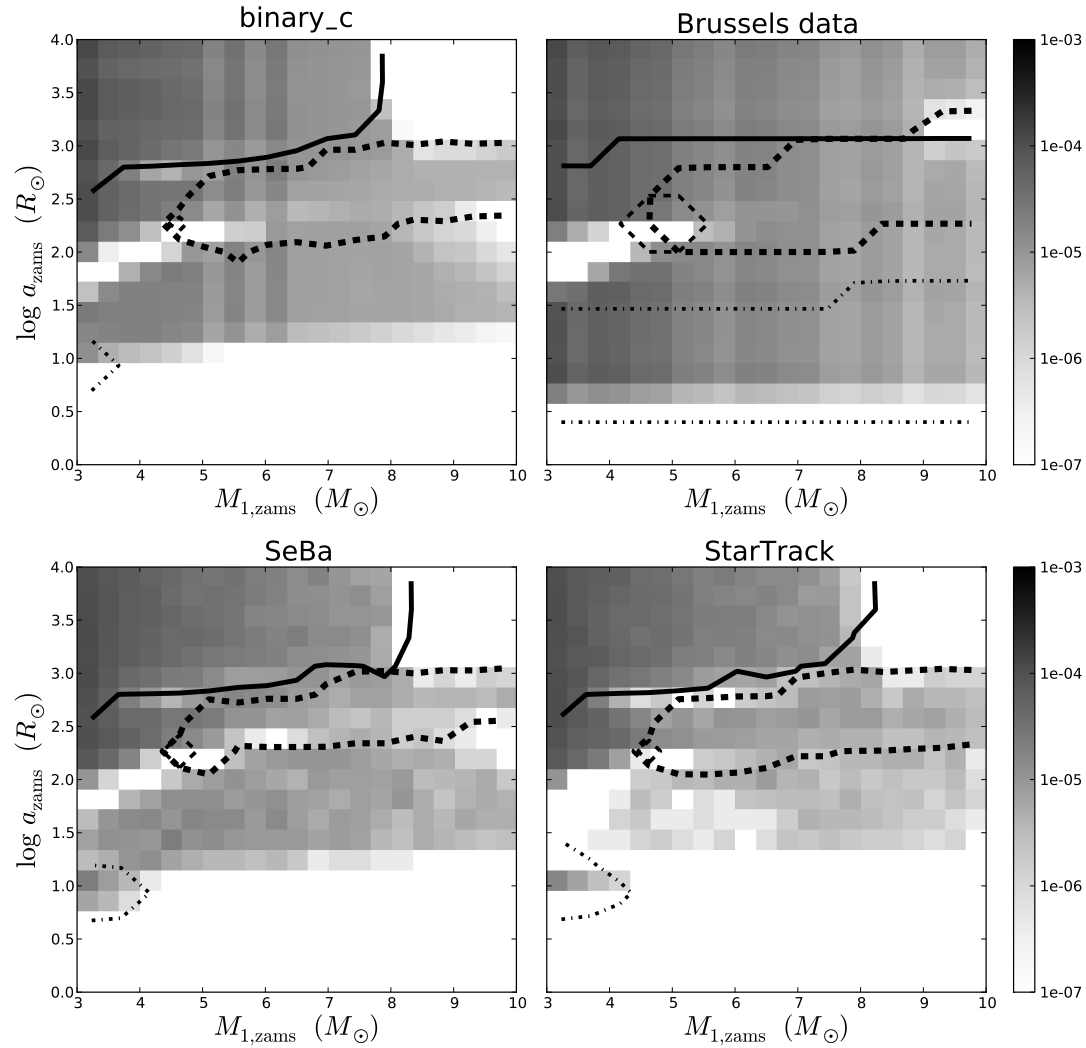


FIGURE 6.7: Initial orbital separation versus initial primary mass for all SWDs in the intermediate mass range. The contours represent the SWD population from a specific channel: channel 1 (solid line), channel 4a (thin dashed line), channel 4b (thick dashed line) and channel 5 (dash-dotted line).

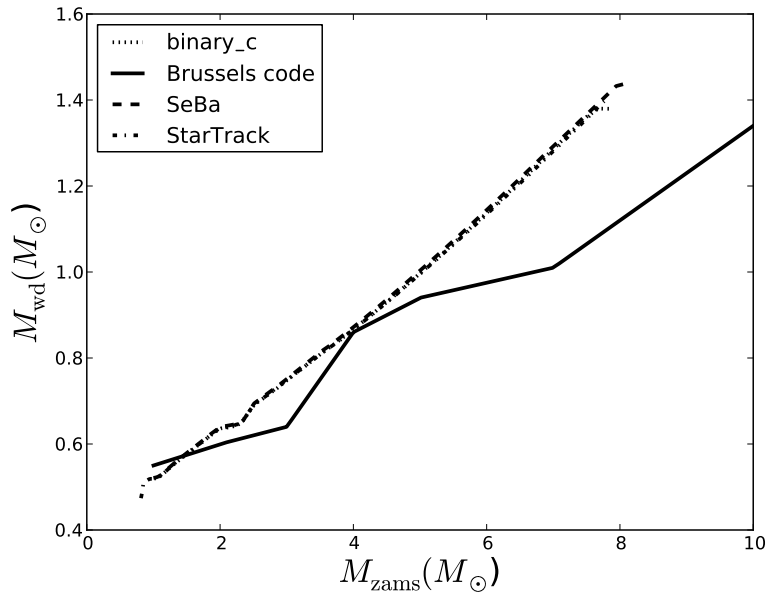


FIGURE 6.8: Initial-final mass relation of single stars that become WDs for the different groups, dotted line shows the results of `binary_c`, solid line the results of the Brussels code, the dashed line the results of `SeBa`, and the dash-dotted line the results of `StarTrack`.

The ZAMS configurations for progenitors of SWDs are shown in Fig. 6.6 and 6.7 with the separation a_{zams} versus primary mass $M_{1,\text{zams}}$. There is a general agreement between the codes about which progenitor systems lead to a SWD system and which systems do not. According to all codes, compact progenitor systems ($a_{\text{zams}} \lesssim 400R_{\odot}$ for the intermediate mass range, while $a_{\text{zams}} \lesssim 30R_{\odot}$ for the low mass range) undergo stable mass transfer for the initial mass transfer episode. Furthermore the codes agree that for most progenitor systems with orbital separations in the range $a_{\text{zams}} \approx (0.1-3) \cdot 10^3 R_{\odot}$ the first phase of mass transfer is unstable. Systems with orbital separations that lie between the ranges described above lead to a merging event, thus no SWD system is formed. Progenitor systems with $a_{\text{zams}} \gtrsim 700R_{\odot}$ for the intermediate mass range ($a_{\text{zams}} \gtrsim 250R_{\odot}$ for the low mass range) are too wide for the primary star to fill its Roche lobe.

The initial-final mass (MiMf)-relation of single stars (see Fig. 6.8) is very similar between `binary_c`, `SeBa` and `StarTrack`, but different than the one from the Brussels code due to different single star prescriptions that are used in the latter code (see Sect. 6.5.1.1 for a discussion). The effect on the population of SWD progenitors can be seen in Fig. 6.7 in the maximum mass of the primary stars which is extended from about $8M_{\odot}$ in `binary_c`, `SeBa` and `StarTrack` to about $10M_{\odot}$ in the Brussels code. For binary stars the relation between WD mass and the initial mass is hereafter called the initial-WD mass (MiMwd)-relation (see Sect. 6.5.1.2 for a discussion). Differences in the MiMwd-relation lead to an increase of systems at small WD masses $\lesssim 0.64M_{\odot}$ in Fig. 6.3 in the Brussels code compared to the

TABLE 6.3: Definitions of abbreviations of stellar types used in the text and figures.

Abbreviation	Type of star
MS	Main-sequence star
HG	Hertzsprung-gap star
GB	Star on the first giant branch (red giants)
AGB	Star on the asymptotic giant branch
He-MS	Star on the equivalent of the main-sequence for hydrogen-poor helium-burning stars
Ev. He-star	Evolved hydrogen-poor helium-burning star
WD	White dwarf

other codes. The gap in WD masses between $0.7\text{-}0.9M_{\odot}$ in the Brussels data in Fig. 6.3 is a result of a discontinuity in the MiMwd-relation between the WD masses of primaries that fill their Roche a second time, and those that do not. In the other codes, the primary WD masses of binaries that evolve through these two evolutionary channels are overlapping. Differences in the stability criteria of mass transfer can be seen in Fig. 6.3 and 6.5, most pronouncedly via the greyscales where the StarTrack code shows a decrease of systems that underwent stable mass transfer (see Sect. 6.5.1.3). Mass transfer is modelled differently in the codes (see Sect. 6.A) leading to an extension to small separations in the Brussels data compared to the other codes (see Fig. 6.7), and an increase in systems that underwent stable mass transfer at $a_{\text{zams}} \approx 10R_{\odot}$ for $M_{1,\text{zams}} \gtrsim 4M_{\odot}$ in Fig. 6.5 (see Sect. 6.5.1.5).

In the next sections, we make a more detailed comparison between the simulated populations of SWDs of the four codes. We distinguish between the most commonly followed evolutionary paths with birthrates larger than $1.0 \cdot 10^{-3} \text{ yr}^{-1}$. We describe each evolutionary path, the similarities and differences, and investigate the origin of these differences. Specific examples are given and discussed for the most common paths. Abbreviations of stellar types are shown in Table 6.3. Paragraphs explaining the evolutionary path, an example evolution and the comparison of the simulated populations for each evolutionary channel are indicated with *Evolutionary path*, *Example* and *Population*, respectively. For some channels, causes for differences between the populations are discussed separately in paragraphs that are indicated by *Effects*. Masses and orbital separations according to each code are given in vector form $[c_1, c_2, c_3, c_4]$ where c_1 represents the value according to the binary_c code, c_2 according to the Brussels code, c_3 according to SeBa, and c_4 according to StarTrack. The examples are given to illustrate the evolutionary path and relevant physical processes. However, note that when comparing different BPS codes, achieving similar results for specific binary populations is more desirable and important than achieving a perfect match between specific, individual binary systems.

6.5.1.1 Channel 1: detached evolution

Evolutionary path Most SWD binaries are non-interacting binaries where the stars essentially evolve as single stars. Most binary processes that are discussed in Sect. 6.2 do not play a role in channel 1.

Example As an example of a system in channel 1, we discuss the evolution of a system that initially contains a $5M_{\odot}$ and $4M_{\odot}$ star in an orbit of $10^4 R_{\odot}$ (and $e_{\text{zams}} = 0$ by assumption). When the primary star becomes a WD its mass is $[1.0, 0.94, 1.0, 1.0]M_{\odot}$ in an orbit of $[1.8, 1.8, 1.8, 1.8] \cdot 10^4 R_{\odot}$. The differences in the resulting SWD system from different BPS codes are small and mainly due to different initial-final mass (MiMf)-relations (see Fig. 6.8). The maximum progenitor mass to form a WD from a single star is $[7.6, 10, 7.9, 7.8]M_{\odot}$ and corresponding maximum WD mass of $[1.38, 1.34, 1.38, 1.4]M_{\odot}$ according to the four codes. The MiMf-relations of the `binary_c` code, `SeBa` and `StarTrack` are very similar. The similarities are not surprising as these codes are based on the same single stellar tracks and wind prescriptions of Hurley et al. [2000]. However, small differences arise in the MiMf-relation as the prescriptions for the stellar wind are not exactly equal. The Brussels code is based on different models of single stars e.g. different stellar winds and a different overshooting prescription (see Appendix 6.A). The result is that the core mass of a specific single star is larger according to the Hurley tracks. In other words, the progenitor of a specific single WD is more massive in the Brussels code.

Population Despite differences for individual systems, the population of non-interacting binaries at WD formation is very similar. The previously mentioned differences in the MiMf-relations are noticeable in the maximum initial primary mass in Fig. 6.6 and 6.7. The distribution of separations at WD formation (see Fig. 6.2 and 6.3) are very similar between the codes. For the intermediate mass range, the separations at SWD formation are $\gtrsim 4.5 \cdot 10^3 R_{\odot}$ for the Brussels code and extend to slightly lower values of $\gtrsim 2.0 \cdot 10^3 R_{\odot}$ for `binary_c`, `SeBa`, and `StarTrack`. For the full mass range, the latter three codes agree that the separations can be as low as $5.0 \cdot 10^2 R_{\odot}$. The progenitor systems of channel 1 have similar separations of $\gtrsim 3.0 \cdot 10^2 R_{\odot}$ for low mass primaries. For intermediate mass stars `binary_c`, `SeBa` and `StarTrack` find that the initial separation is $\gtrsim 0.7 \cdot 10^3 R_{\odot}$ where the Brussels code finds a slightly higher value of $\gtrsim 1.6 \cdot 10^3 R_{\odot}$ (see Fig. 6.6 and 6.7). The minimum separation (at ZAMS and WD formation) for a given primary mass depends on whether or not the primary fills its Roche lobe, which in turn depends on the maximum radius for that star according to the particular single star prescriptions that are used. Even though the progenitor populations are not 100% equal, the characteristics of the SWD population and the birthrates (see Table 6.2) in this channel are in excellent agreement.

6.5.1.2 Channel 2: unstable case C

Evolutionary path One of the most common evolutionary paths of interacting binaries is channel 2, of which an example is shown in Fig. 6.9. In this channel, the primary star

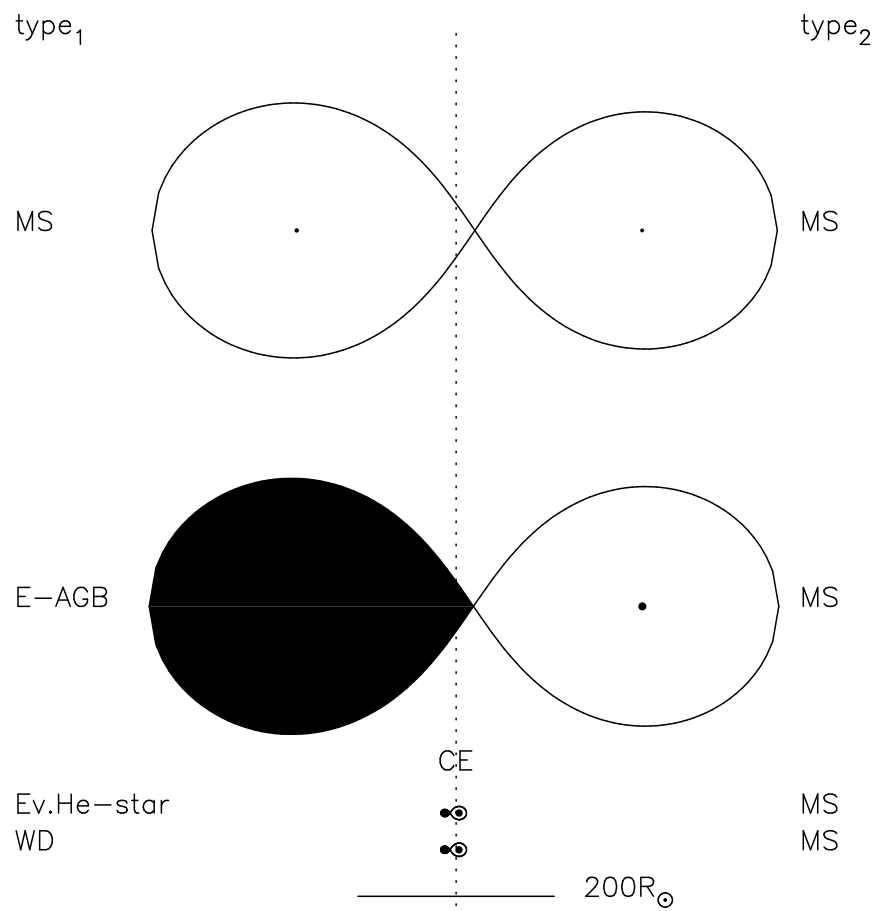


FIGURE 6.9: Example of the evolution of a single white dwarf system in channel 2a. Abbreviations are as in Table 6.3.

fills its Roche Lobe when helium is exhausted in its core, so-called case C mass transfer [Lauterborn, 1970]. As the envelope of the donor star is deeply convective at this stage, generally mass transfer leads to an unstable situation and a CE-phase develops. While the orbital separation shrinks severely, the primary loses its hydrogen envelope. By assumption in this project, the secondary is not affected during the CE-phase. The primary can either directly become a WD or continue burning helium as an evolved helium star as shown in the example of Fig. 6.9. If the primary becomes a WD directly, or indirectly but without further interaction, the evolutionary path is called channel 2a. Evolution according to channel 2b occurs if the primary fills its Roche lobe for a second time when it is a helium star. The second phase of mass transfer can be either stable or unstable.

Example As an example of channel 2a, we discuss the evolution of the binary system in Fig. 6.9. The initial parameters are $M_{1,zams} = 3.5M_{\odot}$, $M_{2,zams} = 3M_{\odot}$ and $a_{zams} = 350R_{\odot}$. The primary star fills the Roche lobe early on the AGB before thermal pulses and superwinds occur. Wind mass loss prior to the CE-phase is small, $[4.4, 0, 4.3, 4.9] \cdot 10^{-2}M_{\odot}$. After the CE-phase the orbital separation is reduced to $[14, 9.1, 14, 14]R_{\odot}$. In this example the primary continuously burns helium as an evolved helium star of mass $[0.78, 0.55, 0.78, 0.78]M_{\odot}$. When the primary exhausts its fuel, it becomes a WD of $[0.76, 0.51, 0.77, 0.76]M_{\odot}$ in an orbit of $[14, 9.1, 14, 14]R_{\odot}$ with a $3M_{\odot}$ MS companion. The most important differences, to be seen between the Brussels code and the other codes, arise from the different single star prescriptions that are used. This affects the resulting mass of a WD from a specific primary, and the resulting orbital separation. Note that while the MiMf-relation for single stars depends on the single star prescriptions (i.e. core mass growth and winds), the MiMwd-relation is also affected by the companion mass and separation (which determine when and which kind of mass transfer event takes place), and the single star prescriptions for helium stars. In other words, the MiMwd-relation represents how fast the core grows on one hand, and the envelope is depleted by mass transfer and stellar winds on the other hand.

Population Despite the differences between individual systems, the different BPS codes agree in which regions of phase space ($M_{1,swd}$, $M_{2,swd}$, a_{swd}) in Fig. 6.10, 6.11, 6.12 and 6.13 the systems from channel 2 lie. The systems of channel 2 evolve towards small separations, with the majority in the range $0.2 - 150R_{\odot}$ at WD formation. In addition, the codes agree on the masses of both stars at formation of the single WD system. In the low mass range `binary_c`, `SeBa` and `StarTrack` agree that $M_{1,swd} \approx 0.5 - 0.7M_{\odot}$ and $M_{2,swd} \approx 0.1 - 2.7M_{\odot}$. In the intermediate mass range the different codes find that $M_{1,swd} \gtrsim 0.64M_{\odot}$, however, the Brussels code finds primary WD masses down to $0.5M_{\odot}$ due to differences in MiMwd-relation. For secondary masses the codes find $M_{2,swd} \approx 0.1 - 7.0M_{\odot}$.

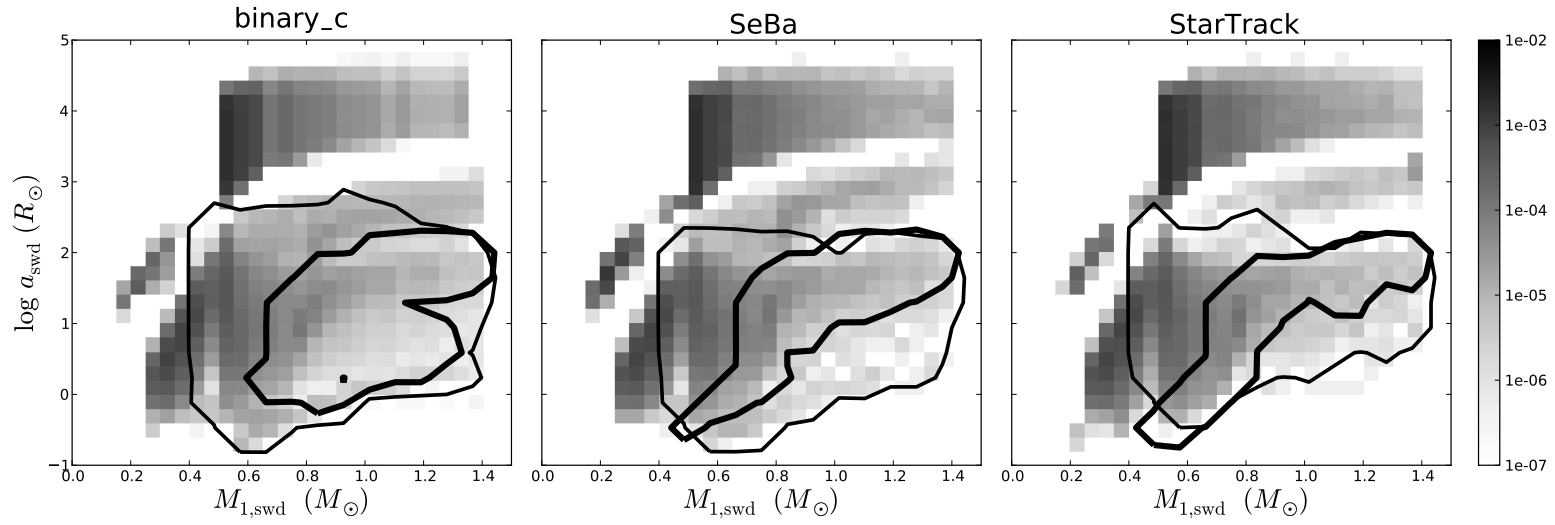


FIGURE 6.10: Orbital separation versus WD mass for all SWDs in the full mass range at the time of SWD formation. The contours represent the SWD population from a specific channel: channel 2a (thin line) and channel 2b (thick line).

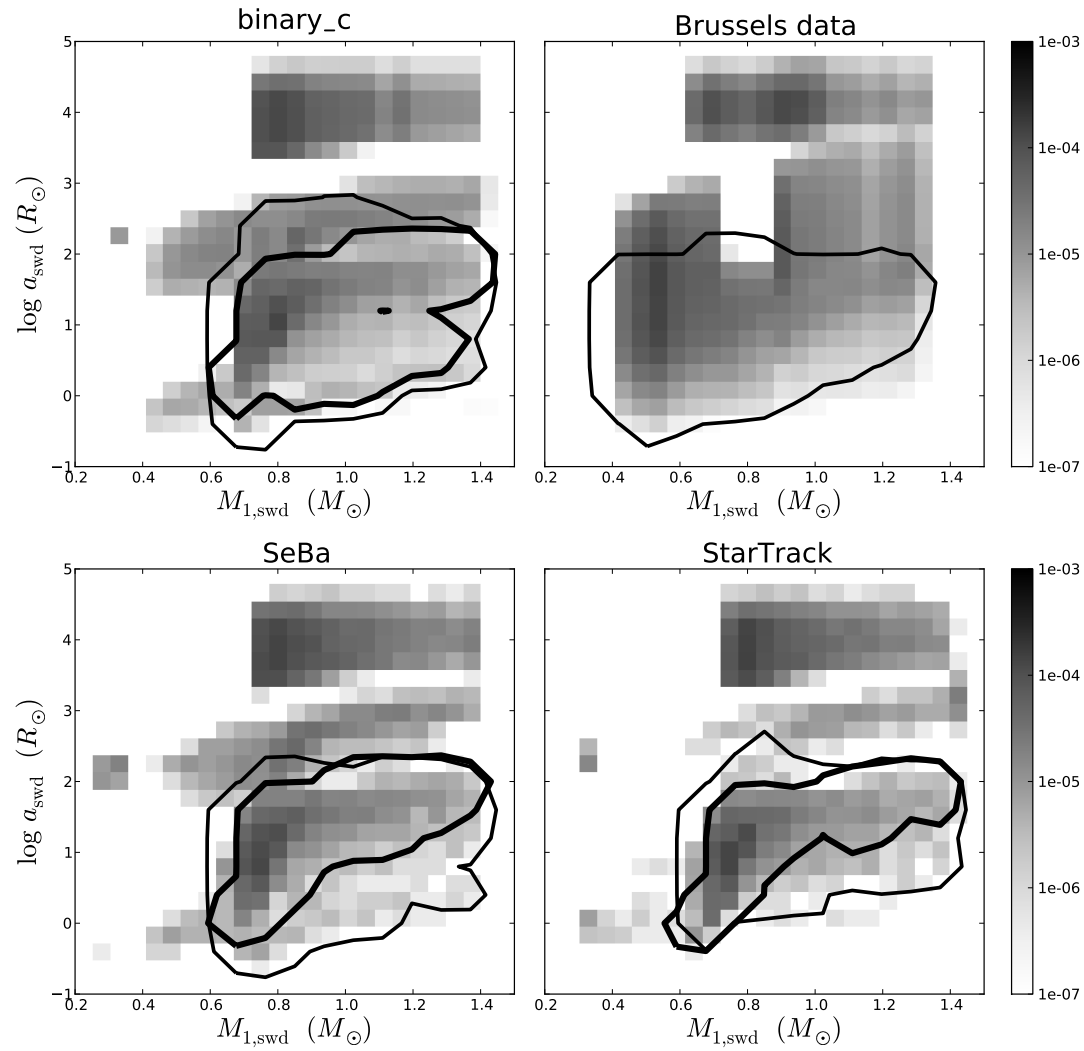


FIGURE 6.11: Orbital separation versus WD mass for all SWDs in the intermediate mass range at the time of SWD formation. The contours represent the SWD population from a specific channel: channel 2a (thin line) and channel 2b (thick line).

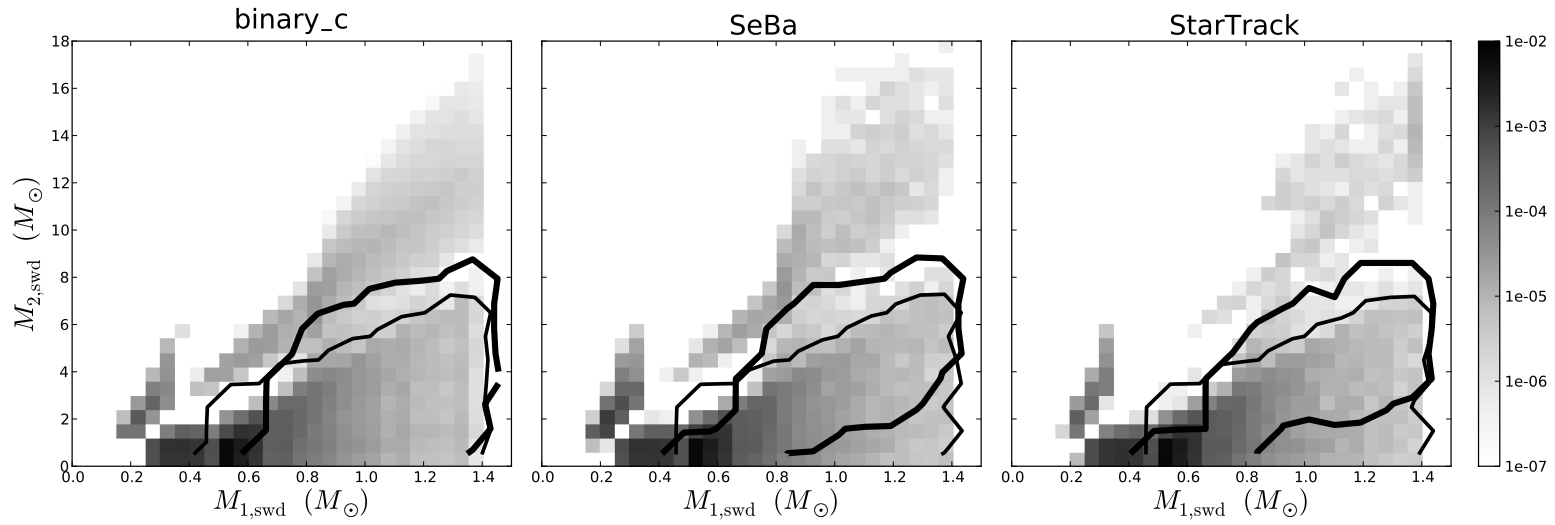


FIGURE 6.12: Secondary mass versus WD mass for all SWDs in the full mass range at the time of SWD formation. The contours represent the SWD population from a specific channel: channel 2a (thin line) and channel 2b (thick line).

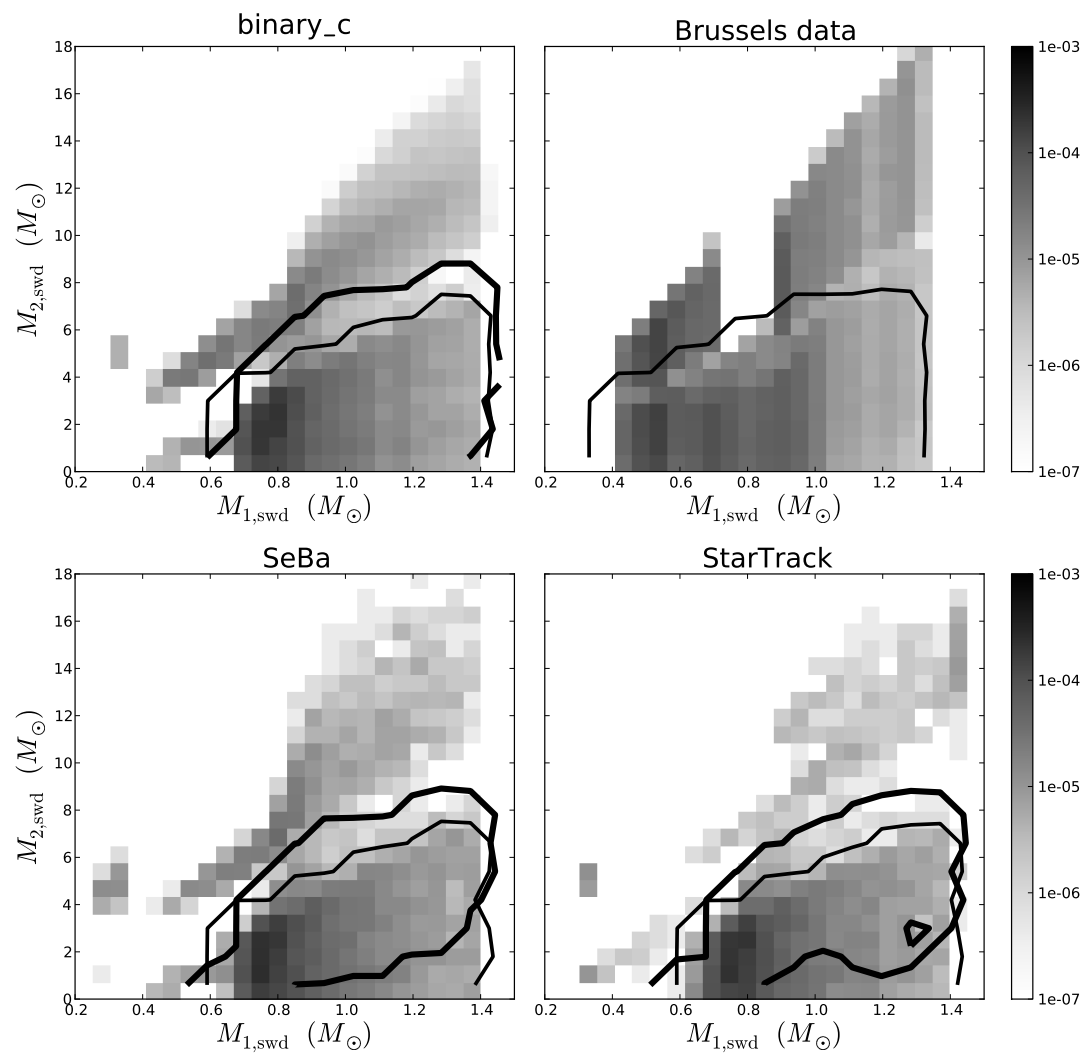


FIGURE 6.13: Secondary mass versus WD mass for all SWDs in the intermediate mass range at the time of SWD formation. The contours represent the SWD population from a specific channel: channel 2a (thin line) and channel 2b (thick line).

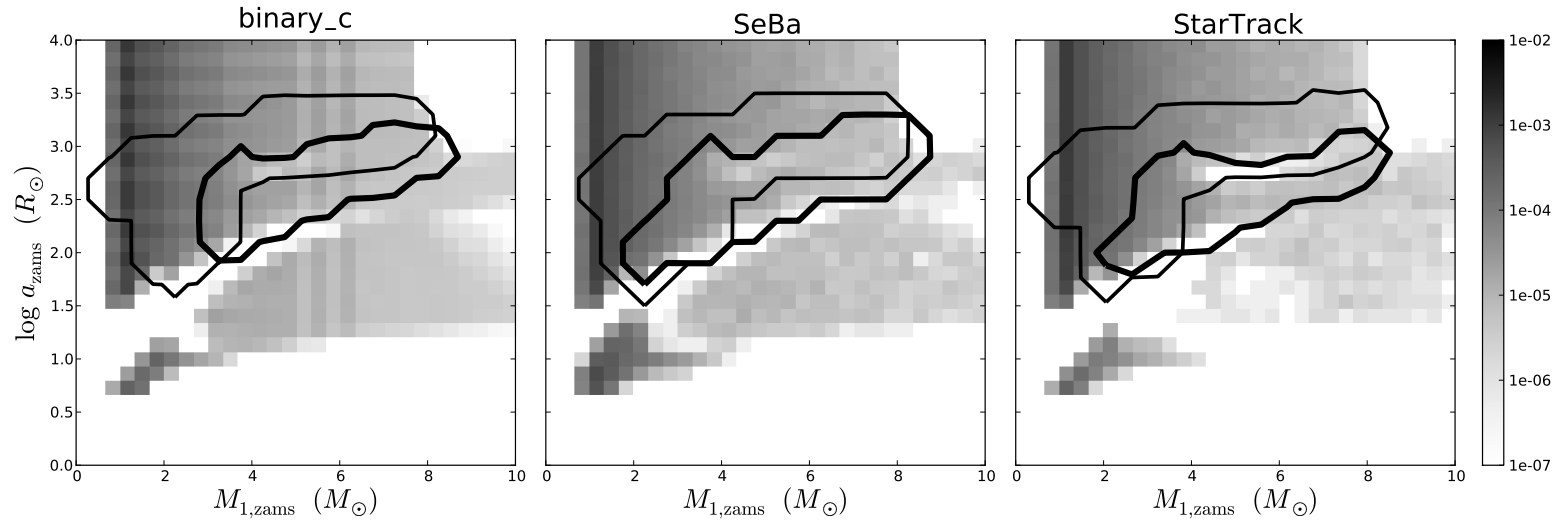


FIGURE 6.14: Initial orbital separation versus initial primary mass for all SWDs in the full mass range. The contours represent the SWD population from a specific channel: channel 2a (thin line) and channel 2b (thick line).

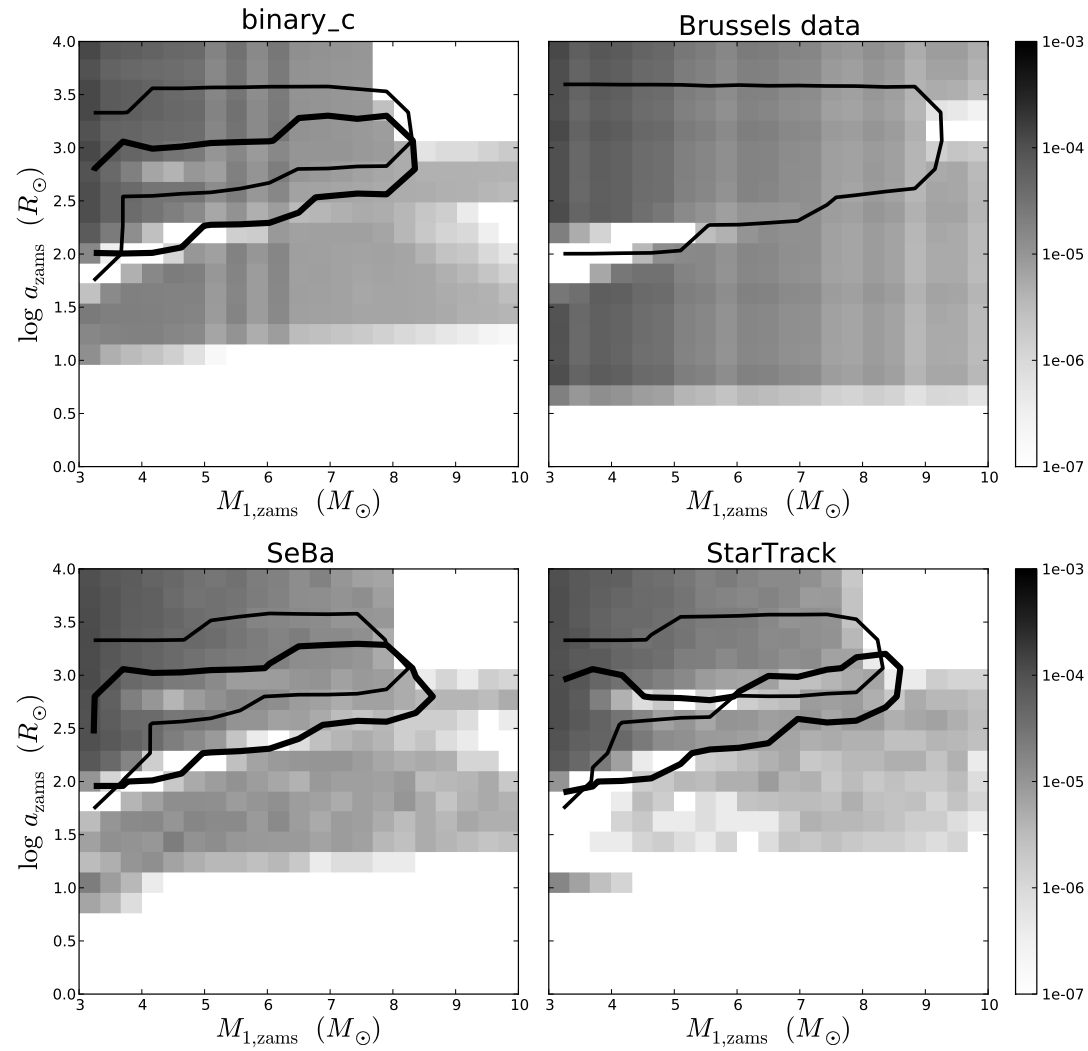


FIGURE 6.15: Initial orbital separation versus initial primary mass for all SWDs in the intermediate mass range. The contours represent the SWD population from a specific channel: channel 2a (thin line) and channel 2b (thick line).

The `binary_c`, `SeBa`, and `StarTrack` codes agree on the initial separation for low mass binaries, which is between $(0.6 - 12) \cdot 10^2 R_\odot$ (see Fig. 6.14), $M_{1,zams} \approx 1.0 - 3.0 M_\odot$ and $M_{2,zams} \approx 0.1 - 3.0 M_\odot$. For intermediate mass binaries in channel 2, there is an agreement between all codes that the initial primary masses lie between $M_{1,zams} \approx 3 - 8.5 M_\odot$ and $M_{2,zams} \approx 0.1 - 7.7 M_\odot$. Due to the MiMwd-relation, the maximum initial primary mass extends to slightly higher values for the Brussels code in comparison with the other codes (see Fig. 6.15). However, for massive primary progenitors e.g. $M_{1,zams} > 9 M_\odot$ in the Brussels code, the envelope mass of the donor is large and therefore a merger is more likely to happen in the simulations of the Brussels code compared to those of the other three codes. The initial orbital separation lies between $(0.1 - 2.4) \cdot 10^3 R_\odot$ (see Fig. 6.15) according to `binary_c`, `SeBa` and `StarTrack`, however, the range is extended to $3.2 \cdot 10^3 R_\odot$ in the Brussels code due to the single star prescriptions of stellar radii.

Effects Comparing channel 2a and 2b separately, the birthrates of SWDs (see Table 6.2) in the full mass range are close between the codes `binary_c`, `SeBa`, and `StarTrack`. In the intermediate mass range for channel 2a, the birthrates of `binary_c`, `SeBa`, and `StarTrack` are essentially identical, and within a factor of 2.5 lower compared to that of the Brussels code. The larger difference with the Brussels code are caused because this code assumes a priori that a white dwarf is formed without a second interaction, thus there is no entry for the Brussels code in Table 6.2 for channel 2b. The birthrates for channel 2b are very similar within a factor of about 1.2 between `binary_c`, `SeBa` and `StarTrack`. Comparing the total birthrate in channel 2 between all codes, the rate of `binary_c`, `SeBa` and `StarTrack` is only lower by about a factor 1.5 compared to the Brussels code, as some systems merge in the second interaction in the simulations of the former codes. Other differences in the simulated populations from this channel are due to the MiMwd-relation as seen in the example, but also due to differences in the criteria for the stability of mass transfer and the prescriptions for the wind mass loss (see below).

The effect of the stellar wind in the example above is negligible, but the effect of wind mass loss becomes more important for systems with more evolved donors. Mass loss from the primary either in the CE-phase or in foregoing wind mass loss episodes affects the maximum orbital separation of the SWD systems directly and through angular momentum loss. In the simulations of the Brussels code, the maximum orbital separations at WD formation are lower ($a_{swd} \lesssim 80 R_\odot$ compared to $\lesssim 150 R_\odot$ for the main group of systems in `binary_c`, `SeBa` and `StarTrack`), as winds are not taken into account and more mass is removed during the CE-phase in this code. More mass loss during a CE-phase leads to a greater shrinkage of the orbit, where as more wind mass loss with the assumption of specific angular momentum loss from the donor (Jeans-mode, see eq. 6.3), leads to an orbital increase.

Another effect arises from the stellar wind in combination with the stability criterion of mass transfer. For systems with high wind mass losses in which the mass ratio has reversed, the first phase of mass transfer can become stable according to `binary_c`, `SeBa`, and `Star-`

Track. Systems in which this happen are not included in channel 2, however, the birthrates are low ($[1.3, -, 6.5, 4.7] \cdot 10^{-4} \text{ yr}^{-1}$ in the full mass range and $[5.4, -, 10, 9.1] \cdot 10^{-5} \text{ yr}^{-1}$ in the intermediate mass range). In general, when a AGB star initiates mass transfer, stable mass transfer is more readily realised in SeBa and StarTrack than in `binary_c`. Therefore the maximum separation of SWDs in channel 2 is highest in the `binary_c` data (up to $650R_{\odot}$). However, only about 1% of systems in channel 2 in the `binary_c` code lie in the region with a separation larger than $70R_{\odot}$ and a WD mass higher than $0.6M_{\odot}$.

The stability of mass transfer is another important effect for the population of systems in channel 2b during the second phase of mass transfer. We only compare the `binary_c` code, SeBa, and StarTrack, as the Brussels code does not consider this evolutionary path. Whether or not the second phase of mass transfer is stable affects the resulting distribution of orbital separations. This effect is shown in Fig. 6.10 as an extension to lower separations $a_{\text{swd}} \lesssim 10R_{\odot}$ for $M_{1,\text{swd}} \gtrsim 0.8M_{\odot}$ in the `binary_c` data due to unstable mass transfer.

There is a difference between StarTrack on one hand, and `binary_c` and SeBa on the other hand regarding the survival of systems in channel 2b during the first phase of mass transfer. Due to a lack of understanding of the CE-phase, generally BPS codes assume for simplicity that when the stars fit in their consecutive Roche lobes after the CE is removed, the system survives the CE phase. However, this depends crucially on the evolutionary state of the stars after the CE. For channel 2b in which the primary continues helium burning in a shell as a non-degenerate helium star, the response of the primary to a sudden mass loss in the CE is not well known. The StarTrack code assumes the stripped star immediately becomes an evolved helium star and corresponding radius, while `binary_c` and SeBa assume the stripped star is in transition from an exposed core to an evolved helium star with a radius that can be a factor of about 1-15 smaller. The uncertainty in the radii of the stripped star mostly affect systems with $M_{1,zams} \gtrsim 5M_{\odot}$ at separations $\gtrsim 450R_{\odot}$ that merge according to StarTrack, and survive according to `binary_c` and SeBa.

Included in channel 2 are systems that evolve through a double CE-phase² in which both stars lose their envelope described in Sect. 6.2 and in eq. 6.9. The double CE-mechanism is taken into account by the `binary_c`, SeBa and StarTrack code. However, there is a difference between StarTrack on one hand, and `binary_c` and SeBa on the other hand regarding the binding energy of the envelope of the secondary star. In StarTrack the binding energy is calculated according to eq. 6.8) with $R_2 = R_{\text{RL},2}$, where as in `binary_c` and SeBa the instantaneous radius at the start of the double CE-phase is taken for the secondary radius. This can have a significant effect on the orbit of the post-double CE-system, leading to an increase of systems at low separations (approximately $1R_{\odot}$) in the `binary_c` and SeBa data compared to the StarTrack data.

²Note that systems in which the double CE-phase results directly in a DWD system are not taken into account for the comparison of SWD systems.

6.5.1.3 Channel 3: stable case B

Evolutionary path For channel 3, mass transfer starts when a hydrogen shell burning star fills its Roche lobe in a stable way before core helium-burning starts [Kippenhahn & Weigert, 1967, case Br]. This can occur when the envelope is radiative or when the convective zone in the upper layers of the envelope is shallow. In this project we assume that stable mass transfer proceeds conservatively and so the secondary significantly grows in mass. Because mass transfer is conservative, the orbit first shrinks and when the mass ratio has reversed the orbit widens. Mass transfer continues until the primary has lost (most of) its hydrogen envelope. At this stage the primary can become a helium WD or, if it is massive enough, ignite helium in its core. In the latter scenario the primary is a He-MS star. Like for channel 2, there are two sub-channels depending on whether the primary star fills the Roche lobe for a second time as a helium star. If the primary does not go through a helium-star phase or does not fill its Roche lobe as a helium star, the system evolves according to channel 3a. In channel 3b there is a second phase of mass transfer.

Example of channel 3a Figure 6.16a shows an example of the evolution of a binary system of channel 3a. The initial parameters are $M_{1,zams} = 4.8M_{\odot}$, $M_{2,zams} = 3M_{\odot}$ and $a_{zams} = 70R_{\odot}$. The masses of He-MS and secondary star are very similar in the BPS codes $[0.82, 0.83, 0.82, 0.82]M_{\odot}$ and $[6.9, 7.0, 7.0, 7.0]M_{\odot}$ respectively. The separations at the moment the helium star forms are $[4.2, 4.3, 4.3, 4.7] \cdot 10^2 R_{\odot}$ and are similar as well. In the subsequent evolution, the primary star effectively evolves as a single helium star before becoming a carbon-oxygen WD and loses $[0.038, 0.14, 0.043, 0.038]M_{\odot}$ during that time and the orbit does not change significantly.

Population from channel 3a Regarding channel 3a, not all codes agree on the ranges of separation and masses (see Fig. 6.21 and 6.22). However, there is an agreement between binary_c, the Brussels code and SeBa that majority of intermediate mass systems originate from systems with $M_{1,zams}$ between 3 and $5M_{\odot}$ and a_{zams} between 10 and $100R_{\odot}$. The SWD population at WD formation is centred around systems with $M_{1,swd} \approx 0.6M_{\odot}$ for the binary_c, Brussels and SeBa codes, and with the majority of separations between about 20 – $1000R_{\odot}$. The SWD systems and their progenitors that are just described are not SWD progenitors according to StarTrack. According to this code, mass transfer is unstable and the system merges. The birthrates of binary_c, the Brussels code and SeBa differ within a factor of about 4 (see Table 6.2). In addition binary_c, SeBa and StarTrack show a good agreement on the different sub-populations for the full mass range. At WD formation these codes show a subpopulation between 15 to about $200R_{\odot}$ with WD masses of between 0.17 and $0.35M_{\odot}$. There is a second subpopulation at about $1R_{\odot}$ with most systems having a WD between 0.4 and $0.8M_{\odot}$.

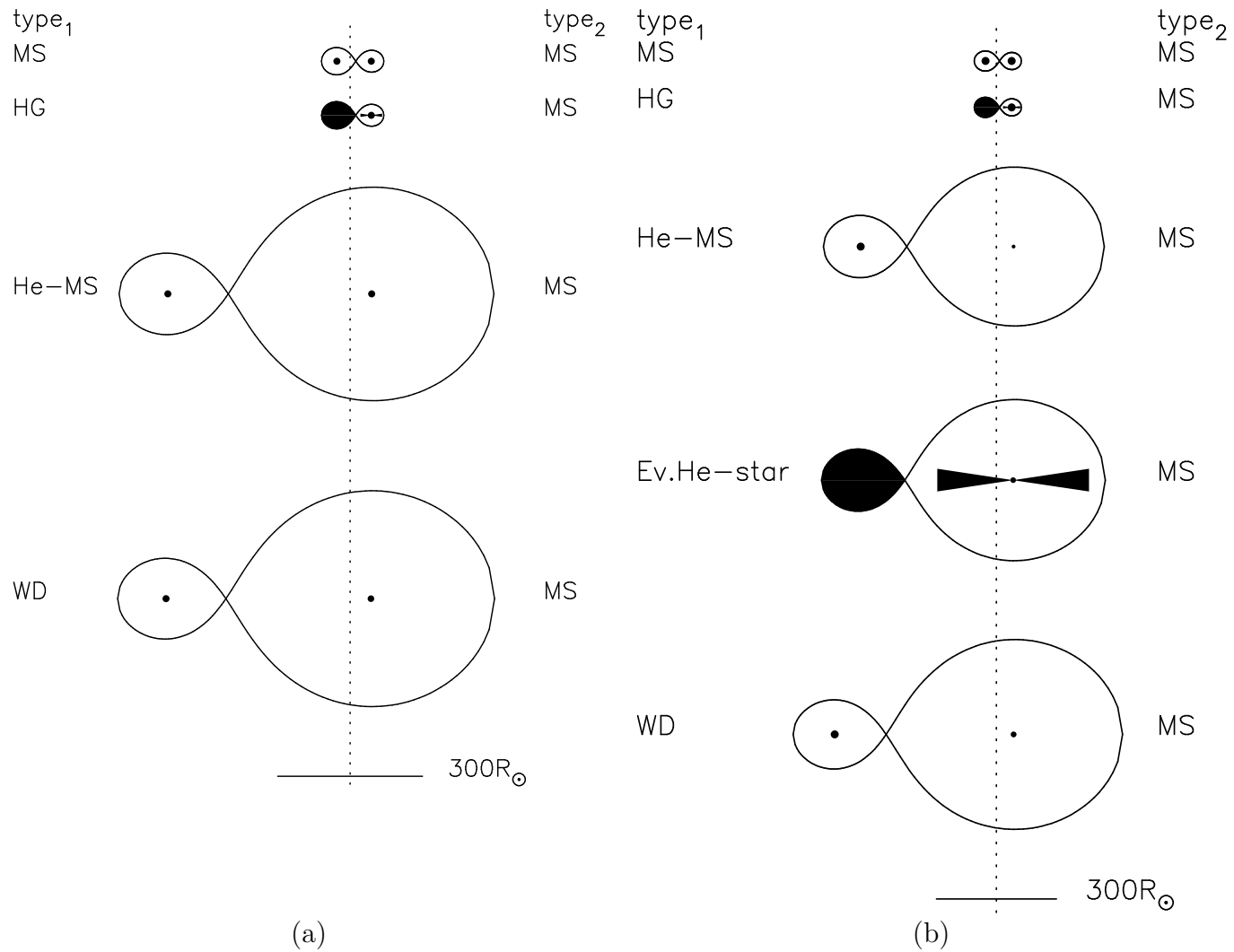


FIGURE 6.16: Example of the evolution of a single white dwarf system in channel 3a (left) and channel 3b (right). Abbreviations are as in Table 6.3.

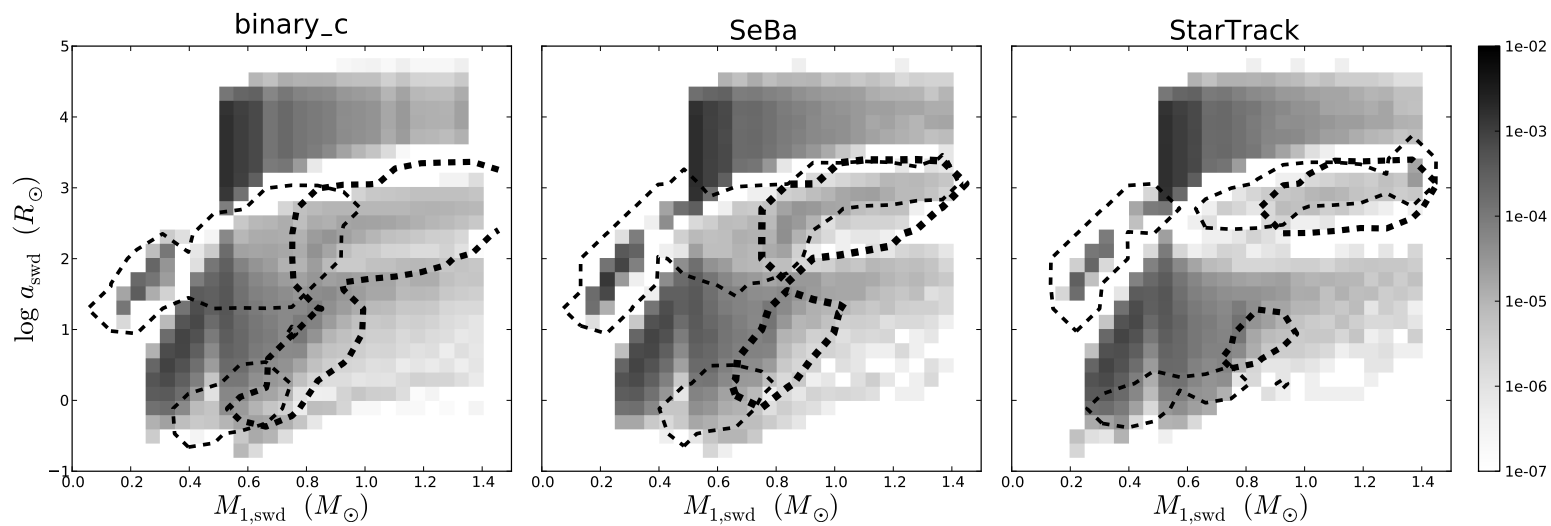


FIGURE 6.17: Orbital separation versus WD mass for all SWDs in the full mass range at the time of SWD formation. The contours represent the SWD population from a specific channel: channel 3a (thin line) and channel 3b (thick line).

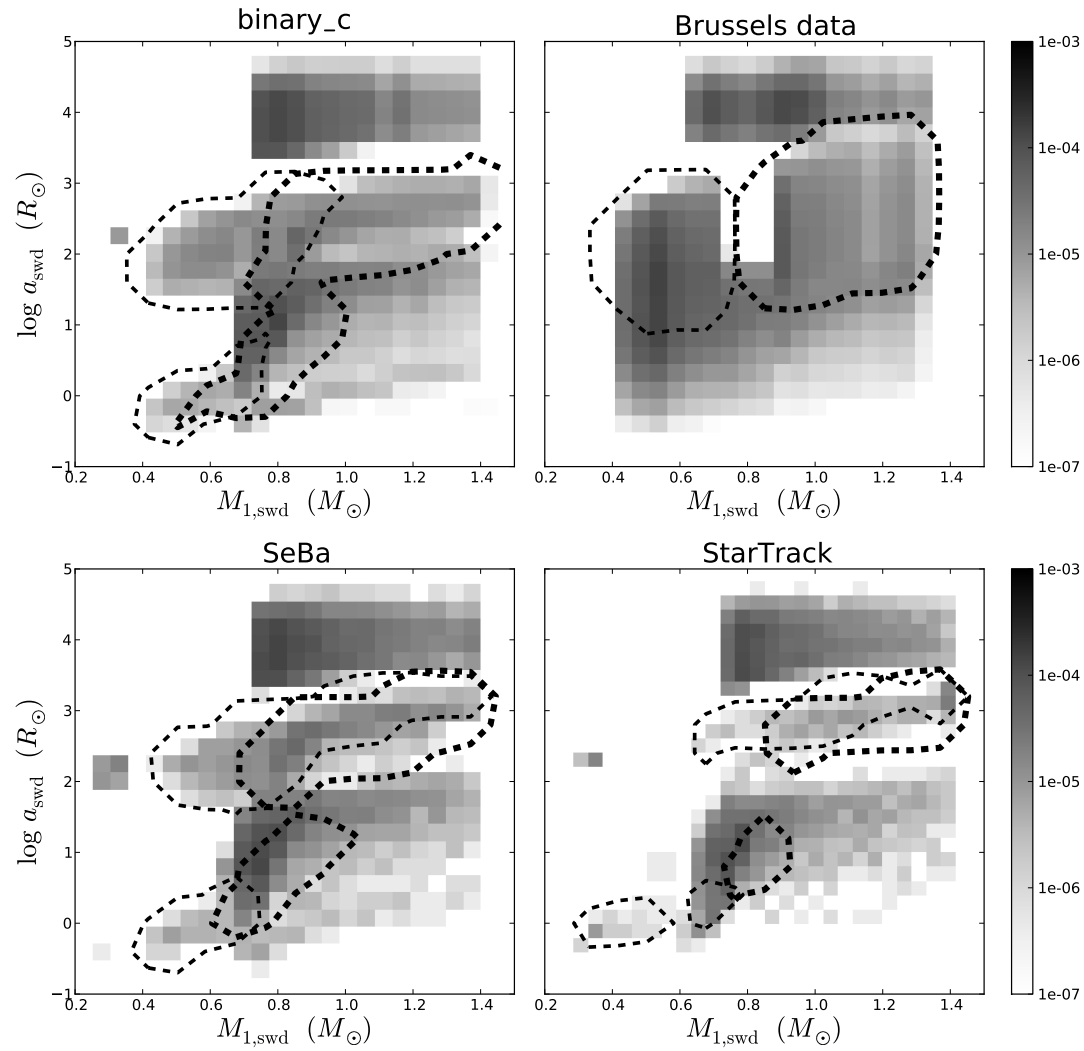


FIGURE 6.18: Orbital separation versus WD mass for all SWDs in the intermediate mass range at the time of SWD formation. The contours represent the SWD population from a specific channel: channel 3a (thin line) and channel 3b (thick line).

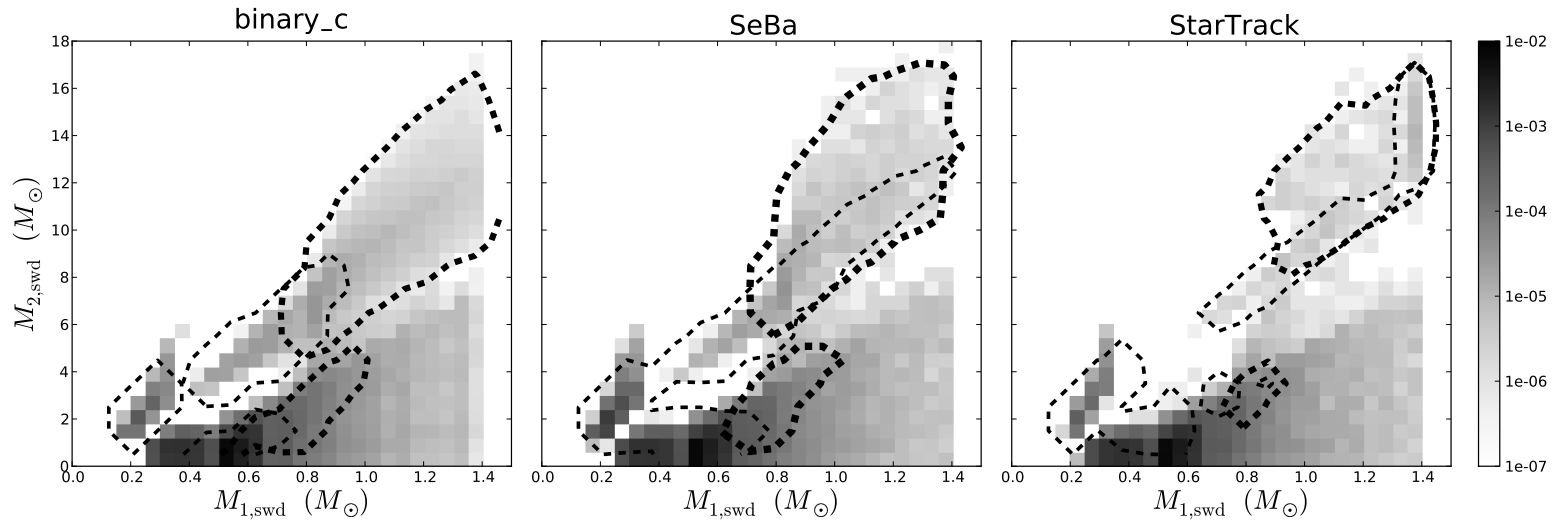


FIGURE 6.19: Secondary mass versus WD mass for all SWDs in the full mass range at the time of SWD formation. The contours represent the SWD population from a specific channel: channel 3a (thin line) and channel 3b (thick line).

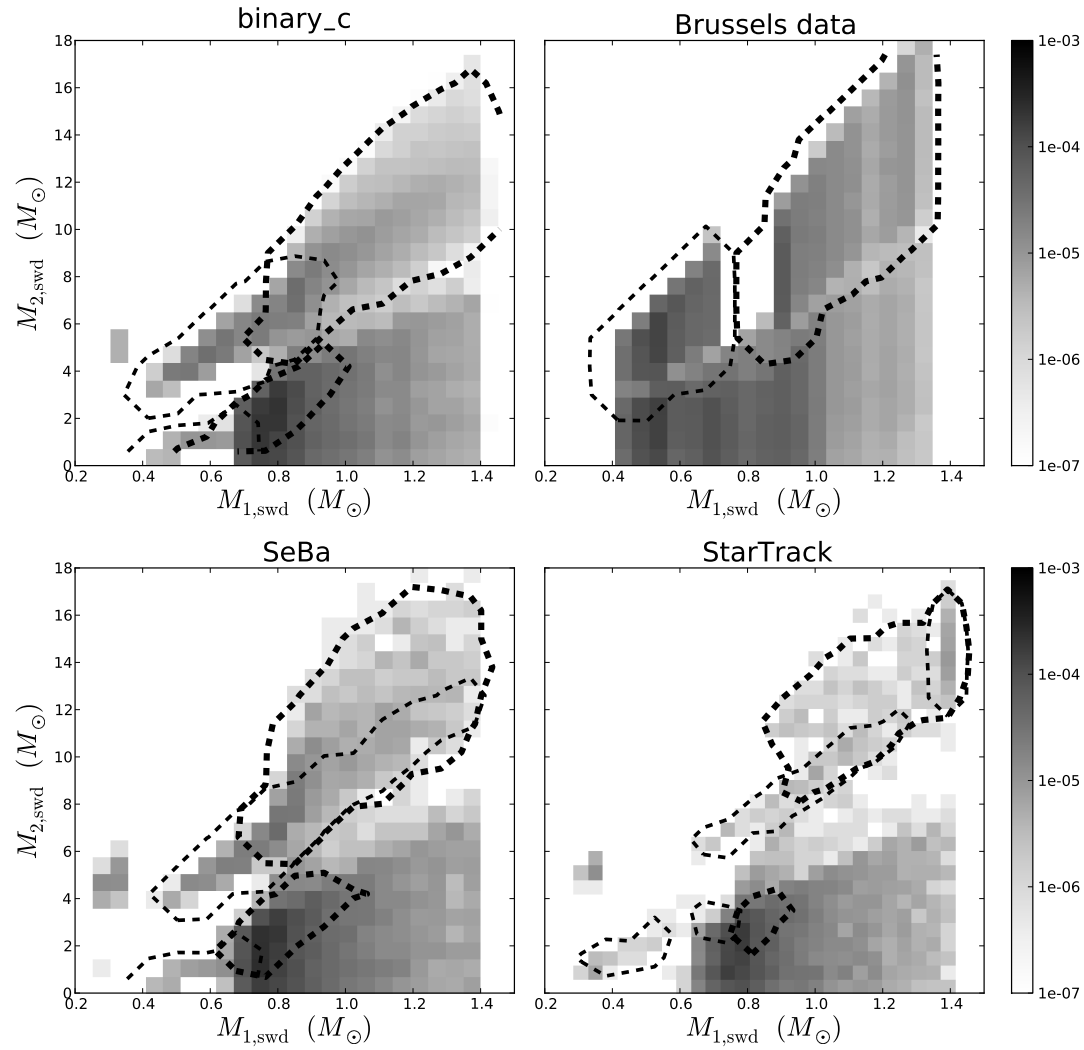


FIGURE 6.20: Secondary mass versus WD mass for all SWDs in the intermediate mass range at the time of SWD formation. The contours represent the SWD population from a specific channel: channel 3a (thin line) and channel 3b (thick line).

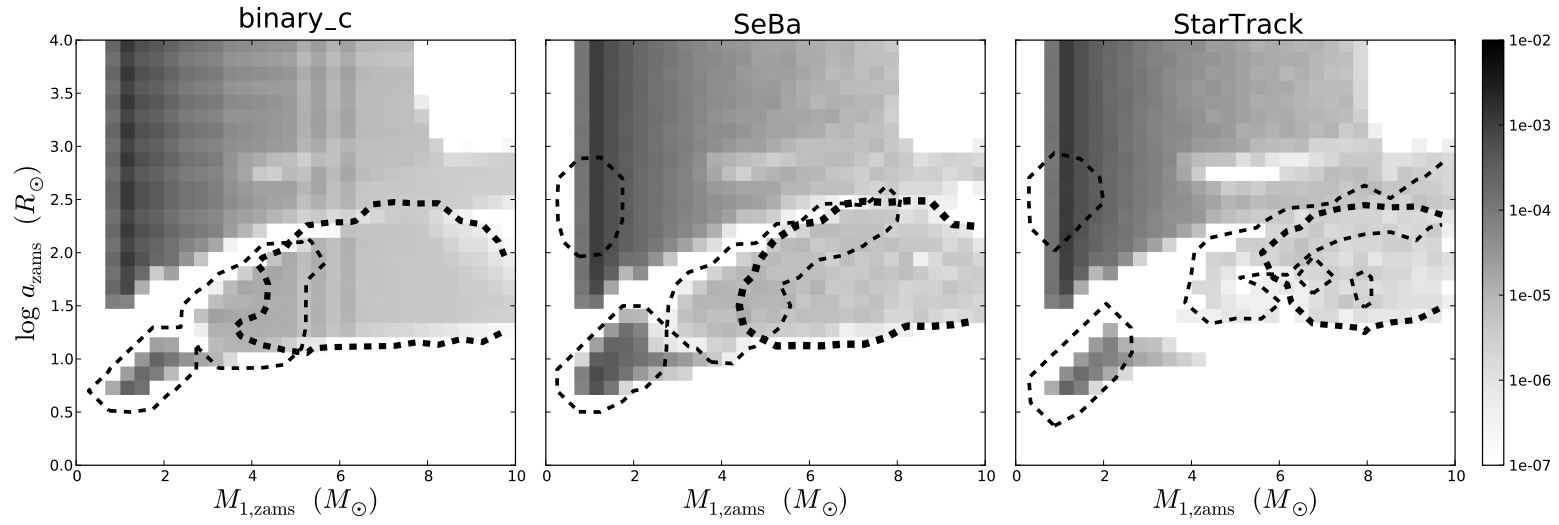


FIGURE 6.21: Initial orbital separation versus initial primary mass for all SWDs in the full mass range. The contours represent the SWD population from a specific channel: channel 3a (thin line) and channel 3b (thick line).

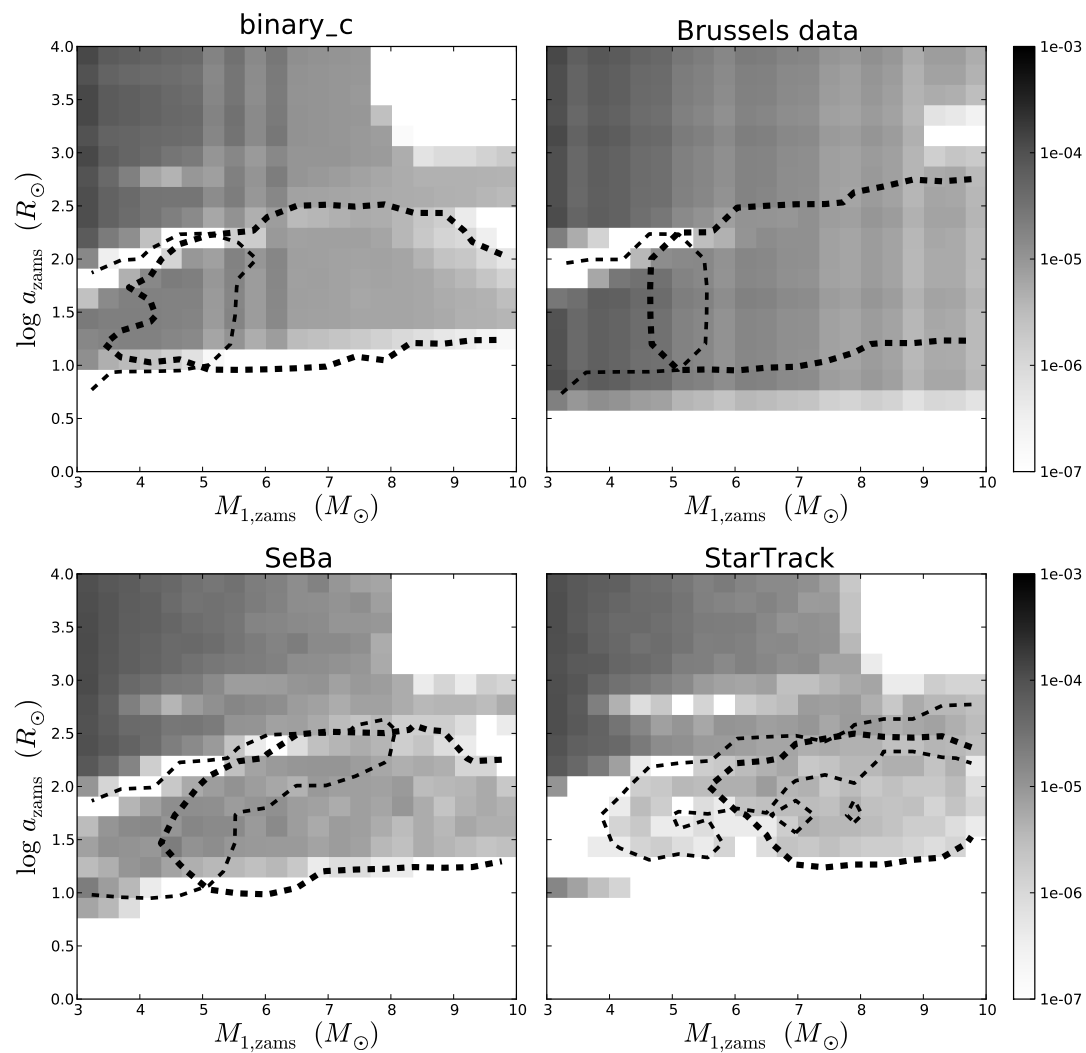


FIGURE 6.22: Initial orbital separation versus initial primary mass for all SWDs in the intermediate mass range. The contours represent the SWD population from a specific channel: channel 3a (thin line) and channel 3b (thick line).

A third population shows mainly WD masses of more than $0.8M_{\odot}$ at separations of more than $300R_{\odot}$, where the population is extended to higher separations and WD masses in the results of SeBa and StarTrack. The third population is also visible in the progenitor population in Fig. 6.21 with primary masses of more than $5M_{\odot}$ and separations of more than about $70R_{\odot}$. Again this population is more extended to high masses and separations according to SeBa and StarTrack. The low mass range of the progenitor population shows predominantly systems in orbits of $5\text{-}15R_{\odot}$. SeBa and StarTrack agree that there is an extra group at high orbital separations $a_{\text{zams}} \approx (1.3 - 4.6) \cdot 10^2 R_{\odot}$.

Example of channel 3b An example of the evolution in channel 3b is shown in Fig. 6.16b. Initially the system has $M_1 = 7M_{\odot}$, $M_2 = 5M_{\odot}$ and $a = 65R_{\odot}$. After the first phase of mass transfer the primary masses $M_1 = [1.4, 1.5, 1.4, 1.4]M_{\odot}$, the secondary masses $M_2 = [11, 11, 11, 11]M_{\odot}$ and separations $a = [3.8, 3.3, 3.8, 4.1] \cdot 10^2 R_{\odot}$. When the primary fills its Roche lobe again, it has lost $[5.8, -, 6.8, 7.3] \cdot 10^{-2} M_{\odot}$ in the wind. The mass transfer phase is stable and the secondary increases in mass to $[11, 11, 11, 11]M_{\odot}$. The primary becomes a WD of $[1.1, 1.0, 0.99, 1.0]M_{\odot}$ in an orbit of $[4.5, 6.5, 5.9, 6.2] \cdot 10^2 R_{\odot}$.

Population from channel 3b The binary_c, Brussels and SeBa codes agree well on the initial systems leading to SWDs through channel 3b. This holds for both the initial mass, namely between about 5 and $10M_{\odot}$ and the initial separation between $0.1 - 3.0 \cdot 10^2 R_{\odot}$. The population of progenitors of channel 3b according to the StarTrack code lies inside the previously mentioned ranges, however, the parameter space is smaller. In addition the four codes agree that at WD formation the majority of companions that are formed through channel 3b are massive, about 6 to $18M_{\odot}$ (for StarTrack 8- $18M_{\odot}$.) The orbits of these systems are wide around $10^3 R_{\odot}$, however, the ranges in separation and WD mass differs between the codes and will be discussed in the next paragraphs. Binary_c, SeBa and StarTrack also show a group of lower mass companions. For binary_c and SeBa these lie in the range $0.8\text{-}4.5M_{\odot}$ with separations of $0.5\text{-}30R_{\odot}$ and $M_{1,\text{swd}}$ mainly between $0.6M_{\odot}$ and $1.0M_{\odot}$. The population of StarTrack agrees with these ranges, however, the parameter space for this population is smaller.

Effects The population of SWDs from channel 3a and 3b are influenced by the MiMwd-relation. An important contribution to the MiMwd-relation comes from the assumed mass losses for helium stars and its mechanism, i.e. in a fast spherically symmetric wind or in planetary nebula (see Appendix 6.A). There is not much known about the mass loss from helium stars either observationally or theoretically. The differences in the MiMwd-relation affect for example the distribution of separations in Fig. 6.18. For channel 3b the separation is $\lesssim 1400R_{\odot}$ for binary_c, SeBa, and StarTrack, but is extended to $6600R_{\odot}$ in the Brussels code. Binaries become wider in the Brussels code, as the WD masses in channel 3 are in general smaller compared to the other three codes.

There is also a difference in the MiMwd-relation between StarTrack on one hand, and binary_c and SeBa on the other hand regarding primaries that after losing their hydrogen envelopes become helium stars. For massive helium stars, binary_c and SeBa find that

these stars will collapse to neutron stars, where as in StarTrack these stars form WDs. For channel 3a the difference occurs for the range of helium star masses of $1.6\text{-}2.25M_{\odot}$. As a result, systems containing massive helium stars are not considered to become SWD systems in binary_c and SeBa. These systems are present in the SWD data of StarTrack at $M_{1,\text{swd}} \gtrsim 1.38M_{\odot}$ in Fig. 6.4 for channel 3a and 3b. The progenitors have high initial masses of $M_{1,\text{zams}} \gtrsim 8M_{\odot}$ and orbital separations of $a_{\text{zams}} \approx 65 - 220R_{\odot}$.

Another effect on the SWD population is the modelling of the mass transfer phases which is inherent to the BPS codes. The value of the mass transfer rate or the length of the mass transfer phase, however, do not have a large effect on the population or the evolution of individual systems from channel 3b in the set-up of the current study. This is because a priori conservative mass transfer is assumed, and therefore the accretion efficiency is not affected by the mass transfer rate. The mass transfer timescale only affects the binary evolution when other evolutionary timescales (such as the wind mass loss timescale or nuclear evolution timescale) are comparable. For example, while for $M_1 \ll M_2$ the orbit increases strongly during RLOF, the orbit increases only moderately during wind mass loss assuming Jeans mode angular momentum loss. The range of separations in Fig. 6.18 is therefore, besides the MiMwd-relation, also affected by the amount of wind mass and wind angular momentum leaving the system during RLOF. The binary_c, SeBa, and StarTrack codes assume wind mass takes with it the specific angular momentum of the donor star (Jeans mode), where as the Brussels code does not take wind mass loss into account during stable mass transfer.

Generally, no significant evolution of the donor star takes place during the mass transfer phase. Therefore with the current set-up, the post-mass transfer masses are determined by their initial mass and for binary_c, SeBa and StarTrack also the evolutionary moment the donor star fills its Roche lobe. However, an exception to this occurs for channel 3b during the second phase of mass transfer. Here the length of the mass transfer phase is important, as the evolutionary time scale of an evolved helium star is very short (of the order of few Myr) and the core grows significantly during this period. As a result the duration of the mass transfer phase becomes important for the resulting WD mass and separation in binary_c, SeBa and StarTrack (see e.g. the example of channel 3b).

A crucially important assumption for the evolutionary outcome of channel 3 are the adopted stability criteria. Despite the importance of the stability criteria, the various implementations have not been compared until this study. We find a clear disagreement between the codes; stable mass transfer is possible in systems with mass ratios $q_{\text{zams}} \gtrsim 0.6$ according to StarTrack, in SeBa $q_{\text{zams}} > 0.35$, in binary_c $q_{\text{zams}} > 0.25$ and $q_{\text{zams}} > 0.2$ in the Brussels code. The effect of the relative large critical mass ratio for StarTrack results in a low birthrate in particular in the intermediate mass range (see Table 6.2 and Fig. 6.22), which results in a lack of SWD systems lower than $300R_{\odot}$ (see Fig. 6.17) and fewer SWD systems with $M_{2,\text{swd}} \lesssim 1.0M_{\odot}$ (see Fig. 6.19). The effect of the relative low critical mass ratio for the Brussels code can be seen in Fig. 6.20 as an extension in the Brussels code

to lower separations $a_{\text{swd}} \lesssim 50$. Systems with lower mass companions initially, go through mass ratio reversal and subsequent expansion of the orbit later in the mass transfer phase.

In the low mass range we find that the stability criteria vary most strongly for donor stars that are early on the first giant branch when they have shallow convective zones in the upper layers of the envelope. In general, stable mass transfer from this type of donor for the same conditions is more readily realised in StarTrack than in `binary_c`, and it is even more readily realised in SeBa. Systems with this kind of donor show in Fig. 6.21 at $M_{1,\text{zams}} < 3M_{\odot}$ a larger range in initial separations for SeBa ($5\text{-}25R_{\odot}$) than for `binary_c` and StarTrack ($5\text{-}18R_{\odot}$). There is also an extra population of SWD systems in the SeBa and StarTrack data with high initial separation $a_{\text{zams}} \approx (1.3 - 4.6) \cdot 10^2 R_{\odot}$ and high initial mass ratio $q_{\text{zams}} \approx M_{2,\text{zams}}/M_{1,\text{zams}} > 0.8$. In these systems the primary fills its Roche lobe stably on the giant branch after the mass ratio has reversed due to wind mass losses. When donors with shallow convective zones are excluded, the birthrate in the full mass range in channel 3a decreases to $1.4 \cdot 10^{-3} \text{ yr}^{-1}$ for SeBa and $7.3 \cdot 10^{-4} \text{ yr}^{-1}$ for StarTrack, which is comparable to the birthrate predicted by `binary_c` (see Table 6.2).

The long-term behaviour of the orbit can be effected by tides. If energy is dissipated, angular momentum can be exchanged between the orbit and the spin of the stars. For this project the `binary_c`, Brussels and SeBa code assume that the spin angular momentum of the stars can be neglected compared to the orbital angular momentum³. As such in their simulations orbital angular momentum is conserved. In the StarTrack code, the orbital and spin angular momentum combined are conserved, under the assumption that the stars are and remain in a synchronized orbit. As a consequence after the first phase of mass transfer in channel 3, the orbits are slightly larger in StarTrack compared to those of the other codes (see the example system of channel 3a and 3b).

Whether or not a primary fills its Roche lobe for a second time is modelled different in the Brussels code than in the other three codes. In the Brussels code stars with an initial mass less than $5M_{\odot}$ are assumed to evolve through channel 3a, and stars with a higher mass evolve through channel 3b. The `binary_c` and SeBa simulations roughly agree with this, see Fig. 6.21. However, the boundary between channel 3a and 3b is determined at run time in `binary_c`, SeBa, and StarTrack. It is dependent on the evolution of the radii and wind mass loss of helium stars, the stability criterion and the separation after the first phase of mass transfer. Therefore differences exist between these codes in the upper limits for ZAMS masses and separations in channel 3a in Fig. 6.21 and at WD formation in Fig. 6.19. `Binary_c`, SeBa, and StarTrack also find that systems that evolve through channel 3a or 3b overlap in WD mass at WD formation (see Fig. 6.18 and 6.20). In the data from the Brussels code, the boundary at WD formation is discontinuous in primary mass causing a gap between 0.7 and $0.9 M_{\odot}$ (see Fig. 6.18 and 6.20). The gap in WD mass in the data from the Brussels code originates as a considerable amount of mass is lost during

³In `binary_c` it is possible to take into account spin angular momentum into the total angular momentum of the system.

the planetary nebula phase of a star that does not initiate a second mass transfer phase. In the other three codes, the mass loss in winds from helium stars is less strong compared to the mass loss in the planetary nebula phase of helium stars in the Brussels code.

The evolution of helium stars (their radii, core masses, wind mass losses, and if they fill their Roche lobes also the stability and mass transfer rates) are important in channel 3. A difference arises between the Brussels code and the others, because of the way helium stars are simulated. In `binary_c`, `SeBa`, and `StarTrack` it is possible that after the first phase of mass transfer, the secondary fills its Roche lobe before the primary moves off the He-MS and becomes a white dwarf. Subsequently the primary becomes a WD before the secondary evolves significantly⁴. This reversal can occur because the evolutionary timescale of a low-mass helium star is very long (about 10^8 yr), while that of the secondary that gained much mass is reduced. As a result, when the first WD is formed, the mass of the secondary and the orbital separation has decreased substantially. These systems lie according to `binary_c`, `SeBa` and `StarTrack` at separations $\lesssim 20R_\odot$, primary WD masses of $\lesssim 1.0M_\odot$ and secondary masses of $\lesssim 4.5M_\odot$ in Fig. 6.17 and 6.19. The birthrates of the systems in `binary_c`, `SeBa` and `StarTrack`, are low ($[1.1, -, 8.6, 0.4] \cdot 10^{-4} \text{ yr}^{-1}$ in the full mass range). In the Brussels code, the evolution of the stars is not followed in time, and this evolutionary track is not considered. As a result in the range of $0.45\text{-}0.7M_\odot$ for the WD mass, the range in secondary masses is broader in the Brussels code.

6.5.1.4 Channel 4: unstable case B

Evolutionary path In this path, a hydrogen shell burning star fills its Roche lobe [Kippenhahn & Weigert, 1967, case Bc], but the mass transfer is unstable. After the CE-phase the primary becomes a helium WD or a He-MS. Again, we differentiate two evolutionary paths within a channel. In channel 4a, the primary becomes a WD directly or the primary becomes a helium star that will evolve into a WD without any further interaction with the secondary. If the primary star fills its Roche lobe for a second time, the system evolves through subchannel 4b. An example of the evolutionary path of channel 4b is shown in Fig. 6.23.

Example Figure 6.23 shows the evolution of a system of channel 4b, that starts its evolution with $M_{1,\text{zams}} = 6M_\odot$, $M_{2,\text{zams}} = 3M_\odot$ and $a_{\text{zams}} = 320R_\odot$. The primary fills its Roche lobe as it ascends the first giant branch. After mass transfer ceases the primary has become a He-MS of mass $[1.1, 1.1, 1.1, 1.1]M_\odot$ in an orbit with a separation of $[7.0, 7.1, 7.0, 7.0]R_\odot$. As the helium star evolves and increases in radius, it initiates the second phase of mass transfer. Soon after mass transfer ceases, the primary becomes a WD with $M_{1,\text{swd}} = [0.81, 0.91, 0.77, 0.79]M_\odot$. The secondary is still on the MS with

⁴Note that it is also possible that the secondary becomes a WD before the primary does [Toonen et al., 2012, Claeys et al. in prep.]. Because of the evolutionary reversal, these systems are not shown in Fig. 6.17 to 6.22 nor included in channel 3. The birthrates, however, are low ($[1.4, -, 5.6, 0.7] \cdot 10^{-4} \text{ yr}^{-1}$ in the full mass range).

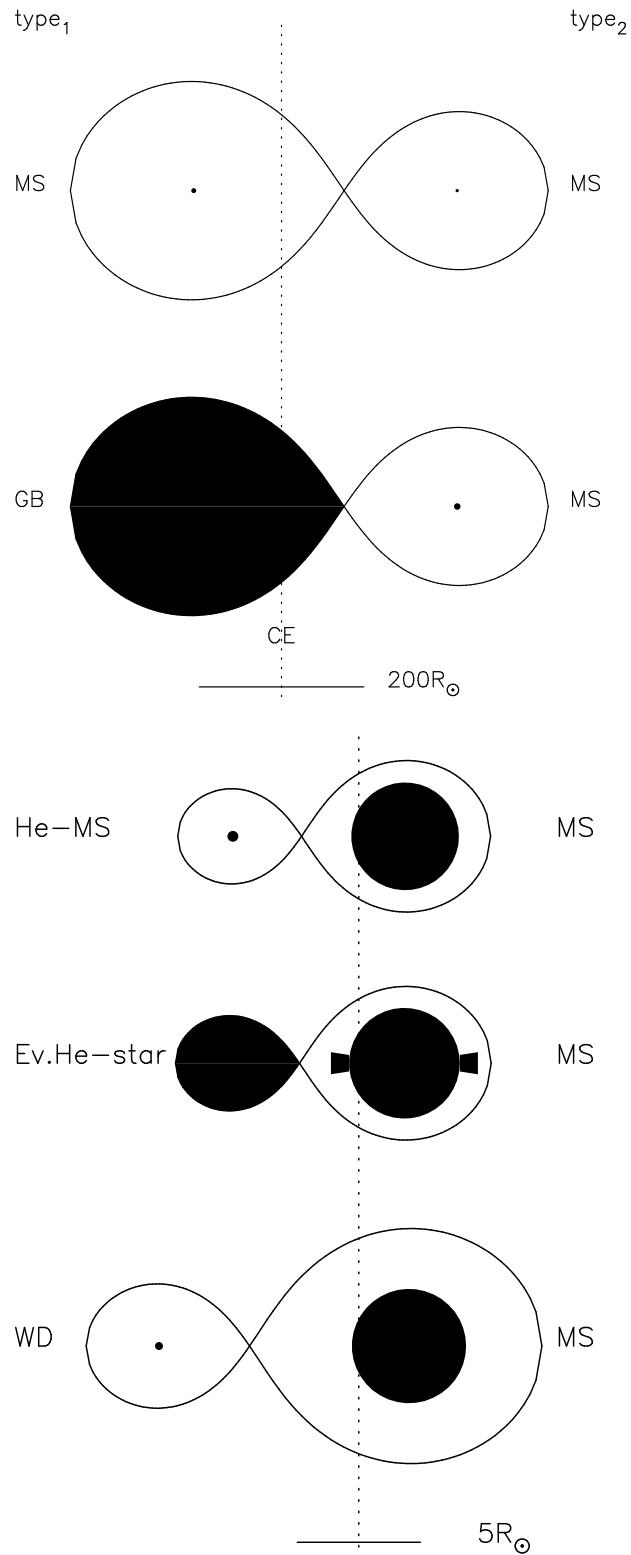


FIGURE 6.23: Example of the evolution of a single white dwarf system in channel 4b. The primary fills its Roche lobe a second time. The top and bottom parts of the figure have different scales due to a common envelope phase, denoted as CE in the figure. Abbreviations are as in Table 6.3.

$M_{2,\text{swd}} = [3.2, 3.2, 3.3, 3.3]M_{\odot}$ and the orbital separation is $a_{\text{swd}} = [10, 9.4, 11, 11]R_{\odot}$. The differences in this example are caused by effects discussed before; the MiMwd-relation including the mass transfer rates from helium rich donors.

Population The codes agree well on the location of the SWDs at WD formation from channel 4a and 4b in Fig. 6.2, 6.3, 6.4 and 6.5, their progenitor systems in Fig. 6.6 and 6.7 and the birthrates of the channels (see Table 6.2). For channel 4a, which predominantly contains low mass binaries, there is an excellent agreement between `binary_c`, `SeBa` and `StarTrack` in the previously mentioned figures as well as in the birthrates (see Table 6.2). The low mass SWDs at WD formation have WDs of $0.25\text{--}0.48M_{\odot}$, companions of $< 1.8M_{\odot}$, in an orbit of $0.5\text{--}100R_{\odot}$, and progenitor systems with $a_{\text{zams}} \approx (0.3\text{--}4.0) \cdot 10^2R_{\odot}$ for $M_{1,\text{zams}} \approx 1\text{--}2M_{\odot}$.

The population of systems that evolve through channel 4b are primarily intermediate mass binaries of mass $M_{1,\text{zams}} \approx 4.5\text{--}10M_{\odot}$ that become WDs of $M_{1,\text{swd}} \approx 0.7\text{--}1.3M_{\odot}$. The majority of systems have initial separations of $a_{\text{zams}} \approx (0.2\text{--}1.0) \cdot 10^3R_{\odot}$. At WD formation the range of separations according to `binary_c`, `SeBa` and `StarTrack` is $4\text{--}1.0 \cdot 10^2R_{\odot}$, however, for the Brussels code it is extended to $0.9\text{--}1.4 \cdot 10^2R_{\odot}$.

Effects There is a difference between the Brussels code on one hand and the other three codes on the other hand, regarding the survival of systems with low initial secondary masses $M_{2,\text{zams}} < 3M_{\odot}$ in channel 4b. This is predominantly due to the difference in the single star prescriptions for the radii of stars. The radius of low-mass secondary-stars are in general larger in `binary_c`, `SeBa` and `StarTrack` than in the Brussels code. Therefore in the former three codes, the stars are more likely to fill their Roche lobe at the end of the CE-phase resulting in a merger. In the Brussels data, these systems survive at small separations ($\lesssim 10R_{\odot}$ at $1M_{\odot}$, see Fig. 6.3). Note that the Brussels code was written for intermediate mass stars (see Sect. 6.3), and in principal the code does not allow for the detailed evolution of stars with initial masses below $3M_{\odot}$.

In addition, the stability of the second phase of mass transfer affects the SWD population of channel 4. If this phase is unstable, the system will evolve to a merger. In the Brussels code, it is assumed that the second phase of mass transfer is always stable, however, this is not the case in the three other codes. Differences in the stability criteria affect the orbital separation of SWD formation for all codes.

6.5.1.5 Channel 5: case A

Evolutionary path In channel 5 mass transfer starts during the core hydrogen burning phase of the donor [Case A, Kippenhahn & Weigert, 1967].

Population The birthrates in the full mass range differ within a factor 2.5 between `binary_c`, `SeBa` and `StarTrack` (see Table 6.2). According to these codes, the progenitors of the primaries in channel 5 are stars of low mass ($1\text{--}4M_{\odot}$) in small orbits ($5\text{--}13R_{\odot}$), see Fig. 6.6. There is a good agreement that the majority of SWDs from channel 5 at WD

formation consists of a primary of mass $0.2\text{-}0.35M_{\odot}$, a secondary of mass $1.8\text{-}5.5M_{\odot}$ in an orbit with a separation of $30\text{-}240R_{\odot}$ (see Fig. 6.2 and 6.4). Binary_c, SeBa and StarTrack further agree on a subchannel ($a_{\text{swd}} \approx 0.4R_{\odot}$ and $M_{1,\text{swd}} \approx 0.3M_{\odot}$ in Fig. 6.2) in which the secondary is a hydrogen-poor helium-star at WD formation (see also channel 3). The birthrates of this subchannel are low ($[4.5, -, 4.8, 18] \cdot 10^{-6} \text{ yr}^{-1}$).

The birthrate of channel 5 in the Brussels code is higher by over a factor 20 compared to binary_c, SeBa and StarTrack (see Table 6.2). For the Brussels code the intermediate mass primaries have an initial mass $M_{1,\text{zams}} \approx 3 - 10M_{\odot}$ and WD mass $M_{1,\text{swd}} \approx 0.45 - 1.3M_{\odot}$, while the other codes show smaller ranges. For the main group of progenitors, these ranges are $M_{1,\text{zams}} \approx 3 - 4M_{\odot}$ and WD mass $M_{1,\text{swd}} \lesssim 0.35M_{\odot}$ (see Fig. 6.2 and 6.6). The initial separation in the Brussels code $a_{\text{zams}} \approx 5 - 22R_{\odot}$, while in binary_c, SeBa and StarTrack $a_{\text{zams}} \approx 8 - 13R_{\odot}$. The separation at SWD formation a_{swd} in the Brussels code is between $20\text{-}350R_{\odot}$, while in the other codes the separation is mainly between $100\text{-}250R_{\odot}$. The range of secondary masses is $M_{2,\text{swd}} \approx 3\text{-}18M_{\odot}$ in the Brussels code, but only $M_{2,\text{swd}} \approx 4\text{-}6M_{\odot}$ in the other codes. Note that the region indicated by the dash-dotted contours in Fig. 6.2, contains systems from channel 5 as well as from channel 3, however, this does not change our conclusion regarding the extended range and birthrates in the Brussels code compared to the other codes.

Effects The differences between the Brussels code and the other codes is caused by the fact that the Brussels population code does not follow the mass transfer event and its mass transfer rate in detail. It considers only the initial and final moment of the mass transfer phase, therefore any intermediate steps in which the system can be closer are disregarded. For example, during conservative mass transfer to an initially less massive companion, the orbital separation first decreases and then increases again after mass ratio reversal. As the orbital separation decreases, the secondary can fill its Roche lobe leading to a contact system, especially as it grows in mass and radius due to the accretion. In the binary_c, SeBa and StarTrack code, it is assumed that the contact phase will lead to a merger or CE-phase for evolved secondaries. The Brussels code assumes that for shallow contact, the merger can be avoided. In other words, the codes have different assumptions for the stability of mass transfer.

6.5.2 Double white dwarfs

In this section we compare and discuss the population of DWDs as predicted by binary_c, the Brussels code, SeBa and StarTrack. Prior to the formation of a second degenerate component, DWDs undergo the evolution as described in the previous section (channel 1 to channel 5). Subsequently, they undergo a second intrusive (series of) event(s) at the time the secondary fills its Roche lobe. As a consequence the processes that influence the evolution of SWDs influence the DWD population as well. Here we will point out the evolutionary processes that are specifically important for DWDs.

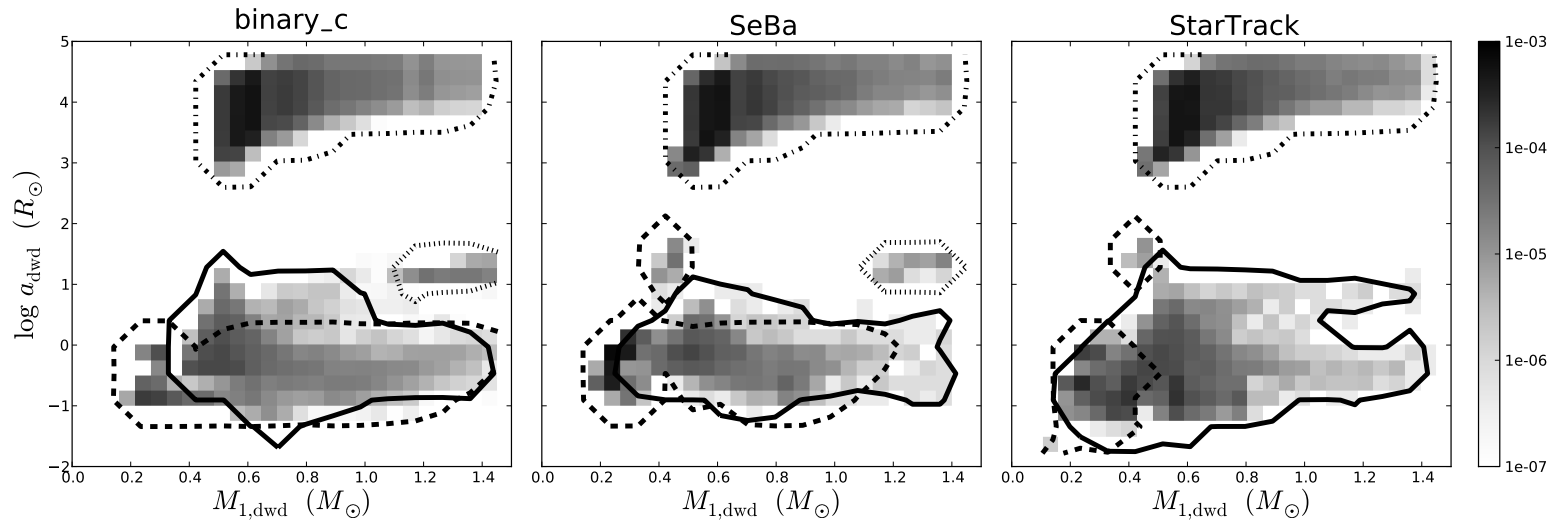


FIGURE 6.24: Orbital separation versus primary WD mass for all DWDs in the full mass range at the time of DWD formation. The contours represent the DWD population from a specific channel: channel I (dash-dotted line), channel II (solid line), channel III (dashed line) and channel IV (dotted line).

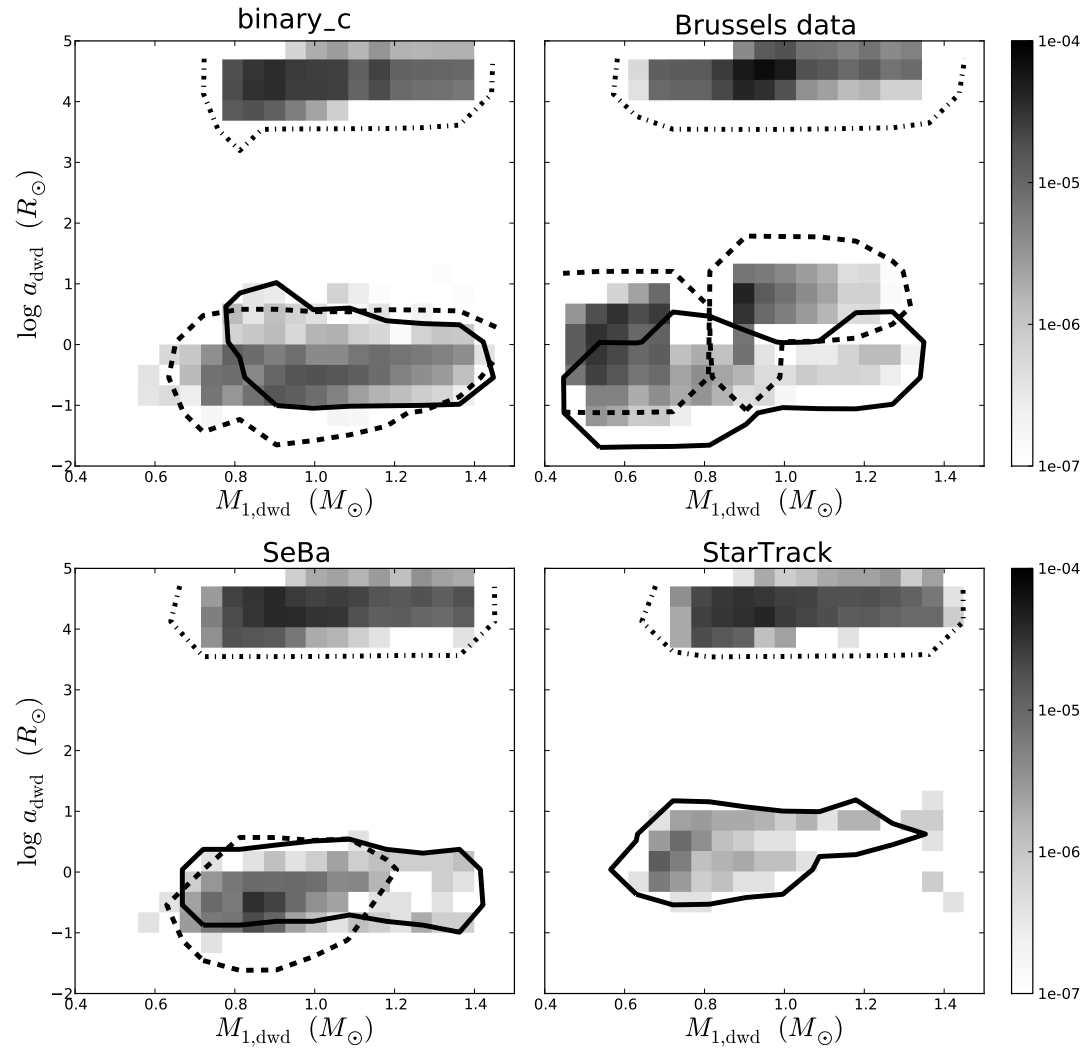


FIGURE 6.25: Orbital separation versus primary WD mass for all DWDs in the intermediate mass range at the time of DWD formation. The contours represent the DWD population from a specific channel: channel I (dash-dotted solid line), channel II (solid line) and channel III (dashed line). The contours of the DWD population from channel III according to StarTrack and channel IV according to all codes are not shown, as the birthrate from this channel is too low.

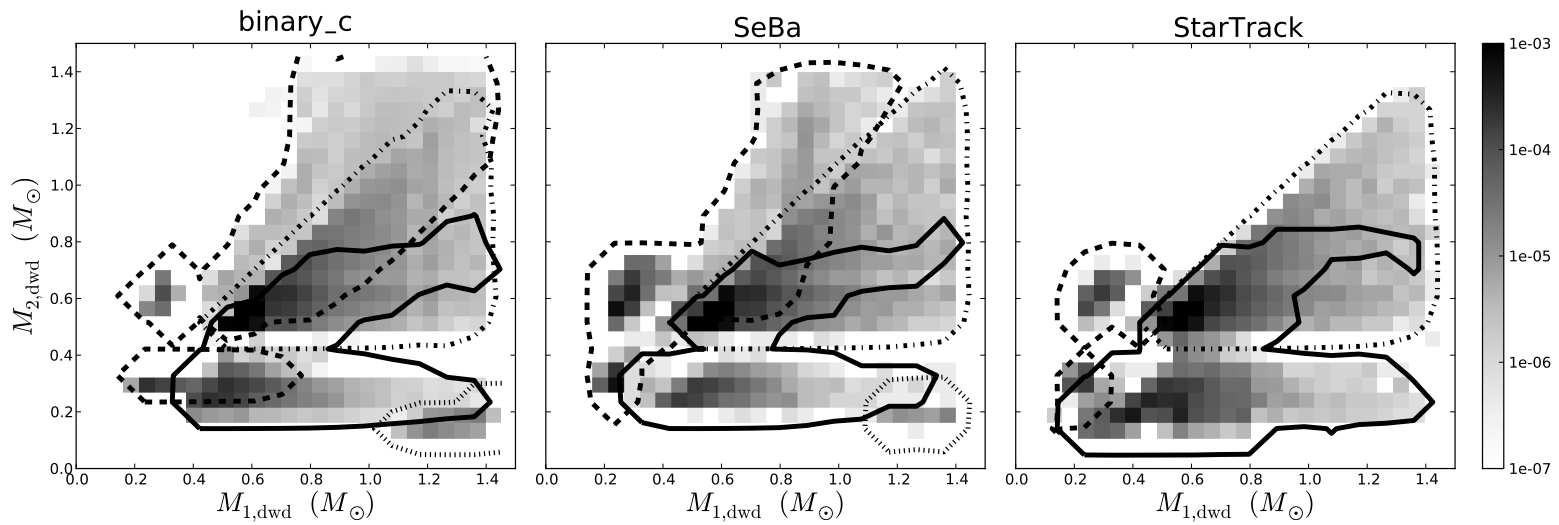


FIGURE 6.26: Secondary WD mass versus primary WD mass for all DWDs in the full mass range at the time of DWD formation. The contours represent the DWD population from a specific channel: channel I (dash-dotted solid line), channel II (solid line), channel III (dashed line) and channel IV (dotted line).

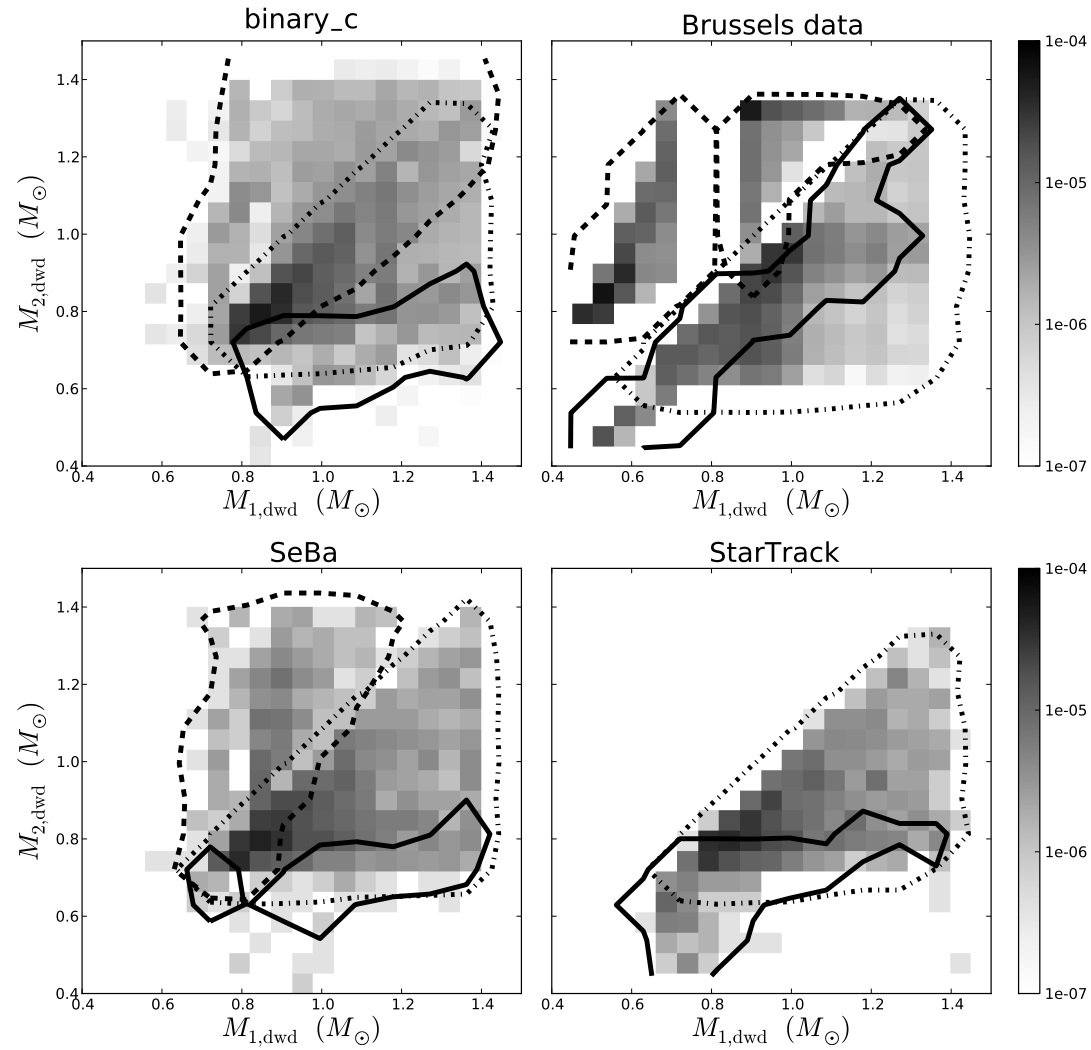


FIGURE 6.27: Secondary WD mass versus primary WD mass for all DWDs in the intermediate mass range at the time of DWD formation. The contours represent the DWD population from a specific channel: channel I (dash-dotted solid line), channel II (solid line) and channel III (dashed line). The contours of the DWD population from channel III according to StarTrack and channel IV according to all codes are not shown, as the birthrate from this channel is too low.

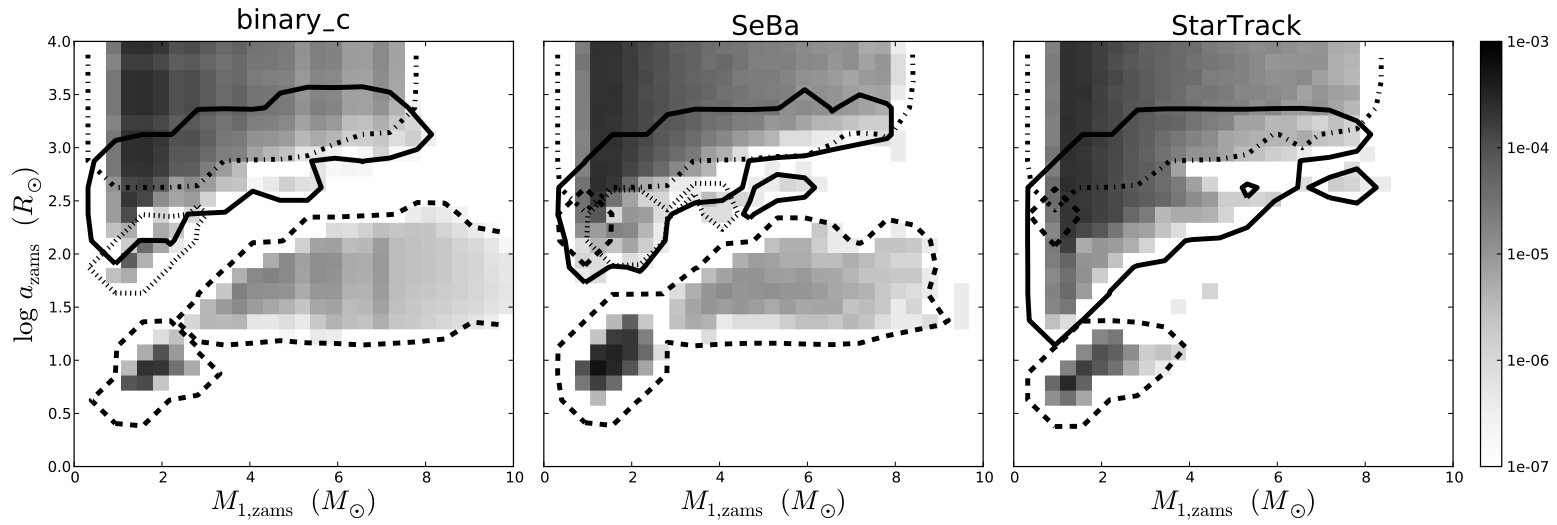


FIGURE 6.28: Initial orbital separation versus initial primary mass for all DWDs in the full mass range. The contours represent the DWD population from a specific channel: channel I (dash-dotted solid line), channel II (solid line), channel III (dashed line) and channel IV (dotted line).

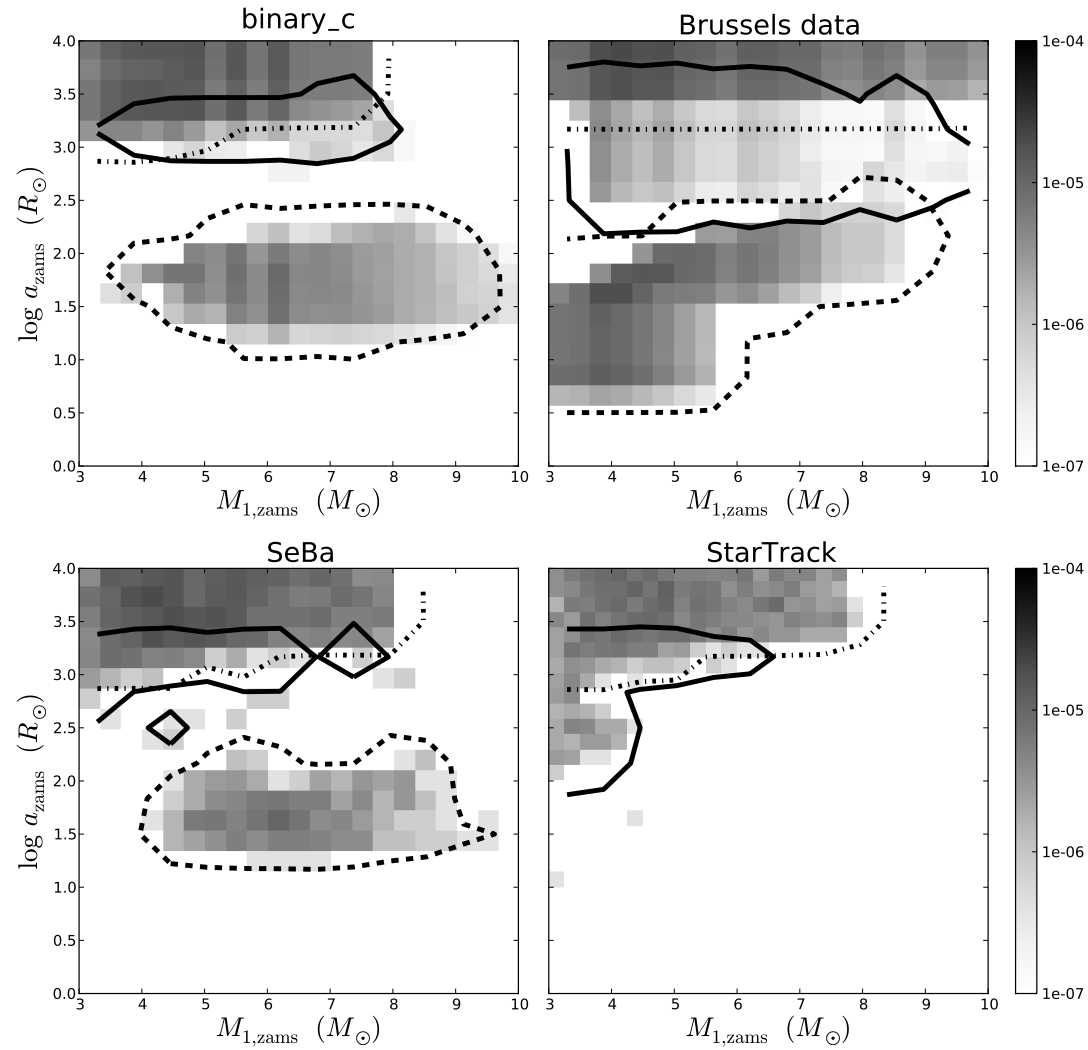


FIGURE 6.29: Initial orbital separation versus initial primary mass for all DWDs in the intermediate mass range. The contours represent the DWD population from a specific channel: channel I (dash-dotted solid line), channel II (solid line) and channel III (dashed line). The contours of the DWD population from channel III according to StarTrack and channel IV according to all codes are not shown, as the birthrate from this channel is too low.

The population of DWDs at DWD formation is shown in Fig. 6.24, 6.25, 6.26, and 6.27 where orbital separation and secondary mass respectively is shown as a function of primary mass for the full and intermediate mass range. The ZAMS progenitors of these systems are shown in Fig. 6.28 and 6.29 for the full and intermediate mass range respectively.

In the full mass range the population of DWDs is comparable between `binary_c`, `SeBa` and `StarTrack` with white dwarf masses of $M_{1,\text{dwd}} \approx 0.2 - 1.4M_{\odot}$ and $M_{2,\text{dwd}} \approx 0.1 - 1.4M_{\odot}$. At large separations $(0.1-5) \cdot 10^4 R_{\odot}$ the codes find systems which are formed without any interaction, see also Fig. 6.24. This figure also shows a population of interacting systems at lower separations, where the majority has separations of $a \approx 0.1 - 10R_{\odot}$. Furthermore there is a good agreement on which progenitors lead to a DWD system and which do not. Figure 6.28 shows several subpopulations of DWD progenitors with comparable binary parameters for `binary_c`, `SeBa` and `StarTrack`; a group of non-interacting systems at $a_{\text{dwd}} \gtrsim 5 \cdot 10^2 R_{\odot}$, a group of systems for which the first phase of mass transfer is stable at $a_{\text{dwd}} \lesssim 25R_{\odot}$ for low mass primaries and $a_{\text{dwd}} \lesssim 2.5 \cdot 10^2 R_{\odot}$ for the full mass range, and a group of systems at intermediate separations that predominantly undergoes a CE-phase for the first phase of mass transfer.

An effect that plays a role for DWDs, has already been noted for SWDs, namely that stable mass transfer is more readily realized in `binary_c` and `SeBa` compared to `StarTrack`. It plays a role for example in Fig. 6.28 in the lack of systems at $M_{1,\text{zams}} > 3M_{\odot}$ and $a_{\text{zams}} < 2.5 \cdot 10^2 R_{\odot}$ in the `StarTrack` data compared to `binary_c` and `SeBa`, and in Fig. 6.26 in the lack of systems with $M_{2,\text{dwd}} > M_{1,\text{dwd}}$. Differences in the interpretations of the double CE-phase, in which both stars lose their envelopes (eq. 6.8), results in larger separations at DWD formation and less mergers in `StarTrack` compared to `binary_c` and `SeBa` (see Fig. 6.25 and Sect. 6.5.2.2). At the same time, the initial separations of systems evolving through a double CE-phase can be smaller in the `StarTrack` data compared to `binary_c` and `SeBa` ($a_{\text{dwd}} \approx 25 - 100R_{\odot}$, see Fig. 6.28). The DWD populations will be discussed in more detail in the following sections.

In the intermediate mass range at DWD formation, two groups of systems can be distinguished in all simulations (see Fig. 6.25). Similar to the full mass range, there is one group of non-interacting systems at separations higher than $6 \cdot 10^3 R_{\odot}$ and a group of interacting systems with separations $\lesssim 20R_{\odot}$. However, the distribution of systems in the latter range, corresponding to different evolutionary paths, varies between the codes. Most DWD systems have primary and secondary WD masses above $0.6M_{\odot}$ in all the codes. The progenitors in the intermediate mass range show the same division in separation in three groups as the progenitors in the full mass range. DWD progenitors with separations $a_{\text{zams}} \lesssim 3 \cdot 10^2 R_{\odot}$ undergo a stable first phase of mass transfer. The components of DWD progenitors with $a_{\text{zams}} \gtrsim 1.5 \cdot 10^3 R_{\odot}$ do not interact. At intermediate separations the first phase of mass transfer is predominantly a CE-phase.

Comparing the `Brussels` code with `binary_c` and `SeBa` (differences with `StarTrack` have the same origin as discussed in the previous paragraph), the most important causes for

differences in the DWD population in the intermediate mass range are the MiMf-relation, the MiMwd-relation, the modelling of the stable mass transfer phase and the survival of mass transfer. The effect of the first three causes on the DWD population, is similar to the effect on the SWD population. Firstly, the differences in the MiMf-relation can be seen in the progenitor population of non-interacting binaries in Fig. 6.29 as an extension to higher primary masses in the Brussels data ($8-10M_{\odot}$, see Sect. 6.5.2.1). Secondly, differences in the MiMwd-relation can be seen in Fig. 6.25 as an extension to lower primary WD masses $M_{1,\text{dwd}} \lesssim 0.64M_{\odot}$ and the discontinuity in primary WD masses around $0.7-0.9M_{\odot}$ (see Sect. 6.5.2.2 and 6.5.2.3). The MiMwd-relation also effects the orbital separation distribution at DWD formation and results in a higher maximum separation in the Brussels code compared to `binary_c` and `SeBa`. Finally, due to the method of modelling of mass transfer there is a disagreement between the codes regarding which systems survive mass transfer, see Fig. 6.29 at $a_{\text{dwd}} \lesssim 20R_{\odot}$ (see Sect. 6.5.2.3). The survival of mass transfer is more important for the DWD population than for the SWD population, as the average orbital separation of DWDs is lower (see Sect. 6.5.2.2 and 6.5.2.3). As the formation of DWDs involves more phases of mass transfer than for SWDs, the differences in the SWD population carry through and are larger in the DWD population.

In the next sections, we differentiate four different evolutionary paths of DWDs. This is based on whether or not mass transfer occurs and if so, if the mass transfer initiated by the primary and secondary is stable or unstable. For clarity we do not distinguish the evolutionary path further e.g. by separating channel 3 and 5, nor channel 3a and 3b. Channel I, II and III represent the most commonly followed evolutionary paths with birthrates larger than $1.0 \cdot 10^{-3} \text{ yr}^{-1}$. Channel IV is included because it stands out in Fig. 6.24 and 6.26, even though the birthrates in this channel are low (see Table 6.2). In each section we describe a specific evolutionary path (marked as *Evolutionary path*), we compare the simulated populations from each code (marked as *Population*) and investigate where differences between the populations come from (marked as *Population* and *Effects*).

6.5.2.1 Channel I: detached evolution

Evolutionary path Channel I involves non-interacting binaries. An example of a system was given for channel 1 in Sect. 6.5.1.1: a $5M_{\odot}$ and $4M_{\odot}$ star in a circular orbit of 10^4R_{\odot} . When the first WD is born, the orbit has increased to $[1.8, 1.8, 1.8, 1.8] \cdot 10^4R_{\odot}$. When the second WD is born, the orbit has increased even more to $[4.9, 5.0, 4.9, 4.9] \cdot 10^4R_{\odot}$ with primary and secondary masses of $[1.0, 0.94, 1.0, 1.0]M_{\odot}$ and $[0.87, 0.86, 0.87, 0.87]M_{\odot}$ respectively.

Population There is a good agreement between the codes on the separations and masses of non-interacting DWDs, initially and at DWD formation. In the full mass range, initial separations are $a_{\text{zams}} \approx (0.5 - 10) \cdot 10^3R_{\odot}$. The codes `binary_c`, `SeBa`, and `StarTrack` find non-interacting DWDs in wide orbits of $a_{\text{dwd}} \approx (0.1 - 5.4) \cdot 10^4R_{\odot}$ and with WD masses between $0.5-1.4M_{\odot}$. In the intermediate mass range, the initial separations are

$a_{\text{zams}} \gtrsim 1.5 \cdot 10^3 R_{\odot}$ for binary_c, SeBa and StarTrack. Both WD masses are $\gtrsim 0.75 M_{\odot}$ and orbits are wide with separations $a_{\text{dwd}} \approx (0.6 - 5.4) \cdot 10^4 R_{\odot}$ for binary_c, SeBa and StarTrack. For the Brussels code, the separations are slightly higher; initially $a_{\text{zams}} \gtrsim 2.8 \cdot 10^3 R_{\odot}$ and at dwd formation $a_{\text{dwd}} \approx (1.3 - 7.2) \cdot 10^4 R_{\odot}$. Furthermore for the Brussels code both WD masses extend to slightly lower values of $\gtrsim 0.65 M_{\odot}$. Small differences between the populations are due to different MiMf-relations and different descriptions for single stars (e.g. stellar radii), as for SWDs from channel 1. The birthrates in channel I are very similar in the full mass range as well as in the intermediate mass range (see Table 6.2).

6.5.2.2 Channel II: CE + CE

Evolutionary path The classical formation channel for close DWDs involves two CE-phases. First the primary star evolves into a WD via a phase of unstable mass transfer, i.e. via the evolutionary path described in Sect. 6.5.1.2 and 6.5.1.4 as channel 2 or 4 respectively. Subsequently the secondary initiates a CE-phase. It should be noted that for binary_c, SeBa and StarTrack this channel includes, systems that evolve through one CE-phase in which both stars lose their (hydrogen) envelope, the so-called double common envelope phase described in Sect. 6.2 and in eq. 6.9. Note that in the Brussels code, the double CE phase is not considered.

Population In the full mass range there is a good agreement between the progenitors according to the binary_c and SeBa code and a fair agreement with the StarTrack code. These three codes find that primaries of $M_{1,\text{zams}} \approx 1 - 8 M_{\odot}$ contribute to this channel. For the majority the primaries have initial separations of $a_{\text{zams}} \approx (0.1 - 2.5) \cdot 10^3 R_{\odot}$. The DWD populations as predicted by binary_c and SeBa are similar, and comparable with the population of StarTrack. WD masses range from $0.35 M_{\odot}$ to $1.4 M_{\odot}$ for primaries and from $0.19 M_{\odot}$ to $0.9 M_{\odot}$ for secondaries for binary_c and SeBa. For StarTrack the ranges are slightly larger; $0.2 - 1.4 M_{\odot}$ for primaries and $0.1 - 0.8 M_{\odot}$ for secondaries. The orbital separation of DWDs from channel II is between a few tenths of solar radii to a few solar radii, however, the specific ranges of the three codes differ. The birthrates in channel II are similar between the three codes (see Table 6.2). In the intermediate mass range the codes agree that primaries and secondaries with initial mass between about 3 to $8 M_{\odot}$ can contribute to channel II. In the Brussels code the mass range is slightly extended to higher masses of $10 M_{\odot}$ for primaries due to the MiMwd-relation. There is an agreement on the initial separation of the majority of system, although the range of separations differs between the codes. For binary_c and SeBa $a_{\text{zams}} \approx (0.7 - 2.5) \cdot 10^3 R_{\odot}$, however, the range for StarTrack is extended to lower values of $a_{\text{zams}} \approx (0.4 - 20) \cdot 10^2 R_{\odot}$ as noted above. Comparing with the Brussels code, the range is extended to lower as well as higher values ($(0.3 - 3.2) \cdot 10^3 R_{\odot}$). The higher maximum initial separation depends on the maximum radius in the single star prescriptions as discussed in channel 1. The difference in the lower minimum initial separation for the Brussels code has been noted

for the SWDs in channel 2 as well. The Brussels code assumes that the primaries in these systems become WDs without a second interaction, where as in `binary_c`, `SeBa` and `StarTrack` these systems merge in the second interaction of the primary star. The separations of DWDs are centred around $0.5R_{\odot}$, however, the distribution of separations is different between the codes: $0.17\text{-}10R_{\odot}$ for `binary_c`, $0.06\text{-}1.18R_{\odot}$ for the Brussels code, $0.14\text{-}3.6R_{\odot}$ for `SeBa` and $0.05\text{-}11R_{\odot}$ for `StarTrack`. Primary WD masses are comparable between the codes, $[0.8\text{-}1.4, 0.5\text{-}1.3, 0.7\text{-}1.4, 0.7\text{-}1.4]M_{\odot}$ where the ranges are the largest for the Brussels code. The maximum WD mass in the Brussels code is lower compared to the other codes due to the MiMwd-relation, see channel 1. The secondary WD masses at a given primary WD mass are lower in `binary_c`, `SeBa` and `StarTrack` ($\lesssim 0.9M_{\odot}$) compared to the Brussels code ($\lesssim 1.3M_{\odot}$).

Effects Several effects influence the distribution of separations in Fig. 6.25. Even though the codes agree that the majority of DWDs from channel II have separation around $0.5R_{\odot}$, the spread around this value varies between the codes. In the full mass range the maximum separation is $8R_{\odot}$ in the `SeBa` data, $22R_{\odot}$ in the `StarTrack` data and $31R_{\odot}$ for `binary_c`. In the intermediate mass range it is $1R_{\odot}$ for the Brussels results, $4R_{\odot}$ in the `SeBa` data, $10R_{\odot}$ for `binary_c` and $11R_{\odot}$ in the `StarTrack` data. The maximum separation is affected by the MiMwd-relation and winds. As seen in channel 2, the maximum orbital separation in the Brussels code is lower as winds are not taken into account and more mass is removed during the CE. The distribution of orbital separation in the Brussels data is also affected in a different way than in the others codes as this code assumes that AGB donors become WDs directly without a second phase of interaction (see also channel 2). In `binary_c`, `SeBa` and `StarTrack` AGB donors can become helium stars, that fill their Roche lobes for a second time, resulting in lower average masses. This effect can be seen in Fig. 6.27 where the secondary mass in `binary_c`, `SeBa` and `StarTrack` is $\lesssim 0.9M_{\odot}$ where as it is extended to $\lesssim 1.3M_{\odot}$ in the Brussels data. Mass loss in combination with the stability criteria, as also discussed for channel 2 causes high separations in the `binary_c` data. However, the relatively high maximum separations found by the `StarTrack` code is not affected much by the difference in the MiMwd-relation and winds, but are affected by differences in the double CE-formalism (see below).

All codes find that initially many DWD systems have high mass ratios, that in `binary_c`, `SeBa` and `StarTrack` lead to a double CE-phase. As discussed for channel 2, there is a difference in the formalism of the double-CE phase between `StarTrack` on one hand, and `binary_c` and `SeBa` on the other hand. As a result the separation after the double CE-phase is smaller according to the latter two codes, and a merger is more likely to happen. The birthrate of systems in the full (intermediate) mass range that evolve through a double CE is $7.2 \cdot 10^{-4} \text{ yr}^{-1}$ ($7.9 \cdot 10^{-5} \text{ yr}^{-1}$) according to `StarTrack`, while the birthrate is $4.6 \cdot 10^{-5} \text{ yr}^{-1}$ ($2.5 \cdot 10^{-5} \text{ yr}^{-1}$) and $1.1 \cdot 10^{-4} \text{ yr}^{-1}$ ($3.2 \cdot 10^{-5} \text{ yr}^{-1}$) for `binary_c` and `SeBa` respectively. An example of systems that merge according to `binary_c` and `SeBa`, but form a DWD according to `StarTrack` are the systems at $a_{zams} \lesssim 120R_{\odot}$ in Fig. 6.28 which lie at

$a_{\text{dwd}} \approx 0.07 - 1.2R_{\odot}$ for $M_{1,\text{dwd}} \lesssim 0.35M_{\odot}$ in Fig. 6.24. An example of systems that survive according to all codes, however, at smaller separations for `binary_c` and `SeBa` compared to `StarTrack`, are systems with $M_{1,\text{dwd}} \gtrsim 0.7M_{\odot}$ and $a_{\text{dwd}} \approx 4 - 10R_{\odot}$ for `StarTrack` and $a_{\text{dwd}} \lesssim 2R_{\odot}$ for `binary_c` and `SeBa`.

An effect that plays a role in channel II concerns the survival of a system during the mass-transfer event. As explained for channel 2, BPS codes compare the radius of the stripped star (i.e. exposed cores) to the corresponding Roche lobe to determine whether or not a merger takes place during the CE event. For donor stars that become WDs directly after mass transfer ceases, i.e. without a hydrogen-poor helium burning phase, the `Brussels` and `StarTrack` code assume a zero-temperature WD where as `binary_c` and `SeBa` assume the exposed core is expanded due to previous nuclear shell burning. The effect of this is that the radius of the stripped star is a factor of about 5 smaller in the `Brussels` and `StarTrack` code than in `binary_c` and `SeBa`. Therefore a merger is less likely to take place. Therefore the minimum separation in the intermediate mass range is 0.06 and $0.05R_{\odot}$ in the `Brussels` code and the `StarTrack` code, respectively. While the minimum separation is about $0.15R_{\odot}$ in `binary_c` and `SeBa`.

6.5.2.3 Channel III: stable + CE

Evolutionary path In channel III, the primary initiates stable mass transfer (alike channel 3 or 5 which are described in Sect. 6.5.1.3 and 6.5.1.5). When the secondary fills its Roche lobe mass transfer is unstable⁵.

Population There is an agreement between the codes about the main parameter space occupied by the DWDs from channel III and their progenitors, however, the codes do not agree completely. The causes for differences in channel III have been discussed previously in the context of SWDs (see the discussion on channel 3 and 5), but they lead to more pronounced differences in the DWD population than in the SWD population.

In the intermediate mass range, the `binary_c`, `Brussels` and `SeBa` code agree on the orbital characteristics of the main progenitors. The initial masses are $M_{1,\text{zams}} \approx 4 - 9M_{\odot}$ and the initial separations $a_{\text{zams}} \approx (0.2 - 2) \cdot 10^2R_{\odot}$. There is also a rough agreement between these codes on the range of masses of both WDs. For primaries `binary_c` and `SeBa` find $M_{1,\text{dwd}} \gtrsim 0.65M_{\odot}$ and the `Brussels` code $M_{1,\text{dwd}} \gtrsim 0.45M_{\odot}$ due to differences in the `MiMwd`-relation. For secondaries these three codes find $M_{2,\text{dwd}} \gtrsim 0.7M_{\odot}$. The maximum mass of

⁵Note that there are two variations of this evolutionary path that are not included in this channel and Fig. 6.24 to 6.29. First, systems in which the secondary becomes a WD before the primary are excluded in this channel. The birthrates of this evolutionary path are low ($[8.6, -, 27, 5.1] \cdot 10^{-5} \text{yr}^{-1}$ in the full mass range. See also the discussion and footnote for channel 3 in Sect. 6.5.1.3 on this evolutionary path. Secondly, for systems with AGB donors that have suffered severe wind mass loss such that the mass ratio has reversed, the first phase of mass transfer can become stable as well. However, consequently the orbit widens to separations comparable to the separations of Channel I such that the secondary will not fill its Roche lobe. The birthrates of this evolutionary path are low as well ($[9.4, -, 6.6, 5.3] \cdot 10^{-4} \text{yr}^{-1}$ in the full mass range).

the primary and secondary white dwarfs varies between 1.2 and $1.4M_{\odot}$. The birthrates are high (a few times 10^{-4} yr^{-1}) in this channel according to `binary_c`, the Brussels code and `SeBa`, however, the birthrate is a factor 1000 lower according to `StarTrack`. In the `StarTrack` simulation there are only two systems in channel III in the intermediate mass range, and therefore we refrain from showing contours for this channel for the `StarTrack` data in Fig. 6.25, 6.27 and 6.29. Figure 6.29 shows an increase of progenitor systems at separations $a_{\text{zams}} \lesssim 20R_{\odot}$ and primary masses $M_{1,\text{zams}} \approx 3 - 5.5M_{\odot}$ in the Brussels simulation compared to those from the other codes. The effect carries through into the DWD population as the increase of systems in the data from the Brussels code with WD primary masses between $0.45-0.7M_{\odot}$. The orbital separation of DWDs in channel III is very similar between `binary_c` and `SeBa`, $a_{\text{dwd}} \approx 0.1 - 1.1R_{\odot}$, however, for the Brussels code $a_{\text{dwd}} \approx 0.3 - 20R_{\odot}$. The existence of wide systems in the Brussels code is not surprising, as this code also finds the widest SWDs from channel 3 in comparison with `binary_c` and `SeBa`. As discussed previously in Sect. 6.5.1.3, this is related to differences in the MiMwd-relation and angular momentum loss from winds. The gap at $M_{1,\text{dwd}} \approx 0.7 - 0.9M_{\odot}$ in Fig. 6.27 in the data from the Brussels code, is caused by the boundary between channel 3a and 3b, as in Fig. 6.20 (see also Sect. 6.5.1.3).

Regarding the populations of progenitors for low mass primaries, `binary_c`, `SeBa` and `StarTrack` agree reasonably well. They both show that most DWDs in channel III have initial separations of $5-20R_{\odot}$. However, the range of initial separations is extended to $25R_{\odot}$ in the population simulated by `SeBa`. `SeBa` and `StarTrack` also show an extra population compared to `binary_c` ($a_{\text{zams}} \approx 140 - 270R_{\odot}$ and $M_{1,\text{zams}} \lesssim 1.2M_{\odot}$). These two differences are due to differences in the stability of mass transfer for donors with shallow convective envelopes, as discussed for channel 3. Comparing the population of DWDs itself for low mass primaries, `binary_c`, `SeBa` and `StarTrack` agree well. The codes show a population of DWDs with primary mass $M_{1,\text{dwd}} \approx 0.2-0.44M_{\odot}$ at a separation of $a_{\text{dwd}} \approx 0.1-1.5R_{\odot}$, with secondary masses $M_{2,\text{dwd}}$ around $0.6M_{\odot}$. The extra population in the `SeBa` and `StarTrack` data lies at $a_{\text{dwd}} \approx 10 - 50R_{\odot}$ and $M_{1,\text{dwd}} \approx 0.4 - 0.47M_{\odot}$. The three codes show systems at $M_{2,\text{dwd}}$ about $0.3M_{\odot}$, where in the `binary_c` data this group is extended to higher primary WD masses of $M_{1,\text{dwd}} \approx 0.2 - 0.7M_{\odot}$ in Fig. 6.26. These systems in `binary_c` mainly evolve through a specific evolutionary path in which there is a phase of stable mass transfer between a He-MS and a WD, a so-called AM CVn-system. The birthrate of these systems is $5.0 \cdot 10^{-4} \text{ yr}^{-1}$ according to `binary_c` and negligible according to the other codes.

Effects The extremely low birthrate of `StarTrack` in the intermediate range is caused by a combination of effects discussed previously. Firstly, stable mass transfer is more readily realised in the other codes compared to `StarTrack` (see channel 3). Only systems with $q_{\text{zams}} \gtrsim 0.6$ undergo stable mass transfer and become SWD systems according to `StarTrack`. For about 60% of these systems, the secondary becomes massive enough to collapse to a neutron star after nuclear burning ceases (in accordance with the other codes). Secondly, the remaining systems merge when the secondary star fills its Roche lobe. For AGB donors

this is more likely to happen in the StarTrack data, because of the difference in the radii of stripped stars compared to binary_c and SeBa (see channel 2b).

The different methods of calculating mass transfer between the Brussels code and the other codes, cause an increase in systems in the data from the Brussels code, similar to channel 5. In particular for DWDs, it is important how the secondary responds to mass gain. The systems that survive in the Brussels code have $q_{\text{zams}} > 0.85$, such that the orbit widens severely due to the mass transfer. However, according to binary_c and SeBa, when the secondary accretes a significant amount of mass and is rejuvenated, its evolutionary timescale is reduced. As the secondary evolves, the system comes in contact and merges. The Brussels code assumes that the merger can be avoided for phases of shallow contact.

The evolution of and mass transfer rates from evolved helium stars donors (see channel 3) are important for channel III. It affects the DWD systems with high masses of the primary progenitor and primary WD, see Fig. 6.27 and 6.29. The range of primary WD masses is extended to $1.2M_{\odot}$ according to SeBa, and $1.3M_{\odot}$ according to the Brussels code and $1.4M_{\odot}$ according to binary_c. Contrary to stable mass transfer from hydrogen rich donors, the core of evolved helium stars can grow significantly during stable mass transfer phases as the timescale for mass transfer can become comparable to the timescale of wind mass loss or nuclear evolution. If the mass transfer phase is relatively short, the core of the donor star does not have time to grow significantly and little mass is lost in the wind. With the assumption of conservative mass transfer, most of the envelope is then transferred to the secondary star which then is more likely to become a neutron star instead of a WD.

Differences in the radii of stripped stars causes a relative lack of close systems for the Brussels code compared to the other codes. For channel II this was discussed in the context of donor stars that become a WD directly. However, in channel III in the intermediate mass range many donor stars continue burning helium after the mass transfer event ceases. The radius of the stripped donor star depends on its mass, and for binary_c, SeBa and StarTrack also on the evolutionary state of the donor stars (see also channel 2). When the donor star is stripped of its envelope before the AGB-phase, the core radius is a factor of about 4-5 larger in the Brussels code compared to binary_c, SeBa and StarTrack. Therefore a merger is more likely to take place in the Brussels code.

6.5.2.4 Channel IV: CE + stable

Evolutionary path In the final evolutionary channel for DWDs, when the primary fills its Roche lobe, mass transfer proceeds in an unstable manner (according to channel 2 or 4 which are described in Sect. 6.5.1.2 and 6.5.1.4). However, when the secondary fills its Roche lobe mass transfer mass to the primary is stable. As a result the primary accretes mass.

Population The systems of channel IV lie in a small and specific region of DWD parameter space (see Fig. 6.24 and 6.26). The birthrates are low, $1.6 \cdot 10^{-4} \text{ yr}^{-1}$ and $5.5 \cdot 10^{-5} \text{ yr}^{-1}$

for `binary_c` and `SeBa` respectively in the full mass range. We do not compare the population of this channel with the Brussels code as the progenitors according to `binary_c` and `SeBa` are low mass binaries and the birthrate in the Brussels code is zero per definition (see also Sect. 6.4.1). We cannot compare the characteristics of the population of `binary_c` and `SeBa` with that of the `StarTrack` code as in the simulations of the latter code there are no systems evolving through channel IV indicating a birthrate of $< 4 \times 10^{-7} \text{ yr}^{-1}$. The birthrate is low according to `StarTrack` as unstable mass transfer is more readily realised in this code compared to `binary_c` and `SeBa` (see also channel 3). The `binary_c` and `SeBa` code agree well on the binary parameters of the population of DWDs at DWD formation from this channel: separations of $10\text{-}30R_{\odot}$ and primary WD masses of $1.1\text{-}1.4M_{\odot}$, and secondary WD masses of $0.15\text{-}0.20M_{\odot}$. The progenitors systems in this channel are similar, $M_{1,\text{zams}} \approx 1 - 3M_{\odot}$ and $a_{\text{zams}} \approx 50 - 400R_{\odot}$. Differences in the population of DWD systems from this channel, their progenitors and the birthrates occur due to the uncertainty in the stability of mass transfer and the mass transfer rate (see also the discussion for channel 3). Note that in the current study we have assumed conservative mass transfer to all accretors, including WDs. This is not a physical picture, so a warning of caution needs to be given to trust the parameters of this population, nonetheless the similarities between the `binary_c` and `SeBa` codes are striking.

6.6 Summary of critical assumptions in BPS studies

In the previous section we compared simulations from four different BPS codes and investigated the causes for the differences. The causes are not due to numerical effects, but are inherent to the codes and the underlying physical principles of the differences are listed below and discussed. The implementations of these principles in each code are described in Appendix 6.A.

- Initial-WD mass-relation;

For single stars or non-interacting stars, the initial-final mass relation for WDs (see Fig. 6.8) is determined by the trade off between the growth of the core and how much mass is lost in stellar winds and the planetary nebula phase. The amount of mass a low or intermediate mass star loses in a stellar wind is small on the MS, but significant in later stages of its evolution.

The WD mass of primary stars is further affected by the mass transfer event, the moment and the timescale of the removal of the envelope mass. If the primary star becomes a hydrogen-poor helium burning star before turning into WD, the MiMwd-relation is influenced by helium star evolution. Of particular importance are the core mass growth versus the mass loss from helium stars and a possible second phase of mass transfer. A related issue, of particular importance for supernova Type Ia rates,

6.6 SUMMARY OF CRITICAL ASSUMPTIONS IN BPS STUDIES

concerns the composition of WDs; what is the range of initial masses for carbon-oxygen WDs or other types of WDs?

The amount of mass that is lost in the wind and in the planetary nebula influences the orbit directly, and indirectly through angular momentum loss. Questions remain about how much mass is lost in the wind of stars, and how much angular momentum is lost with the wind.

- The stability of mass transfer;

For which systems does mass transfer occur in a stable manner and for which systems is it unstable? As binary population synthesis codes do not solve the stellar structure equations, and cannot model stars that are not in hydrostatic or thermal equilibrium, BPS codes rely on parametrisations or interpolations to determine the stability of mass transfer. Theoretical stability criteria for polytropes exist [Hjellming & Webbink, 1987], but are lacking for most real stars [but see de Mink et al., 2007; Ge et al., 2010, 2013, for MS stars].

The critical mass ratio for stable mass transfer with hydrogen shell-burning donors differs between the codes from $q \gtrsim 0.2$ in the Brussels code to $q \gtrsim 0.6$ in StarTrack. A difference for low mass stars between binary_c, SeBa and StarTrack arises from the uncertainty of the mass transfer stability of donors with shallow convective envelopes. In a recent paper, Woods et al. [2012] show that mass transfer between a hydrogen shell-burning donor ($M_{1,zams} = 1 - 1.3M_{\odot}$) and a main-sequence star can be stable when non-conservative. The effect on the orbit is a modest widening.

- Survival of mass transfer;

For which systems does mass transfer lead to a merger and which system survive the mass transfer phase, in particular when mass transfer is unstable? As for the stability of mass transfer, the inability of BPS codes to model stars that are not in hydrostatic and thermal equilibrium, makes BPS codes rely on additional prescriptions, that are not (fully) available in literature. Regarding the survival of mass transfer, different assumptions for the properties (e.g. radii) of stripped stars lead to differences in the results of the four BPS codes, see e.g. channel II and III. For donor stars in which the removal of the envelope due to mass transfer leads to an end in nuclear (shell) burning and a WD is formed directly, it is unclear how much the core is bloated just after mass transfer ceases compared to a zero-temperature WD [Hurley et al., 2000]. For donor stars that are stripped of their hydrogen envelopes due to mass transfer, but helium burning continues, it is unclear how fast the transition takes place from an exposed core to an (evolved) helium star (see channel 2b).

- Stable mass transfer;

Modelling of the stable mass transfer phase in great detail is not possible in BPS codes, as for the stability of mass transfer. Therefore BPS codes rely on simplified methods

to simulate stable mass transfer events. In this project, the different approaches to model the event do not lead to large differences in the synthetic stellar populations, however, differences do exist most strongly for channel 3b and 5.

The evolution of the mass transfer rate during the mass transfer phase can have a strong effect on the resulting binary. However, in the current set-up of this project that assumes conservative mass transfer, the importance is greatly reduced. The mass transfer rates are only important when the timescale of other effects (e.g. wind mass loss or nuclear evolution) become comparable to the mass transfer timescale, as in channel 3b.

An effect of the approach to model stable mass transfer phases is that mergers are less likely to happen in the Brussels code compared to the other codes. The approach of `binary_c`, `SeBa` and `StarTrack` is to follow the mass transfer phase in time, with approximations of the mass transfer rate. In the Brussels code, the mass transfer phases are not followed in detail. Instead it only considers the initial and final situation from interpolations of a grid of detailed calculations. Regarding channel 5 mass transfer, it is important to better understand which contact systems lead to a merger and which not. From observations, many Algol systems are found which have undergone and survived a phase of shallow contact.

- The evolution of helium stars;
A large fraction of interacting systems go through a phase in which one of the stars is a helium star, for SWDs roughly 15% in the full mass range and roughly 50% in the intermediate mass range. Not much is known about these objects about e.g. the stellar evolution, winds or mass transfer stability. Also the mass transfer rate is important, in particular for evolved helium stars whose evolutionary and wind loss timescales can become comparable to the mass transfer timescales. Therefore small differences in the mass transfer rate can lead to large differences in the resulting WD. This is especially important for massive WDs, e.g. SNIa rates.

The assumptions that were equalised for this project will lead to a larger diversity in the simulated populations as different codes make different assumptions (see Appendix 6.B) and these should be taken into account when interpreting BPS results. The influence of the parameters that were equalised has not been studied here, not qualitatively nor quantitatively. The assumptions are:

- The CE-prescription and efficiency;
- Accretion efficiency during stable mass transfer;
- Angular momentum loss;
- Tidal effects;

- Magnetic braking;
- Wind accretion;
- The initial distribution of primary mass, mass ratio and orbital separation.

Despite the significance of these phenomena to binary evolution and the enormous effort of the community, all efforts so far have not been successful in understanding them. Several prescriptions exist for the first six phenomena and the effect on the evolution of the binary can be severely different. For example regarding the CE-phase, it is unclear how efficient orbital energy can be used to expel the envelope and if other sources of energy can be used, such as recombination, rotational, tidal or magnetic energy [Iben & Livio, 1993; Han et al., 1995; Politano & Weiler, 2007; Webbink, 2008; Zorotovic et al., 2010; De Marco et al., 2011; Zorotovic et al., 2011a; Davis et al., 2012; Ivanova et al., 2013]. Also, predictions for the efficiency of mass accretion onto WDs vary strongly and the SNIa rate is severely affected by this uncertainty [Bours et al., 2013]. Furthermore, the adopted mode of angular momentum loss has a strong effect on the evolution of the orbit (see Fig. 6.1 and Sect. 6.2.1.1). It is also not clear how the different prescriptions for tidal evolution affect the populations. However, in Sect. 6.5.1.3 we found that spin-orbit coupling (assuming orbits are continuously synchronised), only has a small effect on the final separation of the SWD systems. The effect of different initial distributions [see e.g. Duquennoy & Mayor, 1991; Kouwenhoven et al., 2007] of binary parameters can be severe with respect to the importance of a certain evolutionary channel, e.g. birthrates, number density or events per solar mass of created stars [see e.g. Eggleton et al., 1989; de Kool & Ritter, 1993; Davis et al., 2010, Claeys et al. in prep.]. Furthermore, the importance of a certain channel is affected by the boundaries of the distribution through the normalisation of the simulation. In Appendix 6.B.7 we show that for the typical assumptions of the four codes this effect can be a factor 0.5-2 on the birthrates. The typical assumptions for each code for all equalised parameters are described in Appendix 6.B.

6.7 Conclusion

In this paper we studied and compared four binary population synthesis codes. The codes involved are the `binary_c` code [Izzard et al., 2004, 2006, 2009, Claeys et al. in prep.], the Brussels code [De Donder & Vanbeveren, 2004; Mennekens et al., 2010, 2012], SeBa [Portegies Zwart & Verbunt, 1996; Nelemans et al., 2001c; Toonen et al., 2012] and StarTrack [Belczynski et al., 2002b, 2008a; Ruiters et al., 2009b; Belczynski et al., 2010a]. We focused on low and intermediate mass binaries that evolve into single white dwarf systems (containing a WD and a non-degenerate companion) and double white dwarf systems. These populations are interesting for e.g. post-common envelope binaries, cataclysmic variables, single degenerate as well as double degenerate supernova Type Ia progenitors. For this

project input assumptions in the BPS codes were equalised as far as the codes permit. This was done to simplify the complex problem of comparing BPS codes that are based on many (often different) assumptions. In this manner inherent differences between and numerical effects within the codes were investigated.

Regarding the single white dwarf population, we identified five evolutionary paths. There is a general agreement on what initial parameters of $M_{1,zams}$, $M_{2,zams}$ and a_{zams} lead to SWD binaries through each formation channel. When the SWD system is formed, there is an agreement on the orbital separation range for those systems having undergone stable or unstable mass transfer. Furthermore there is a general agreement on the stellar masses after a phase of stable or unstable mass transfer.

Regarding the double white dwarf population, similar evolutionary paths can be identified in the various codes. There is an agreement on which primordial binaries lead to DWD systems through stable and unstable mass transfer respectively, and a rough agreement on the characteristics ($M_{1,dwd}$, $M_{2,dwd}$ and a_{dwd}) of the DWD population itself. Double white dwarfs go through more phases of evolution than single degenerate systems. The uncertainty in their evolution builds up through each mass transfer phase. The white dwarfs are formed with comparable masses, but at different separations.

We found that differences between the simulated populations arise not due to numerical differences, but due to different inherent assumptions. The most important ones that lead to differences are the MiMf-relations (of single stars), the MiMwd-relation (of binary stars), the stability of mass transfer, the mass transfer rate and in particular helium star evolution. Different assumptions between the codes are made for these topics as theory is poorly understood and sometimes poorly studied. Therefore we suggest further research into these topics e.g. with a detailed (binary) stellar evolution code to eliminate the differences between BPS codes.

In addition some assumptions were equalised for the comparison that affect the results of the comparison. These are the initial binary distributions, the common envelope prescription and efficiency, the accretion efficiency, angular momentum loss during RLOF, tidal effects, magnetic braking and wind accretion. We leave the study of their effects on stellar populations for another paper.

In Sect. 6.3 a short description is given of each code. In Appendix 6.A and 6.B, a more detailed overview is given of the typical assumptions of each code outside the current project. These should be taken into account when interpreting results from the BPS codes. Furthermore, we recommend using these sections as a guideline when deciding which code or results to use for which project. Finally we would like to encourage other groups involved in BPS simulations, to do the same test as described in this paper and compare the results with the figures given in this paper. More detailed figures are available on request.

Concluding, we found that when the input assumptions are equalised as far as possible within the codes, we find very similar populations and birthrates. Differences are caused by different assumptions for the physics of binary evolution, not by numerical effects. So

although the four BPS codes use very different ways to simulate the evolution of these systems, the codes give similar results and are adequate.

Acknowledgements

The authors would like to thank G. Nelemans, M. van der Sluys, O. Pols, D. Vanbeveren, W. van Rensbergen, & R. Voss for very helpful discussions on this project. ST thanks S. Portegies Zwart, JSWC thanks R.G. Izzard and AJR thanks I. Seitenzahl and K. Belczynski for thoughtful comments and general discussion. The authors are very grateful to those involved in the Lorentz Center workshops “Stellar mergers” (2009) and “Observational signatures of Type Ia supernova progenitors” (2010), who provided the inspiration to carry out this long-awaited work. Furthermore the authors are grateful for the contributions to an early version of this project in 2002-2003 from K. Belczynski, C. Fryer, J. Hurley, V. Kalogera, G. Nelemans, S. Portegies Zwart and C. Tout, and in 2009-2010 from A. Bogomazov, P. Kiel, B. Wang and L. Yungelson. The work of ST and JSWC was supported by the Netherlands Research School for Astronomy (NOVA).

6.A Backbones of the BPS codes

The structure of BPS codes can vary strongly, which complicates the process of comparing BPS codes. Some aspects of the code are relatively simple to adapt in order to let assumptions of different groups converge, where as other aspects are inherent to the code and are not straightforward to change. For example, where some codes use results from detailed single star evolution codes, written down in analytical formulae [e.g. Eggleton et al., 1989; Hurley et al., 2000] to compute stellar parameters, others use the results of detailed binary evolution codes – a grid over which one can interpolate – and those results are integrated into the population code [e.g. De Donder & Vanbeveren, 2004]. The inherent differences will create differences between the results of the different groups. The main differences are summarised in Table 6.4 and a more complete overview is given below. For most of the points the influence on a population it not immediately clear, therefore their effects are discussed in Sect. 6.6.

TABLE 6.4: Numerical treatments in the different codes which are inherent to them. (Further explanation can be found in Sect. 6.A)

	binary_c	Brussels code	SeBa	StarTrack
Single star prescriptions	HPT00	VB98	HPT00	HPT00
Stability of RLOF	q_{crit}	$R_{\text{conv}}, q_{\text{crit}}$	ζ	$\zeta, q_{\text{ddi}}^{(1)}$
Mass transfer rate	$R_{\text{d}}/R_{\text{RL}}^{(2)}$	$R_{\text{d}}/R_{\text{RL}}^{(2)}$	$\zeta \rightarrow \frac{M}{\tau_*}^{(3)}$	$\zeta \rightarrow \frac{M}{\tau_*}^{(3)}$
Wind (AGB)	R75, VW93, HPT00	HG97	R75, VW93, HPT00	R75, VW93, HPT00
AML (wind)	Donor (HTP02)	No	Donor	Donor
Helium star evolution	Yes	Not explicit	Yes	Yes
Population synthesis	Grid based	Grid based	Monte Carlo	Monte Carlo

NOTES: References in the table: HPT = Hurley et al. [2000], VB98 = Vanbeveren et al. (1998), R75 = Reimers [1975], VW93 = Vassiliadis & Wood [1993], HG97 = van den Hoek & Groenewegen [1997], HTP02 = Hurley et al. [2002].

(1) Mass ratio threshold for delayed dynamical instability [Hjellming & Webbink, 1987], dependent on evolutionary state of the donor.

(2) R_{RL} is the Roche radius of the donor star.

(3) τ_* = Characteristic timescale of mass transfer. Can be nuclear, Kelvin-Helmholtz, timescale of magnetic braking or of gravitational wave radiation.

6.A.1 Single star prescriptions

The single star prescriptions, either given by analytical formulae or included in a grid of binary systems over which can be interpolated, determine which mass the WD will have when the star loses its envelope. Furthermore they determine the radii during the evolution of the star and therefore the moment at which the star fills its Roche lobe.

- *binary_c*, *SeBa*, *StarTrack*: the codes use analytical fitting formulae [Hurley et al., 2000] from detailed single star evolution tracks. These tracks are based on an overshooting constant $\delta_{\text{ov}} = 0.12$ [based on Pols et al., 1998]. In *binary_c* different AGB models can be used, based on detailed models of Karakas et al. [2002] for thermally pulsating AGB stars (TP-AGB). However, these are not used for this work. Prior to the work of Toonen et al. [2012], the single star prescriptions in *SeBa* were based on Eggleton et al. [1989].
- *Brussels code*: intermediate mass single star prescriptions are taken from Schaller et al. [1992]. These tracks include convective overshooting by means of the following prescription: the overshooting distance d_{over} is directly proportional to the pressure scale height H_p according to $d_{\text{over}} = 0.2H_p$. This corresponds to a slightly lower degree of overshooting than in the codes that use the overshooting constant $\delta_{\text{ov}} = 0.12$ in the stability criteria, the latter corresponding to a d_{over}/H_p between 0.22 and 0.4 depending on mass [see Hurley et al., 2000]. Stellar parameters which do not depend on whether the star is part of an interacting binary system are taken directly from this reference. Other stellar parameters, such as the remnant mass after RLOF, are taken from the detailed binary evolution code.

6.A.2 Stability of mass transfer

At the moment that one of the stars fills its Roche lobe mass transfer can proceed in a stable manner or the system can evolve into a CE-phase (see Sect. 6.2.1). In the simulation of the evolution of a binary system the entire stellar structure is not explicitly followed in detail, and consequently, ‘stability checks’ must be built-in to BPS codes to determine if RLOF will lead to a CE-phase.

- *binary_c*: for every type of donor star and type of accretor star a critical mass ratio (q_{crit}) is given. The mass ratio of the system during mass transfer is compared with the critical mass ratio for stable mass transfer and determines if mass transfer will proceed in a stable manner or not. An overview can be found in Claeys et al. (in prep.). Note that in that paper two possibilities are described for the stability of Roche lobe overflowing helium stars to non-degenerate accretors. For this project the criterion as described in Hurley et al. [2002] is used.

- *Brussels code*: the boundary between stable and unstable RLOF is determined by whether the outer layers of the donor star are radiative or deeply convective respectively. For each stellar mass, the minimum stellar radius R_{conv} is given for which the envelope is convective. If the orbital period of the system under investigation is smaller than the theoretical orbital period at the time when $R_{\text{RL}} = R_{\text{conv}}$, mass transfer will proceed in a stable way.

If the mass ratio between the two stars is extreme ($q = M_a/M_d < 0.2 = q_{\text{crit}}$), an instability [Darwin, 1879] can take place in close binary systems through tidal interactions. The more massive star will be unable to extract sufficient angular momentum from the orbit to remain in synchronized rotation, resulting in a mass transfer episode that quickly becomes dynamically unstable. Tidal interaction will cause the secondary to spiral into the donor's outer layers, a process that is treated identically to the common envelope evolution (hence with $\beta = 0$).

- *SeBa*: the stability and rate of mass transfer are dependent on the reaction to mass change of the stellar radii and the corresponding Roche lobes. The change in the Roche radius R_{RL} due to loss and transfer of mass M is given by

$$\zeta_{\text{RL}} \equiv \frac{d \ln R_{\text{RL}}}{d \ln M}, \quad (6.14)$$

the adiabatic (i.e. immediate) response of the donor star's radius R is given by

$$\zeta_{\text{ad}} \equiv \frac{d \ln R}{d \ln M}. \quad (6.15)$$

For every Roche lobe filling system, ζ_{RL} and ζ_{ad} are compared at every timestep. If $\zeta_{\text{RL}} < \zeta_{\text{ad}}$ we assume mass transfer proceeds in a stable manner [e.g. Webbink, 1985; Pols & Marinus, 1994]. When $\zeta_{\text{RL}} > \zeta_{\text{ad}}$, mass transfer is dynamically unstable leading to a CE-phase.

The value of ζ_{RL} is calculated numerically by transferring a test mass of $10^{-5} M_{\odot}$. The advantage of this is that, because $\zeta_{\text{RL}} = \zeta_{\text{RL}}(M_d, M_a, a)$ and so ζ_{RL} is dependent on the mass accretion efficiency of the secondary, the (de)stabilising effect [see Soberman et al., 1997] of non-conservative stable mass transfer is taken into account automatically. Appropriate recipes of ζ_{ad} are implemented in the code for every type of donor star. An overview can be found in Toonen et al. [2012], appendix A3 therein. Furthermore, the orbital angular momentum is compared with the stellar spin angular momenta, to check whether a Darwin instability is encountered [Darwin, 1879].

- *StarTrack*: When a non-degenerate star fills its Roche lobe, ζ_{ad} and ζ_{RL} are calculated, similar to the case of SeBa. The value of ζ_{ad} is determined by removing mass from the star over a 1-year timestep [Belczynski et al., 2008a]. The value of ζ_{RL} is determined by transferring a small amount (1%) of the star's mass toward the companion. In

cases where the mass loss is so rapid such that the star loses thermal equilibrium, a ‘diagnostic diagram’ is used to predict the stability of mass transfer [see description in Belczynski et al., 2008a, sect. 5.2]. The diagnostic diagram is a numerical tool that was first calibrated using detailed stellar evolution calculations of massive stars, and is currently being updated to include a range of stellar models for low- and intermediate-mass stars.

In addition, there is also a check for a possible delayed dynamical instability. This occurs for stars with $M_d/M_a > q_{\text{ddi}}$, with q_{ddi} based on Hjellming & Webbink [1987], or when a Darwin instability is encountered, or when the trapping radius of the accretion stream [King & Begelman, 1999] exceeds the Roche radius of the accreting star [see Ivanova et al., 2003; Belczynski et al., 2008a, sect. 5.4]. This latter point however, is not considered for this work.

6.A.3 Stable mass transfer

To take into account various driving mechanism of stable RLOF, such as thermal readjustment or nuclear evolution of the donor, approximate prescriptions are used to determine the mass transfer rate. Note that mass transfer rate refers to the mass lost by the donor, which will always be equal to or greater than the mass accretion rate, which refers to the mass gained by the companion.

- *binary_c*: the mass transfer rate is calculated as a function of the ratio of the stellar radius and the Roche radius [based on Whyte & Eggleton, 1980]. A function is generated which follows the radius more closely during mass transfer on a thermal timescale and more loosely when the star is in thermally equilibrium. A smooth transition is build-in between the two. The formulation can be found in Claeys et al. (in prep.). That paper also shows that the resulting mass transfer phases are comparable to that of the detailed binary stellar evolution code STARS [based on Eggleton, 1971] in the duration of the mass transfer phases and the mass transfer rates for a set of models. This method indirectly considers mass transfer on the nuclear and thermal timescale, but also on the timescale of gravitational wave radiation or magnetic braking are considered.
- *Brussels code*: the mass transfer rates are not explicitly calculated in the population code. It considers merely the initial and final masses. These are interpolated from the results of the detailed binary evolution code. The latter calculates the mass transfer rate during stable RLOF iteratively, by investigating how much mass needs to be lost during the current timestep for the donor star to remain confined by its Roche lobe (within the order of a few percent).
- *SeBa*: ζ_{RL} is compared with appropriate values of ζ_{eq} to determine if mass transfer is driven by the thermal readjustment or the nuclear evolution of the donor star. ζ_{eq}

represents the response of the donor star’s radius R as it adjusts to the new thermal equilibrium:

$$\zeta_{\text{eq}} = \left(\frac{d \ln R}{d \ln M} \right)_{\text{th}}. \quad (6.16)$$

Appropriate recipes of ζ_{eq} are implemented for every type of donor star. Mass transfer is driven by the nuclear evolution of the donor star if $\zeta_{\text{RL}} < \min(\zeta_{\text{ad}}, \zeta_{\text{eq}})$. In that case we assume mass transfer proceeds on the nuclear timescale of the donor star [e.g. Webbink, 1985; Pols & Marinus, 1994]. If $\zeta_{\text{eq}} < \zeta_{\text{RL}} < \zeta_{\text{ad}}$, RLOF is dynamically stable and driven by thermal readjustment of the donor, so that mass transfer proceeds on the thermal timescale of the donor star.

In addition, stable mass transfer can be driven by angular momentum loss from magnetic braking or gravitational wave emission. When the timescale of angular momentum loss is shorter than the mass loss timescale determined above, we assume mass transfer is driven by angular momentum loss. For more detail see Appendix A.3 of Toonen et al. [2012].

- *StarTrack*: For non-degenerate donors ζ_{RL} and ζ_{ad} are calculated, along with the thermal timescale τ_{KH} [based on Kalogera & Webbink, 1996]. Additionally, the equilibrium mass transfer timescale τ_{eq} is calculated as a combination of RLOF both driven by angular momentum loss and the nuclear evolution of the star and/or the changes due to magnetic braking and gravitational wave radiation [see Belczynski et al., 2008a]. If $\tau_{\text{eq}} > \tau_{\text{KH}}$ the mass losing star is in thermal equilibrium and mass transfer proceeds on $\dot{M}_{\text{eq}} = M/\tau_{\text{eq}}$. If $\tau_{\text{eq}} \leq \tau_{\text{KH}}$ mass transfer proceeds on a thermal timescale, given by $\dot{M}_{\text{KH}} = M/\tau_{\text{KH}}$. If \dot{M}_{eq} becomes positive the star falls out of equilibrium and the stability of mass transfer is determined by the *diagnostic diagram* [see Belczynski et al., 2008a]. In the case of WD donors, the mass transfer rate is always driven by gravitational radiation.

6.A.4 Wind mass loss

The driving mechanisms of the wind and the explicit rate at which this material is lost are not yet completely understood. This results in different prescriptions to describe the rate of wind mass loss and the amount that can be lost [e.g. Wachter et al., 2002]. We only discuss the wind-prescriptions that are relevant for low and intermediate mass stars.

- *binary_c*, *SeBa*, *StarTrack*: for stars up to the early AGB the prescription of Reimers [1975] is adopted (with $\eta = 0.5$). To describe the wind mass loss of stars on the TP-AGB a prescription based on Vassiliadis & Wood [1993] is implemented. Both prescriptions are defined in Hurley et al. [2000]. In *binary_c* and *StarTrack* different prescriptions for the wind mass loss are available that used by different users of the respective codes.

- *Brussels code*: For intermediate mass interacting binaries, the initial-final mass relation of WDs is determined by assuming the wind prescription of van den Hoek & Groenewegen [1997]. However, it should be noted that in the BPS code a star in an interacting binary does not have wind mass loss. For the most massive stars, wind mass loss is as is described in Vanbeveren et al. [1998].

6.A.5 Angular momentum loss from winds

Section 6.2.1.1 describes the importance of angular momentum loss (AML) and the effect on the orbit. Not only mass lost during RLOF, but also wind carries angular momentum, which is lost when it leaves the system. The same prescriptions as described in Sect. 6.2.1.1 can be applied to AML when material is lost through a wind and different prescriptions are used in the BPS codes.

- *binary_c*: different prescriptions of angular momentum loss through a stellar wind are available in *binary_c*. In this study as in Claeys et al. (in prep.), wind angular momentum loss is as described in Hurley et al. [2002]. When no material is accreted by the companion star, the wind takes specific angular momentum of the donor.
- *Brussels code*: Mass lost by a stellar wind in non-interacting systems is lost through the Jeans mode. Interacting systems do not have wind mass loss prior to interaction.
- *SeBa, StarTrack*: the material lost by a wind that is not accreted by the companion is lost from the system with specific angular momentum from the donor.

6.A.6 Evolution of helium stars

A helium star is formed after a hydrogen-rich star with a helium core loses its hydrogen-rich envelope. When the core is not degenerate at that time, the evolution of the star continues as a helium-burning star. Uncertainties in the evolution of helium stars encompass the growth of this star, the wind mass loss and mass transfer phase, such as the stability and rate.

- *binary_c, SeBa, StarTrack*: the evolutionary tracks and wind prescription are based on Hurley et al. [2000]. The stability of mass transfer and the rate are described in previous sections.
- *Brussels code*: helium star evolution is not explicitly included in the code. It is assumed that the donor star always loses its entire H-rich envelope in one episode and becomes a white dwarf afterwards, except in the case where a donor fills its Roche lobe for a second time as a helium star. In this case mass transfer is followed as described in Sect. 6.A.3, however, time-dependent evolutionary aspects of the helium star are not followed. This simplification is made because the intermediate step is not believed to

have a large influence on the eventual masses and separation. However, this implicitly means that the most massive star will always become a white dwarf first, which is not necessarily the case when helium star evolution is explicitly followed. For stars that lose mass during the planetary nebula phase, no resulting angular momentum loss is taken into account.

6.A.7 Generating the initial stellar population

The initial population can be chosen by a Monte Carlo method, or the choice can be made grid-based. Nevertheless, if the method is well performed both methods should give the same results for a high enough resolution.

- *binary_c*: $N_{M_{1,zams}} \times N_{M_{2,zams}} \times N_{a_{zams}}$ binaries are simulated, with $M_{1,zams}$, $M_{2,zams}$, a_{zams} chosen in logarithmic space. A probability is calculated for every system determined by the defined initial distributions.
- *Brussels code*: the code works with a three-dimensional grid of initial parameters: primary mass $M_{1,zams}$, mass ratio q_{zams} and orbital period P_{zams} . According to the initial mass function, initial mass-ratio distribution and initial orbital period (or separation) distribution, each grid point is assigned a certain weight. Every system corresponding to such a grid point is then taken through its evolution.
- *SeBa, StarTrack*: initial parameters $M_{1,zams}$, $M_{2,zams}$, a_{zams} and the initial eccentricity e_{zams} are chosen randomly on a Monte-Carlo based-approach where the probability functions are given by the initial distributions. With this method, the resolution is highest in those regions of parameter space where most systems lie.

6.B Typical variable assumptions in BPS codes

Some aspects of the codes that are not straightforward to change have been discussed in the previous section. However, other aspects of the codes are relatively simple to adapt. These aspects are often contained in relatively isolated and parametrised functions. For this project we equalised these aspects in the codes as far as possible. However, we do not believe that all the assumptions made for this project are realistic. Previous publications of results from these BPS codes are based on different assumptions. Although we do not compare the effect of the different assumptions on stellar populations in this work, it is good to realise which assumptions are generally used. Therefore the usual assumptions made by the authors in their corresponding BPS code are summarised in Table 6.5 and are discussed in more detail below. Typical assumptions may vary between different users of the BPS codes.

TABLE 6.5: Equalised assumptions for this research and the usual assumptions of the authors in the corresponding BPS codes.

	binary_c	Brussels code	SeBa	StarTrack	This research
β (RLOF)	Variable	Conditional ⁽¹⁾	Variable	Conditional ⁽¹⁾	1
AML (RLOF)	Isotropic re-emission	Ring ⁽²⁾ ($\eta = 1.5 \frac{(M_d + M_a)^2}{M_d M_a}$)	Orbit ⁽²⁾ ($\eta = 2.5$)	Orbit ⁽²⁾ ($\eta = 1$)	Orbit ($\eta = 1$)
CE ⁽³⁾	α (v2)	α (v1)	$\gamma\alpha$ (T12)	α (v1)	α (v1)
$\alpha_{ce}\lambda_{ce}/\gamma$	Variable ⁽⁴⁾	1	2/1.75	1	1
Wind accretion	B-H ⁽⁵⁾	No	B-H ⁽⁵⁾	No ⁽⁶⁾	No
Tides	Z77, H81, HTP02	Z77	PZV96	Z77, H81, HTP02, C07	No
Magn. braking	RVJ83	No	RVJ83	IT03	No

NOTES: References in the table: T12 = Toonen et al. [2012], Z77 = Zahn [1977], H81 = Hut [1981], HTP02 = Hurley et al. [2002], PZV96 = Portegies Zwart & Verbunt [1996], B08 = Belczynski et al. [2008a], C07 = Claret [2007], RVJ83 = Rappaport et al. [1983], IT03 = Ivanova & Taam [2003].

- (1) Constant for non-degenerate accretors, variable for accretion onto a WD.
- (2) Except during accretion onto a compact object, AML = isotropic re-emission.
- (3) v1 = prescription Webbink [1984], v2 = prescription Hurley et al. [2002].
- (4) Based on detailed stellar structure models [for the description see Izzard, 2004, Claeys et al. in prep.].
- (5) B-H = Prescription based on Bondi & Hoyle [1944].
- (6) Wind accretion is taken into account for neutron star and black hole accretors assuming B-H-accretion⁽⁵⁾.

6.B.1 Accretion efficiency

In this project mass transfer is assumed to be conservative to all types of stars. However, in general, the accretion efficiency depends on the type of accreting star and the mass transfer rate.

- *binary_c*, *SeBa*: in the case of non-degenerate accretors with radiative envelopes, the accretion efficiency mainly depends on the mass transfer rate and the thermal timescale of the accreting star. In the case of non-degenerate objects with convective envelopes, mass is transferred conservatively. In the case of a degenerate accretors, the accretion efficiency depends on the mass of the degenerate object and the mass transfer rate.
- *Brussels code*: the accretion efficiency onto a non-degenerate object is taken to be constant. If the mass ratio is below 0.2, mass transfer is unstable and the accretion efficiency is assumed to be zero (see Sect. 6.A.2). To ensure continuity, between mass ratios 0.2 and 0.4 a linear interpolation is used for the accretion efficiency, between 0 and β (usually 1). Note that for popcorn this transition was not implemented and the accretion efficiency is one between 0.2 and 0.4. In case of a degenerate accreting object, the regions in the (companion mass, orbital period)-parameter space from Hachisu et al. [2008] are used to determine in which cases the white dwarf can stably accrete up to $1.4 M_{\odot}$. In all other cases, mass transfer towards white dwarfs is assumed to become unstable, and is treated as a common envelope phase.
- *StarTrack*: the accretion efficiency onto a non-degenerate object is taken to be constant. In the case of a degenerate accreting object, the accretion efficiency depends on the mass of the accreting object and the mass transfer rate [see Belczynski et al., 2008a, sect. 5 therein].

6.B.2 Angular momentum loss during RLOF

In BPS codes a wide range of prescriptions are used to describe angular momentum loss when material is lost in a phase of stable RLOF. See Sect. 6.2.1.1 for the different prescriptions of angular momentum loss and a discussion of the importance of the effect on the orbit.

- *binary_c*: in this work and the standard model in Claeys et al. (in prep.) the material not accreted during the stable RLOF phase is lost as isotropic re-emission.
- *Brussels code*: the material is lost through the second Lagrangian point such that angular momentum is lost from a circumbinary ring with $a_{\text{ring}} = 2.3$.
- *SeBa*: when the accretor is a non-degenerate star, the material lost carries 2.5 times the specific orbital angular momentum of the binary [Portegies Zwart, 1995; Nelemans

et al., 2001c]. In the case of a degenerate accretor, the material lost carries specific orbital angular momentum of the accreting star.

- *StarTrack*: when the accretor is a non-degenerate star, the material lost carries one time the specific orbital angular momentum. In the case of a degenerate accretor, the material lost carries specific orbital angular momentum of the accreting star.

6.B.3 Common envelope evolution

The evolution of a CE-phase is highly uncertain. For this reason, various BPS codes employ different CE-prescriptions (see Sect. 6.2.1.2) and CE-efficiencies (such as α_{ce}) and both aspects are often varied within a BPS study for comparison. Here, we briefly describe the CE-parametrisations that are implemented most often by the authors in the four different codes.

- *binary_c*: to describe CE-evolution the prescription based on Hurley et al. [2002] is used. In the standard model of Claeys et al. (in prep.) α_{ce} is one, while λ_{ce} depends on the type of star, its mass and luminosity [see Izzard, 2004, Claeys et al. in prep.]. However, in the BPS code also the γ -prescription can be used.
- *Brussels code, StarTrack*: For standard calculations, the prescription based on Webbink [1984] is used, where α_{ce} and λ_{ce} are both one. In both codes different values for α_{ce} and λ_{ce} can be implemented, as well as the γ -prescription [for further information about the version of the γ -prescription implemented in StarTrack see Belczynski et al., 2008a; Ruiters et al., 2011].
- *SeBa*: the standard model for simulating CE-evolution in SeBa is the γ -prescription, unless the binary contains a compact object or the CE is triggered by a Darwin instability [Darwin, 1879] for which the α -formalism based on Webbink [1984] is used. The γ -formalism is introduced by Nelemans et al. [2000] in order to better reproduce the mass ratio distribution of observed double white dwarfs. The mass loss reduces the angular momentum of the system according to:

$$\frac{J_i - J_f}{J_i} = \gamma \frac{M_{d,env}}{M_d + M_a}, \quad (6.17)$$

where J_i and J_f are the angular momenta of the pre- and post-mass transfer binary respectively. The motivation for this formalism is the large amount of angular momentum available in binaries with similar mass objects that possibly can be used to expel the envelope. In SeBa γ is taken to be equal to 1.5, and $\alpha_{ce} \times \lambda_{ce}$ is equal to two.

6.B.4 Wind accretion

Material that is lost in the form of a stellar wind can be partly accreted by the companion star. The amount depends on properties of the wind (e.g. the velocity), the accreting star and the binary system (e.g. the separation). However, the exact amount accreted is ill-constrained.

- *binary_c*, *SeBa*: the accretion efficiency of wind material is determined by the Bondi-Hoyle prescription [Bondi & Hoyle, 1944]. In *binary_c* the accretion efficiency based on the wind Roche-lobe overflow model can be used [Mohamed & Podsiadlowski, 2007, 2012; Abate et al., 2013], however, is not used for this work.
- *Brussels code*: no material lost in the form of a stellar wind is accreted by the companion star.
- *StarTrack*: material lost through a wind is in general not accreted by the companion star, except when the companion star is a neutron star or a black hole.

6.B.5 Tides

The general picture of tidal effects is clear, however, uncertainties remain due to missing knowledge about for example some dissipative processes.

- *binary_c*: tidal evolution is implemented as described by Hurley et al. [2002], which is based on Hut [1981]; Zahn [1977].
- *Brussels code*: tidal evolution is a described by Zahn [1977].
- *SeBa*: tidal evolution is implemented as described by Portegies Zwart & Verbunt [1996].
- *StarTrack*: tidal evolution is implemented as described by Claret [2007], as well as Hurley et al. [2002], which is based on Hut [1981]; Zahn [1977].

6.B.6 Magnetic braking

Magnetic braking is important for low mass stars with convective envelopes. Nevertheless, this process is not fully understood and different prescriptions co-exist.

- *binary_c*, *SeBa*: both codes use the prescription of Rappaport et al. [1983].
- *Brussels code*: the code is not used for the evolution of stellar objects with a mass lower than $3M_{\odot}$, therefore magnetic braking is not considered.
- *StarTrack*: the prescription of Ivanova & Taam [2003] is used in standard calculations.

TABLE 6.6: Effect on the normalisation of different boundaries for the initial distribution of binary parameters. The initial distributions are as in Table 6.1. The normalisation factor is defined as the ratio of the number of systems for the given boundary conditions and the total number of systems using the typical boundary conditions (as given in the top line). The normalisation factor is used to convert the number of systems in the simulation to physical quantities such as birthrates, number density, events per solar mass of created stars.

Normalisation factor	min M M_{\odot}	max M M_{\odot}	min a R_{\odot}	max a R_{\odot}	min q	max q
1	0.1	100	5	1e6	$0.1M_{\odot}/M_{1,zams}$	1
1.0	0.1	80	5	1e6	$0.1M_{\odot}/M_{1,zams}$	1
1.0	0.1	150	5	1e6	$0.1M_{\odot}/M_{1,zams}$	1
0.6	0.1	100	5	1e4	$0.1M_{\odot}/M_{1,zams}$	1
1.7	0.1	100	5	1e6	$0.01/M_{1,zams}$	1
1.4	0.08	100	5	1e6	$0.08/M_{1,zams}$	1

6.B.7 Initial population

The choice for an initial distribution and the respective boundaries can severely affect the importance of a certain evolutionary channel through the normalisation of the simulation. Table 6.6 shows the effect of different boundary conditions considered in the standard simulations of the respective BPS codes compared to the boundary conditions assumed in this study. It shows that different boundary conditions affect the birthrates by a factor of about 0.5 to 2. The assumptions made by the authors with their respective codes are summarised in Table 6.7. Different aspects which need extra clarification are discussed below. Note that other users of the BPS codes under study here, other than the authors, may use different distribution functions and/or ranges.

- *binary_c*: the initial eccentricity is zero Hurley et al. [2002]. The minimum initial separation is varied between $5R_{\odot}$ or the minimum separation at which a binary system with a certain mass is initially detached. The minimum and maximum masses and separations are based on the work of Kouwenhoven et al. [2007].
- *Brussels code*: the initial eccentricity is zero. A minimum and maximum initial orbital period of one day and 3650 days is assumed. In order to compare with the other codes, a conversion of orbital period to separations is given in Table 6.7.
- *SeBa, StarTrack*: a distribution for the initial eccentricities is assumed (see Table 6.7). The initial semi-major axis is chosen between $10^6 R_{\odot}$ and the minimum initial separation is the minimum separation at which a binary system with a certain mass is initially detached.

TABLE 6.7: Equalised initial distribution and range of binary parameters and the usual distributions and ranges of the authors for the corresponding BPS codes.

What?	binary_c	Brussels code	SeBa	StarTrack	This research
$f(M_{1,zams})$	KTG93	KTG93	KTG93	KTG93	KTG93
$M_{1,zams,min} (M_{\odot})$	0.1	0.1	0.1	0.08	0.1
$M_{1,zams,max} (M_{\odot})$	80	120	100	150	100
$f(a_{zams})$	$\propto a^{-1}$	$\propto a^{-1}$	$\propto a^{-1}$	$\propto a^{-1}$	$\propto a^{-1}$ (A83)
$a_{zams,min} (R_{\odot})$	$\max(5, (R_a + R_b)/(1 - e_0))$	$2 - 12^{(1)}(P = 1d)$	$(R_a + R_b)/(1 - e_0)$	$2(R_a + R_b)/(1 - e_0)$	5
$a_{zams,max} (R_{\odot})$	5e6	$5.8e2 - 2.2e3^{(1)}(P = 3650d)$	1e6	1e6	1e6
$f(q_{zams})$	Flat	Flat	Flat	Flat	Flat
$q_{zams,min}$	$0.01M_{\odot}/M_{1,zams}$	$0.1M_{\odot}/M_{1,zams}$	0	$0.08M_{\odot}/M_{1,zams}$	$0.1M_{\odot}/M_{1,zams}$
$q_{zams,max}$	1	1	1	1	1
$f(e_{zams})$	-	-	H75	H75	-
$e_{zams,min}$	-	-	0	0	-
$e_{zams,max}$	-	-	1	1	-
Max time (Gyr)	13.7	15	13.5	15	13.7
Binary fraction (%)	100	100	50-100	50	100

NOTES: $f(\xi)$ is the distribution of parameter ξ . '-' Indicates that no distribution of initial eccentricities is considered, instead $e_{zams} = 0$ a priori. Otherwise the distribution of initial eccentricities is $f(e_{zams})$ with e_{zams} between $e_{zams,min}$ and $e_{zams,max}$.

References in the table: KTG93 = Kroupa et al. [1993], A83 = Abt [1983], H75 = Heggie [1975]

(1) Separations given for the binary masses under investigation.

BIBLIOGRAPHY

- C. Abate, O. R. Pols, R. G. Izzard, et al., 2013. *A&A*, 552:A26.
- B. Abbott, R. Abbott, R. Adhikari, et al., 2004. *Phys. Rev. D*, 69(12):122001.
- H. A. Abt, 1983. *ARA&A*, 21:343–372.
- R. D. Alexander, G. A. Wynn, A. R. King, et al., 2011. *MNRAS*, 418:2576–2583.
- P. Amaro-Seoane, S. Aoudia, S. Babak, et al., 2012a. *ArXiv:1201.3621*.
- P. Amaro-Seoane, S. Aoudia, S. Babak, et al., 2012b. *ArXiv:1202.0839*.
- T. Augusteijn, R. Greimel, E. J. M. van den Besselaar, et al., 2008. *A&A*, 486:843–853.
- C. Badenes, J. Harris, D. Zaritsky, et al., 2009. *ApJ*, 700:727–740.
- K. Belczynski, M. Benacquista, & T. Bulik, 2010a. *ApJ*, 725:816–823.
- K. Belczynski, T. Bulik, C. L. Fryer, et al., 2010b. *ApJ*, 714:1217–1226.
- K. Belczynski, T. Bulik, A. Heger, et al., 2007. *ApJ*, 664:986–999.
- K. Belczynski, T. Bulik, & V. Kalogera, 2002a. *ApJ*, 571:L147–L150.
- K. Belczynski, T. Bulik, & A. J. Ruiter, 2005. *ApJ*, 629:915–921.
- K. Belczynski, M. Dominik, T. Bulik, et al., 2010c. *ApJ*, 715:L138–L141.
- K. Belczynski, V. Kalogera, & T. Bulik, 2002b. *ApJ*, 572:407–431.
- K. Belczynski, V. Kalogera, F. A. Rasio, et al., 2008a. *ApJS*, 174:223–260.
- K. Belczynski, V. Kalogera, A. Zezas, et al., 2004. *ApJ*, 601:L147–L150.
- K. Belczynski, R. E. Taam, E. Rantsiou, et al., 2008b. *ApJ*, 682:474–486.
- K. Belczynski, G. Wiktorowicz, C. L. Fryer, et al., 2012. *ApJ*, 757:91.
- D. H. Berger, D. R. Gies, H. A. McAlister, et al., 2006. *ApJ*, 644:475–483.
- R. D. Blandford & J. P. Ostriker, 1978. *ApJL*, 221:L29–L32.
- J. J. Bochanski, A. A. West, S. L. Hawley, et al., 2007. *AJ*, 133:531–544.
- A. I. Bogomazov & A. V. Tutukov, 2009. *Astronomy Reports*, 53:214–222.
- A. I. Bogomazov & A. V. Tutukov, 2011. *Astronomy Reports*, 55:497–504.
- S. Boissier & N. Prantzos, 1999. *MNRAS*, 307:857–876.
- A. Bonačić Marinović, R. G. Izzard, M. Lugaro, et al., 2006. *Mem. Soc. Astron. Italiana*, 77:879.

BIBLIOGRAPHY

- H. Bondi & F. Hoyle, 1944. *MNRAS*, 104:273–+.
- M. C. P. Bours, S. Toonen, & G. Nelemans, 2013. *A&A*, 552:A24.
- T. S. Boyajian, H. A. McAlister, G. van Belle, et al., 2012. *ApJ*, 746:101.
- G. E. Brown, 1995. *ApJ*, 440:270–279.
- W. R. Brown, M. Kilic, C. Allende Prieto, et al., 2010. *ApJ*, 723:1072–1081.
- W. R. Brown, M. Kilic, C. Allende Prieto, et al., 2013. *ApJ*, 769:66.
- W. R. Brown, M. Kilic, J. J. Hermes, et al., 2011. *ApJ*, 737:L23+.
- A. Büning & H. Ritter, 2004. *A&A*, 423:281–299.
- E. Cappellaro & M. Turatto, 2001. In *The Influence of Binaries on Stellar Population Studies*, editor D. Vanbeveren, volume 264 of *ASSL*, page 199. Kluwer Academic Publishers, Dordrecht.
- J. A. Cardelli, G. C. Clayton, & J. S. Mathis, 1989. *ApJ*, 345:245–256.
- X. Chen, C. S. Jeffery, X. Zhang, et al., 2012. *ApJ*, 755:L9.
- J. S. W. Claeys, O. R. Pols, J. Vink, et al., 2011. *ArXiv:1101.5601*.
- A. Claret, 2007. *A&A*, 467:1389–1396.
- K. R. Covey, Ž. Ivezić, D. Schlegel, et al., 2007. *AJ*, 134:2398–2417.
- G. Darwin, 1879. *Phil. Trans. Roy. Soc.*, 170:447–538.
- P. J. Davis, U. Kolb, & C. Knigge, 2012. *MNRAS*, 419:287–303.
- P. J. Davis, U. Kolb, & B. Willems, 2010. *MNRAS*, 403:179–195.
- J. H. J. de Bruijne, 2012. *Ap&SS*, 341:31–41.
- E. De Donder & D. Vanbeveren, 2004. *New A Rev.*, 48:861–975.
- M. de Kool & H. Ritter, 1993. *A&A*, 267:397–409.
- M. de Kool, E. P. J. van den Heuvel, & E. Pylyser, 1987. *A&A*, 183:47–52.
- O. De Marco, J.-C. Passy, M. Moe, et al., 2011. *MNRAS*, 411:2277–2292.
- S. E. de Mink, N. Langer, R. G. Izzard, et al., 2013. *ApJ*, 764:166.
- S. E. de Mink, O. R. Pols, & R. W. Hilditch, 2007. *A&A*, 467:1181–1196.
- P. A. Denissenkov, F. Herwig, L. Bildsten, et al., 2013. *ApJ*, 762:8.
- J. D. M. Dewi & T. M. Tauris, 2000. *A&A*, 360:1043–1051.
- R. Di Stefano, 2010. *ApJ*, 712:728–733.
- M. Dominik, K. Belczynski, C. Fryer, et al., 2012. *ApJ*, 759:52.
- G. Duchêne & A. Kraus, 2013. *ArXiv:1303.3028*.
- R. A. Dupke & R. E. White, III, 2000. *ApJ*, 528:139–144.
- A. Duquennoy & M. Mayor, 1991. *A&A*, 248:485–524.
- P. P. Eggleton, 1971. *MNRAS*, 151:351–+.
- P. P. Eggleton, 1972. *MNRAS*, 156:361–+.
- P. P. Eggleton, M. J. Fitchett, & C. A. Tout, 1989. *ApJ*, 347:998–1011.
- C. R. Evans, I. Iben, Jr., & L. Smarr, 1987. *ApJ*, 323:129–139.
- J. Farihi, D. W. Hoard, & S. Wachter, 2010. *ApJS*, 190:275–296.
- C. L. Fryer, A. J. Ruitter, K. Belczynski, et al., 2010. *ApJ*, 725:296–308.
- H. Ge, M. S. Hjellming, R. F. Webbink, et al., 2010. *ApJ*, 717:724–738.

- H. Ge, R. F. Webbink, X. Chen, et al., 2013. In *IAU Symposium*, editors C. M. Zhang, T. Belloni, M. Méndez, et al., volume 290 of *IAU Symposium*, pages 213–214.
- S. Geier, H. Hirsch, A. Tillich, et al., 2011. *A&A*, 530:A28.
- S. Geier, S. Nesslinger, U. Heber, et al., 2007. *A&A*, 464:299–307.
- M. Gilfanov & Á. Bogdán, 2010. *Nature*, 463:924–925.
- E. Glebbeek, O. R. Pols, & J. R. Hurley, 2008. *A&A*, 488:1007–1015.
- O. Graur & D. Maoz, 2012. *ArXiv:1209.0008*.
- O. Graur & D. Maoz, 2013. *MNRAS*, 430:1746–1763.
- I. Hachisu & M. Kato, 2001. *ApJ*, 558:323–350.
- I. Hachisu, M. Kato, & K. Nomoto, 1996. *ApJ*, 470:L97.
- I. Hachisu, M. Kato, & K. Nomoto, 1999b. *ApJ*, 522:487–503.
- I. Hachisu, M. Kato, & K. Nomoto, 2008. *ApJ*, 679:1390–1404.
- I. Hachisu, M. Kato, & K. Nomoto, 2010. *ApJ*, 724:L212–L216.
- I. Hachisu, M. Kato, K. Nomoto, et al., 1999. *ApJ*, 519:314–323.
- A. S. Hamers, O. R. Pols, J. S. W. Claeys, et al., 2013. *MNRAS*, 430:2262–2280.
- J. M. Hameury, A. R. King, & J. P. Lasota, 1989. *MNRAS*, 237:39–47.
- J. M. Hameury, A. R. King, J. P. Lasota, et al., 1993. *A&A*, 277:81.
- Z. Han, P. P. Eggleton, P. Podsiadlowski, et al., 2001. In *Evolution of Binary and Multiple Star Systems*, editors P. Podsiadlowski, S. Rappaport, A. R. King, et al., volume 229 of *Astronomical Society of the Pacific Conference Series*, page 205.
- Z. Han & P. Podsiadlowski, 2004. *MNRAS*, 350:1301–1309.
- Z. Han, P. Podsiadlowski, & P. P. Eggleton, 1995. *MNRAS*, 272:800–820.
- Z. Han, P. Podsiadlowski, P. F. L. Maxted, et al., 2002. *MNRAS*, 336:449–466.
- B. M. S. Hansen, 1999. *ApJ*, 520:680–695.
- D. C. Heggie, 1975. *MNRAS*, 173:729–787.
- W. Hillebrandt & J. C. Niemeyer, 2000. *ARA&A*, 38:191–230.
- L. A. Hillenbrand & R. J. White, 2004. *ApJ*, 604:741–757.
- M. S. Hjellming & R. F. Webbink, 1987. *ApJ*, 318:794–808.
- J. B. Holberg & P. Bergeron, 2006. *AJ*, 132:1221–1233.
- D. A. Howell, 2001. *ApJ*, 554:L193–L196.
- H. Hu, E. Glebbeek, A. A. Thoul, et al., 2010. *A&A*, 511:A87+.
- S.-S. Huang, 1966. *Annales d’Astrophysique*, 29:331–+.
- R. M. Humphreys & K. Davidson, 1994. *PASP*, 106:1025–1051.
- J. R. Hurley, O. R. Pols, & C. A. Tout, 2000. *MNRAS*, 315:543–569.
- J. R. Hurley, C. A. Tout, & O. R. Pols, 2002. *MNRAS*, 329:897–928.
- P. Hut, 1980. *A&A*, 92:167–170.
- P. Hut, 1981. *A&A*, 99:126–140.
- I. Iben, Jr. & M. Livio, 1993. *PASP*, 105:1373–1406.
- I. Iben, Jr. & A. V. Tutukov, 1984. *ApJS*, 54:335–372.
- I. Iben, Jr. & A. V. Tutukov, 1985. *ApJS*, 58:661–710.

BIBLIOGRAPHY

- I. Iben, Jr. & A. V. Tutukov, 1996. *ApJS*, 105:145–+.
- N. Ivanova, K. Belczynski, J. M. Fregeau, et al., 2005. *MNRAS*, 358:572–584.
- N. Ivanova, K. Belczynski, V. Kalogera, et al., 2003. *ApJ*, 592:475–485.
- N. Ivanova, S. Justham, X. Chen, et al., 2013. *A&A Rev.*, 21:59.
- N. Ivanova & R. E. Taam, 2003. *ApJ*, 599:516–521.
- R. G. Izzard, 2004. *Nucleosynthesis in binary stars*. Ph.D. thesis, Institute of Astronomy, Cambridge.
- R. G. Izzard, T. Dermine, & R. P. Church, 2010. *A&A*, 523:A10.
- R. G. Izzard, L. M. Dray, A. I. Karakas, et al., 2006. *A&A*, 460:565–572.
- R. G. Izzard, E. Glebbeek, R. J. Stancliffe, et al., 2009. *A&A*, 508:1359–1374.
- R. G. Izzard, C. A. Tout, A. I. Karakas, et al., 2004. *MNRAS*, 350:407–426.
- P. G. Jonker, C. G. Bassa, G. Nelemans, et al., 2011. *ApJS*, 194:18.
- H. E. Jorgensen, V. M. Lipunov, I. E. Panchenko, et al., 1997. *ApJ*, 486:110.
- V. Kalogera & R. F. Webbink, 1996. *ApJ*, 458:301.
- A. I. Karakas, J. C. Lattanzio, & O. R. Pols, 2002. *PASA*, 19:515–526.
- A. Kashi & N. Soker, 2011. *MNRAS*, 417:1466–1479.
- M. Kato & I. Hachisu, 1994. *ApJ*, 437:802–826.
- M. Kato & I. Hachisu, 1999. *ApJ*, 513:L41–L44.
- M. Kilic, W. R. Brown, C. Allende Prieto, et al., 2011a. *ApJ*, 727:3–+.
- M. Kilic, W. R. Brown, J. J. Hermes, et al., 2011b. *MNRAS*, 418:L157–L161.
- M. Kilic, W. R. Brown, S. J. Kenyon, et al., 2011c. *MNRAS*, 413:L101–L105.
- A. R. King & M. C. Begelman, 1999. *ApJ*, 519:L169–L171.
- A. R. King, J. Frank, U. Kolb, et al., 1996. *ApJ*, 467:761.
- A. R. King, D. J. Rolfe, & K. Schenker, 2003. *MNRAS*, 341:L35–L38.
- R. Kippenhahn & E. Meyer-Hofmeister, 1977. *A&A*, 54:539–542.
- R. Kippenhahn & A. Weigert, 1967. *ZAp*, 65:251.
- C. Knigge, I. Baraffe, & J. Patterson, 2011. *ApJS*, 194:28.
- C. Knigge, A. R. King, & J. Patterson, 2000. *A&A*, 364:L75–L79.
- C. Kobayashi & K. Nomoto, 2009. *ApJ*, 707:1466–1484.
- C. Kobayashi, T. Tsujimoto, K. Nomoto, et al., 1998. *ApJ*, 503:L155.
- M. B. N. Kouwenhoven, A. G. A. Brown, S. F. Portegies Zwart, et al., 2007. *A&A*, 474:77–104.
- P. M. Kowalski & D. Saumon, 2006. *ApJ*, 651:L137–L140.
- R. P. Kraft, J. Mathews, & J. L. Greenstein, 1962. *ApJ*, 136:312–315.
- A. L. Kraus & L. A. Hillenbrand, 2007. *AJ*, 134:2340–2352.
- M. Kromer, S. A. Sim, M. Fink, et al., 2010. *ApJ*, 719:1067–1082.
- P. Kroupa, C. A. Tout, & G. Gilmore, 1993. *MNRAS*, 262:545–587.
- R. P. Kudritzki, A. Pauldrach, & J. Puls, 1987. *A&A*, 173:293–298.
- S. R. Kulkarni & M. H. van Kerkwijk, 2010. *ApJ*, 719:1123–1131.
- R. L. Kurucz, 1993. *SYNTHE spectrum synthesis programs and line data*.

- R. L. Kurucz & E. H. Avrett, 1981. *SAO Special Report*, 391.
- J.-P. Lasota, 2001. *New A Rev.*, 45:449–508.
- D. Lauterborn, 1970. *A&A*, 7:150–159.
- B. Leibundgut, G. A. Tammann, R. Cadonau, et al., 1991. *A&AS*, 89:537–579.
- W. Li, A. V. Filippenko, R. R. Treffers, et al., 2001. *ApJ*, 546:734–743.
- W. Li, J. Leaman, R. Chornock, et al., 2011. *MNRAS*, 412:1441–1472.
- X.-D. Li & E. P. J. van den Heuvel, 1997. *A&A*, 322:L9–L12.
- X.-D. Li & E. P. J. van den Heuvel, 2002. In *Cosmic Chemical Evolution*, editors K. Nomoto & J. W. Truran, volume 187 of *IAU Symposium*, pages 103–108.
- V. M. Lipunov, K. A. Postnov, M. E. Prokhorov, et al., 2009. *Astronomy Reports*, 53:915–940.
- T. Lisker, U. Heber, R. Napiwotzki, et al., 2005. *A&A*, 430:223–243.
- M. Livio, 2000. In *Type Ia Supernovae, Theory and Cosmology*, editor J. C. Niemeyer & J. W. Truran, page 33. Cambridge Univ. Press.
- M. Livio & B. Warner, 1984. *The Observatory*, 104:152–159.
- M. López-Morales, 2007. *ApJ*, 660:732–739.
- A. J. Loveridge, M. V. van der Sluys, & V. Kalogera, 2011. *ApJ*, 743:49.
- J. MacDonald, 1986. *ApJ*, 305:251–260.
- A. Maeder & G. Meynet, 1989. *A&A*, 210:155–173.
- D. Maoz & C. Badenes, 2010. *MNRAS*, 407:1314–1327.
- D. Maoz & F. Mannucci, 2012a. *PASA*, 29:447–465.
- D. Maoz & F. Mannucci, 2012b. *PASA*, 29:447–465.
- D. Maoz, F. Mannucci, & T. D. Brandt, 2012. *MNRAS*, 426:3282–3294.
- D. Maoz, F. Mannucci, W. Li, et al., 2011. *MNRAS*, 412:1508–1521.
- D. Maoz, K. Sharon, & A. Gal-Yam, 2010. *ApJ*, 722:1879–1894.
- T. R. Marsh, 2011. *Classical and Quantum Gravity*, 28(9):094019–+.
- T. R. Marsh, B. T. Gänsicke, D. Steeghs, et al., 2011. *ApJ*, 736:95–+.
- P. F. L. Maxted & T. R. Marsh, 1999. *MNRAS*, 307:122–132.
- P. F. L. Maxted, T. R. Marsh, & R. C. North, 2000. *MNRAS*, 317:L41–L44.
- J. Melnick, R. Terlevich, & P. P. Eggleton, 1985. *MNRAS*, 216:255–271.
- X. Meng, X. Chen, & Z. Han, 2009. *MNRAS*, 395:2103–2116.
- X. C. Meng, W. C. Chen, W. M. Yang, et al., 2011. *A&A*, 525:A129.
- N. Mennekens, D. Vanbeveren, & J. P. De Greve, 2012. *ArXiv:1212.0313*.
- N. Mennekens, D. Vanbeveren, J. P. De Greve, et al., 2010. *A&A*, 515:A89+.
- E. J. A. Meurs & E. P. J. van den Heuvel, 1989. *A&A*, 226:88–107.
- S. Mohamed & P. Podsiadlowski, 2007. In *15th European Workshop on White Dwarfs*, editors R. Napiwotzki & M. R. Burleigh, volume 372 of *Astronomical Society of the Pacific Conference Series*, page 397.
- S. Mohamed & P. Podsiadlowski, 2012. *Baltic Astronomy*, 21:88–96.
- F. Mullally, C. Badenes, S. E. Thompson, et al., 2009. *ApJ*, 707:L51–L55.

BIBLIOGRAPHY

- U. Munari, R. Sordo, F. Castelli, et al., 2005. *A&A*, 442:1127–1134.
- R. Napiwotzki, N. Christlieb, H. Drechsel, et al., 2001. *Astronomische Nachrichten*, 322:411–418.
- R. Napiwotzki, G. Tovmassian, M. G. Richer, et al., 2005. In *Planetary Nebulae as Astronomical Tools*, editor R. Szczerba, G. Stasińska, & S. K. Gorny, volume 804 of *AIP Conf. Ser.*, pages 173–176.
- A. Nebot Gómez-Morán, B. T. Gänsicke, M. R. Schreiber, et al., 2011. *A&A*, 536:A43.
- G. Nelemans, 2010. *Ap&SS*, 329:25–31.
- G. Nelemans, R. Napiwotzki, C. Karl, et al., 2005. *A&A*, 440:1087–1095.
- G. Nelemans, S. Toonen, & M. Bours, 2013. In *IAU Symposium*, volume 281 of *IAU Symposium*, pages 225–231.
- G. Nelemans & E. P. J. van den Heuvel, 2001. *A&A*, 376:950–954.
- G. Nelemans, F. Verbunt, L. R. Yungelson, et al., 2000. *A&A*, 360:1011–1018.
- G. Nelemans, L. R. Yungelson, & S. F. Portegies Zwart, 2001a. *A&A*, 375:890–898.
- G. Nelemans, L. R. Yungelson, & S. F. Portegies Zwart, 2001b. *A&A*, 375:890–898.
- G. Nelemans, L. R. Yungelson, & S. F. Portegies Zwart, 2004. *MNRAS*, 349:181–192.
- G. Nelemans, L. R. Yungelson, S. F. Portegies Zwart, et al., 2001c. *A&A*, 365:491–507.
- S. Neo, S. Miyaji, K. Nomoto, et al., 1977. *PASJ*, 29:249–262.
- M. Nielsen, G. Nelemans, & R. Voss, 2010. In *AIP Conf. Ser.*, editor K. Werner & T. Rauch, volume 1273 of *AIP Conf. Ser.*, pages 279–282.
- H. Nieuwenhuijzen & C. de Jager, 1990. *A&A*, 231:134–136.
- K. Nomoto, 1982. *ApJ*, 257:780–792.
- K. Nomoto & I. Iben, Jr., 1985. *ApJ*, 297:531–537.
- K. Nomoto, H. Saio, M. Kato, et al., 2007. *ApJ*, 663:1269–1276.
- K. Nomoto, F.-K. Thielemann, & K. Yokoi, 1984. *ApJ*, 286:644–658.
- K. Nomoto, H. Umeda, C. Kobayashi, et al., 2000. In *American Institute of Physics Conference Series*, editors S. S. Holt & W. W. Zhang, volume 522 of *American Institute of Physics Conference Series*, pages 35–52.
- T. Nugis & H. J. G. L. M. Lamers, 2000. *A&A*, 360:227–244.
- J. E. O’Donnell, 1994. *ApJ*, 422:158–163.
- Y. Osaki, 1996. *PASP*, 108:39.
- R. O’Shaughnessy, K. Belczynski, & V. Kalogera, 2008. *ApJ*, 675:566–585.
- W. Packet & J. P. De Greve, 1979. *A&A*, 75:255–257.
- B. Paczyński & R. Sienkiewicz, 1972. *Acta Astron.*, 22:73–91.
- B. Paczynski, 1976. In *Structure and Evolution of Close Binary Systems*, editor P. Eggleton, S. Mitton, & J. Whelan, volume 73 of *IAU Symposium*, page 75. Kluwer, Dordrecht.
- R. Pakmor, S. Hachinger, F. K. Röpkke, et al., 2011. *A&A*, 528:A117.
- R. Pakmor, M. Kromer, F. K. Röpkke, et al., 2010. *Nature*, 463:61–64.
- R. Pakmor, M. Kromer, S. Taubenberger, et al., 2012. *ApJ*, 747:L10.
- J.-C. Passy, O. De Marco, C. L. Fryer, et al., 2012. *ApJ*, 744:52.

- J. Patterson, 1984. *ApJS*, 54:443–493.
- J. Patterson, 2009. *ArXiv e-prints*.
- J. Patterson, J. Kemp, A. Shambrook, et al., 1998. *PASP*, 110:380–395.
- S. Perlmutter, G. Aldering, G. Goldhaber, et al., 1999. *ApJ*, 517:565–586.
- K. Perrett & et al., 2012. *AJ*, 144:59.
- P. C. Peters, 1964. *Physical Review*, 136:1224–1232.
- M. M. Phillips, 1993. *ApJ*, 413:L105–L108.
- A. J. Pickles, 1998. *PASP*, 110:863–878.
- L. Piersanti, S. Gagliardi, I. Iben, Jr., et al., 2003. *ApJ*, 598:1229–1238.
- P. Podsiadlowski, 1991. *Nature*, 350:136–138.
- M. Politano & K. P. Weiler, 2007. *ApJ*, 665:663–679.
- O. R. Pols, R. G. Izzard, R. J. Stancliffe, et al., 2012. *A&A*, 547:A76.
- O. R. Pols & M. Marinus, 1994. *A&A*, 288:475–501.
- O. R. Pols, K.-P. Schröder, J. R. Hurley, et al., 1998. *MNRAS*, 298:525–536.
- O. R. Pols, C. A. Tout, P. P. Eggleton, et al., 1995. *MNRAS*, 274:964–974.
- S. Portegies Zwart, 2013. *MNRAS*, 429:L45–L49.
- S. Portegies Zwart, S. McMillan, S. Harfst, et al., 2009. *New A*, 14:369–378.
- S. F. Portegies Zwart, 1995. *A&A*, 296:691.
- S. F. Portegies Zwart, 2000. *ApJ*, 544:437–442.
- S. F. Portegies Zwart, H. Baumgardt, P. Hut, et al., 2004. *Nature*, 428:724–726.
- S. F. Portegies Zwart, S. L. W. McMillan, P. Hut, et al., 2001. *MNRAS*, 321:199–226.
- S. F. Portegies Zwart & H. N. Spreeuw, 1996. *A&A*, 312:670–674.
- S. F. Portegies Zwart & F. Verbunt, 1996. *A&A*, 309:179–196.
- S. F. Portegies Zwart & L. R. Yungelson, 1998. *A&A*, 332:173–188.
- D. Prialnik, 1986. *ApJ*, 310:222–237.
- D. Prialnik & A. Kovetz, 1995. *ApJ*, 445:789–810.
- J. L. Prieto, K. Z. Stanek, & J. F. Beacom, 2008. *ApJ*, 673:999–1008.
- D. Raghavan, H. A. McAlister, T. J. Henry, et al., 2010. *ApJS*, 190:1–42.
- S. Rappaport, F. Verbunt, & P. C. Joss, 1983. *ApJ*, 275:713–731.
- A. Rebassa-Mansergas, B. T. Gänsicke, P. Rodríguez-Gil, et al., 2007. *MNRAS*, 382:1377–1393.
- A. Rebassa-Mansergas, B. T. Gänsicke, M. R. Schreiber, et al., 2010. *MNRAS*, 402:620–640.
- D. Reimers, 1975. *Memoires of the Societe Royale des Sciences de Liege*, 8:369–382.
- P. M. Ricker & R. E. Taam, 2008. *ApJ*, 672:L41–L44.
- P. M. Ricker & R. E. Taam, 2012. *ApJ*, 746:74.
- A. G. Riess, A. V. Filippenko, P. Challis, et al., 1998. *AJ*, 116:1009–1038.
- P. Rodríguez-Gil, M. Santander-García, C. Knigge, et al., 2010. *MNRAS*, 407:L21–L25.
- G. Roelofs, C. Bassa, R. Voss, et al., 2008. *MNRAS*, 391:290–296.
- G. H. A. Roelofs, P. J. Groot, G. F. Benedict, et al., 2007a. *ApJ*, 666:1174–1188.
- G. H. A. Roelofs, G. Nelemans, & P. J. Groot, 2007b. *MNRAS*, 382:685–692.

BIBLIOGRAPHY

- F. K. Röpkke, M. Kromer, I. R. Seitenzahl, et al., 2012. *ApJ*, 750:L19.
- A. J. Ruiter, K. Belczynski, M. Benacquista, et al., 2009a. *ApJ*, 693:383–387.
- A. J. Ruiter, K. Belczynski, M. Benacquista, et al., 2010. *ApJ*, 717:1006–1021.
- A. J. Ruiter, K. Belczynski, & C. Fryer, 2009b. *ApJ*, 699:2026–2036.
- A. J. Ruiter, K. Belczynski, & T. E. Harrison, 2006. *ApJ*, 640:L167–L170.
- A. J. Ruiter, K. Belczynski, S. A. Sim, et al., 2011. *MNRAS*, 417:408–419.
- A. J. Ruiter, S. A. Sim, R. Pakmor, et al., 2012. *ArXiv:1209.0645*.
- A. J. Ruiter, S. A. Sim, R. Pakmor, et al., 2013. *MNRAS*, 429:1425–1436.
- H. Saio & K. Nomoto, 1985. *A&A*, 150:L21–L23.
- A. Sandage, 1972. *ApJ*, 178:1–24.
- K. Sato, K. Tokoi, K. Matsushita, et al., 2007. *ApJ*, 667:L41–L44.
- C. D. J. Savoury, S. P. Littlefair, V. S. Dhillon, et al., 2011. *MNRAS*, 415:2025–2041.
- B. E. Schaefer & A. C. Collazzi, 2010. *AJ*, 139:1831–1843.
- G. Schaller, D. Schaerer, G. Meynet, et al., 1992. *A&AS*, 96:269–331.
- E. Schatzman, 1950. *Annales d’Astrophysique*, 13:384.
- E. Schatzman, 1962. *Annales d’Astrophysique*, 25:18–+.
- D. J. Schlegel, D. P. Finkbeiner, & M. Davis, 1998. *ApJ*, 500:525.
- M. R. Schreiber & B. T. Gänsicke, 2003. *A&A*, 406:305–321.
- B. J. Shappee & T. A. Thompson, 2012. *ArXiv:1204.1053*.
- M. M. Shara, M. Livio, A. F. J. Moffat, et al., 1986. *ApJ*, 311:163–171.
- K. J. Shen & L. Bildsten, 2007. *ApJ*, 660:1444–1450.
- K. J. Shen, L. Bildsten, D. Kasen, et al., 2012. *ApJ*, 748:35.
- S. A. Sim, F. K. Röpkke, W. Hillebrandt, et al., 2010. *ApJ*, 714:L52–L57.
- M. S. Sipior, S. Portegies Zwart, & G. Nelemans, 2004. *MNRAS*, 354:L49–L53.
- A. Skumanich, 1972. *ApJ*, 171:565–+.
- G. E. Soberman, E. S. Phinney, & E. P. J. van den Heuvel, 1997. *A&A*, 327:620–635.
- S. Starrfield, W. M. Sparks, & J. W. Truran, 1974. *ApJS*, 28:247–270.
- S. Starrfield, J. W. Truran, W. M. Sparks, et al., 1972. *ApJ*, 176:169.
- A. Stroerer, U. Heber, T. Lisker, et al., 2007. *A&A*, 462:269–280.
- R. E. Taam & P. M. Ricker, 2010. *New A Rev.*, 54:65–71.
- R. E. Taam & E. L. Sandquist, 2000. *ARA&A*, 38:113–141.
- S. Toonen, G. Nelemans, & S. Portegies Zwart, 2012. *A&A*, 546:A70.
- T. Totani, T. Morokuma, T. Oda, et al., 2008. *PASJ*, 60:1327–.
- C. A. Tout, 2005. In *The Astrophysics of Cataclysmic Variables and Related Objects*, editors J.-M. Hameury & J.-P. Lasota, volume 330 of *Astronomical Society of the Pacific Conference Series*, page 279.
- C. A. Tout, S. J. Aarseth, O. R. Pols, et al., 1997. *MNRAS*, 291:732–+.
- G. Tovmassian, L. Yungelson, T. Rauch, et al., 2010. *ApJ*, 714:178–193.
- G. H. Tovmassian, R. Napiwotzki, M. G. Richer, et al., 2004. *ApJ*, 616:485–497.
- D. M. Townsley & L. Bildsten, 2004. *ApJ*, 600:390–403.

- D. M. Townsley & B. T. Gänsicke, 2009. *ApJ*, 693:1007–1021.
- P.-E. Tremblay, P. Bergeron, & A. Gianninas, 2011. *ApJ*, 730:128.
- T. Tsujimoto, K. Nomoto, Y. Yoshii, et al., 1995. *MNRAS*, 277:945–958.
- A. Tutukov & L. Yungelson, 1979. In *Mass Loss and Evolution of O-Type Stars*, editors P. S. Conti & C. W. H. De Loore, volume 83 of *IAU Symposium*, pages 401–406.
- H. Uthas, C. Knigge, & D. Steeghs, 2010. *MNRAS*, 409:237–246.
- S. van den Bergh & G. A. Tammann, 1991. *ARA&A*, 29:363–407.
- L. B. van den Hoek & M. A. T. Groenewegen, 1997. *A&AS*, 123:305–328.
- M. van der Sluys, M. Politano, & R. E. Taam, 2010. In *American Institute of Physics Conference Series*, editors V. Kologera & M. van der Sluys, volume 1314 of *American Institute of Physics Conference Series*, pages 13–18.
- M. V. van der Sluys, F. Verbunt, & O. R. Pols, 2006. *A&A*, 460:209–228.
- L. M. van Haften, G. Nelemans, R. Voss, et al., 2013. *A&A*, 552:A69.
- M. H. van Kerkwijk, P. Chang, & S. Justham, 2010. *ApJ*, 722:L157–L161.
- D. Vanbeveren, E. De Donder, J. van Bever, et al., 1998. *New A*, 3:443–492.
- D. Vanbeveren & C. De Loore, 1994. *A&A*, 290:129–132.
- D. Vanbeveren, N. Mennekens, & J. P. De Greve, 2012. *A&A*, 543:A4.
- D. Vanbeveren, N. Mennekens, W. Van Rensbergen, et al., 2013. *A&A*, 552:A105.
- E. Vassiliadis & P. R. Wood, 1993. *ApJ*, 413:641–657.
- F. Verbunt, 1984. *MNRAS*, 209:227–240.
- F. Verbunt & C. Zwaan, 1981. *A&A*, 100:L7–L9.
- J. S. Vink, A. de Koter, & H. J. G. L. M. Lamers, 2000. *A&A*, 362:295–309.
- J. S. Vink, A. de Koter, & H. J. G. L. M. Lamers, 2001. *A&A*, 369:574–588.
- R. Voss & G. Nelemans, 2008. *Nature*, 451:802–804.
- A. Wachter, K.-P. Schröder, J. M. Winters, et al., 2002. *A&A*, 384:452–459.
- B. Wang, X. Chen, X. Meng, et al., 2009a. *ApJ*, 701:1540–1546.
- B. Wang & Z. Han, 2012. *New A Rev.*, 56:122–141.
- B. Wang, X.-D. Li, & Z.-W. Han, 2010. *MNRAS*, 401:2729–2738.
- B. Wang, X. Meng, X. Chen, et al., 2009b. *MNRAS*, 395:847–854.
- B. Warner, 1987. *MNRAS*, 227:23–73.
- B. Warner, 1995. *Cambridge Astrophysics Series*, 28.
- R. F. Webbink, 1984. *ApJ*, 277:355–360.
- R. F. Webbink, 1985. *Stellar evolution and binaries*, pages 39–+.
- R. F. Webbink, 2008. In *ASSL*, editor E. F. Milone, D. A. Leahy, & D. W. Hobill, volume 352 of *ASSL*, page 233. Springer, Berlin.
- J. Whelan & I. Iben, Jr., 1973. *ApJ*, 186:1007–1014.
- C. A. Whyte & P. P. Eggleton, 1980. *MNRAS*, 190:801–823.
- B. Willems & U. Kolb, 2004. *A&A*, 419:1057–1076.
- T. E. Woods, N. Ivanova, M. van der Sluys, et al., 2010. In *AIP Conf. Ser.*, editor V. Kologera & M. van der Sluys, volume 1314 of *AIP Conf. Ser.*, pages 24–25.

BIBLIOGRAPHY

- T. E. Woods, N. Ivanova, M. V. van der Sluys, et al., 2012. *ApJ*, 744:12.
- X.-J. Xu & X.-D. Li, 2010. *ApJ*, 716:114–121.
- K. Yakut & P. P. Eggleton, 2005. *ApJ*, 629:1055–1074.
- O. Yaron, D. Prialnik, M. M. Shara, et al., 2005. *ApJ*, 623:398–410.
- S.-C. Yoon, P. Podsiadlowski, & S. Rosswog, 2007. *MNRAS*, 380:933–948.
- D. G. York, J. Adelman, J. E. Anderson, Jr., et al., 2000. *AJ*, 120:1579–1587.
- L. R. Yungelson, 2005. In *White dwarfs: cosmological and galactic probes*, editors E. M. Sion, S. Vennes, & H. L. Shipman, volume 332 of *Astrophysics and Space Science Library*, pages 163–173.
- L. R. Yungelson, 2010. *Astronomy Letters*, 36:780–787.
- L. R. Yungelson & M. Livio, 2000. *ApJ*, 528:108–117.
- L. R. Yungelson, M. Livio, A. V. Tutukov, et al., 1994. *ApJ*, 420:336–340.
- L. R. Yungelson, A. V. Tutukov, & M. Livio, 1993. *ApJ*, 418:794.
- J.-P. Zahn, 1977. *A&A*, 57:383–394.
- M. Zorotovic, M. R. Schreiber, & B. T. Gänsicke, 2011a. *A&A*, 536:A42.
- M. Zorotovic, M. R. Schreiber, B. T. Gänsicke, et al., 2010. *A&A*, 520:A86+.
- M. Zorotovic, M. R. Schreiber, B. T. Gänsicke, et al., 2011b. *A&A*, 536:L3.

SUMMARY

This thesis presents several studies on the formation and evolution of compact binaries with white dwarf (WD) components. Although the evolution of low-mass single stars is fairly well understood, many questions remain about the processes involved in binary interactions. This thesis focuses on common-envelope evolution and the efficiency of mass accretion onto WDs. We study several populations of binary stars; detached binaries with a WD and a main-sequence star component, WDs accreting from non-degenerate companions, detached double white dwarf binaries, and merging double white dwarfs systems.

A method that is often applied in this thesis, is the modelling of the formation and evolution of binary populations with a binary population synthesis (BPS) code. BPS is a very useful method to study the macroscopic characteristics of a population of binaries and the processes that govern the evolution of a specific binary population. As part of this thesis, the BPS code SeBa [Portegies Zwart & Verbunt, 1996; Nelemans et al., 2001c] was thoroughly updated (see chapter 5 and 2).

Chapter 2: Common-envelope evolution

Crucially important for the formation of close binary systems with degenerate components is the common-envelope phase. However, despite of its importance, the phenomenon is not understood well. The uncertainty in common-envelope evolution is one of the major uncertainties in the predictions of binary population synthesis studies (see also chapter 3 and 5). In the second chapter of this thesis we study common-envelope evolution itself, by analysing the formation of post-common envelope binaries (PCEBs). PCEBs consisting of a WD and a main-sequence star in a detached binary. PCEBs are ideal to study common-envelope evolution as the evolution of the binary including its stellar components are relatively simple.

Using the BPS code SeBa, we simulated a population of PCEBs, with the novelty that we assume a realistic model of the Galaxy that takes into account the observational selection

SUMMARY

effects that are inherent to the PCEB sample. We find that for the main evolutionary path of PCEBs the CE-efficiency must be low, at which energy can be used to expel the envelope in the CE-phase. The main formation channel consists of a CE-phase caused by a red giant that fills its Roche lobe due to a dynamical instability. Other channels in which CE-phase is initiated by a star on the asymptotic giant branch or by a tidal instability can not be constrained with the current observations of PCEBs.

From previous BPS-studies and evolutionary reconstruction studies, a picture of CE-evolution is emerging that varies among types of binary systems (e.g. for different mass ratios and different types of stars evolved in the CE-phase). The first phase of mass transfer in progenitor systems of double white dwarfs (DWDs) leads to a modest widening of the orbit [Nelemans et al., 2000, 2001c]. These progenitors are thought to be of fairly equal mass. CE-evolution in binaries with low mass ratios and non-degenerate components leads to a strong contraction of the orbit [Chapter 2, Zorotovic et al., 2010]. However, CE-evolution in systems with low mass ratios and a WD component leads to a much less strong reduction of the orbital separation [such as in the second phase of mass transfer in the progenitors of DWD systems Nelemans et al., 2000].

Chapter 3: Mass retention efficiency of accreting white dwarfs

The third chapter of this thesis concern the supernova Type Ia (SNIa) progenitors from the single-degenerate (SD) channel, a WD accreting from a non-degenerate companion. According to various binary population synthesis studies, the theoretical rates of the single-degenerate channel are lower than those of the double-degenerate channel and the observed rates. However, the theoretical rates vary over four orders of magnitude [Nelemans et al., 2013].

We find that the efficiency of mass retention of an accreting WD is crucially important for the SD SNIa progenitor systems. However, it is poorly understood because of processes such as novae. Furthermore the assumptions for the mass retention efficiency vary strongly amongst different binary population synthesis codes [Ruiter et al., 2009b; Mennekens et al., 2010; Wang et al., 2010; Yungelson, 2010; Claeys et al., 2011]. We implemented different prescriptions for the mass retention efficiencies [Nomoto et al., 2007; Ruiter et al., 2009b; Yungelson, 2010] in SeBa and found that the SNIa rate is affected by a factor 3-4 up to more than a factor 100. In comparison the uncertainty in the common-envelope evolution affects the SD SNIa rate by a factor of about 0.7-3 [Chapter 3, Wang et al., 2010; Ruiter et al., 2009b; Mennekens et al., 2010; Claeys et al., 2011] and up to an order of magnitude for extreme changes in the CE-efficiency α (Claeys et al. in prep.). Furthermore, our SNIa models recover the trend in the predicted rates of different BPS studies. However, they do not fully explain the large disagreements between them. Other BPS assumptions play a

role as well, such as the stability of mass transfer and the evolution of the mass transfer rates.

Chapter 4: Mass transfer variability towards accreting white dwarfs

In the previous chapter we discussed the effect of the uncertainty in the WD retention efficiency on the predictions for the SD SNIa rate. In chapter 4 we study another possible source of uncertainty for the growth of WDs; mass transfer cycles. The canonical retention efficiencies are calculated under the assumption of a constant mass transfer rate, however, it is possible that accreting WD systems are influenced by effects that cause the mass transfer rate to fluctuate on various timescales.

We show that if long-term mass transfer variability is present in accreting WD systems, the regimes that allow for WD growth are enhanced. Long-term variability can be induced by irradiation of the donor star by the accreting WD or by cyclic variations of the Roche lobe from mass loss episodes [Knigge et al., 2011] for example. We find that there are both theoretical and observational support for long-term mass transfer variability in accreting WD binaries.

Mass transfer variability and subsequent enhanced retention efficiencies is likely to impact the properties of accreting WD binaries, such as cataclysmic variables and SNIa progenitors in the single-degenerate channel. WDs in cataclysmic variables are on average more massive than single WDs, however, an understanding of this phenomenon is lacking. Regarding SNIa progenitors, we included the effects of mass transfer variability in our BPS model, and found that the parameter space of WDs that evolve to SNIa events significantly widens. The effect, however, on the SNIa rate is modest, e.g. a factor of about 2-3 on the integrated rate. When mass transfer variability is included in our model, the synthetic SNIa rate is comparable with the lower limit of the observed rates [Maoz & Mannucci, 2012b; Perrett & et al., 2012; Maoz et al., 2012; Graur & Maoz, 2013]. Concluding, the theoretical SD SNIa rate is fairly uncertain, because the effective mass retention efficiency is strongly dependent on the details of the accretion process such as the mass transfer rate, and overall not understood well (see also chapter 3).

Chapter 5: Double white dwarf binaries as supernovae Type Ia progenitors

The fifth chapter of this thesis concerns the progenitors of supernovae Type Ia events from DWD mergers. Our goal is to predict the SNIa rate from the double-degenerate channel with a binary population synthesis approach. The difficulty is that the number of observed

SUMMARY

SNIa progenitors is too small to constrain our simulations. Fortunately, the population of observed DWDs (of all flavours and masses) can be used instead, because this population is closely related to the SNIa progenitors. In agreement with Nelemans et al. [2000] and Nelemans et al. [2001c], we find that our model using the α -CE prescription is not consistent with the observed DWD population, where as our model using the γ -CE prescription is.

Regarding SNIa progenitors, however, the difference between the models is modest. The time-integrated rate of SNIa event decreases by a factor of about 1.5 when assuming the γ -CE prescription instead of the α -prescription. The shapes of the delay-time distributions of both models match well with observations, however, the normalization is a factor of about 7-12 lower than the observed SNIa rates. The observed rates come from a variety of methods [for a review see Maoz & Mannucci, 2012a] in galaxy clusters.

After publication of chapter 5, new measurements from volumetric surveys were published [Perrett & et al., 2012; Maoz et al., 2012; Graur & Maoz, 2013]. These studies found SNIa rates that are a factor 1.5-5 lower than the previous studies. This diminishes the problem of too low SNIa rates predicted by our work. At this moment it is unclear if there is an enhancement of SNeIa in cluster galaxies or if the different observed integrated rates are due to systematic effects [see also Maoz et al., 2012].

Chapter 6: Binary population synthesis

The last chapter of this thesis describes the PopCORN project, which stand for population synthesis of compact objects research network. For this project we have collaborated with three other BPS research groups to compare the corresponding BPS codes. The goal is to investigate whether differences in the simulated populations are due to numerical effects, or whether they can be explained by differences in the input physics. The comparison focuses on the evolution of low- and intermediate-mass binaries containing one or more WDs. We show that when input assumptions are equalized, the simulated populations are very similar. The main differences between the results arise from deviating input assumptions for physical processes in binary evolution. The most important assumptions are the initial-final mass relation for WDs, the stability of mass transfer, survival of mass transfer, stable mass transfer and helium star evolution. Processes that were equalised between the code for this project and therefore not studied are a.o. the prescription for common-envelope evolution, accretion efficiency, angular momentum loss, magnetic braking and the initial distributions of primary mass, mass ratio and orbital separation. The processes on these two lists must be taken into account when interpreting BPS results, but should also motivate the astrophysics community to conduct further research into these topics.

It remains to conduct a BPS code comparison for the progenitors of systems in the single-degenerate channel to understand better the differences in the predicted SNIa rates (see also chapter 3) as well as for binary systems with massive components (e.g. the progenitors

of X-ray binaries) for which other processes are relevant such as rotation and stellar winds.

Conclusion

The PopCORN project (chapter 6) has brought forward two important results. Within the equalised assumptions of the project, differences in the predictions of macroscopic characteristics of a population are not caused by numerical effects or a lack of accuracy in the codes. However, the project has also pointed out (once again) the importance of the assumptions for binary processes that are not understood fully or not understood at all. In order to improve the results from BPS modelling, a better understanding of these assumptions is necessary and it is very important to take into account the uncertainty in the assumptions when making and interpreting BPS models.

The simplicity of the evolution of PCEBs makes the population of PCEBs ideal to study common-envelope evolution. By taking into account the observational selection effects, a direct comparison with observations could be made for the first time (see chapter 2). On the other hand the evolution of DWDs is more complicated. It can involve stable and unstable mass transfer and multiple phases of mass transfer (see chapter 5). In particular the evolution of DWD mergers as SNIa progenitors is hard to model, because this population is biased to the most massive WD progenitors whose evolution often involves a second, additional phase of mass transfer. This phase is initiated by a star when it is hydrogen-poor and helium-burning. Besides assumptions for binary evolution, other assumptions should be taken into account in the interpretation of results as well. An example is that often in BPS studies, a constant star formation rate is assumed for the Milky Way for simplicity. However, for SNIa progenitors from the double-degenerate channel, the synthetic rate is very sensitive to the recent star formation rate because the average delay time is short. Therefore, the rate can be overestimated significantly if a constant star formation rate for the full history of Milky Way is assumed (see chapter 5).

So far, BPS studies have been hampered by the low number of observed binaries of a specific population. However, over recent years a vast improvement has been made in this respect, in particular for DWDs and binaries containing hydrogen-poor helium burning stars (i.e. hot subdwarfs). The ELM survey [Brown et al., 2010] focuses on discovering and characterizing the population of extremely low-mass (ELM) WDs in the Milky Way and has found over 50 DWDs with ELM components [Brown et al., 2013]. Another survey that makes use of the Sloan Digital Sky Survey [York et al., 2000] is the SWARMS survey [Badenes et al., 2009; Mullally et al., 2009] which aims to find massive, close DWDs as possible progenitors of SNIa events. Furthermore, the ESO Supernova Ia Progenitor Survey (SPY) has increased the number of DWDs [Napiwotzki et al., 2001; Nelemans et al., 2005], as well as the number of subdwarfs [Lisker et al., 2005; Stroeger et al., 2007]. Regarding subdwarfs, their observed number has increased further by a.o. MUCHFUSS [Geier et al.,

SUMMARY

2011] which aims at finding hot subdwarfs with compact companions like massive WDs, neutron stars or black holes.

Large samples, but most importantly homogeneous samples, are fundamental for testing and constraining the BPS models. An example of this is the population of DWDs, with which common-envelope evolution can be studied. The observed mass ratio distribution of DWDs lead Nelemans et al. [2000] to propose the γ -prescription, however, the γ -prescription does not reproduce the visible population of PCEBs well. Woods et al. [2012] suggested that DWDs can be created by stable mass transfer between a red giant and a main-sequence star. It is not clear yet if this channel is wide enough to create a significant amount of DWDs. However, if this is the case, we can study the effect of stable, non-conservative mass transfer and the corresponding mass and angular momentum loss. Regarding the ELM WD binaries, these have not been studied yet in a binary population synthesis approach, and at the moment it is not clear if BPS results are in contradiction with the large amount of observed ELM binaries.

Traditionally BPS studies have focused on predicting and comparing population sizes (e.g. space densities, merger rates) and population characteristics (e.g. distribution of periods, masses, mass ratios) of a specific population. However, due to the increase in the observed number of binaries of multiple populations, BPS studies can start conducting comparisons between populations (e.g. relative population sizes). For example, comparing the populations of subdwarf binaries, DWDs and PCEBs can lead to a more complete picture of common-envelope evolution across binary types (see also chapter 2).

In conclusion, because of the advent of large scale surveys such as the Sloan Digital Sky Survey or in the future Gaia [de Bruijne, 2012], it is an excellent moment to conduct BPS studies. The surveys are providing us with an unprecedented number of binaries, and most importantly homogeneously selected binaries that can help us to improve our understanding of binary evolution.

SAMENVATTING

Als je 's avonds omhoog kijkt naar de hemel, kun je ze zien: sterren. Daar heb je wel een beetje geluk voor nodig, want het weer moet meezitten. Met nog meer geluk kun je ook de maan zien of een paar planeten. In ons zonnestelsel is er een ster, de zon, en acht planeten die om de zon heen draaien. De meeste sterren brengen hun leven echter niet in hun eentje door, maar ze hebben andere sterren als nabije burens. Sterstelsels bestaan vaak uit twee sterren zoals bij een dubbelster, maar stelsels met meerdere sterren zijn ook bekend [Duchêne & Kraus, 2013]. In dit proefschrift bestuderen we de evolutie van dubbelstelsels.

Introductie

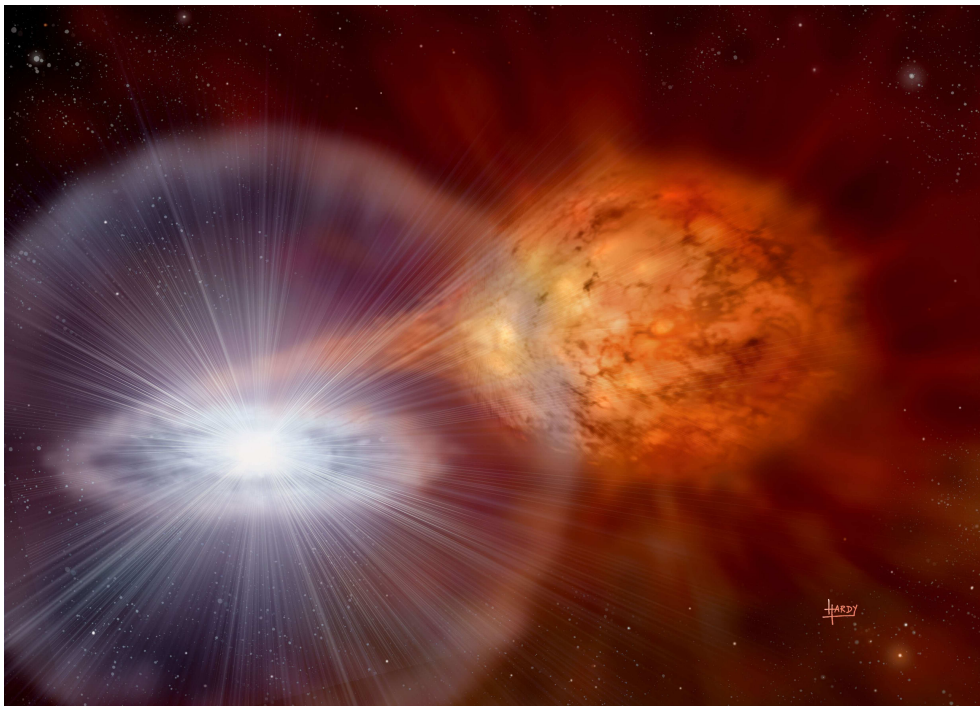
Het leven van een ster...

Sterren komen voor in veel verschillende soorten en maten. De zon is een tamelijk standaard ster met een massa van $1.98 \cdot 10^{30}$ kg. Dit wordt ook wel een zonsmassa genoemd: $1M_{\odot}$. Er bestaan sterren met een massa van 10% van de zon ($0.1M_{\odot}$) tot meer dan 100 keer de massa van de zon ($>100M_{\odot}$). De simpelste beschrijving voor een ster is een bol van gas dat in evenwicht is. De zwaartekracht duwt de materie van de ster naar het midden van de ster, terwijl de gasdruk de materie naar buiten duwt de ruimte in. Als gevolg van dit evenwicht, heeft de ster een hoge dichtheid en hoge temperatuur. De temperatuur wordt gehandhaafd door de productie van energie binnenin de ster. De belangrijkste bron van energie in een ster is kernenergie. Bij het fuseren van twee atoomkernen wordt een zwaardere kern gevormd, maar er komt daarnaast ook een grote hoeveelheid energie vrij. Energieverlies aan het oppervlak van een ster is wat wij zien als het licht van sterren.

Als sterren ouder worden, verandert de evenwichtspositie langzaam (maar in sommige fasen snel). Op de lange termijn wordt de evolutie van een ster gedreven door verschillende fasen van kernfusie. Aanvankelijk bestaan sterren voornamelijk uit waterstof. In de kern

SAMENVATTING

wordt waterstof gefuseerd tot helium, en om de kern zit een omhulsel van waterstof. Deze sterren worden hoofdrekssterren (main-sequence, MS) genoemd. Als de brandstof in de kern op is, krimpt de kern. Als de dichtheid en temperatuur in de kern voldoende groot worden, dan zal helium gefuseerd worden tot koolstof en zuurstof. In elk mogelijk later stadium worden steeds zwaardere elementen geproduceerd. De structuur van een ster lijkt op die van een ui (of Shrek); een kern met lagen materie daarom heen. Hoe dieper de laag in de ster ligt, hoe meer zwaardere elementen in de laag te vinden zijn. De meeste sterren eindigen hun leven wanneer kernfusie niet meer kan optreden. Deze objecten krimpen en koelen dan verder, totdat er nieuw evenwicht is gevonden. Bij dit evenwicht neemt een kwantummechanische druk ('ontaarding') de rol van de gasdruk over. Het object is nu ongeveer 50 tot 100 keer kleiner dan bij zijn geboorte. Deze uitgebrande sterren worden witte dwergen genoemd.



FIGUUR 1: Dubbelstersysteem bestaande uit een ster (rechts) die massa overdraagt naar een witte dwerg (links). De stroom van materie vormt een schijf om de witte dwerg. Er heeft zonet een nova-explosie plaats gevonden op de witte dwerg. Hierdoor wordt materie van het oppervlak van de witte dwerg afgeblazen, en dit kun je nog zien als de bol om de witte dwerg. (credits: David A. Hardy, www.astroart.org)

.. met zijn tweeën

Als twee sterren deel uit maken van een dubbelstersysteem, draaien ze een baan om elkaar heen. Als de sterren dicht genoeg bij elkaar staan, vindt er interactie plaats tussen de

sterren. Hierdoor verandert de evolutie van het systeem en de twee sterren. Een voorbeeld van een interactie is massa-overdracht (zie figuur 1). Hierbij stroomt er materie van een ster (de donor) naar de andere ster (de begeleider). Als gevolg van de massa-overdracht kan het systeem samensmelten; je houdt dan een enkele ster over. Maar als het dubbelstersysteem blijft bestaan, is de donor vaak zijn omhulsel verloren. Hierdoor wordt de evolutie van de donor beëindigd (een witte dwerg wordt gevormd) of op z'n minst aanzienlijk verkort (er is minder brandstof). De begeleider kan alle materie accreteren die wordt overgedragen, of alleen een gedeelte ervan, of zelfs helemaal geen materie. In de laatste twee gevallen verliest het dubbelstersysteem materie.

Alhoewel de evolutie van enkele sterren zoals de zon redelijk goed begrepen wordt, zijn er nog veel vragen over processen in dubbelsterevolutie. Dit proefschrift richt zich op twee belangrijke processen die, afhankelijk van je humeur, niet volledig of volledig niet begrepen worden. Deze twee processen zijn accretie op witte dwergen en instabiele massa-overdracht.

- Accretie op witte dwergen;

Accretie op witte dwergen is een ingewikkeld proces. Het hoeft niet zo te zijn dat de geaccreteerde materie ook daadwerkelijk op de witte dwerg zal blijven liggen. In eerste instantie wordt de geaccreteerde materie snel verspreid over het oppervlak van de witte dwerg. Afhankelijk van de snelheid van de massa-overdracht, kan er kernfusie optreden in de geaccreteerde laag [Nomoto, 1982; Nomoto et al., 2007; Shen & Bildsten, 2007], zowel op een stabiele [Whelan & Iben, 1973; Nomoto, 1982] als instabiele manier [Schatzman, 1950; Starrfield et al., 1974]. Bij lage snelheden hoopt de materie zich op op het oppervlak. Wanneer kernfusie begint, verspreidt de verbranding zich vliegensvlug door de laag. Zulke uitbarstingen worden novae genoemd, wat 'nieuwe sterren' betekent (zie figuur 1). Tijdens zo'n uitbarsting wordt een gedeelte of zelfs alle geaccreteerde materie door de witte dwerg uitgestoten en het is zelfs mogelijk dat oppervlaktemateriaal van de witte dwerg verloren wordt [Priyalnik, 1986; Priyalnik & Kovetz, 1995; Townsley & Bildsten, 2004; Yaron et al., 2005]. Bij hoge snelheden van de massa-overdracht vindt er continue kernfusie plaats op het oppervlak van de witte dwerg. Dit soort dubbelsterren zendt röntgenstraling uit. Bij nog hogere snelheden vormt de materie een omhulsel rondom de witte dwerg. Een wind kan vervolgens een gedeelte van het omhulsel van de witte dwerg afstoten.

Samenvattend, een witte dwerg kan alleen groeien in massa wanneer de accretie plaatsvindt binnen een relatief klein bereik van massaoverdrachtssnelheden. Bovendien brengt accretie op witte dwergen verschillende fascinerende tafereelen teweeg, zoals röntgenstraling en nova-uitbarstingen.

- Massa-overdracht;

Als de massa-overdracht op een stabiele manier verloopt [Webbink, 1985; Hjellming & Webbink, 1987; Pols & Marinus, 1994; Soberman et al., 1997], dan blijft de donor

SAMENVATTING

(qua druk) in evenwicht. De interne structuur van de ster wordt aangepast aan een de nieuwe massa en bijbehorende nieuwe druk, dichtheid en temperatuur. De baan van de twee sterren verandert ten gevolge van de herschikking (of het verlies) van massa en draaimoment. Vaak zijn de banen wijder na de massa-overdracht.

Bij instabiele massa-overdracht neemt de snelheid van de massa-overdracht snel toe als een op hol geslagen paard. Het omhulsel van de donor zal ook de begeleider omhullen, zodat het dubbelstersysteem een gezamenlijk omhulsel heeft [common-envelope, CE Paczynski, 1976; Webbink, 1984]. In hun baan om elkaar gaan de begeleider en de kern van de donor nu door een dichte mist van materie. Hierdoor ondervinden ze veel wrijving, waardoor ze snelheid verliezen en hun baan steeds kleiner wordt. Instabiele massa-overdracht leidt dan ook vaak tot een samensmelting van de twee sterren. Echter als door de wrijving het gezamenlijke omhulsel voldoende energie wint om aan het systeem te ontsnappen, kan een samensmelting worden voorkomen. Wat overblijft is een compacte dubbelster. Instabiele massa-overdracht speelt een essentiële rol in de vorming van vele soorten compacte dubbelsterren en daarmee ook in dit proefschrift.



FIGUUR 2: Sterrenstelsel NGC 4526 en supernova 1994D. Supernova 1994D was een supernova van type Ia, die plaatsvond aan de rand van het sterrenstelsel. De supernova is ongeveer even helder als het centrum van het sterrenstelsel. Deze foto is gemaakt door de Hubble Space Telescope. (credits: NASA/ESA, The Hubble Key Project Team en The High-Z Supernova Search Team)

Supernovae van type Ia

Supernovae spelen een essentiële rol in dit proefschrift. Het zijn een van de meest energieke en explosieve gebeurtenissen in het heelal. Voor een korte tijd is een enkele supernova intens helder. Ze zijn dan helderder dan sterrenstelsels zoals onze Melkweg, die bestaan uit honderden miljarden sterren (zie figuur 2). De helderheid van supernovae maakt het mogelijk om supernovae waar te nemen op grote afstand van de Aarde.

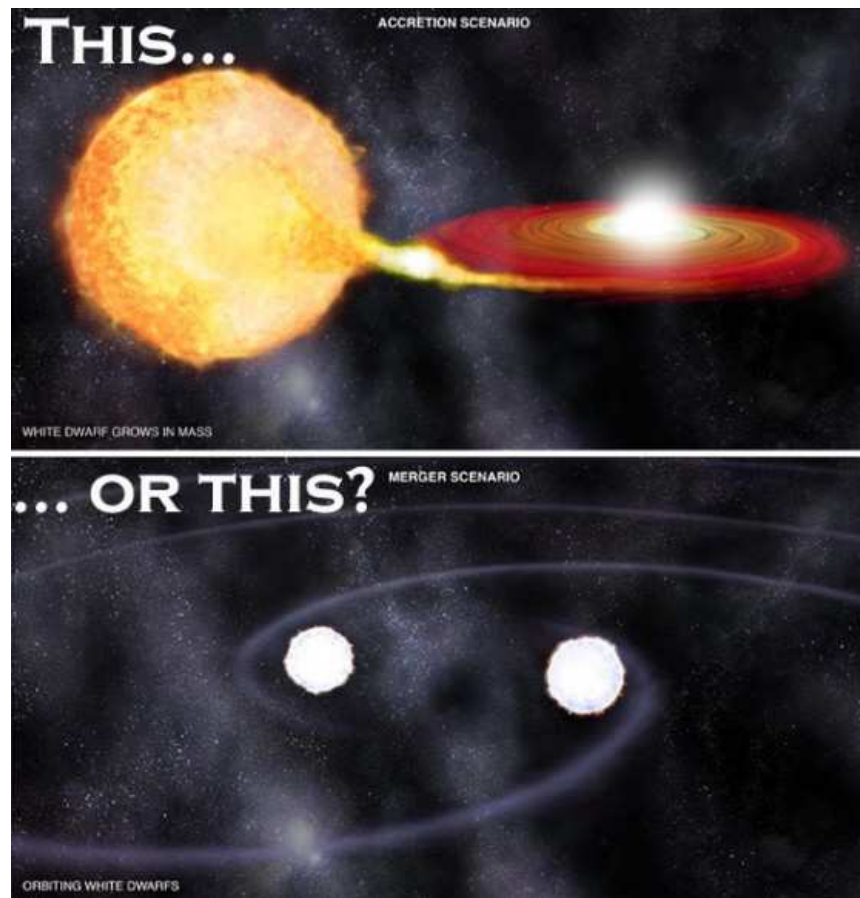
Een specifiek soort supernova, type Ia, heeft een bijzondere eigenschap. De helderheid van een supernova van type Ia verandert in de tijd op een specifieke manier [Phillips, 1993]. Hierdoor kunnen we schatten hoe ver weg een supernova staat. Als een supernova verder weg staat, lijkt de supernova minder helder. Het bepalen van afstanden in het heelal is lastig, en daarom spelen supernovae van type Ia een belangrijke rol in de extragalactische sterrenkunde. Het meest belangrijke resultaat (in ieder geval in mijn ogen) is dat het heelal versneld uitdijt [bv Riess et al., 1998; Perlmutter et al., 1999]. Supernovae van type Ia spelen ook een belangrijke rol in galactische sterrenkunde, vanwege het uitstoten van zware elementen zoals ijzer.

Ondanks het grote belang van supernovae van type Ia, worden ze theoretisch nog slecht begrepen. Over het algemeen wordt aangenomen dat een supernova van type Ia een exploderende witte dwerg is. Wanneer kernfusie plaatsvindt in een witte dwerg, komt er in een korte tijd zoveel energie vrij, dat de witte dwerg binnen de kortste keren explodeert. De details van het ontbrandingsmechanisme worden nog slecht begrepen en meerdere evolutiepaden zijn voorgesteld om de fusie aan de gang te brengen. De klassieke evolutiepaden (zie figuur 3) hebben te maken met de maximale massa van een witte dwerg. Dit heet de Chandrasekhar massa en is ongeveer 1,4 keer de massa van de zon. Als de witte dwerg massiever wordt, raakt de ster uit evenwicht; de zwaartekracht wint dan van de ontappingsdruk.

In het eerste klassieke evolutiepad [single degenerate model, SD, Whelan & Iben, 1973] accreteert een koolstof-zuurstof witte dwerg materie van de andere ster in het dubbelsterstelsel. Als de massa van de witte dwerg $\sim 1,4M_{\odot}$ bereikt, wordt aangenomen dat een supernova van type Ia plaatsvindt. In het tweede klassieke evolutiepad [double degenerate model, DD, Webbink, 1984; Iben & Tutukov, 1984] smelten twee witte dwergen, bestaande uit koolstof en zuurstof, samen. Als de gezamenlijke massa van de witte dwerg groter is dan $\sim 1,4M_{\odot}$, vindt wederom de supernova-explosie plaats.

Dit proefschrift

In dit proefschrift worden verschillende studies gepresenteerd over de vorming en evolutie van compacte dubbelsterren. Waarnemingen van een bepaalde groep van dubbelsterren geven ons informatie over de eigenschappen van deze dubbelsterpopulatie, zoals de verdeling van de periode van hun baan of de massaverhouding van de twee sterren. Deze



FIGUUR 3: De twee klassieke evolutiekanalen voor supernovae van type Ia. Boven geeft het scenario weer waarin een witte dwerg materie accreteert van een ster, en onder het scenario waarin twee witte dwergen samensmelten. (credits: Bad Astronomy/Discovery).

eigenschappen worden bepaald door de processen die de dubbelsterpopulatie ondergaan is. Door de eigenschappen te bestuderen, kunnen we processen bestuderen die (nog) niet in detail gesimuleerd of waargenomen kunnen worden.

We maken daarvoor gebruik van het software pakket SeBa⁶. SeBa is een computerprogramma dat de evolutie van dubbelsterren van geboorte tot aan sterfte kan simuleren. Vanwege de snelheid van SeBa, is SeBa uitermate geschikt om de eigenschappen van populaties van stersystemen te bestuderen. Computerprogramma's zoals SeBa worden dubbelsterpopulatie-synthese codes (binary population synthesis, BPS) genoemd.

In dit proefschrift richten we ons op twee processen in het bijzonder: instabiele massa-overdracht en accretie op witte dwergen. Deze processen zijn van belang in dubbelsterren waarvan een of twee van de componenten witte dwergen zijn. De soorten dubbelsterren die we bestuderen in dit proefschrift zijn:

⁶De naam SeBa is afgeleid van een Egyptisch woord voor 'onderwijzen', 'de poort naar kennis' of '(dubbel)ster' [Portegies Zwart, 2000]. De exacte betekenis ligt aan de spelling van de hiërogliefen.

- dubbelsterren met een witte dwerg en een hoofdreeksster, die een fase van instabiele massa-overdracht zijn ondergaan (post-common-envelope binaries, PCEBs);
- dubbelsterren met een witte dwerg en een begeleider, waarbij de begeleider massa overdraagt naar de witte dwerg totdat een supernova van type Ia plaatsvindt;
- dubbelsterren met twee witte dwergen die zodanig samensmelten dat een supernova van type Ia plaatsvindt.

Hoofdstuk 2: Instabiele massa-overdracht

Instabiele massa-overdracht is een van de meest belangrijke processen in dubbelsterevolutie. Veel dubbelsterren die we waarnemen hebben tenminste een zo'n fase gehad in hun evolutie. Tegelijkertijd is instabiele massa-overdracht een van de minst begrepen processen in dubbelsterevolutie. In welke systemen leidt instabiele massa-overdracht to een samensmelting en welke systemen overleven als dubbelster? Hoe verandert de baan van een dubbelster als gevolg van instabiele massa-overdracht? Krimpt de baan sterk? Dit heeft een gevolg op de verdere evolutie van het systeem. De onzekerheid in het verloop van instabiele massa-overdracht veroorzaakt een van de grootste onzekerheden in de voorspellingen van dubbelsterpopulatie-synthese codes (zie ook hoofdstuk 3 en 5).

In het eerste hoofdstuk bestuderen we het proces van instabiele massa-overdracht door de vorming van PCEBs te bestuderen. PCEBs zijn dubbelsterren die bestaan uit een witte dwerg en een hoofdreeksster en die in hun vorming door een fase van instabiele massa-overdracht zijn gegaan. Deze systemen zijn ideaal om instabiele massa-overdracht te bestuderen omdat de evolutie van de systemen relatief eenvoudig is.

Met behulp van SeBa hebben we een populatie van PCEBs gesimuleerd. Het vernieuwende aan dit model is dat voor het eerst een realistisch model voor de Melkweg is aangenomen. Bovendien houden we rekening met observationele selectie-effecten. Het probleem is dat een hoofdreeksster vaak veel helderder is dan een witte dwerg, zodat de meeste PCEBs niet als zodanig waargenomen zouden worden, maar als een enkele hoofdreeksster.

Wij vinden dat de instabiele massa-overdrachtsfase voor de meeste PCEBs moet leiden tot een sterke krimp van de baan, in tegenstelling tot eerdere studies over de vorming van dubbele witte dwergen [Nelemans et al., 2000, 2001c]. De waargenomen dubbele witte dwergen zijn door twee fases van instabiele massa-overdracht gegaan. De laatste keer krimpt de baan, maar veel minder sterk van bij PCEBs. De eerste keer kan de baan zelfs een beetje uitzetten. Hieruit moeten we opmaken dat de standaard, uniforme beschrijving van instabiele massa-overdracht voor meerdere typen dubbelsterren niet werkt.

Hoofdstuk 3: Hoe efficiënt kan een witte dwerg groeien door accretie?

Er zijn twee klassieke evolutiepaden voor een supernova van type Ia (zie figuur 3). In het ene pad accreteert een witte dwerg van een begeleidende ster, en in het andere pad smelten twee dubbele witte dwergen samen (zie ook de introductie). Voor beide evolutiepaden is de vraag, kun je wel echt een supernova van type Ia vormen via deze weg, en zo ja hoeveel supernovae dan? BPS studies voorspellen dat het aantal supernovae van het eerste evolutiepad lager ligt dan die van het andere evolutiepad. De voorspellingen voor het eerste evolutiepad liggen echter ver uit elkaar, maximaal ongeveer een factor 1000 [Nelemans et al., 2013].

Wij vinden dat theoretisch voorspellingen voor het aantal supernovae type Ia cruciaal afhangen van hoe efficiënt een witte dwerg kan accreteren. Accretie naar witte dwergen is een ingewikkeld proces, vanwege nova-uitbarstingen en kernfusie van het geaccreteerde materiaal. De aannames voor de accretie-efficiëntie verschillen dan ook sterk tussen BPS codes [Ruiter et al., 2009b; Mennekens et al., 2010; Wang et al., 2010; Yungelson, 2010; Claeys et al., 2011]. Om te onderzoeken hoe sterk het effect is van de verschillende efficiënties op het aantal supernovae, hebben we drie verschillende efficiënties [Nomoto et al., 2007; Ruiter et al., 2009b; Yungelson, 2010] geïmplementeerd in SeBa. Afhankelijk van de aangenomen efficiënties, verschilt het totale aantal supernovae met een factor 3 tot 4, of zelfs meer dan een factor 100. De onzekerheid in de instabiele massa-overdrachtsfase leidt slechts tot een onzekerheid in het aantal supernovae van een factor 0,7 tot 3, en tot maximaal een factor 10 voor extreme veranderingen [Wang et al., 2010; Ruiter et al., 2009b; Mennekens et al., 2010; Claeys et al., 2011, dit proefschrift, Claeys et al. in prep]. De trend in onze modellen komt overeen met de trend in de voorspellingen van andere codes. Van de andere kant kunnen de modellen de verschillen in de voorspellingen niet volledig verklaren. Dat betekent dat naast de accretie-efficiëntie ook andere processen een rol spelen, zoals bijvoorbeeld de stabiliteit van massa-overdracht. Ons onderzoek heeft aangetoond dat de efficiëntie van accretie naar witte dwergen van fundamenteel belang is voor het begrijpen van de bijdrage van dit evolutiepad aan het totale aantal supernovae van type Ia.

Hoofdstuk 4: Variabiliteit van de snelheid van massa-overdracht naar witte dwergen

In het vorige hoofdstuk hebben we laten zien dat de efficiëntie van accretie naar witte dwergen vrij onzeker is, en dat deze onzekerheid doorwerkt in de onzekerheid op het aantal supernovae van type Ia. In dit hoofdstuk bespreken we nog een andere bron van onzekerheid voor de groei van witte dwergen. De klassieke accretie-efficiënties gaan namelijk uit van een constante snelheid van de massa-overdracht, maar het is mogelijk dat de snelheid schommelt op verschillende tijdschalen.

We laten zien dat als de schommeling plaatsvindt op een lange tijdschaal, de witte dwerg efficiënter kan groeien in massa. Het bereik van snelheden van de massa-overdracht waarin een witte dwerg efficiënt kan groeien is groter in het nieuwe model. Dit beïnvloedt verschillende soorten dubbelsterren, maar natuurlijk ook de systemen die tot een supernova van type Ia kunnen leiden in het eerste klassieke evolutiepad. In het nieuwe model is het evolutiepad veel wijder, maar er komen relatief maar weinig dubbelsterren terecht op dit pad. Als rekening gehouden wordt met de variabiliteit in de snelheid van de massa-overdracht, neemt het totale aantal supernovae van type Ia toe met een factor 2 tot 3. Kort samengevat, omdat de accretie-efficiëntie sterk afhankelijk is van de details van de massa-overdracht en over het algemeen niet goed begrepen wordt, is het theoretische aantal supernovae van type Ia van dit evolutiepad tamelijk onzeker.

Hoofdstuk 5: Supernovae van type Ia veroorzaakt door samensmeltende dubbele witte dwergen

Het doel van dit hoofdstuk was om een voorspelling te maken voor het aantal supernovae van type Ia per jaar van samensmeltende dubbele witte dwergen. Is dit klassieke evolutiepad een belangrijke manier om supernovae van type Ia te vormen? Om nauwkeurige voorspellingen te kunnen doen, is het belangrijk dat onze modellen overeenkomen met de waargenomen populatie van dubbele witte dwergen die op het punt staan samen te smelten. Voorspellen we de juiste massa's en periodes voor deze dubbelsterren? Het probleem is dat er nog geen systemen waargenomen zijn waarvan we verwachten dat bij het samensmelten een supernova ontstaat.

In hoofdstuk 5 hebben wij onderzocht of onze modellen overeenkomen met de gehele waargenomen populatie van dubbele witte dwergen. Alhoewel deze systemen geen supernovae van type Ia zullen vormen, is hun evolutie wel heel vergelijkbaar met die systemen die wel deel uit maken van het klassieke evolutiepad. In overeenstemming met Nelemans et al. [2000] en Nelemans et al. [2001c], vinden we dat de standaard manier om een instabiele massa-overdracht te simuleren, een populatie geeft die niet in overeenstemming is met de waargenomen dubbele witte dwergen. De alternatieve beschrijving voor instabiele massa-overdracht van Nelemans et al. [2000] geeft een populatie die wel in overeenstemming is met de waargenomen populatie.

De verschillen tussen het aantal supernovae van type Ia per jaar voor de twee beschrijvingen zijn gering. Het totale aantal supernovae van type Ia is 1,5 keer lager wanneer de alternatieve beschrijving aangenomen wordt. Aan de andere kant, de consensus op het moment van publicatie van hoofdstuk 5 was dat het waargenomen aantal supernovae hoger lag, ongeveer tien keer zo hoog [voor een overzicht zie Maoz & Mannucci, 2012a]. Hieruit zou je de conclusie trekken, dat het klassieke evolutiepad van samensmeltende witte dwergen niet het dominante evolutiepad voor supernovae van type Ia is. Echter, na de publicatie zijn nieuwe waarnemingen gepubliceerd. Deze artikelen vinden een aantal supernovae dat

1,5 tot 5 keer [Perrett & et al., 2012; Maoz et al., 2012; Graur & Maoz, 2013] lager ligt dan bij de oude waarnemingen. Op dit moment is het onduidelijk of dit verschil in de waarnemingen wordt veroorzaakt door verschillen tussen types van sterrenstelsels, of door een systematisch effect in de analyse.

Hoofdstuk 6: Het simuleren van dubbelsterpopulaties

In het laatste hoofdstuk van mijn proefschrift wordt het PopCORN project beschreven. PopCORN staat voor 'population synthesis of compact objects research network', ofwel 'onderzoeksverband voor het simuleren van populaties met compacte sterren'. Voor dit project hebben we samengewerkt met drie andere onderzoeksgroepen die BPS studies verrichten met hun eigen BPS codes. We hebben gekeken naar dubbelsterren met een of twee witte dwergen. Het doel was om de codes te vergelijken en de verschillen in de voorspellingen van de onderzoeksgroepen te begrijpen. Worden deze verschillen veroorzaakt door verschillen in de aannames in de fysica van dubbelsterevolutie, of door numerieke effecten (doen de codes hun berekeningen wel precies genoeg)?

Als eerste stap hebben we met vier BPS codes dezelfde dubbelsterpopulaties gesimuleerd en vergeleken met elkaar. Voor deze simulaties hebben we de initiële aannames zoveel mogelijk gelijk gesteld. Wij vonden dat de gesimuleerde populaties erg vergelijkbaar zijn. De belangrijkste verschillen tussen de gesimuleerde populaties worden veroorzaakt door afwijkende aannames voor bepaalde processen in dubbelsterevolutie die nog niet goed begrepen worden. Een voorbeeld hiervan is de stabiliteit van massa-overdracht. Een volgende stap voor het project zou zijn om te onderzoeken of en wat voor effect de gelijkgestelde initiële aannames hebben op dubbelsterpopulaties. Het is belangrijk om rekening te houden met de aannames van beide groepen bij het interpreteren van de resultaten en voorspellingen van BPS studies. Wij hopen ook de sterrenkundige gemeenschap te motiveren om de processen achter deze aannames verder te bestuderen.

CURRICULUM VITÆ

I was born on the the 31st of May 1984 in the 'Radboud ziekenhuis' (UMC St. Radboud) in Nijmegen. I attended primary school in Nieuw-Bergen at the 'Klimop' school and secondary school at the 'Elzendaelcollege' in Boxmeer. In 2002, I moved to Leiden to study Astronomy at Leiden University. The Bachelor research project, I did together with Caroline Bovée on the age, metallicity, and mass-to-light ratio of early-type galaxies. We worked with Jesus Falcón Barroso and Michele Cappellari in the group of Tim de Zeeuw. I enjoyed the Bachelor in astronomy very much, and continued in Leiden with a Master in astronomy. I received my M.Sc. cum laude.

For the major research project of the Master program, I worked again with Jesus Falcón Barroso and Tim de Zeeuw as well as John Beckman, Kambiz Fathi, and Anne-Marie Weijmans. The project was about the kinematics of the ionized gas in NGC 6946 from measurements with a Fabry-Pérot interferometer. At my initiative, part of this project was performed at the Instituto de Astrofísica de Canarias in La Laguna, Tenerife, Spain. The results of the project were later published in the *Astrophysical Journal*.

After working in the field of observational astronomy, I wanted to gain experience in the field of theoretical astrophysics. For the minor research project, I worked on the stochastic gravitational wave background from star-massive black hole fly-bys in the LISA frequency band with Clovis Hopman and Marc Freitag. This project resulted in my first first-author publication.

During my studies, I was also involved in preparation trainings for highschool students as head teacher and assistant-teacher in mathematics. The courses have been set up to help high school students prepare for their final exams to the best of their abilities.

In 2008, I moved to Nijmegen to take up a Ph.D. position at the Radboud University under the supervision of Gijs Nelemans. The first part of my PhD focused on updating the extensive software package SeBa. SeBa can be used to model the formation and evolution of binary populations. In the second part, we studied several populations of binaries with white dwarf components, and the physical processes that are relevant for these populations.

CURRICULUM VITÆ

We have used SeBa to test our hypotheses. Furthermore I have lead a collaboration of four BPS research groups on the comparison of the respective binary population synthesis codes. The results of these projects have been presented at conferences in Munich (Germany), Kraków (Poland), Noordwijkerhout (The Netherlands), Padua (Italy), Tübingen (Germany), Mykonos (Greece) etc. and can be found in this thesis.

I have very much enjoyed doing research, as well as the scientific collaborations and discussions, conference visits, contributions to astronomy education and public outreach. I have been an academic teaching assistant for several courses and co-supervised an undergraduate and a graduate student in their research projects. In the latter case, the project lead to a publication (see chapter 3). Public outreach has consisted of guided telescope tours and lectures at public observing nights, university open days, associations for weather and astronomy etc.

In 2011, I was awarded a Frye Stipend 2011 for talented female PhD candidates at the Radboud University Nijmegen. This award gave me the opportunity to visit the Department of Physics at the University of Warwick (United Kingdom) for a ten week internship. I collaborated with Boris Gänsicke amongst others.

I will start a postdoctoral position with Simon Portegies Zwart at Leiden Observatory, Leiden University to work on simulating star cluster formation with the Astrophysical Multipurpose Software Environment (AMUSE).

LIST OF PUBLICATIONS

Published

- The effect of common-envelope evolution on the visible population of post-common-envelope binaries
Toonen, S., Nelemans, G., accepted in A&A
- Population synthesis of ultracompact X-ray binaries in the Galactic bulge
van Haften, L. M., Nelemans, G., Voss, R., Toonen, S., Portegies Zwart, S. F., Yungelson, L. R., van der Sluys, M. V., 2013, A&A, 552, 69
- Single degenerate supernova type Ia progenitors. Studying the influence of different mass retention efficiencies
Bours, M. C. P., Toonen, S., Nelemans, G., 2013, A&A, 552, 24
- Supernova Type Ia progenitors from merging double white dwarfs. Using a new population synthesis model
Toonen, S., Nelemans, G., Portegies Zwart, S.F., 2012, A&A, 546, 70
- The gravitational wave background from star-massive black hole fly-bys
Toonen, S., Hopman, C., Freitag, M., 2009, MNRAS, 398, 1228
- Quantifying Resonant Structure in NGC 6946 from Two-dimensional Kinematics
Fathi, K., Toonen, S., Falcón-Barroso, J., Beckman, J. E., Hernandez, O., Daigle, O., Carignan, C., de Zeeuw, P. T., 2007, ApJ, 667, 137

Submitted

- PopCORN: Hunting down the differences between binary population synthesis codes
Toonen, S., Claeys, J.S.W., Mennekens, N., Ruiter, A.J.R., submitted to A&A

LIST OF PUBLICATIONS

- On Double degenerate type Ia supernova progenitors as supersoft X-ray sources: A population synthesis analysis using SeBa
Nielsen, M.T.B., Nelemans, G., Voss, R., Toonen, S., submitted to A&A
- Enhanced growth of white dwarfs caused by mass-transfer variability
Toonen, S., Voss, R., Knigge, C., will be submitted to MNRAS

Proceedings

- Binary population synthesis and SNIa rates
Toonen, S., Nelemans, G., Bours, M., Portegies Zwart, S. F., 2013, arXiv, 1302, 0837
- Progenitors of Supernovae Type Ia
Toonen, S., Nelemans, G., Bours, M., Portegies Zwart, S.F., Claeys, J.S.W., Mennekens, N., Ruiter, A.J.R., 2013, ArXiv, 1302, 0495
- Double White Dwarf Merger Rates
Toonen, S., Nelemans, G., Portegies Zwart, S.F., 2013, IAUS, 281, 223
- Single Degenerate Progenitors of Type Ia Supernovae
Bours, M., Toonen, S., Nelemans, G., 2013, IAUS, 281, 248
- Theoretical Delay Time Distributions
Nelemans, G., Toonen, S., Bours, M., 2013, IAUS, 281, 225
- POPCORN: A comparison of binary population synthesis codes
Claeys, J. S. W.; Toonen, S.; Mennekens, N., 2012, arXiv, 1211, 0809
- A New Population Synthesis Model: Preliminary Results for Close Double White Dwarf Populations
Toonen, S., Nelemans, G., Portegies Zwart, S. F., 2010, AIPC, 1314, 266
- New population synthesis model: Preliminary results for close double white dwarf populations
Toonen, S., Nelemans, G., Portegies Zwart, S. F., 2010, AIPC, 1273, 283
- The Pattern Speeds of NGC 6946
Toonen, S., Fathi, K., Falcón-Barroso, J., Beckman, J. E., de Zeeuw, P. T., 2008, ASPC, 390, 322

ACKNOWLEDGEMENTS

Last but not least, I would like to express my thanks to all those who contributed to the realization of this thesis. I am very grateful and honoured for all the help, love, care, friendship, patience, support, and listening ears that I have received over the years. There are a few people I would like to thank in particular.

I am very grateful to my supervisor Gijs. Gijs, it was a great pleasure to work together with you. Your schedule is busy, but you always made time to answer my questions. How long is our list of possible things to further improve in SeBa? I have learned a lot from you, about the evolution of binary systems, and also about project management, but also about life in general. You once gave some advice⁷ at a tough moment, that I appreciate very much:

‘Some you win, some you loose.

If you focus on the ones you loose, you never get anywhere.’

Furthermore, I owe many thanks to Joke. Your dedication, joy and interest in binary physics, have made it a pleasure to collaborate with you. We must have driven each others office mates crazy by coming by so often to each others desks with questions. But we succeeded and together with Ashley and Nicki and all others involved we finished the PopCORN project!

Thanks to Rasmus, Marc and Evert for your patience and interest in questions when I was confused about any process in binary evolution. I appreciate that your door was always open. I also want to thank Pim, Martin and Wim for the computer support you have given me. I have learned a lot from you, and without you I would still be installing software. Thank you Kars, for listening to and answering all my questions about surveys and properties of observed binaries. Your resilience to stress is legendary and an example for me. Lastly, I want to thank my office mates and everyone at the department for the

⁷though I take it the quote originally comes from Jan Kuijpers

ACKNOWLEDGEMENTS

nice atmosphere at lunchtime, coffee breaks, cake breaks, Friday night drinks etc. Even if sometimes the number of cake breaks in a week seems to be getting out of hand!

Many thanks to my friends and family for your support and help through the years. Thank you Cor and Babs in particular, for your friendship during my Bachelor, Master and now PhD-degree. Special thanks to Cor for creating the cover for this thesis. Ook wil ik heel graag mijn ouders bedanken voor jullie steun en adviezen. Jullie staan altijd voor me klaar en dat waardeer ik heel erg. Ik vind het heel leuk dat jullie altijd de krantenberichtjes over sterrenkunde voor mij bewaren! Emilio, thank you very much for your love, friendship and support. Thank you for all the cups of tea you brought to me when I was trying to finish this thesis frantically. I hope that we can be together for a long time (an astrophysical timescale!) and that I can return the same love, friendship and support to you.